

NGU Report 98.081

The geology of the Engebøfjell eclogite deposit
and its regional setting

Report no.: 98.081	ISSN 0800-3416	Grading: <i>Open</i> Confidential to 04.05.2003	
Title: The geology of the Engebøfjell eclogite deposit and its regional setting.			
Authors: Korneliussen, A., Braathen, A., Erambert, M., Lutro, O. and Ragnhildstveit, J.		Client: DuPont	
County: Norway		Commune: Naustdal	
Map-sheet name (M=1:250.000) Florø		Map-sheet no. and -name (M=1:50.000) 1117.1 Fjaler	
Deposit name and grid-reference: Engebøfjellet UTM 310300 6822700		Number of pages: 121	Price (NOK):
		Map enclosures: 2	
Fieldwork carried out: the authors	Date of report: 04.05.1998	Project no.: 1900.05	Person responsible: <i>T. G. Beres</i>
<p>Summary:</p> <p>The Engebøfjellet eclogite deposit is situated at the northern side of Førdefjord near the small community Vevring in Naustdal kommune, Sogn og Fjordane county, W. Norway. Geologically the Førdefjord area belongs to the «Western Gneiss Region», between the Devonian Kvamshesten basin to the south and the Devonian Håsteinen basin to the North. Recent mapping divide the Førdefjord region into two major geologic units: the Hegreneset complex and the Helle complex. The Hegreneset complex (oldest) contains a variety of amphibolitic, eclogitic and gabbroic rocks, together with tonalitic to dioritic gneisses. The Helle complex comprises mainly granitic and granodioritic gneisses.</p> <p>The Engebøfjellet eclogite is a 2.5 km long, folded, lens-formed body surrounded by hybrid mafic-felsic country-rocks belonging to the Hegreneset complex. The protolith to the eclogite is believed to be a Proterozoic Fe and Ti-rich gabbroic intrusion. The transformation into eclogite is related to Caledonian high-pressure metamorphism at approx. 400 Ma. In this process, ilmenite in the gabbro protolith was replaced by rutile. The Ti-enriched parts of the eclogite are now rutile ore.</p> <p>Preliminary investigations of rutile at Engebøfjellet have been carried out by a variety of companies since the early 1970's without identifying its full ore potential. In 1995, however, an agreement was made between DuPont/Conoco and the local company, Fjord Blokk, which at that time started a test production of eclogite blocks at Engebøfjellet to be used in breakwater/sea-wall constructions, and a small core-drilling program was set up. Drilling results were promising and the drilling program was extended; by the end of 1997, a total of 15000 m had been drilled, and a large rutile resource identified.</p> <p>This report gives a regional geologic overview of the Førdefjord region including a new 1:50000 scale map, and lithologic, mineralogical, geochemical and structural information for the Engebøfjellet eclogite deposit based on investigations in the field and of drill-cores by NGU in collaboration with DuPont, Conoco and Fjord Blokk.</p>			
Keywords: fagrapport	geologic mapping	eclogite	
titanium	rutile	Caledonian	
Western Gneis Region			

CONTENTS

	page
1. Introduction	8
2. The Førdefjord region	8
3. The Engebøfjell eclogite	10
4. Summary and recommendations for future works	20
5. References	22

APPENDIX

- Appendix 1: Regional bedrock map, Førdefjorden region.
- Appendix 2: Lithologic and structural map of Engebøfjellet
- Appendix 3: Geology of the Førdefjord region
- Appendix 4: Structural geology, Engebøfjellet
- Appendix 5: Mineralogy, Engebøfjellet
- Appendix 6: Plots of analytical data, Engebøfjellet
- Appendix 7: Surface sample list, Engebøfjellet
- Appendix 8: Major and trace element analyses
- Appendix 9: Miscellaneous photographs

FIGURES

Figures to the main text

- Fig. 1: Computer image of the Engebøfjell eclogite
- Fig. 2: Overview photographs of Engebøfjellet.
- Fig. 3: Photograph of Engebøfjellet viewed from the fjord.
- Fig. 4: Fe_2O_3 - TiO_2 plot of core analyses.
- Fig. 5: Fe_2O_3 - TiO_2 plot of surface samples.
- Fig. 6: Rutile vs. TiO_2 in core samples.
- Fig. 7: Photograph of eclogite lenses that are folded and stretched.
- Fig. 8: Summary diagram of observed structures and mineral parageneses of the Engebøfjell eclogite

Figures in Appendix 3

- Fig. A3.1: Simplified geologic map, Sognefjord to Nordfjord.
- Fig. A3.2: Block diagram, Sunnfjord area.
- Fig. A3.3 - A3.16: Miscellaneous photographs.
- Fig. A3.17: Geological N-S cross sections across Førdefjord.
- Fig. A3.18: Structures in the Førdefjord region. Stereo-plots.

Figures to Appendix 4

- Fig. A4.1: Structural fabric map of the Engebøfjell eclogite.
- Fig. A4.2: Structural cross-sections of the Engebøfjell eclogite.
- Fig. A4.3: Possible primary feature in the ferro eclogite .
- Fig. A4.4: Tight to isoclinal F_2 -fold of the S_1 foliation in a sheared version of the ferro eclogite.
- Fig. A4.5: Tight to isoclinal F_2 -fold of the S_1 foliation in a sheared version of the ferro eclogite.
- Fig. A4.6: Tight F_3 -antiform of S_2 foliation(?) in ferro eclogite.
- Fig. A4.7: Strongly sheared, isoclinally folded lenses of partly retrograded

eclogite in amphibole-gneiss (retrograded eclogite) with a dominant amphibolitic S_3 foliation.

Fig. A4.8: Partly retrograded eclogite lenses in quartz-mica matrix.

Fig. A4.9: D_1 structural data.

Fig. A4.10: D_2 structural data.

Fig. A4.11: D_3 structural data.

Fig. A4.12: D_4 structural data.

Fig. A4.13: Microphotograph of eclogite with S_2 foliation.

Fig. A4.14: Microphotograph of amphibolitised eclogite with S_3 foliation.

Fig. A4.15: Microphotograph of ferro eclogite with D_5 fractures.

Figures to Appendix 5

Fig. A5.1: Microphotograph of massive leucogabbroic eclogite: coronitic texture.

Fig. A5.2: Microphotograph of recrystallized leucogabbroic eclogite.

Fig. A5.3: Microphotograph of leucogabbroic eclogite with post- D_1 omphacite.

Fig. A5.4: Microphotograph of recrystallized ferro eclogite.

Fig. A5.5: Microphotograph of carbonate-rich eclogite.

Fig. A5.6: Retrogression of eclogite along D_5 fractures.

Fig. A5.7: Composition of garnets in eclogites from Engebøfjellet

Fig. A5.8: Compositional profiles in garnet from ferro eclogite

Fig. A5.9: Classification of amphiboles from Engebøfjellet according to Leake (1978)

Fig. A5.10: Substitution in eclogite amphiboles.

Fig. A5.11: Photomicrograph showing extensive symplectitic retrogression in eclogite.

Fig. A5.12: Photomicrograph showing incipient retrogr. of eclogite along grain boundaries.

Fig. A5.13: Retrogressive textures, Ti-oxides

Figures to Appendix 6

Fig. A6.1: Fe_2O_3 - TiO_2 plot of X-Met core analyses of leuco-, transit.- and ferro eclogite.

Fig. A6.2: Fe_2O_3 - TiO_2 plot of X-Met core analyses of leuco eclogites.

Fig. A6.3: Fe_2O_3 - TiO_2 plot of X-Met core analyses of transitional eclogites.

Fig. A6.4: Fe_2O_3 - TiO_2 plot of X-Met core analyses of ferro eclogites.

Fig. A6.5: Fe_2O_3 - TiO_2 plot of X-Met core analyses of amphibolite unit rocks.

Fig. A6.6: Fe_2O_3 - TiO_2 plot of X-Met core analyses of amphibolites.

Fig. A6.7: Fe_2O_3 - TiO_2 plot of X-Met core analyses of garnet amphibolites.

Fig. A6.8: Fe_2O_3 vs. TiO_2 , P_2O_5 , La and Zr for core samples analysed by XRF.

Fig. A6.9: Fe/Mg vs. TiO_2 , P_2O_5 , La and Zr for core samples analysed by XRF.

Fig. A6.10: Zr - Y^*3 - Ti/100 triangular diagram, Engebøfjell core samples.

Fig. A6.11: Chondrite normalised REE-patterns for Engebøfjell core samples.

Figures to Appendix 9

Fig. A9.1: Photographs of core and thin-section of ferro eclogite.

Fig. A9.2: Photographs of ferro eclogite cores.

Fig. A9.3: Microphotographs of retrograded eclogite.

Fig. A9.4: Microphotographs showing alteration of rutile to ilmenite and titanite in ferro eclogite.

Fig. A9.5: Photographs of leucoeclogite in core and thin-section.

Fig. A9.6: Photograph of retrograded eclogite varieties (cores).

Fig. A9.7: Photographs of amphibolite unit rocks (cores).

Fig. A9.8: Photograph of core with sharp contact between amphibolite and ferro eclogite.

TABLES

Tables in the main text

Table 1: Exploration history, Engebøfjellet

Table 2: Major lithologic units in the Engebøfjellet - Vevring area.

Tables in Appendix 5

Table A5.1: Garnet composition in eclogites from Engebøfjellet

Table A5.2: Eclogite pyroxenes from Engebøfjellet

Table A5.3: Eclogite-facies amphiboles from Engebøfjellet

Table A5.4: Eclogite minerals from Engebøfjellet.

Table A5.5: Temperature estimates on eclogites from Engebøfjellet.

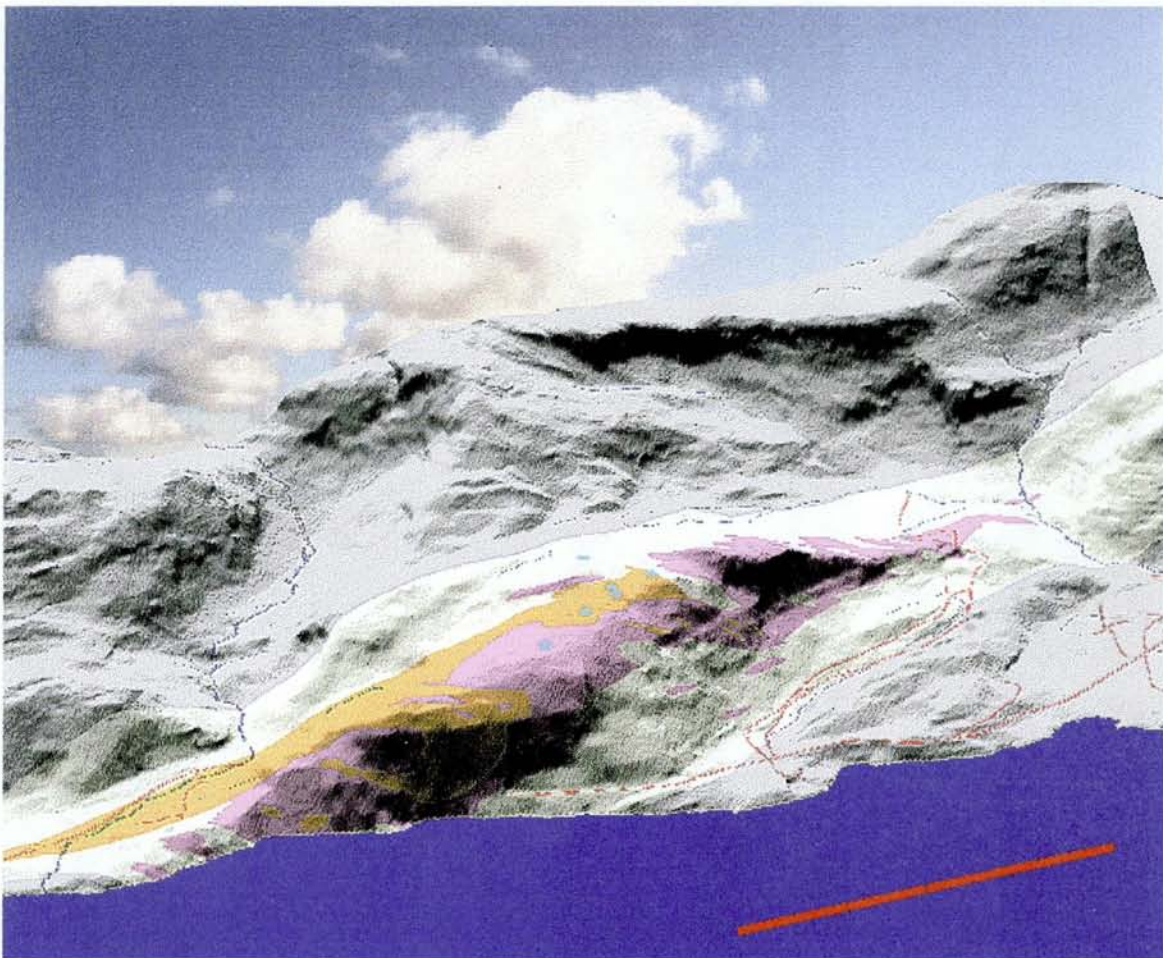


Fig. 1: Computer image of the Engebøfjellet eclogite with Førdefjord in the foreground. The ferroeclogite (ore type) is in pink and the leuco- to transitional eclogite in yellow. The image was made by Eiof Erichsen (NGU) based on available digital topographic and geological maps. The green dots are field sites for spectrometer measurements (see report on air-borne remote sensing in the Førdefjord area by Follestad (in prep.)). The scale-bar in the fjord is 1 km. Height of mountain to the right is 618 m.a.s.l. and the highest point of the Engebøfjell eclogite is 312 m.a.s.l.



Fig. 2: Overview photographs of Engebøfjellet. Upper photo: Engebøfjellet viewed from Redal in the east. Lower photo: Engebøfjellet seen from helicopter westwards, with outer Førdefjord and Vevring in the background



Fig. 3: The southern slopes of the central part of Engebøfjellet seen from the fjord.

1. Introduction

The mountain-ridge named Engebøfjellet (Figs. 1 - 2, Appendix 2) is located at the north side of the Førdefjord in western Norway, as shown on the regional bedrock map of the Førdefjord region (Appendix 1). Rocks of the region belong to the Western Gneiss Region, which is dominated by Precambrian ortho-gneisses (e.g., Kullerud et al. 1986; Milnes et al. 1988; Milnes et al. 1996, Andersen and Jamtveit 1990). These rocks reveal mineral parageneses indicating metamorphic P-T conditions reaching amphibolite -, and locally granulite facies. There are also numerous bodies of eclogite in the western part of the province (e.g., Griffin et al., 1985, 1987; Krogh and Carswell 1995), among them the Engebøfjellet eclogite (Korneliussen and Furuhaug 1991; Korneliussen 1996; Korneliussen and Erambert 1997).

Since 1992 NGU has collaborated with DuPont in the investigation of rutile-bearing eclogites in W. Norway, resulting in several significant new discoveries. The existence of the Engebøfjell eclogite, however, has been known since the 1970s (Korneliussen 1980 b; Korneliussen and Foslie 1985, Korneliussen and Furuhaug 1991); see summary of exploration history (Table 1). In 1995, the company Fjord Blokk started test-production of eclogite blocks for breakwater material at the eastern end of the deposit. A meeting was held between Fjord Blokk and DuPont/Conoco in July 1995 which resulted in a collaboration in the continued investigation of Engebøfjellet and initiation of a core-drilling program.

NGU has been involved in the planning of the investigations, follow-up of the core-drilling in the field, analytical work on cores, core-logging, mapping, and gravimetric investigations in the surroundings of Engebøfjellet (Korneliussen 1996, Korneliussen and Erambert 1997, Muring and Gellein 1996, 1997, Muring et al. 1997).

The purpose of this report is to give an update review of the geology of the Engebøfjell eclogite deposit and its surroundings in the light of these investigations

2. The Førdefjord region (see Appendix 3 for further details)

The Førdefjord area is a part of the Proterozoic Western Gneiss Region of Norway. This area and adjacent areas to the south and north, are folded into regional east-west trending folds, interpreted to be the result of late-Palaeozoic N-S compression. Two major units are present in the area: the Hegreneset complex and the Helle complex.

The Hegreneset complex consists of a variety of mafic, mainly eclogitic rocks, and crosscutting, homogeneous grey to grey-green tonalitic, dioritic and granodioritic intrusives. The mafic and felsic rocks are in many places intimately mingled, in several places with a broad intrusive contact zone where the grey intrusives have abundant basic xenoliths. The Hegreneset complex crops out continuously on the southern side of Førdefjord from Hegreneset in the west to near Førde in the east. It seems to be situated in a major late-Caledonian east-west elongated dome structure. On the northern side of the Førdefjord, it crops out in the Engebø area, and from Engebø it can be followed discontinuously eastwards, surrounded by rocks of the Helle complex.

Table 1: Exploration history, Engebøfjellet.

Early 1970's	The Elkem geologist Hans-Peter Geis was probably the first geologist to recognize the Engebøfjellet eclogite as a rutile deposit in the early '70's. He made a sampling profile through the Engebøfjellet road-tunnel.
1978-79	Additional sampling was done within a cooperation project between NGU and Elkem on rutile-bearing eclogites in Sunnfjord.
1979	Frank Barkve and Tore Birkeland focused on Engebøfjellet in an investigation of heavy rocks as breakwater material. That was the start of a long and complex process which resulted in Fjord Blokk's eclogite mining operation in 1995.
1984-85	Several companies were active at Engebøfjellet in the mid-80's investigating the rutile and breakwater material/aggregate possibilities.
1990	NGU made a W-E sampling profile along the deposit (Korneliussen and Furuhaug 1991).
1992	Signing of agreement between DuPont and NGU to jointly investigate the rutile potential of eclogites in W.Norway.
1991	R. McLimans (DuPont), S. Parr (Stokke Industri) and A. Korneliussen (NGU) visited Engebøfjellet on a rutile/eclogite excursion in W. Norway, followed by a sample profile through the road tunnel later the same year by McLimans and K. Davies (also from DuPont).
1995	Fjord Blokk and Conoco/DuPont made an agreement for a joint rutile investigation of Engebøfjellet, followed by core-drilling, beneficiation tests, surface sampling and geologic mapping activities. At first, the intent was to drill 400 m in the eastern part of Engebøfjellet near Fjord Blokk's quarry and financial support was given by the Prospecting Fund. The drilling started in October 1995. Shortly afterwards, the drilling program was extended.
1996-97	Continued investigations of the rutile potential incl. 15000 meters of core drilling, gravimetric investigations, structural and lithological mapping and mineralogical investigations

At Mt. Fureviknipa on the southern side of the fjord, banded eclogite represents eclogitized layered gabbro. Westwards from Fureviknipa, anorthosite and leucogabbro constitute part of the same basic complex; the anorthosite contains lenses of retrograded eclogites. The large basic complex south of Førdefjord, including Mt. Fureviknipa, therefore consists mostly of plutonic layered cumulate rocks. Southwest of Mt. Fureviknipa, a fine-grained, banded to laminated, basic rock of either intrusive or extrusive origin occurs. This rock shows extensive mesoscopic, ductile, disharmonic folding under eclogite facies conditions; and resembles the Engebøfjellet eclogite. In some places, such as the country-rocks to the Engebøfjellet eclogite body, mafic and felsic rocks occur in a characteristic deformed cm-dm scale banded succession as well as in larger units.

The Helle complex consists mainly of granitic to granodioritic gneisses, in many places migmatitic and/or banded. The granitic gneisses are red to grey. A number of younger red granites altered to gneiss, and minor basic intrusives are also included in the complex. Due to the complex, polyphase, and generally strong deformation in the area, rocks with varied structures and textures occur.

3. The Engebøfjellet eclogite

The Engebø - Vevring area is characterised by a series of mafic rocks (eclogitic and amphibolitic) intermixed with grey gneisses. These rocks belong to the «amphibolite unit» in the Engebøfjell geologic map (Appendix 2). The eclogitic rocks are mainly of a garnet-poor, amphibole-rich type, with gradational transitions into garnet-amphibolites and amphibolites. Generally, the eclogite to amphibolite transition is an effect of retrogression. The grey gneisses which are intimately associated with the mafic rocks, are of two types: cm-dm thick leucocratic bands (quartz + feldspar + white-mica) alternating with mafic bands of garnet amphibolites and eclogites (see Fig. A9.7 in Appendix 9), and granodioritic to tonalitic gneisses within units several meters to several tens of meters thick. The Engebøfjellet eclogite and the surrounding undifferentiated mafic and felsic rocks belong to the Hegreneset complex, see the Førdefjord geologic map (Appendix 1). Larger units of granitoid gneisses belong to the Helle complex.

The Engebøfjell eclogite forms a 2.5 km long E-W-trending lens (see the geological map in Appendix 2) with a distinctly massive character compared to the surrounding rocks. It is believed to represent a Proterozoic gabbroic intrusion that experienced crystal fractionation processes leading to the enrichment of Fe and Ti, and transformed into eclogite during Caledonian high-pressure metamorphism at approx. 400 Ma. In this process ilmenite in the eclogite protolith has been replaced by rutile, and the Ti-enriched parts of the body is now rutile ore. The TiO_2 -content of the ore is illustrated in the Fe_2O_3 - TiO_2 plots (Fig. 4 and 5).

The Engebøfjell geologic map (Appendix 2) is based primarily on a combination of geologic observations in the field and an interpretation of TiO_2 - and Fe_2O_3 -analyses of surface samples. The central and western half of Engebøfjellet has been better mapped than the eastern half, mainly because the overburden is more extensive in the east. Another reason is that the eastern part of Engebøfjellet is strongly deformed with country-rocks frequently folded into the main eclogite body.

In the Engebøfjell geologic map, the body is subdivided into two major eclogite types based on their varying iron and titanium contents: (1) The *ferro eclogite* is Fe_2O_3 -, TiO_2 - and garnet-rich; >14% Fe_2O_3 , >3% TiO_2 and > 25% garnet, respectively. In general, it has a more massive character than the other eclogite varieties found at Engebøfjellet, although in parts it is significantly banded and folded. This eclogite is the rutile ore-type eclogite, the major volume of which is found in the central and western parts of the deposit. This eclogite occasionally shows fairly sharp contacts to the leuco eclogite (see below), but usually the contacts are gradational over several decimetres to several meters via a «transitional» eclogite variety. Rutile- and garnet-rich, and fairly massive eclogite layers in the Fjord Blokk quarry in the E, and the rutile-rich parts of Dh1, 2 and 3 (see Korneliussen and Erambert 1997) are unmapped eastward extensions of this eclogite type.

(2) The *leuco- and transitional eclogite* is TiO_2 - and Fe_2O_3 -poor (<14% Fe_2O_3 and < 3% TiO_2), locally with preserved gabbroic protolith textures. Metagabbroic

relict textures are more abundant in the western parts of the deposit, whereas this rock-type not has been mapped in the eastern part of Engebøfjellet.

Geochemistry: The geochemistry of the Engebøfjell eclogite is a reflection of its complex geologic evolution, and mirrors both primary magmatic chemical variation in the Proterozoic gabbroic protolith and probably also the influence of Caledonian metamorphism.

Based on a large number of Fe_2O_3 and TiO_2 analyses of cores by a portable XRF spectrometer (Fig. 4) and analyses of surface samples (Fig. 5), some general features can be observed. Firstly, the Fe_2O_3 - TiO_2 chemical variation is continuous from leuco eclogite and through transitional eclogite into ferro eclogite. Secondly, the ferro eclogite (>14% Fe_2O_3 and >3% TiO_2 , approx.) can be split into two groups, a «normal ferro eclogite» that is a direct-line continuation from the leuco - transitional eclogite trend illustrated by the solid line in Fig. 4, and a «Ti-enriched ferro eclogite», illustrated by the stippled line in Fig. 4. It is believed that the reason for this split-up of the ferro eclogite is caused by crystal fractionation processes in the gabbroic protolith. The metamorphic influence is considered minor, although evidence for this interpretation is not documented. Thirdly, some ferro eclogite samples at approx. 18% Fe_2O_3 are distinctly enriched in P_2O_5 (0.5-2% P_2O_5 vs. the normal values of < 0.2% P_2O_5), as shown in Fig. A6.8 in Appendix 6. This eclogite variety is called «P-rich ferro eclogite». Unfortunately no field-criteria has been developed to distinguish these ferro eclogite varieties in the field; at present they can only be recognised in terms of their chemical compositions. Amphibolite unit rocks, which are easily recognisable in the field, tend to be enriched in elements such as La and Zr compared to the leuco-, transitional- and ferro eclogites, indicating a distinct precursor and/or a different geologic evolution.

A large number of surface samples have been taken across the eclogite body. In the Fe_2O_3 - TiO_2 diagram (Fig. 5), these samples plot along a continuous trend in which titanium is positively correlated with iron, although a significant number of samples are anomalously enriched in TiO_2 compared with the “normal” trend. An unknown number of samples in the lower Fe_2O_3 - TiO_2 ranges represent amphibolite unit rocks; this does not, however, change the overall character of the plot.

In comparison, a Fe_2O_3 and TiO_2 plot of all core analyses done by the X-Met portable XRF, is shown in Fig. 4. The eclogite type is defined by core logging that has not taken in account cm-dm scale variations in the core with either low or high Fe_2O_3 and TiO_2 contents; therefore a number of samples plot well outside their normal field. In this diagram the three eclogite varieties plot in fields with gradual contacts. This plot shows the same overall pattern as for the surface samples (Fig. 5). In this plot the ferro eclogite can be subdivided into two major varieties; one that represents a distinct TiO_2 -enrichment, the other represent a continuation of a «normal» linear Fe_2O_3 - TiO_2 enrichment incorporating the leuco- and transitional eclogites.

The core-samples that were analysed for both major- and trace elements (Fig. A6.8 in Appendix 6), show a similar trend.

Table 2: Major lithologic units in the Engebøfjell - Vevring area.

The rocks enclosing the Engebøfjell eclogite body

Granitoid gneisses (undifferentiated)	The granitoid gneisses represent Proterozoic granitic and tonalitic plutonic rocks belonging to the Helle complex. They intruded into the mafic and felsic rocks of the Hegreneset complex and were extensively deformed by the Caledonian orogeny.
Amphibolite unit (undifferentiated)	This unit is characterised by cm- to dm-scale alternating mafic- and felsic bands. The mafic components are eclogitic to amphibolitic (retrograded eclogite) and the felsic component resembles tonalite or diorite. These rocks are now strongly deformed and metamorphosed due to the Caledonian orogeny. This unit represents an older part of the Hegreneset complex into which the Engebøfjell protolith gabbro intruded. See photograph in Fig. A9.7 (Appendix 9).

The Engebøfjell eclogite rocks

Leuco eclogite	Fine-grained eclogite with a fairly low garnet content. In varieties with minor deformation a gabbroic texture is preserved. <i>Leuco- and transitional eclogite</i> is distinguished from ferroeclogite by its leucocratic character incl. lower garnet content. The increase in iron and titanium values is gradual. See photograph in Fig. A9.5 (Appendix 9).
Transitional eclogite	Eclogite intermediate between the leuco- and the ferro eclogite.
Ferro eclogite	The ferro eclogite (ore type) is a relatively massive, dark, garnet-rich eclogite with a distinct rutile-content. A characteristic feature that is commonly seen is a series of thin cracks (D ₅) in which the eclogite has been retrograded (amphibolitised). Occasionally 1-2 mm large holes after a leached-out mineral can be seen along certain zones in this eclogite. See photograph in Fig. A9.1 (Appendix 9).

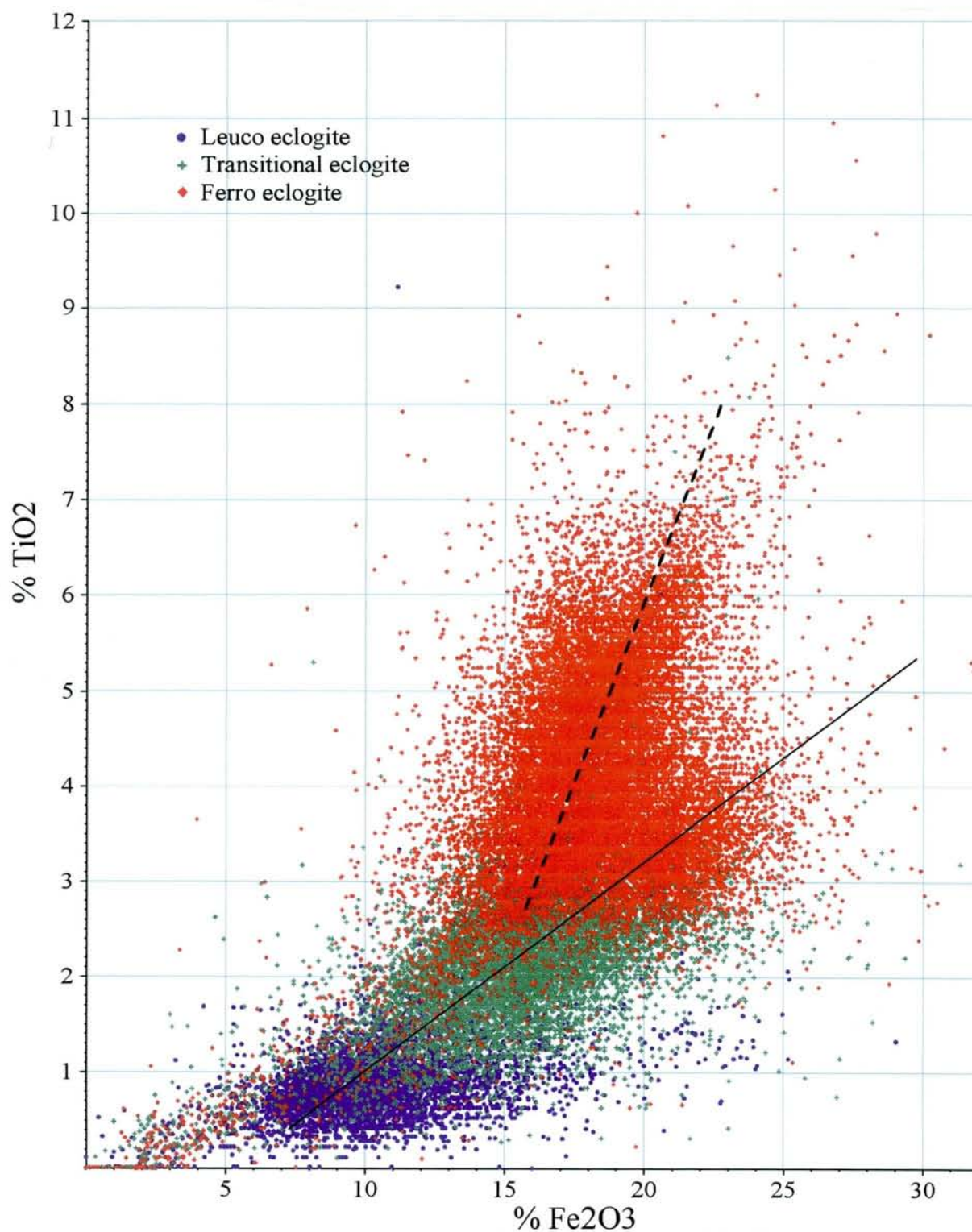


Fig. 4: Fe₂O₃ -TiO₂ plot of analyses done by the X-Met portable XRF directly on cores, based on data from a corelog database (Englog.mdb) of core sections defined as leuco-, transitional - and ferro eclogite, respectively. Individual samples that plot far outside the main field for the respective rocktype, for example ferro eclogite samples with low Fe₂O₃ and TiO₂ contents, indicate small-scale inhomogeneities within the rock type picked up by the X-Met analyser. The solid line indicates the normal Fe-Ti enrichment trend and the dashed line the enrichment trend for the Ti-rich ferro eclogite.

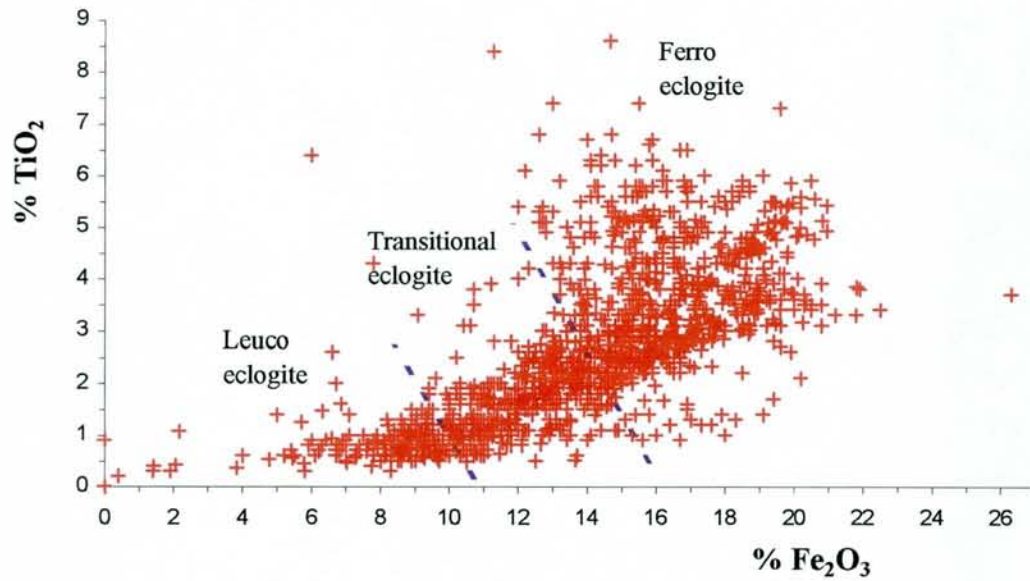


Fig. 5: Fe_2O_3 - TiO_2 plot of surface samples taken at Engebøfjellet with the fields for leuco -, transitional - and ferro eclogite. An unknown number of samples in the lower Fe_2O_3 - TiO_2 ranges represent amphibolite unit rocks. This does not, however, change the overall character of the plot.

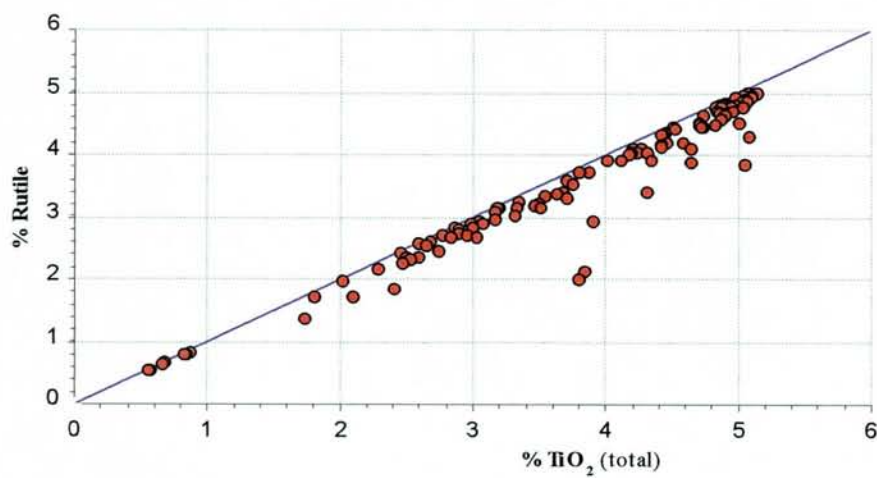


Fig. 6: % rutile vs. % TiO_2 (total), core samples. The analytical data are given in Appendix 8.

Rutile is determined by the so-called *rutile analytical procedure* ($\% \text{ rutile} = \% \text{TiO}_2$ (analysed by XRF) - $\% \text{TiO}_2$ (dissolved in HCl; analysed by ICP)). In this procedure rutile is not dissolved while ilmenite is dissolved by HCl. Silicates are not dissolved in HCl, i.e. TiO_2 in silicates will come out as rutile by this method. The method is only to be used on rocks, such as eclogites, where TiO_2 in silicates are low enough to be neglected for practical purposes. In the typical Engebøfjell eclogite more than 90% of the titanium in the rock occurs as rutile, as illustrated in Fig. 6. Those samples in Fig. 6 that plot well away from the line $\text{rutile}/\text{TiO}_2 = 1$ have a distinct portion of retrograde ilmenite formed during the deformational episodes D_3 , D_4 and D_5 . Microphotographs of ferro eclogite showing different stages of retrograde overprinting are shown in Figs. A9.3 - 4 (Appendix 9).

Mineralogy (see Appendix 5 for more detailed information): The Engebøfjell gabbroic protolith was metamorphosed under eclogite-facies P and T conditions of 15-17 kbar and ca. 600°C. Eclogitisation corresponds to a complete mineralogical change. No relict of magmatic minerals was found in the Engebøfjell eclogite. The degree of textural equilibration of the eclogites is dependent on their deformational history during the eclogite-facies metamorphism (D_1 and D_2 phases). The leucocratic rocks show a textural evolution from coronites to foliated eclogites. In coronitic leuco eclogites (e.g. "massive leuco eclogite"), albite, together with phengite, zoisite and quartz, forms microcrystalline pseudomorphs after plagioclase. Small granular amphibole and clinopyroxene has replaced magmatic mafic phases. Coronas of garnet separate felsic and mafic domains, underlining the former grain boundaries and the relict gabbroic texture. In more deformed rocks, segregations after plagioclase have become coarser-grained and taken an elongate shape; they contain paragonite, phengite and clinozoisite. The mafic matrix surrounding them is recrystallised into a fine-grained assemblage of garnet, clinopyroxene and amphibole. Completely recrystallized leuco eclogites are found at the deformed margins of the massive leuco eclogite body. The melanocratic rocks, with Ti ore potential, are generally completely recrystallized into foliated eclogites. On average, eclogites from Engebøfjell are fine-grained rocks, either as a result of strong deformation (ferro eclogites) or lack of complete recrystallisation (coronitic leuco eclogite). Ferro eclogites are generally granular, with a grain size less than 0.5 mm.

Eclogite paragenesis comprises garnet, omphacite, amphibole, phengite, clinozoisite, quartz, dolomite, rutile and pyrite. Accessory minerals are apatite, allanite and zircon. Ti is now mainly residing in rutile, mostly as matrix grains (0.5 mm); a minor amount forms numerous but tiny inclusions within silicates. Discrete ilmenite grains are recorded in one sample. Modal as well as mineral chemical variations are found from ferro- to transitional and leuco- eclogites. Ferro eclogites are usually rich in garnet (from ca. 25% to 55%) and rutile (3-6%). Within this group, bulk-rock chemical variations are expressed by modal variations in garnet, clinopyroxene and amphibole as well as in minor phases like quartz, clinozoisite, phengite, rutile and apatite. Transitional eclogites show an increase in clinopyroxene (omphacite); large amphibole porphyroblasts are common. Within this group, coarser-grained eclogites contain omphacite porphyroclasts sheared within a fine-grained matrix of omphacite, garnet, amphibole, carbonate and mica. Leucocratic rocks are enriched in mica, clinozoisite, and often in amphibole and quartz; garnet forms generally less than 20% of the rock. Omphacite characteristically forms elongate porphyroblasts, up to 2-3 cm long. Some leuco eclogites are layered on the mm-cm scale and contain numerous phengite (carbonate-bearing quartz-rich layers). Concurrently with the modal changes, mineral compositions also evolve. The

almandine garnet become richer in Mg (pyrope component), from Alm 56-65 Spe 1-5 Pyr 9-17 Gro 17-24 And 1-7 in ferro- and transitional eclogites to Alm 52 Spe 2 Pyr 24 Gro 21 And 2 in one leuco eclogite. Both clinopyroxene and amphibole show an increase in Al and Na, evolving from chloromelanitic omphacite (Jd 21-35) to omphacite (Jd 45) and from actinolitic hornblende to barroisite.

Fluid-rock interaction was frequent at all stages in the history of these rocks. The abundance of volatile-bearing minerals (mainly amphibole, phengite, clinozoisite, dolomite and apatite) characterizes eclogite-facies parageneses from Engebøfjellet. Amphibole is ubiquitous, in amounts ranging from trace to being the main Na- and Ca-bearing phase (40-50%). Dolomite is common, varying in abundance from a few scattered grains to a major phase. Abundant eclogite-facies veining (quartz, omphacite, garnet, carbonate, phengite...) indicate that the fluid pressure was high during this event.

Retrogression of the eclogites is often seen dependant on both deformation and fluid infiltration and occurred predominantly along shear zones and margins of the lens. Garnet amphibolites represent the first retrogression stage (D_3). Amphibolites within major shear zones (D_4) contain amphibole (hornblende type), epidote and plagioclase; garnet breaks down. Static retrogression of eclogites to symplectitic assemblages of the same minerals is observed in undeformed areas near these shear zones. The mineral assemblages indicate that the D_4 deformation occurred under conditions characteristic of the epidote-amphibolite facies. Local coronitic retrogression along late fractures and mineral filling in the veins (actinolite, epidote, chlorite, calcite, quartz, magnetite, ilmenite and/or titanite) represent a greenschist facies overprint (D_5). During retrogression, rutile is replaced by ilmenite along grain rim and fractures. This transformation generally amounts to less than 10% in eclogites with minor retrogression but can reach more than 95% in totally amphibolitized samples. Only trace amounts of titanite occur in a few late D_5 veins or as thin coronas around rutile/ilmenite grains in extensively retrograded eclogites.

Structural geology (see Appendix 4 for additional information). Deformation of the Engebøfjellet eclogite and the surrounding rocks may be separated into six stages, designated D_1 to D_6 . Prior to deformation magmatic layering(?) may have existed in the rocks. Metamorphic conditions and mineralogy for this primary phase can not be established due to later, overprinting metamorphic events. The first observable stage, D_1 , is shown as isoclinal folds (F_1) of the mineralogical banding in the protolith rocks. A dominant transposition foliation (S_1), often parallel to this banding, was developed. Metamorphic conditions during the first stage of deformation probably reached eclogite facies, as indicated by formation of garnet and omphacite (Carswell, 1990; Yardley, 1989). Orientation of the F_1 axes, which have a subhorizontal, E-W orientation, may be explained by N-S shortening. However, later non-coaxial deformation, with potential rotation, make any conclusion speculative.

After formation of the S_1 foliation, an elongated omphacite formed in the eclogite rocks (post- D_1). Since this mineral has grown superimposed on to the foliation, and with a random orientation, it probably relates to a period of static P conditions.

During the following D_2 stage, the S_1 foliation is folded into tight to isoclinal F_2 -folds. In these structures, a spaced cleavage generated near the fold-hinges. In the F_2 fold-limbs, which suffered the most D_2 strain, a new penetrative foliation (S_2) was formed. This foliation, which is very fine grained and mylonitic(?), represents the dominant fabric in the Engebøfjellet Eclogite. One good example of a F_2 -fold is illustrated in cross-section D-D' (Fig. A4.2 in Appendix 4), whereas the Fureåsen area (see Appendix 2), near the top of Engebøfjellet, shows well exposed outcrop-scale

structures. Metamorphic conditions during the D_2 stage reached eclogite facies, as suggested by the stable minerals garnet+omphacite along the S_2 foliation. Field observations of kinematic indicators in the D_2 high strain zones reveal both dextral and sinistral shear-sense for separate zones, respectively, i.e. parallel to the WNW-ESE lineation. One way to interpret this pattern is that the eclogite body suffered regional, coaxial N-S shortening during the D_2 phase.

The following D_3 stage folds the S_2 foliation into tight F_3 -folds. A spaced cleavage formed in the hinges of these folds, whereas distinct meter-wide shear-zones (S_3) generate in the fold-limbs. At other places, the eclogitic S_2 foliation is reactivated as shear-zones. In both cases the eclogite is retrograded into (garnet-) amphibolite. Growth of amphibole+garnet+plagioclase in these late high-strain zones indicate amphibolite facies, garnet zone metamorphic conditions (Yardley, 1989) during the D_3 stage. The best example of a F_3 fold is found in the quarry (see cross-section A-A', Fig. A4.2 in Appendix 4), where the F_3 fold-pair and amphibolitic shear-zones relate to the D_3 stage.

The D_4 stage is characterized by the formation of meter-wide shear zones (S_4), which have been observed at a few locations. One of these structures cuts through the F_3 fold in the quarry (described above); thus it post-dates the F_3 -folding. Along the margin of the S_4 high-strain zones, the eclogite is retrograded into amphibolite, whereas the shear-zones contain amphibole+plagioclase(?) + biotite+epidote+quartz. The lack of garnet, and growth of biotite, suggest that these shear-zones formed under epidote-amphibolite to upper greenschist facies, and biotite zone conditions (Yardley, 1989), maybe from a progressive continuation of the D_3 stage.

Shear-sense indicators (e.g., Hamner and Passchier, 1991) for both the D_3 and D_4 stages, such as composite shear fabrics, shear-folds and wings around mechanical strong bodies (Fig. 7), support non-coaxial sinistral shear. This movement was subhorizontal, parallel to the stretching lineation, and resulted in internal shortening by stacking and folding of the first order lens. Thus, the deformation mechanism probably was sinistral transpression.

The S_4 shear-zones and all older structures are truncated by sub-vertical N-S striking joints of the D_5 stage. These joints are filled with epidote + quartz (+ carbonate + chlorite), whereas the wall-rocks often show cm-wide zones where omphacite+ blue amphibole+garnet is replaced by green amphibole. These mineral associations indicate epidote-amphibolite to greenschist facies conditions during the D_5 stage. The N-S, vertical orientation of the fractures, and their tensile nature, suggest that this deformation relates to N-S, horizontal shortening.

It is worth to mention that similar fractures are found in eclogites several km south of Engebøfjellet. There, steep tensile fractures strikes NW-SE. This change in orientation from N to S may relate to late, open folding in the area; folds that possibly are associated with W-directed movement in the detachment zone. These folds are suggested to have a late Devonian - Early Carboniferous age (e.g. Torsvik et al. 1987). Thus, these late, tensile fractures constitute a possible marker that may help to establish late-/post-Caledonian folding of the Precambrian basement.

The last deformation observed in the rocks, the D_6 stage, is present as two populations of brittle faults: (i) N-S striking, moderately to steeply east and west dipping normal faults, and (ii) sub-vertical, NNW-SSE and NE-SW striking strike-slip faults. Slip on the faults is indicated by separation of markers in the rock, as well as lineations on the slip-surfaces (slickensides). These kinematic indicators suggest formation of the faults during N-S shortening, which triggered E-W extrusion/extension. Greenschist facies or lower P-T conditions during the D_6 stage is

suggested from the brittle style of deformation. This type of structures are suggested by Braathen (1998) to reflect Carboniferous - Permian deformation in the region.

The suggested deformation sequence and its tectonic implications is important in a regional perspective. The steep E-W orientation of foliations (S_2 and S_3) seen in the Engebøfjell area are not continuous to the E. There, the main foliation successively changes to moderate N dips. However, the high-strain zone of Engebøfjellet appears to be continuous into the eastern area. Thus high-strain zone bounds an open box-like antiform further S, which has an other high-strain zone as its southern margin. Internal foliation in the antiform probably predates the shearing in the fold-limbs. In the Fureviknipa area W of Førde, a distinct fold-pair is evident. The southern antiform is open and upright, and is probably truncated by the detachment zone, whereas the synform further N is tight and S-verging. The upper limb of the synform reveals a high-strain zone that may correlate with the Engebøfjell shear-zone.

Fig. 8 give a summary of observed structures and mineral parageneses of the Engebøfjell eclogite.

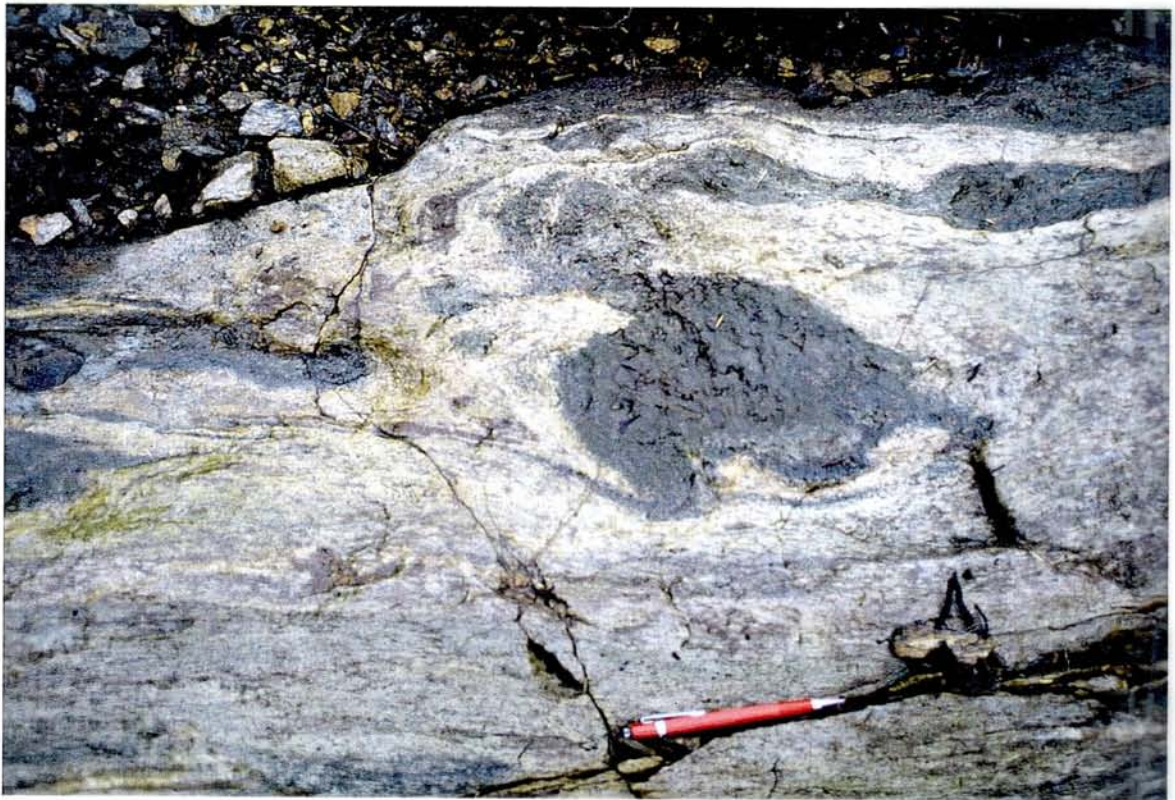


Fig. 7: Photograph of eclogite lenses that are folded and stretched within a sinistral shear system. The eclogite lenses floats in a quartz-mica matrix with a S_3 foliation, to which the shearing relates.

STRUCTURAL AND METAMORPHIC EVOLUTION OF THE ENGEBØFJELLET ECLOGITE


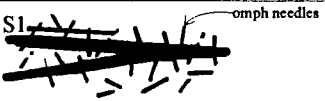

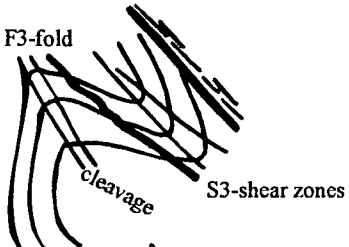
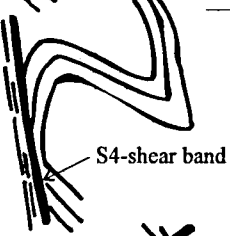
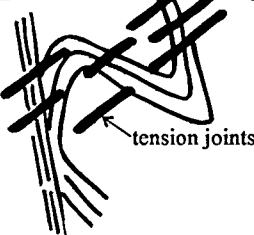
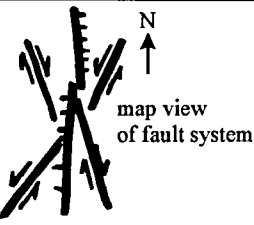
stage	observed structures	style of deformation	metamorphic facies - stable minerals
D1		horizontal shortening(?); isoclinal folding, penetrative foliation/banding	eclogite facies
post-D1		no deformation; static conditions	eclogite facies; static growth of prismatic omph
D2		coaxial horizontal N-S shortening (?); tight to isoclinal folds, penetrative foliation in high strain zones, cleavage in folds	eclogite facies; omph+gnt; +qtz+pheng +czo+amph
D3		non-coaxial sinistral transpression; tight folds, shear zones in fold-limbs, cleavage	amphibolite facies; amph+gnt+plag
D4		continued sinistral transpression (?); meter-wide shear zones	amphibolite facies; amph+bio(?) +epi+ qtz
D5		N-S compression; verticale tension fractures	amphibolite to greenschist facies; amph+epi +qtz(+carbo)
D6		N-S compression; brittle normal faults and conjugate strike-slip faults	brittle conditions, lower greenschist facies (?); epi+qtz(+carbo)

Fig. 8: Summary diagram of observed structures and mineral parageneses of the Engebøfjellet eclogite.

Thus, at least two old foliations can be distinguished in the regional map-pattern, in addition to the mylonitic foliation in the detachment zone. The oldest foliation, which could be Sveconorwegian in age (1000-1200 Ma), occurs in hinge-areas of regional folds. There, isoclinal sheet-like folds within the foliation indicate that significant strain affected the rock at this stage, and that primary, possibly older structures were transposed. A younger foliation is superposed on the older fabric in high-strain zones that are found in the fold-limbs. This foliation, which can be correlated with the S_3 and/or S_4 fabric of Engebøfjellet, reveals subhorizontal stretching lineations, whereas shear-sense indicators suggest sinistral shear. Eclogites and eclogite facies fabrics, probably Caledonian in age (Andersen and Jamtveit 1990), are retrograded into amphibolite-facies rocks in the D_3/D_4 high-strain zones. This faulting/shearing occurred at significant crustal depths. If this reasoning is valid, then sinistral transcurrent movements occurred on moderate to steeply dipping shear-zones at some stage of the Caledonian orogeny of Western Norway.

4. Summary and recommendations for future work

The Engebøfjellet eclogite deposit is situated at the northern side of Førdefjord near the small community Vevring in Naustdal kommune, Sogn og Fjordane county, W. Norway. Geologically the Førdefjord area belong to the «Western Gneiss Region», between the Devonian Kvamshesten basin to the south and the Devonian Håsteinen basin to the North. Recent mapping divide the Førdefjord region into two major geologic units: the Hegreneset complex and the Helle complex. The Hegreneset complex (oldest) contains a variety of amphibolitic, eclogitic and gabbroic rocks, together with tonalitic to dioritic gneisses. The Helle complex comprises mainly granitic and granodioritic gneisses.

The Engebøfjellet eclogite is a 2.5 km long, complexly deformed, lens-formed body surrounded by hybrid mafic-felsic country-rocks belonging to the Hegreneset complex. The protolith to the eclogite is believed to be a Fe and Ti-rich Proterozoic gabbroic intrusion. The transformation into eclogite is related to Caledonian high-pressure metamorphism at approx. 400 Ma. In this process, ilmenite in the gabbro protolith was replaced by rutile. The Ti-enriched part of the eclogite is now rutile ore.

The eclogite mineralogy is closely related to structural and metamorphic events. Two eclogite facies deformation events (D_1 and D_2), two amphibolite facies events (D_3 and D_4), one amphibolite to greenschist facies event (D_5) and one late brittle fault event (D_6) under lower greenschist conditions, are recognised. Rutile is affected by the D_3 , D_4 and D_5 events by the alteration to ilmenite and also to titanite (mainly D_5), while the effect of D_6 is insignificant.

Engebøfjellet is one of the most extensively drilled eclogites in the world, and approx. 15.000 meters of cores are available. These cores represent a unique material for

geological, petrological and mineralogical research on the eclogite itself as well as its relations to metamorphic and structural episodes and to the country-rocks. Continued research on the genesis of the Ti-ore will inevitably lead to new data that can be used in the ore-evaluation work. Extensive geologic knowledge of Engebøfjellet and its geologic surroundings might stimulate to the development of effective exploration methods to discover other Ti-rich eclogites in the Førdefjord area and elsewhere.

To establish a good geological model for the Engebøfjellet eclogite and its surroundings, a dynamic process needs to be developed which takes account to a complex set of interrelated parameters. For example, the mineralogy is strongly affected by structural and metamorphic episodes, and the variations in the metamorphic character within the eclogite are related to structural episodes which have channeled the flow of metamorphic fluids and allowed the reequilibration of mineral assemblages to happen. At the present state of knowledge, the mechanisms that have been active are known in principle, yet their details remain obscure.

A series of continued investigations are suggested to establish a «complete» geological model to be used in the continued ore investigations:

1. *3D lithologic model.* Based on the Engebøfjell geologic map and the core-log data (this subject has not been discussed in this report) a 3-dimensional geologic model should be made.
2. *The relations between mineralogy, structural geology and metamorphism* need to be further investigated, incl. the pressure - temperature evolution in relation to the eclogitisation and superimposed retrogressive events.
3. *The titanium distribution among minerals in the eclogite and the effects of retrogression.* The titanium distribution in the eclogite should be further investigated, i.e. the portion of titanium that occurs as rutile vs. titanium within ilmenite and silicates. Available analytical data show a distinct variation in the rutile/TiO₂ - ratio; this is to some extent related to alteration of the eclogite rock, as indicated by an increased magnetic susceptibility, but other factors might be important. The details of this need to be further investigated.
4. *Rutile mineral chemistry* (not discussed in this report). Rutile occurs in several eclogite varieties such as leuco-/transitional eclogite, ferro eclogite, re-crystallised, probably metasomatic eclogite varieties (omphacite - garnet - quartz - white mica rocks), and quartz- /quartz-omphacite veins. It is likely that the fluid composition varied during the formation of these rocks and that these difference are reflected in the rutile trace element mineral chemistry. Mineral chemical studies by a combination of electron microprobe and ICP-MS laser ablation analyses are suggested.
5. *Eclogite- country rock relations.* The ore-genetic evolution within the eclogite and the relations to the country rocks should be further investigated by additional geological mapping, major- and trace element geochemistry, and geochronological work

5. References (for main text and appendixes)

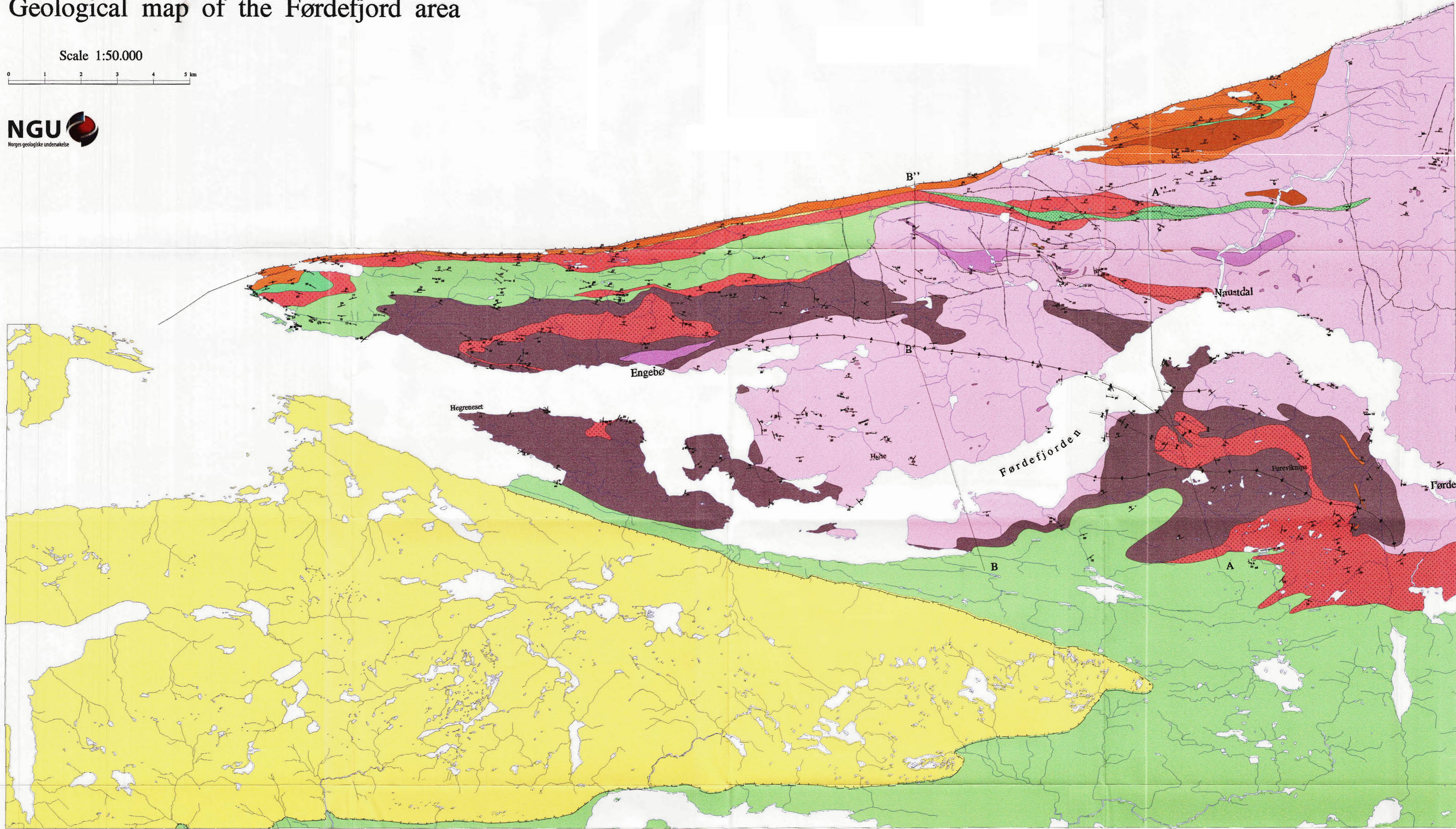
- Andersen, T.B. and Jamtveit, B. 1990. Uplift of deep crust during orogenic extensional collapse: A model based on field studies in the Sogn-Sunnfjord region of Western Norway. *Tectonics* 9, 1097-1111.
- Andersen, T.B., Osmundsen, P.T. and Jolivet, L. 1994. Deep crustal fabrics and model for the extensional collapse of the southwest Norwegian Caledonides. *J. struct. geol.* 16, 1191-1203.
- Bryhni, I. and Lutro, O. 1991. NAUSTDAL. Berggrunnsgeologisk kart 1218-3, foreløpig utgave, NGU.
- Bryhni, I. 1966. Reconnaissance studies of gneisses, Ultrabasites, eclogites and anorthosites in outer Nordfjord, Western Norway. NGU, 241, 1-68.
- Braathen, A. 1998: Polyphase brittle faulting in the Sunnfjord region, Western Norway: kinematic and timing. NGU report no. 98.007, 42 p.
- Carswell, D. A. 1990. Eclogite and eclogite facies: Definition and classification. In: *Eclogite Facies Rocks*, Blackie, Glasgow, 1-13.
- Cho, M. and Ernst, W.G., 1991: An experimental determination of calcic amphibole solid solution along the join tremolite-tschermakite. *American Mineral.*, 76, 985-1001.
- Cuthbert, S.J., 1985: Petrology and tectonic settings of relatively low-temperature eclogites and related rocks in the Dalsfjord area, Sunnfjord, West Norway. Unpubl. PhD thesis, Univ. of Sheffield.
- Dewey, J.F., Ryan, P.D. and Andersen, T.B. 1993: Orogenic uplift and collapse, crustal thickness, fabrics and metamorphic phase changes: The role of eclogites. In: *Magmatic Processes and Plate Tectonics* (edited by Prichard, H.M., Alabaster, T., Harris, N.B.W. and Neary, C.R.). *Spec. Publ. geol. Soc. Lond.* 76, 325-343.
- Dietler, T.N, Koestler, A.G and Milnes, A.G. 1985: A preliminary structural profile through the Western Gneiss Complex, Sognefjord, southwestern Norway. *Norsk Geol. Tidsskr.* 65, 233-235.
- Ellis, D.J. and Green, D.H., 1979: An experimental study of the effect of Ca upon garnet-clinopyroxene Fe-Mg exchange equilibria. *Contrib. Mineral. Petrol.*, 71, 13-22.
- Gilbert, M.C., Helz, R.T., Popp, R.K. and Spear, F.S., 1982: Experimental studies of amphibole stability. In: Veblen, D.R. and Ribbe, P.H. (Eds): *Amphiboles: Petrology and Experimental Phase Relations*. Min. Soc. America, Reviews in Mineralogy, Vol. 9B, pp 229-353.
- Gjelsvik, T., 1952: Metamorphosed dolerites in the gneiss area of Sunnmøre on the west coast of southern Norway. *Norsk Geologisk Tidsskrift*, 30, 33-134.
- Godard, G., 1981: Lambeaux probables d'une croûte océanique subductée: les éclogites de Vendée (Massif Armoricaïn - France) . PhD thesis, Univ. of Nantes.
- Graham, C.M., Maresch, W.V., Welch, M.D. and Pawley, A.R., 1989: Experimental studies on amphiboles: a review with thermodynamic perspectives. *Eur. J. Mineral.*, 1, 535-555.
- Green, D.H. and Ringwood, A.E., 1967: An experimental investigation of the gabbro to eclogite transformation and its petrological applications. *Geochim. Cosmochim. Acta*, 31, 767-833.
- Griffin, W.L., Austrheim, H., Brastad, K., Bryhni, I., Krill, A.G., Krogh, E.J., Mørk, M.B.E, Qvale, H. and Tørudbakken, B 1985: High-pressure metamorphism in the Scandinavian Caledonides. In *The Caledonide Orogen; Scandinavia and related areas*, vol. 2., 783-801. John Wiley and Sons. Chichester, United Kingdom.

- Griffin, W. L. 1987. 'On the eclogites of Norway' -65 years later. *Mineralog. Mag.* 51, 333-343.
- Hamner, S., and Passchier, C., 1991. Shear-sense indicators: a review. *Geol. Surv. Canada Paper* 90-17, 72 p.
- Helz, R.T., 1973: Phase relations of basalts in their melting range at $\text{PH}_2\text{O} = 5$ kbar as a function of oxygen fugacity. Part I : mafic phases. *J. Petrology*, 14, 249-302.
- Holland, T.B.J., 1980: The reaction albite \Leftrightarrow jadeite + quartz determined experimentally in the range 600-1200 °C. *American Mineral.*, 65, 129-134.
- Kildal, E.S. 1970: Geologisk kart over Norge, berggrunnskart Måløy, 1:250.000, norsk utgave. NGU.
- Korneliussen, A. 1980: Jern og titanforekomster tilknyttet gabbroide, amfibolittiske og eklogittiske bergarter i Sunnfjord. Unpubl. NGU-report no. 1717/3, 40p.
- Korneliussen, A. and Foslie., G. 1985: Rutile-bearing eclogites in the Sunnfjord region of Western Norway, *Nor. geol. Unders.* 402, 65-71.
- Korneliussen, A. and Furuhaug, L. 1991. Fureviknipa og Engebøfjellet rutilforekomster ved Førdefjorden, Sogn og Fjordane. *NGU-report no. 91.171*, 17 p.
- Korneliussen, A. 1994: Rutile-bearing eclogites in Western Norway. NGU report 94.013 to DuPont (confidential until 1 Jan. 1999), 152 p.
- Korneliussen, A. 1996: Core-drilling at Engebøfjellet 1995-96; Dh1 to Dh5. NGU report 96.062 to DuPont (confidential until 1 May 2001), 155 p.
- Korneliussen, A. and Erambert, M. 1997: Core-drilling at the Engebøfjell rutile-bearing eclogite 1995/96; Dh1 to Dh10. NGU report 97.014 to DuPont (confidential until 31 Desember 2001), 141 p.
- Korneliussen, A. Og Furuhaug, L. 1991: Fureviknipa og Engebøfjellet rutilforekomster ved Førdefjorden, Sogn og Fjordane. NGU-report 91.159, 28p.
- Krogh, E. And Carswell, D.A. 1995: HP and UHP eclogites and garnet peridotites in the Scandinavian Caledonides. In Coleman, R.G. and Wang, X. 1995: Ultrahigh pressure metamorphism, 244 - 298.3
- Krogh, E.J., 1980: Geochemistry and petrology of glaucophane-bearing eclogites and associated rocks from Sunnfjord, Western Norway. *Lithos*, 13, 355-380.
- Krogh, E.J., 1988: The garnet-clinopyroxene Fe-Mg geothermometer - a reinterpretation of existing experimental data. *Contrib. Mineral. Petrol.*, 99, 44-48.
- Kullerud, K., Tørudbakken, B.O. and Ilebekk, S. 1986: A compilation of radiometric age determinations from the Western Gneiss region, South Norway. *Nor. geol. Unders.* 406, 17-42.
- Leake, B., 1978: Nomenclature of amphiboles. *Mineral. Mag.*, 42, 533-563.
- Maniar, P. D. and Piccoli, P. M. 1989. Tectonic discrimination of granitoids. *Geol. Soc. Am. Bull.* 101, 635-643.
- Mauring, E. 1996: Interpretation of a gravity profile across the Engebøfjellet rutile-bearing eclogite deposit. NGU report no. 96.061, 14 p.
- Mauring, E. and Gellein, J. 1996: Interpretation of a gravity profile across the Engebøfjell rutile-bearing eclogite deposit. NGU report no. 96.061.
- Mauring, E. and Gellein, J. 1997: Interpretation of gravity profiles at the Engebøfjell rutile-bearing eclogite deposit. NGU report no. 97.173, 29 p.
- Mauring, E., Gellein, J. and Korneliussen, A. 1997: Interpretation of two gravity profiles across the Engebøfjell rutile-bearing eclogite deposit. NGU report no. 97.002, 21 p.
- Milnes, A.G, Wennberg, O.P., Skår, Ø. and Koestler, A.G. 1997: Contraction, extension and timing in the South Norwegian Caledonides; the Sognefjord transect. In Burg, J.P. and Ford, M. (eds): *Orogeny through time*. *Geol. Society of London Spec. Publ.* 121, 123-148.
- Mørk, M.B.E, 1985: A gabbro to eclogite transition on Flemsøy, Sunnmøre, Western Norway. *Chem. Geol.*, 50, 283-310.

- Pearce, J. A., Harris, N. B. W. and Tindle, A.G. 1984. Trace element discrimination diagram for tectonic interpretation of granitic rocks. *Journ. of Petrol.* 25 956-983.
- Pognante, U. and Kienast, J.R., 1987: Blueschist and eclogite transformations in Fe-Ti gabbros: a case from the Western Alps ophiolites. *J. Petrology*, 28, 271-292.
- Powell, R., 1985: Regression diagnostics and robust regression in geothermometer/geobarometer calibration: the garnet-clinopyroxene geothermometer revisited. *J. metamorphic Geol.*, 3, 231-243.
- Rubie, D.C., 1990: Mechanisms of reaction-enhanced deformability in minerals and rocks. In: Barber, D.J. and Meredith, P.G. (Eds) *Deformation processes in minerals, ceramics and rocks*. Unwin Hyman, pp 262-295.
- Rutter, E.H. and Brodie, K.H., 1995: Mechanistic interactions between deformation and metamorphism. *Geological Journal*, 30, 227-240.
- Smith, D. C. 1988. A review of the peculiar mineralogy of the Norwegian coesite-eclogite province, with crystal-chemical, petrological, geochemical and geodynamical notes and an extensive bibliography. In: *Smith, D.C. (ed): Eclogite and Eclogite-facies Rocks. Development in Petrology 12. Elsevier Science, Amsterdam. 1-206.*
- Torsvik, T.H., Sturt, B.A., Ramsay, D.M. and Vetti, V. 1987. The tectono-magnetic signature of the Old Red Sandstone and Pre-Devonian strata in the Håsteinen area, western Norway, and implications for the later stages of the Caledonian Orogeny. *Tectonics*, 6, 305-322.
- Waters, D.J. and Martin, H.N. 1993: Geobarometry in phengite-bearing eclogites. Seventh meeting of the European Union of Geosciences; abstract supplement. *Terra Abstracts*. 5, suppl. 1, 410-411.
- Yardley, B.W.D. 1989: *An introduction to metamorphic petrology*. Longman. 248 s.

Geological map of the Førdefjord area

Scale 1:50.000



Legend

The Kvamshesten devonian basin and its basement

Sandstone, conglomerate, metasedimentary, metavolcanic and intrusive rocks, undifferentiated

The Lykkjebø Group

Ultramafic rock
Mica schist
Quartzite

The Eikefjord Group

Ultramafic rock
Meta-gabbro
Meta-anorthosite
Mylonitic gneiss, in places with layers of meta-anorthosite and amphibolite

Basement

Mica schist
Quartzite
Blastomylonitic gneiss
Meta-gabbro, amphibolite
Granitic orthogneiss
Augengneiss
Granitic to granodioritic gneiss
Ultramafic rock
Anorthosite
Eclogite
Eclogite, amphibolite, metagabbro and grey gneiss (quartz-dioritic?) undifferentiated

Strongly deformed and retrogressed Caledonian rocks

Helle Complex

Hegreneset Complex

Geological symbols

Lithological contact
Normal fault
Minor fault, joint
Foliation, schistosity, banding; the dip value is shown, 25° towards SE, vertical, horizontal
Fold axis with the plunge value shown, 25° towards E, horizontal
Lineation with the plunge value shown, 25° towards E, horizontal
Synform, axial-plane trace
Antiform, axial-plane trace
A—A' Line of section

The map is based on the bedrock maps Eikefjord 1118 II (Bryhni & Lutro 1991) and Naustdal 1218 III (Bryhni & Lutro 1991) with additional mapping in 1996 by J. Ragnhildstveit og O. Lutro. The map is compiled at the Geological Survey of Norway in 1996 by Ole Lutro

Reference to the map: Lutro, O. og Ragnhildstveit, R. - 1996
Geological map of the Førdefjord area, bedrock map, scale 1:50.000
Geological Survey of Norway

GEOLOGY OF THE ENGEBØFJELL ECLOGITE DEPOSIT, SOGN OG FJORDANE

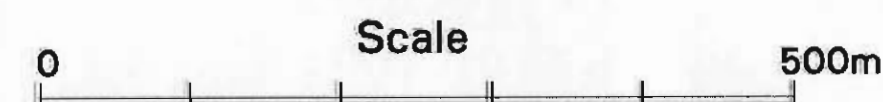
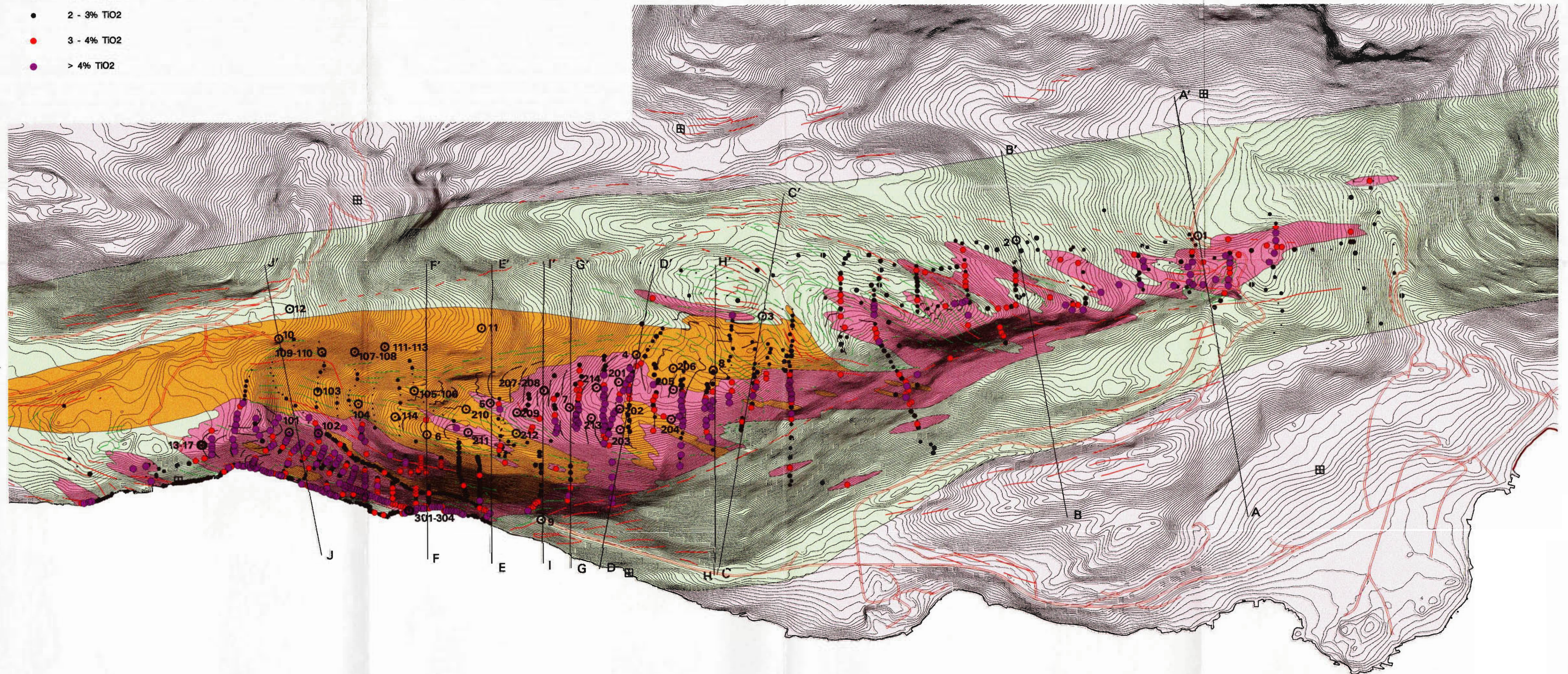
LEGEND

- | | |
|---|---|
| <ul style="list-style-type: none"> 1 Ferro eclogite (ore type) 2 Leuco - and transitional eclogite 3 Amphibolite unit (undiff. amphibolite, eclogite and gray gneiss) 4 Granitoid gneisses, undiff. | <ul style="list-style-type: none"> — D1 fabric — D2 fabric — D3 and D4 fabric Vertical profile (See NGU-report 97.014) ⊙ Drillhole position with number ⊞ End of gravimetric profile — Roads |
|---|---|

Samples (TiO₂)

- < 1% TiO₂
- 1 - 2% TiO₂
- 2 - 3% TiO₂
- 3 - 4% TiO₂
- > 4% TiO₂

Map compiled by Are Korneliussen and Torbjørn Sørdal. Mapping by Are Korneliussen, Muriel Erambert and Alvar Braathen (structures). Sampling by Leif Furuhaug, Jomar Staw, Eric Ahrenberg, Matt Halls, Roger McLimans, Odd Sagegg, David Falkenstern, Are Korneliussen, Ole Grammelvedt and Håvard Jendem.



Equidistance = 2.5 meter

Appendix 3

Geology of the Førdefjord region

By Jomar Ragnhildstveit

Contents

1. Geologic background
2. Main geologic units
 - 2.1 The Hegreneset complex
 - 2.2 The Helle complex, and deformed rocks of uncertain relationships
3. Caledonian structures in the Førdefjord area
4. General remarks on the occurrence of eclogite

1. Geological background

The Førdefjord area is already covered by map sheet Måløy, scale 1:250.000 (Kildal 1970), whereas the northern part is covered by the 1:50.000 scale map sheets Eikefjord 1118-1 and Naustdal 1218-3, scale 1:50.000 (Bryhni and Lutro 1991). Nearby areas have been regionally mapped and described by Bryhni (1966, and references therein). The structural geology of the area has been studied by Dewey et al. (1994) and Dewey et al. (1993). Several eclogite bodies in the Sunnfjord region have been mapped by Korneliussen and co-workers during earlier stages of the project. There also exist a number of detailed mineralogical-petrological studies of eclogites elsewhere in the Western Gneiss Region (see review paper by Griffin 1987, Carswell 1990 and Smith 1988).

The Førdefjord area belongs to the 'Western Gneiss Region', structurally situated in the footwall below the Kvamshesten and Standalen late-Caledonian (Devonian) detachment faults (part of Nordfjord - Sogn detachment), between the Devonian Kvamshesten basin to the south and the Håsteinen basin to the north (Fig. A3.1). The detachments are truncated by several semibrittle to brittle faults, e.g. the Dalsfjord fault

(Torsvik et al. 1987), which partly form the boundary to the basins (Andersen and Jamtveit 1990). The Førdefjord area, together with adjacent areas to the south and north, are folded into regional east-west trending folds, supposed to be a result of late-Palaeozoic N-S compression with the detachment mylonites more folded than the brittle faults along the basins (Torsvik et al. 1987). One of these regional east-west trending folds is the Førdefjord antiform (Fig. A3.2). Rocks on the flanks of the Førdefjord antiform have been divided into three zones of different deformation styles (se Fig. A3.2) as they approach the Devonian detachment faults. The deformation styles represent the transition from lower crustal eclogite facies condition to middle and upper crustal amphibolite and greenschist facies conditions.

As part of the project «Rutile provinces in Norway», the bedrock geology west of Førde, on both sides of the Førdefjord, has been mapped by O. Lutro and J. Ragnhildstveit, during 14 days in June 1996. Based on the field data, a revised, regional, digital, geologic map of the Førdefjord area has been compiled (Appendix 1). A brief description of the rocks follows. Locality descriptions of rocks and structures are stored digitally in an excel database.

2. Main geologic units

At least two, mainly intrusive, units seem to be present in the area. They are informally called the *Hegreneset complex* (box 16-19 in Appendix 1), including the Engebøfjell eclogite, and the *Helle complex* (box 13-15). The Hegreneset complex consists of K-poor rocks while the Helle complex mainly consists of more K-rich rocks. In addition, strongly sheared and variably retrogressed rocks (box 9-12, Appendix 1) with uncertain relationships occur near the late-Caledonian detachments. Rocks belonging to the Helle complex are found to intrude rocks of the Hegreneset complex, but might also contain older rocks. A relatively sharp contact exist between the two complexes west of Vatnevatnet (UTM coord. 312500E 6819400N), indicating a sheared intrusive contact there.

The subdivision into three different structural and metamorphic zones (Andersen and Jamtveit 1990, as seen on Fig. A3.2), is considered inconvenient for practical mapping purposes due to mingling of the different deformation types. Eclogites within the strongly deformed rocks have been reported by Andersen et al. (1994), in the deformation zones 2 and 3 of Fig. A3.2, represented for instance by the Vårdalsneset eclogite south of the area (Dalsfjord). In the mapped area the rocks near the late-Caledonian detachments seem to be of little economic interest with respect to rutile due to the retrogression. However, a garnet mica schist within the strongly sheared rocks is found to contain about 1.5 modal % rutile.

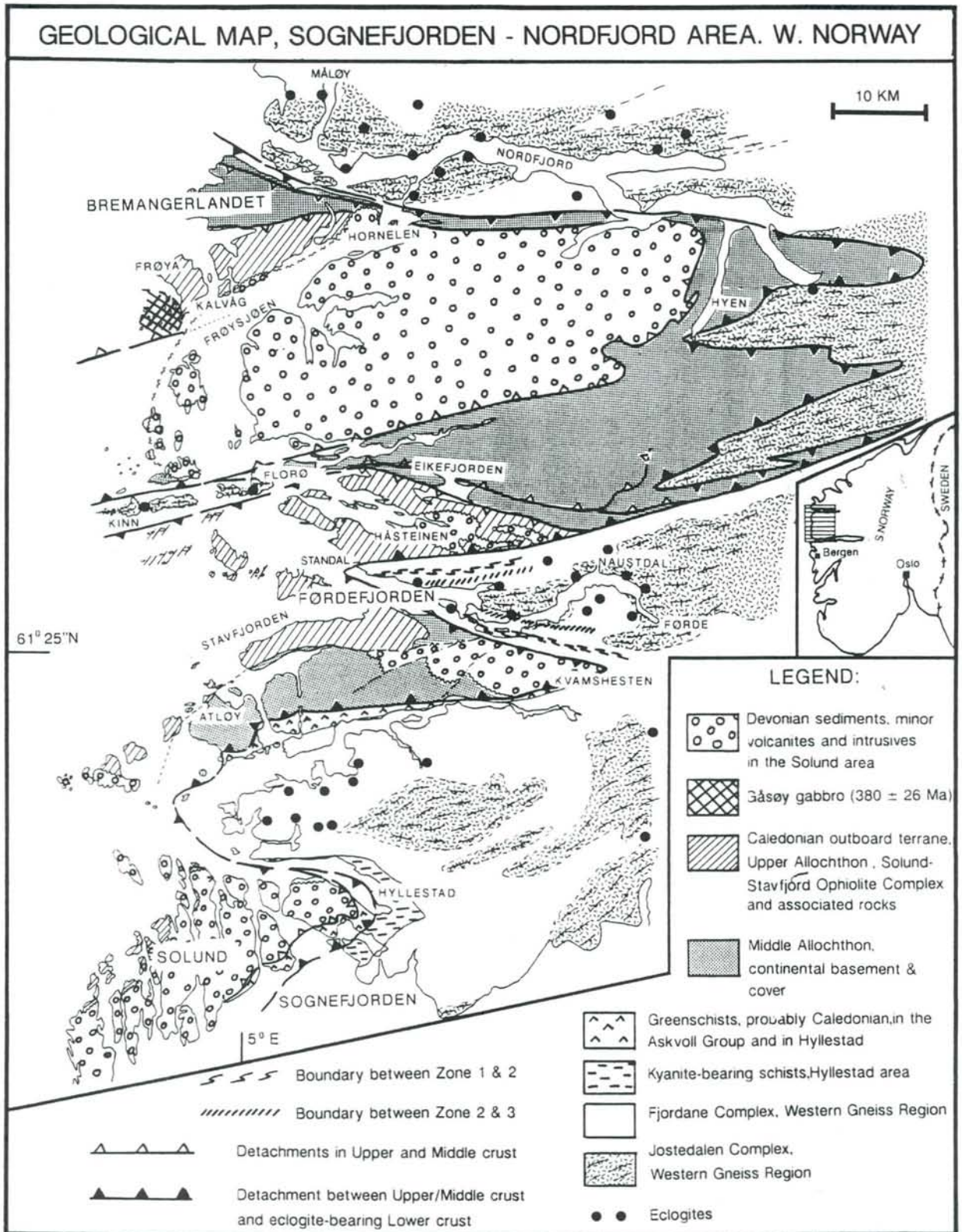


Fig. A3.1: Simplified geologic map of Western Norway between Sognefjord and Nordfjord (Andersen & Jamtveit 1990, Fig. A1).

2.1. The Hegreneset complex

The Hegreneset complex (box 16-19, Appendix 1) consists of two main units; basic to ultramafic, mainly eclogitized rocks, and cross-cutting, homogeneous grey to grey-green tonalitic to dioritic and granodioritic intrusives. The two main units are in many places intimately mixed with one another; several places with a broad intrusive contact zone where the grey intrusives contain abundant basic xenoliths (Fig. A3.4). There may be a gradation from the most basic to the most felsic members in the complex, and the rocks are probably genetically related in some way. However, the grey intrusives cross-cut layered basic rocks (loc. JRA9625), and probably also folded and banded basic rocks (Fig. A3.5). The complex may therefore have had a more complex development. In order to differentiate between the two main units within the complex, i.e. the intermediate and the basic members, much more fieldwork has to be carried out. They are therefore mapped as a single unit (box 19, Appendix 1).

The Hegreneset complex crops out continuously from Hegreneset in the west to near Førde in the east, on the southern side of the Førdefjord. The Hegreneset complex seem to be situated in a major late-Caledonian east-west elongated dome structure. North of the Førdefjord, the Hegreneset complex crop out in the Engebø area, and more discontinuous, as some large and many small rafts surrounded by rocks of the Helle complex further eastward from the Engebø area. Towards the detachment south of Førdefjord, rocks belonging to the Hegreneset complex have been severely sheared and retrogressed to phyllonitic gneiss (box 11, Appendix 1). The deformation within the area is, however, strong in most places, with the development of mylonitic to phyllonitic rocks. The eclogites generally seem to be best preserved in the central part of the dome structure, away from the detachment zones.

Basic to ultrabasic rocks including eclogites. The oldest rocks in the area are found to be basic rocks, mostly eclogitized. These rocks are often distinctly retrograded but with relict eclogite mineralogy present. Occasionally the basic rocks occur as garnet amphibolites, amphibolites or even greenschists-phyllonites. The basic rocks range from fine-grained, partly banded or laminated, to coarse grained, but a substantial part of the rocks are fine-grained. The basic rocks are probably mostly of intrusive origin. At least two different types of layered basic rocks occur. At Mt. Fureviknipa (Fig. A3.6), banded eclogite crop out, representing eclogitized, layered gabbro. Further west (loc. JRA96137 and JRA96139), anorthosite and leucogabbro constitute part of the same basic complex. The anorthosite contains lenses of retrograded eclogites. The large basic complex south of the Førdefjord, including Mt. Fureviknipa, therefore consists mostly of plutonic, partly layered and cumulate rocks. Southwest of Mt. Fureviknipa, a fine-grained, banded to laminated, basic rock of uncertain origin occurs. The rock shows extensive mesoscopic, ductile, disharmonic folding under eclogite facies conditions (Fig. A3.7), a rock type that is somewhat similar to the rock at loc. JRA9659 and to the Engebøfjellet eclogite. The origin of some of the basic rocks have already been discussed to some extent during earlier stages of the project, and basaltic pillow-lava structures have been reported by different geologists. Pillow-like structures have been observed, but they are considered to be of secondary eclogite facies origin related to shearing and boudin formation. These boudins are in many places associated with

light coloured quartz-phengite rich horizons along their surrounding lenticular shear zones.

Tonalitic to dioritic and granodioritic rocks. The grey gneisses show mostly tonalitic modal composition, but vary from tonalitic (and granodioritic) to dioritic composition. They usually are more homogeneous than their basic inclusions in areas of intimate mixing between the two types. The grey gneisses are mostly completely recrystallized and contain either biotite, muscovite or both, but not amphibole. Plagioclase grains are mainly unaltered albite(-oligoclase, $An < 20$). However relict saussuritized grains may occur, and also rocks with strongly saussuritized plagioclase have been observed (JRA9698). Chemical analyses of nine grey gneiss samples outside the mapped area (Korneliussen) plot mostly as quartz- diorite to tonalite and granite. They have subalkaline, calc-alkaline compositions and straddle the boundary line between the metaluminous and peraluminous field (according to Maniar and Picolli 1989, Fig. A3). They mostly plot as volcanic arc granites (according to Pearce et al. 1984, Nb/Y and Rb/Nb + Y diagrams).

2.2. The Helle complex, and deformed rocks of more uncertain relationships

The Helle complex (box 13-15, Appendix 1) comprises mainly granitic to granodioritic gneisses, in many places more or less migmatitic and/or banded. The granitic gneisses are red to grey in colour. A number of younger red granites altered to gneiss, and minor basic veins are also included in the complex. Due to the complex and mostly strong deformation in the area, especially near the late-Caledonian detachment zones, rocks with the most varied structures and textures occur. In many cases therefore, rocks within the Helle complex are difficult to distinguish from grey gneisses belonging to the Hegreneset complex, and from rocks of more uncertain relationships. A description of the many variations in rock types is beyond the scope of this work. For instance, even a single protolith may have widely varying appearance from place to place due to different types and intensity of structural overprinting.

Away from the late-Caledonian detachments, relatively homogeneous rocks with variable deformation occur. There are also areas or zones dominated by highly ductile deformation, consisting of fine-grained gneisses of heterogeneous to more homogeneous composition. There are also zones of more typical mylonitic gneisses and augen gneisses with stretching lineation and asymmetric folding.

Closer to the late-Caledonian detachment zone, retrograde shear zones containing mylonites and phyllonites predominate.

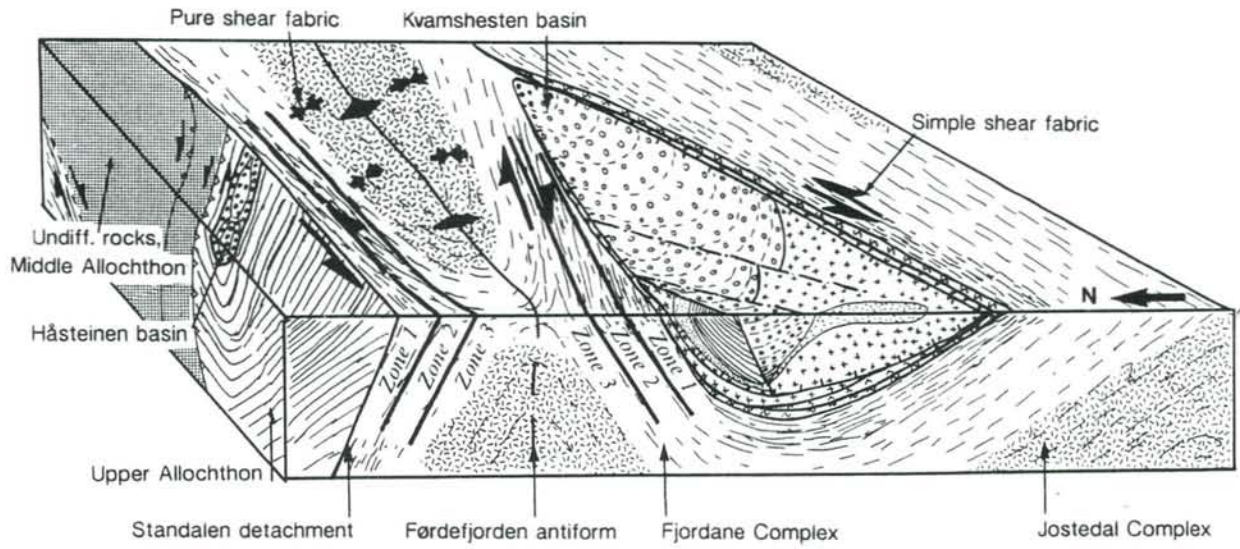


Fig. A3.2: Block diagram with N-S and E-W sections of the central Sunnfjord area showing the Førdefjorden antiform (Andersen & Jamtveit 1990, Fig. A6).



Fig. A3.3: Photo JRA96113 (see explanation in the text).



Fig. A3.4: Photo JRA9675(1) (see explanation in the text).



Fig. A3.5: Photo JRA96129 (3) (see explanation in the text).



Fig. A3.6: Photo JRA96135 towards east. (See explanation in the text).

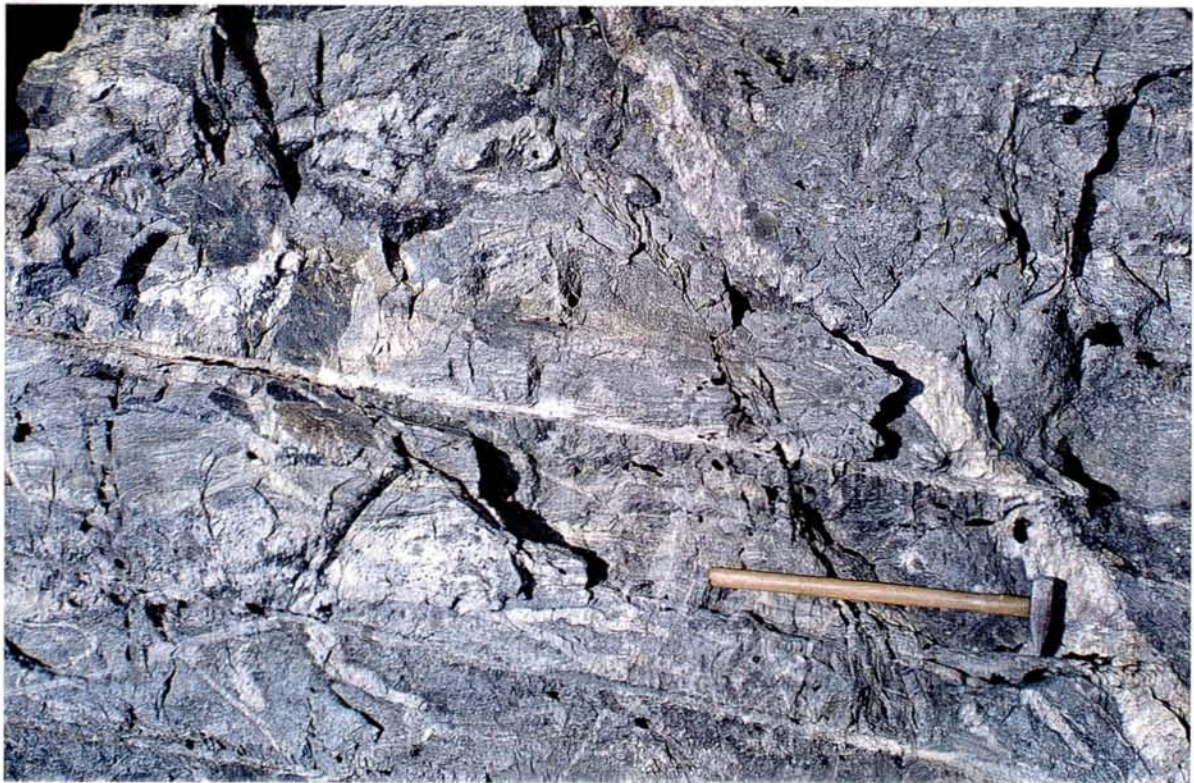


Fig. A3.8: Photo JRA96100 towards west. (See the explanation in the text).



Fig. A3.7: Photo JRA96129 (2) (see explanation in the text).

Description of rocks within the Helle complex, and deformed rocks of more uncertain relationships:

- ◇ *Grey gneisses in the Helle complex.* The grey gneisses range from granitic to tonalitic and dioritic in composition. They are mostly medium- to fine-grained (epidote)-muscovite-biotite gneisses, often metamorphically differentiated, or otherwise altered. The modal composition can be somewhat difficult to estimate in the field. In most cases it is difficult to decide whether some of the grey gneisses represent younger granitoids of the Helle complex, or if they are part of the Hegreneset complex.
- ◇ *Migmatitic gneisses in the Helle complex.* Originally, part of the intrusives in the Helle complex were more or less migmatitic (Fig. A3.8). The rocks have been transformed into banded or foliated gneisses. They mostly consist of granitic to granodioritic compositions and crop out in relatively large areas. Most of the gneisses in the area north of Naustdal are migmatitic. The migmatitisation is mostly pre-kinematic, but migmatitisation is also observed to be post-kinematic (Caledonian?, Fig. A3.9).
- ◇ *Banded gneisses in the Helle complex.* The banded gneisses are mostly fine- to medium grained, partly light coloured and glassy. They consist mostly of red to grey granitic to granodioritic bands and grey gneiss bands of different compositions, and at places also minor amphibolite bands/lenses (Fig. A3.10). There are also more homogeneous banded gneisses (Fig. A3.11, and 2.12), and banded mylonitic gneisses (Fig. A3.13). The banded gneisses have previously, at least partly, been assumed to be of supracrustal origin (see map sheet Måløy). However, the banded appearance in the mapped area seems to be mostly a result of deformation of style B or C (see above). In most cases, the banded gneisses are therefore likely to represent deformed intrusives. Especially, hybrid rocks along intrusive contacts have been altered to banded gneisses (Fig. A3.3). The banded gneisses alternate with more homogeneous, partly migmatitic intrusives.
- ◇ *Augen gneisses in the Helle complex.* Narrow zones of augen gneisses are shown on earlier maps of the region and in nearby areas. In the mapped area, augen gneisses represent different lithologies which have attained eye-structures due to regional deformation or more localized shears along different shear zones. They represent both different protoliths and different deformation styles. The augen gneisses are of two types. The one type represents originally relatively coarse grained or porphyric intrusives which have changed to flaser and augen texture depending on the intensity of the deformation. The other type is related to more localized shear zones, represented by mylonites and porphyroblastic gneisses of widely varying eye-structure and composition. Such augen gneisses of variable composition and appearance are a characteristic feature in the northern part of the area, but are elsewhere relatively rare.
- ◇ *Younger diabases in the Helle complex.* In addition to eclogites and amphibolites in the Hegreneset complex, younger diabases are observed in the Helle complex (Fig. A3.14). The diabases are characterised by homogeneous composition and sharp contacts, in contrast to the more irregular basic rocks within the Hegreneset complex. These younger diabases are partly eclogitized. Their ages are unknown relative to the younger granitic gneisses, and they constitute only a very small, economically unimportant part of the rocks.
- ◇ *Younger granitic gneisses in the Helle complex.* Many small to larger red granites (box 13, Appendix 1) and granitic veins, altered to granitic gneisses, are scattered in the area. They are probably mostly of Sveconorwegian age, and have crosscut the gneissic foliation in the surrounding host rocks several places (e.g. Fig. A3.9). They have also been observed to crosscut banded and folded gneisses. Other places they are strongly deformed and form part of the banded gneisses.
- ◇ *Rocks close to the late-Caledonian - Devonian detachment zones.* Near the late-Caledonian detachment faults both to the north, south and west, all rock types are affected by retrogression and strong deformation. The rocks consist of mylonitic and phyllonitic gneisses derived from both the Hegreneset and the Helle complex, and also comprise

rocks of more uncertain origin. Major shear zones, and maybe even some thrusts, exist in these areas, especially in the northern part. The basic rocks are retrograded to low grade amphibolites.

- ◇ *Mylonites, phyllonites and mica gneiss.* In the Solheim area (JRA96102-108) in the north-eastern part of the map area, grey gneisses alternate with garnet free amphibolites (rock no. 4 on Appendix 1). The assemblage probably represent a retrograded equivalent of the Hegreneset complex. In the southern part of the area, the rocks of the Hegreneset complex are strongly altered, mostly to phyllonites, in a relatively broad zone (rock no. 3 on Appendix 1). Small amounts of anorthosites (JRA114) are observed within the zone.
- ◇ *Quartz-rich rock (quartzite ?).* A quartzite-like rock (JRA9649, impure quartzite?) crops out in contact with eclogite in the transition zone to the more sheared rocks in the north. The quartzite-like rock is only a few meter thick. It may represent a meta-sandstone or, more likely, it may have formed as a hydrothermal vein along a shear zone, or as vein fillings.
- ◇ *Garnet mica schist.* A zone of fine- to medium-grained tourmaline-bearing, chlorite-amphibole-garnet-biotite-muscovite mica schist (JRA9652, box 9, Appendix 1), containing abundant quartz lenses, has been mapped in the northern part of the area. The rock may represent a Palaeozoic meta-sediment. The surrounding gneisses to the north and south of the mica schist are strongly sheared in a relatively broad zone. A thin-section of the mica schist is found to contain about 1.5% rutile and no titanite. No eclogite has been found in that area. Further eastward along the strike, this zone widens, and south of Skeisknausen it consists of phyllonitic, dioritic? gneiss, at places carrying quartz lenses. Strongly sheared and retrograded rocks occur locally in the zone at that area. In the strike-continuation along the valley-side further east, only gneisses have been observed. The rock is shown as a mica schist on map sheet Måløy (Kildal 1970). In the eastern part (JRA9689) however, the rock seems to represent a phyllonite, derived from a dioritic? rock. Similar phyllonitic rocks are also described by Andersen and Jamtveit (1990) and regarded to be deformed diorites.



Fig. A3.9: Photo JRA96101 towards west. (See the explanation in the text).



Fig. A3.10: Photo JRA9699 towards WNW. (See explanation in the text).



Fig. A3.11: Photo JRA9664(1) towards east. (See explanation in the text).



Fig. A3.12: Photo JRA9664(2) towards east. (See explanation in the text).

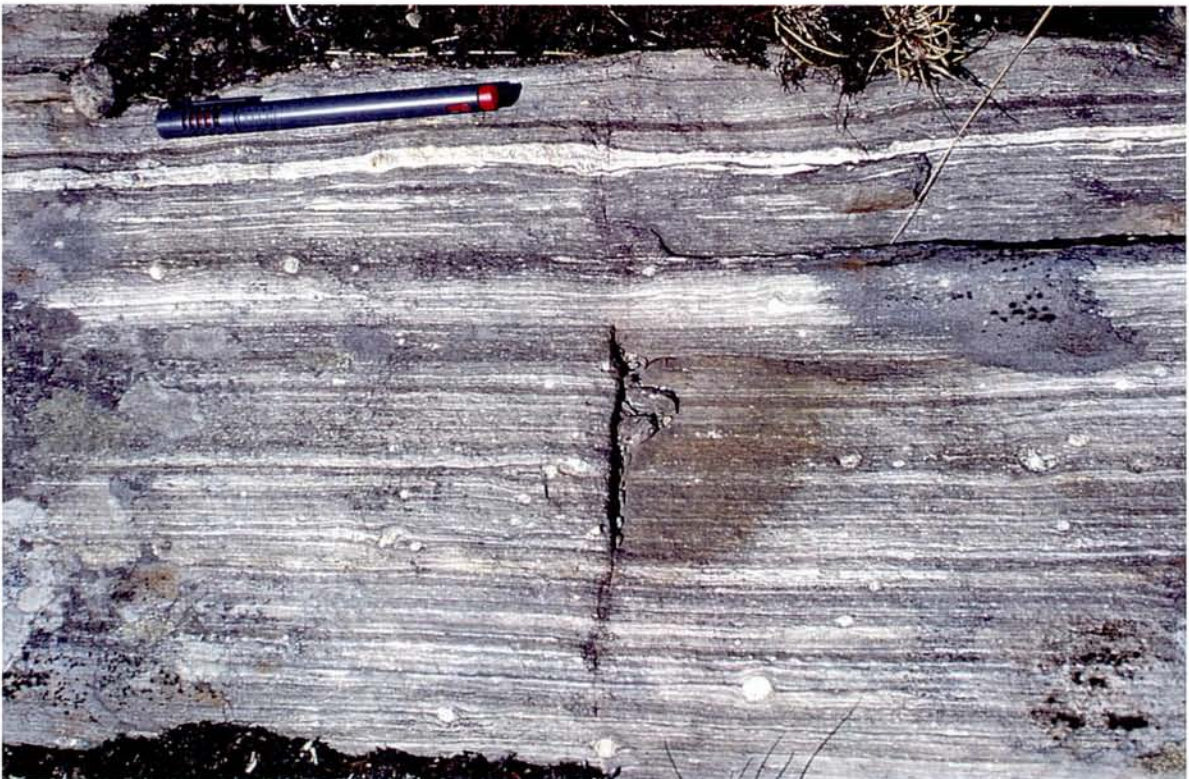


Fig. A3.13: Photo JRA9671. Horizontal surface. Left is towards west. (See explanation in the text).



Fig. A3.14: Photo JRA9678 towards east. (See explanation in the text).



Fig. A3.15: Photo JRA9672 towards east. (See explanation in the text).



Fig. A3.16: Photo JRA9665 towards 110° east. (See explanation in the text).

3. Caledonian structures in the Førdefjord area

The complicated structural evolution related to the Caledonian orogeny include early eclogite facies (coaxial?) structures, and late non-coaxial structures formed under amphibolite to greenschist facies conditions during the postorogenic "collapse" (cf. Andersen and Jamtveit, 1990; Andersen et al., 1994).

Early Caledonian structures are best preserved away from the detachments. In such areas, high-ductile deformation-zones developed under eclogite facies conditions. These zones contain high amplitude, isoclinal, intrafolial, modified folds (Fig. A3.11 and 2.12), and eyefolds/sheath folds are frequent. The ductile deformation zones typically branch or change to broader and less prominent zones along their strike.

The late-Caledonian simple shear and asymmetric folding (e.g. Fig. A3.16) probably started under eclogite facies condition. Thereafter the deformation gradually changed character to low grade conditions which are especially prominent near the detachments. Near the detachments, stretching lineations trend approximately east-west and plunge sub-horizontal to moderately east or west. The foliation dips towards north near the northern detachment, mostly associated with sinistral shearing. Near the southern detachment, the foliation dips towards south, (sense of shear not determined). The poles

to the foliations define a great circle which dips 70° towards east (Fig. A3.18). On a macro scale, the foliations therefore seem to define an antiform plunging 20° towards west. This plunge and overall geometry seem to verify the existence of the Førdefjord antiform (Fig. A3.17). Several subordinate fold hinge lines to the antiform are indicated on the map (Appendix 1). The orientations of late-Caledonian fold axes show more variation than the stretching lineations. The plunge-directions of the fold axes are NE to SE (Fig. A3.18). Away from the detachment, the folds verge mostly towards west, varying from NW to SW. The folds probably formed, and was modified, during the top-to-the-west movement. In the area around Mt. Fureviknipa, S of the Førdefjord, the folding is more variable. For instance there is a moderate to steeply east-plunging macro fold closing to the east. This reflects probably an eastward change in the general Caledonian influence on the basement and hence eclogite formation.

4. General remarks on the occurrence of eclogites

It is suggested that the relatively early Caledonian deformation was important for eclogite formation. It seems that the eclogitization has not been complete throughout the area for this and probably other reasons. The impression is that the mafic rocks in the eastern parts, for instance the Fureviknipa and Naustdal area, are generally rather less eclogitized and/or more retrograded than eclogites in the more western parts, for instance at Engebø. The late-Caledonian shear zones near the detachments are unfavourable for eclogite preservation. Therefore, no well preserved eclogites have been found near the detachments (Appendix 1). As a result the economic interesting eclogites seem to be situated in central part the area. Based on this study, the most promising area for further prospecting, in addition to the Engebø area, may be the area to the south of Førdefjord, close to the Engebø eclogite.

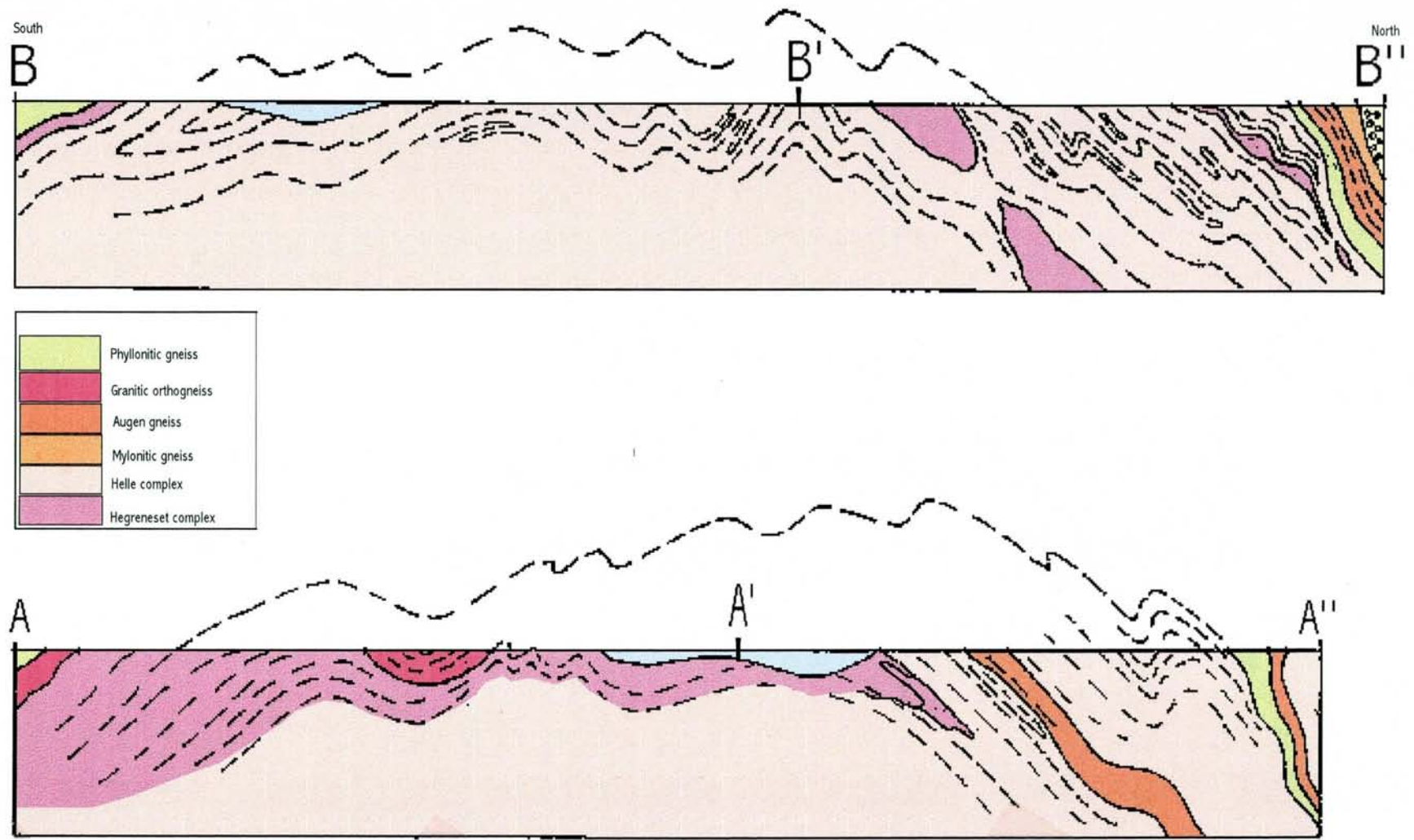


Fig. A3.17: North-South cross sections of the late-Caledonian fold style across Førdefjord. The locations of the cross sections are shown on Appendix 1.

J. Raagild et al. 97

Structures in the F rdefjord area

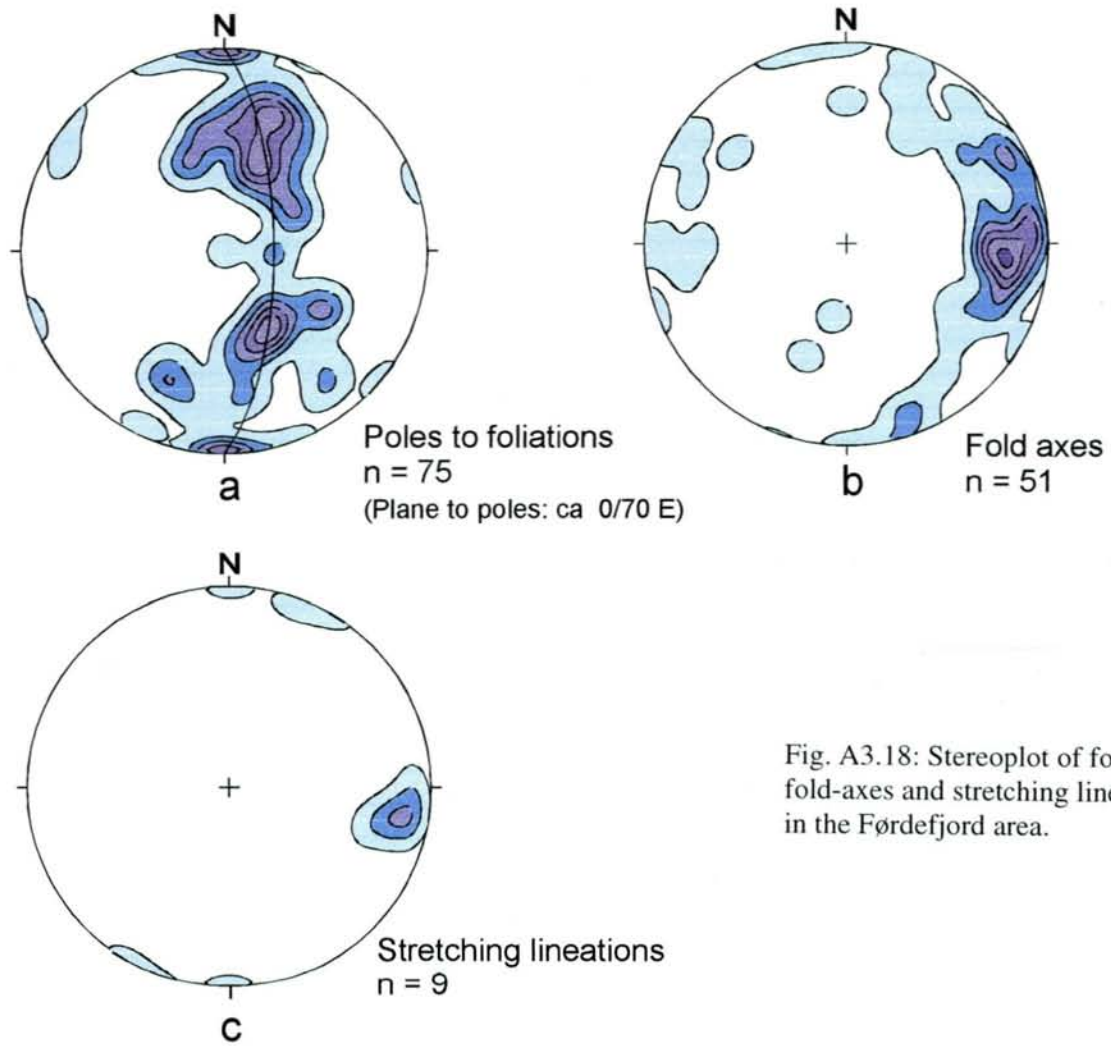


Fig. A3.18: Stereoplot of foliations, fold-axes and stretching lineations in the F rdefjord area.

Appendix 4

Structural geology, Engebøfjellet

By Alvar Braathen

Contents

	page
4.1. Map-scale structures	3
4.2. Sequence and style of deformation	5
4.3. Orientation of meso-scale structures	11
4.4. Micro-scale structures and fabrics	17

Figures

- Fig.A4.1: Structural fabric map of the Engebøfjell eclogite.
- Fig.A4.2: Structural cross-sections of the Engebøfjell eclogite
- Fig.A4.3: Possible primary feature in the ferro eclogite.
- Fig.A4.4: Tight to isoclinal F_2 fold of the S_1 foliation in a sheared version of the ferro eclogite
- Fig.A4.5: Isoclinal F_2 -fold of the S_1 foliation in sheared ferro eclogite
- Fig.A4.6: Tight F_3 -antiform of S_2 foliation (?) in ferro eclogite.
- Fig.A4.7: Strongly sheared, isoclinally folded lenses of partly retrograded eclogite in amphibole-gneiss with a dominant amphibolitic S_3 foliation.
- Fig.A4.8: Partly retrograded eclogite lenses in quartz-mica matrix
- Fig.A4.9: D_1 structural data of the Engebøfjellet eclogite.
- Fig.A4.10: D_2 structural data of the Engebøfjellet eclogite.
- Fig.A4.11: D_3 structural data of the Engebøfjellet eclogite.
- Fig.A4.12: Stereoplots of D_4 , D_5 and D_6 structural data.
- Fig.A4.13: Microphotograph of thin section
- Fig.A4.14: Microphotograph of thin section.
- Fig.A4.15: Microphotograph of thin section.

Structural geology, Engebøfjellet

In this description of structural observations, the following topics are addressed, in a macroscale to microscale order:

- macro- and mesoscale map patterns and cross-section geometries,
- overprinting structural relationships and the sequence and style of deformation,
- orientations of mesoscale folds and fabrics, and
- foliations and stable mineral parageneses based on field and thin section studies.

4.1. Map-scale structures

The Engebøfjellet Eclogite forms an elongated lens or body with an E-W long axis; its length exceeds 2.5 km and its width is approximately 0.5 km at the most. In map-view the body is asymmetric with a sigmoidal shape (Fig.A4.1).

The eclogite lens consists of several distinct rock types (see above). Two rocks form massive, well preserved bodies: The more mafic part of the first order eclogite lens is the ferro eclogite that forms a wide body in the central part (see Fig.A4.1), and several smaller bodies along the southern margin of the main lens. At most places, the ferro eclogite has a distinct massive character. Detailed observations show that it has been deformed under eclogite facies conditions. This is supported by thin section studies, showing strong orientation of garnet, clinopyroxene, rutile and reduction in grain size. Some parts show a compositional mineral banding that may represent the primary layering/banding in the protolith. The other massive rock type is the leucogabbroic eclogite which in general occur north of the ferro eclogite (Fig.A4.1.). In the leucogabbroic eclogite some parts show a poorly developed banding or foliation. There are also indications for relict primary textures.

Both massive rock types described above have a more deformed counterpart, i.e. a tectonized rock, that is well foliated. Along the margin of the ferro eclogite, a zone of foliated/banded ferro eclogite, some meters wide, defines a transition to more strained parts of the leucogabbroic eclogite. The latter well foliated and banded rock is present across a wide area around the ferro eclogite (see Appendix 2). This unit is separated in the cross-sections as «sheared eclogite» (Fig.A4.2). Other rocks in the cross-sections, all characterized by a well developed foliation, are; (i) the quartz-phengite gneiss within the first order lens, (ii) the marginal rock to the first order body, present as eclogite lenses, often partly retrograded, in sheared quartz-mica rich matrix, and (iii) external rocks such as amphibolite, dioritic-tonalitic gneiss and granitic augen gneiss.

Four N-S cross-sections (Fig.A4.2; see Fig.A4.1 for location) describe the vertical geometry of the first order eclogite lens. In order to construct the distribution of rocks in the subsurface, both drill-hole data, where present, and down-plunge projection of observed structures, are incorporated into the sections. Since most folds and cut-off lines have steep plunges, and clearly change plunge along strike, the later method is regarded as uncertain.

Thus, deeper portions of the cross-sections are interpretative in nature, although consistent with gravimetric data from the area (Mauring 1996 and Mauring et al. 1997). In order to follow the margin of the first order eclogite lens, which shows lateral changes in rock composition, this boundary is outlined between the various cross-sections (Fig.A4.2).

Cross-section A-A' (Fig.A4.2), located near the eastern end of the eclogite lens, shows the predominant sub-vertical orientation of lithological contacts in this area. The northern margin consists of amphibolite that is separated by an inferred shear zone from the leucogabbroic eclogite, and further south, the ferro eclogite. There, a prominent fold-pair of the eclogite banding/foliation, and probably the contact of the two eclogite types, are present. The fold-pair consists of a synform to the north and an antiform further south, both folds with an elliptical shape. They have an open to tight interlimb angle and the axial surfaces are steeply inclined to the north, thus, they verge slightly to the south. Shear-zones in the fold-limbs modify the fold geometry and fracture the ferro-eclogite into two or more mega-lenses. One shear-zone, striking WNW-ESE, cuts the fold-pair and the other amphibolitic shear-zones, thus, it probably formed late in the deformation history (see below). To the south an amphibolitic shear zone separates the ferro-eclogite from a wide zone of foliated, partly retrograded eclogite as lenses in quartz-mica rich matrix. There the foliation dips sub-vertical to steeply north. The later dip is consistent with the orientation of the foliation in dioritic gneiss further south.

Cross-section B-B'' (Fig.A4.2) is located to the central part of the first order eclogite lens. To the north in this section the lithological contacts are defined by steep shear zones, bounding large rock-bodies of augen gneiss, amphibolite and sheared eclogite. Further south similar shear zones, all dipping steeply to the north, split the cross-section into several blocks. The northern block on the profile consists of foliated/sheared eclogite, commonly partly retrograded, that contains more massive megalenses of both ferro eclogite and leucogabbroic eclogite. These lenses contain the hinge zone of meso-folds surrounded by well foliated, sheared out limbs. A distinct zone of quartz-phengite gneiss, 5-10-m wide, forms a band that is isoclinally folded parallel to the foliation. A central block constitutes the main body of the first-order eclogite lens, both when it comes to volume of massive eclogite and also high concentration of rutile. This block is composed of a 3-400-m wide body of ferroeclogite that is folded and sheared together with leucogabbroic eclogite along the northern margin. An approximately 100-m wide transition zone forms a boundary towards massive leucogabbroic eclogite to the north. Further south, two blocks consisting of eclogite lenses in quartz-mica matrix, and dioritic-tonalitic gneiss, respectively, terminate cross-section B-B''. In both units, the foliation dips steeply to the north.

Cross-section C-C'' (Fig.A4.2), which is located ca. 500-m west of cross-section B-B'' (see Fig.A4.1), is constructed through to the widest part of the main eclogite lens. In its northern part, shear-contacts between augen gneiss and amphibolite, and the internal foliation of these rocks, dip steeply north and south. The following block to the south, composed of sheared eclogite with massive eclogite lenses and infolded quartz-phengite gneiss, reveals the same geometric patterns as the northern block in cross-section B-B''. The next block to the south, the ferroeclogite, as displayed in cross-section C-C'', constitutes a wide body that is bound to the north and south by leucogabbroic eclogite. The transition zone between the two

rocks shows intense, tight to isoclinal, elliptical folding and a well developed foliation in fold-limbs; fold-hinges develop a spaced cleavage. South of the central block, in the cliff-side, an area of sheared and partly retrograded large eclogitic lenses dominates the cross-section. These rocks are followed by a unit of eclogite lenses in quartz-phengite matrix near the base of the cliff. There, the foliation dips steeply to the north.

Cross-section D-D'' (Fig.A4.2) is located near the western end of the first order eclogite lens, where the lens is approximately 700-m wide. There, amphibolite and augen gneiss bound the lens to the north whereas dioritic-tonalitic gneiss forms the southern margin. Foliation in both gneissic units dip steeply to the north. The central part of the cross-section reveals a distinct fold-pair of the foliation in the ferro eclogite, and the contact towards the leucogabbroic eclogite (Fig.A4.2, cross-section D-D''). This fold-structure is tight to isoclinal, with an elliptical fold shape, and the axial surface is steeply inclined to the north (NNE). A crenulation cleavage is well developed in the fold-knee. The fold-pair is truncated by an amphibolitic shear-zone to the north, as illustrated by the map-pattern (see Appendix 2). This truncation is evident to the east. Further south, near the margin of the eclogite body, a transitional zone of steeply north dipping sheared eclogite, commonly partly retrograded, forms the boundary towards dioritic gneiss.

4.2. Sequence and style of deformation

Overprinting structural relationships are found throughout the area in macro- and meso-scale. For example the internal foliation of the first order eclogite lens is truncated or sheared out and retrograded along the margin of the lens, thus the internal structure of the lens predate the surrounding foliation.

In meso-scale, a detailed structural history can be established with basis in refolding of folds and cross-cutting foliations. In the following, the key observations for this subdivision are described; however, similar overprinting relationships are present at many locations throughout the area.

Some observations suggest that some primary features (magmatic layering and dikes) still exist in the massive eclogites, f.ex., the variations in the mineral concentration/composition (Fig.A4.3), as described in chapter 3.1. This layering is almost everywhere transposed into a foliation (S_1) of the first deformation stage, D_1 , except in the hinge-zone of isoclinal F_1 -folds (Fig.A4.4). There, older relationships may be preserved.

Along the margin of the massive eclogite bodies, as well as in the central-east part of the first order lens, the S_1 foliation/banding is overprinted by a new eclogite fabric, the S_2 foliation of the D_2 stage. This S_2 foliation is developed as an axial-surface parallel zonal crenulation or spaced cleavage in open to tight, elliptical F_2 folds near the massive eclogite bodies. With increasing distance to the massive rocks, the shearing is more intense and F_2 folds are isoclinal, and often shear out to lenses or boudins, whereas the S_1 foliation in the fold-limbs is entirely transposed into a penetrative S_2 foliation (Fig.A4.5). In the latter case, a stretching lineation of elongated quartz and omphacite is formed.

In the area around the quarry (Fig.A4.1) the eclogite foliation ($S_2?$) is folded into an open to tight F_3 fold-pair (see Fig.A4.2, cross-section A-A'). There, the plunge of mesoscopic fold axes varies, from moderately east-plunging to sub-vertical orientations. At some places near the fold-hinges a spaced fracture cleavage, sub-parallel to the axial surface, is developed (Fig.A4.6).

This cleavage is at places characterized by growth of amphibole. Meter wide amphibolitic shear zones (S_3 foliation) partly truncate and modify the fold-limbs. Thus, the D_3 -stage overprint the earlier deformations and retrograde the eclogite into (garnet -) amphibolite. In macroscale, this retrograde S_3 foliation forms the margin to the first order eclogite lens, i.e. it constitutes the main foliation in the surrounding rocks. All these marginal rocks to the eclogites show a well developed stretching lineation defined by quartz, mica and amphibole. Based on the orientation of the internal fabric in the first order eclogite lens, the S_3 foliation clearly truncates and transposes the eclogite fabrics (Figs. 3.7 and 3.8).

Near the quarry, both the above mentioned F_3 -folds and associated shear zones are truncated in the interlimb area (see enclosed map and Fig.A4.2, cross-section A-A') by a meter-wide shear zone (S_4) that retrograde the eclogites. A stretching lineation of elongated quartz and amphibole is seen in the zone. This relationship documents that even later deformation (D_4) affected parts of the first order lens.

Late tensile fractures (S_5) cross-cut all fabrics (S_1 to S_4) of the first order lens (Figs. 3.4 and 3.5). The fractures are normally 0.1 to 1 cm wide with quartz, epidote, or locally carbonate and chlorite, filling. Along the margin of the joints, the omphacite retrograded to amphibole over a distance of ca. 1 cm.

The final deformation, D_6 , of the area is shown as the formation of brittle joints and faults that truncate all earlier structures. Mesoscopic faults can be documented on the basis of displacement of marker beds or bands, whereas net-slip is suggested from slip-lines on the fault surfaces. This suggests that two types of faults are present in the area; two sets of strike-slip faults and one set of normal faults. Some of the surfaces of the fractures are coated by fibrose epidote and/or quartz. Joints are locally filled with brown carbonate.

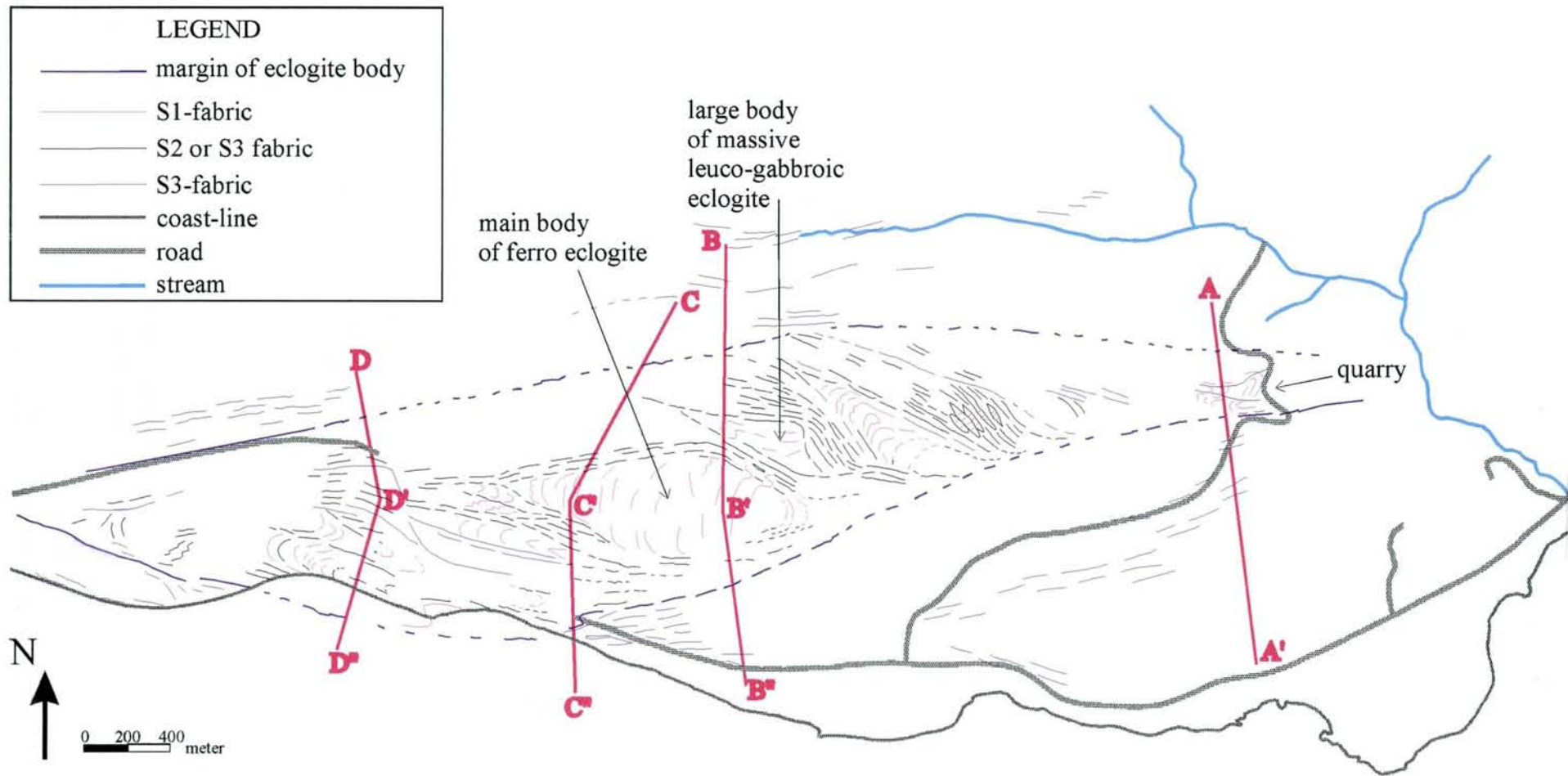


Fig.A4.1: Structural fabric map of the Engebøfjell eclogite. Different colours represent the various fabrics present within and near the eclogite body. The line segments are consistent with strike to the fabrics, which in most cases dips steeply north or south.

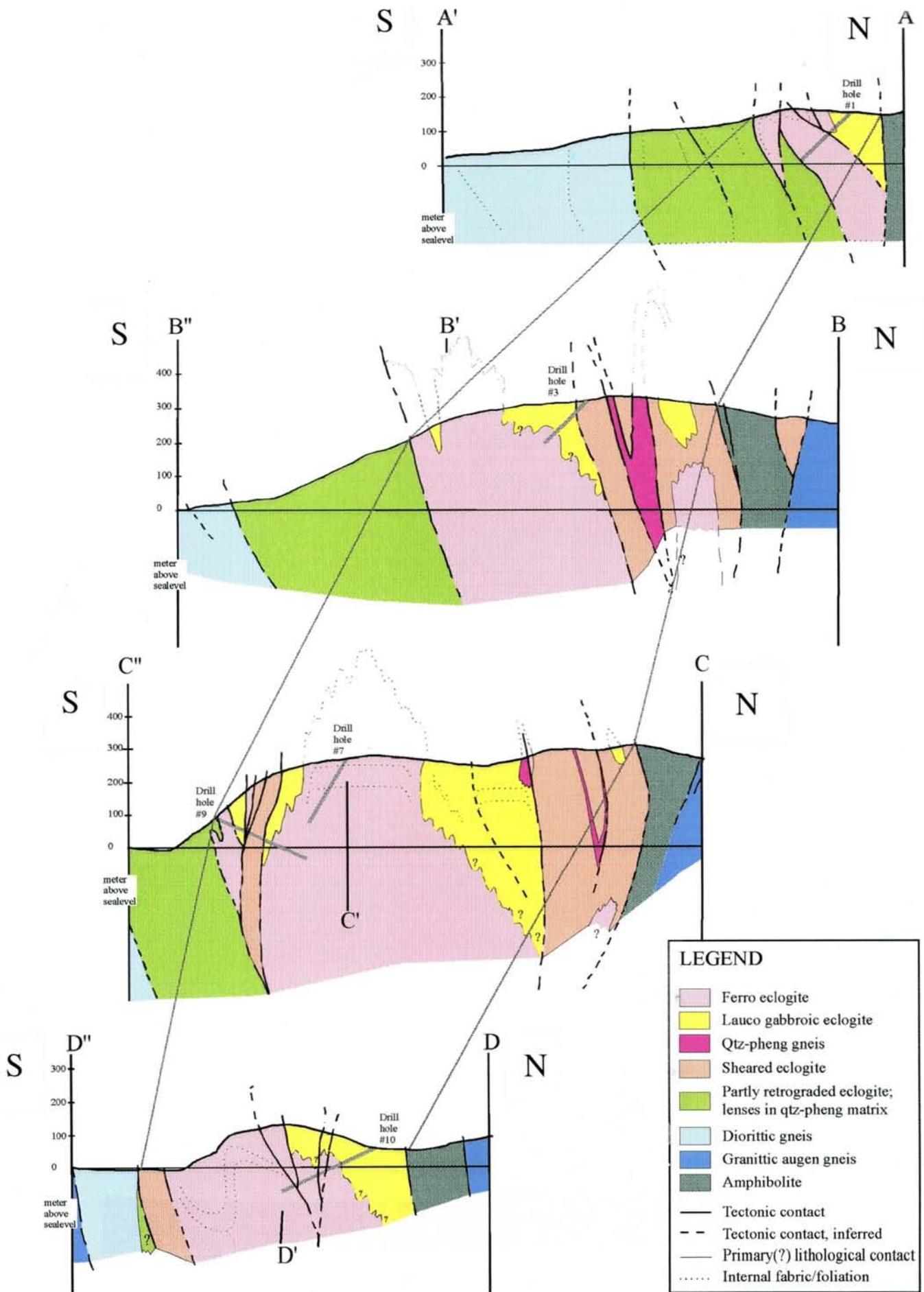


Fig.A4.2: Structural cross-sections of the Engebøfjell eclogite. See text for descriptions and Fig.A4.1. for locations. Vertical vs. horizontal scale is 1:1.



Fig.A4.3. Possible primary feature in the ferro eclogite (dike?). Note the variation in grain size and composition. The black host rock consists of very fine grained garnet and omphacite, whereas the central, green dike(?) reveals both fine grained - and coarse, prismatic omphacite.



Fig.A4.4. Tight to isoclinal F_2 fold of the S_1 foliation in a sheared version of the ferro eclogite. The garnet-rich band in the core of the fold may form an isoclinal F_1 fold with a px-rich core that is folded in the F_2 . Both folds are cross-cut by fractures (S_5) with amphibole along the margins.

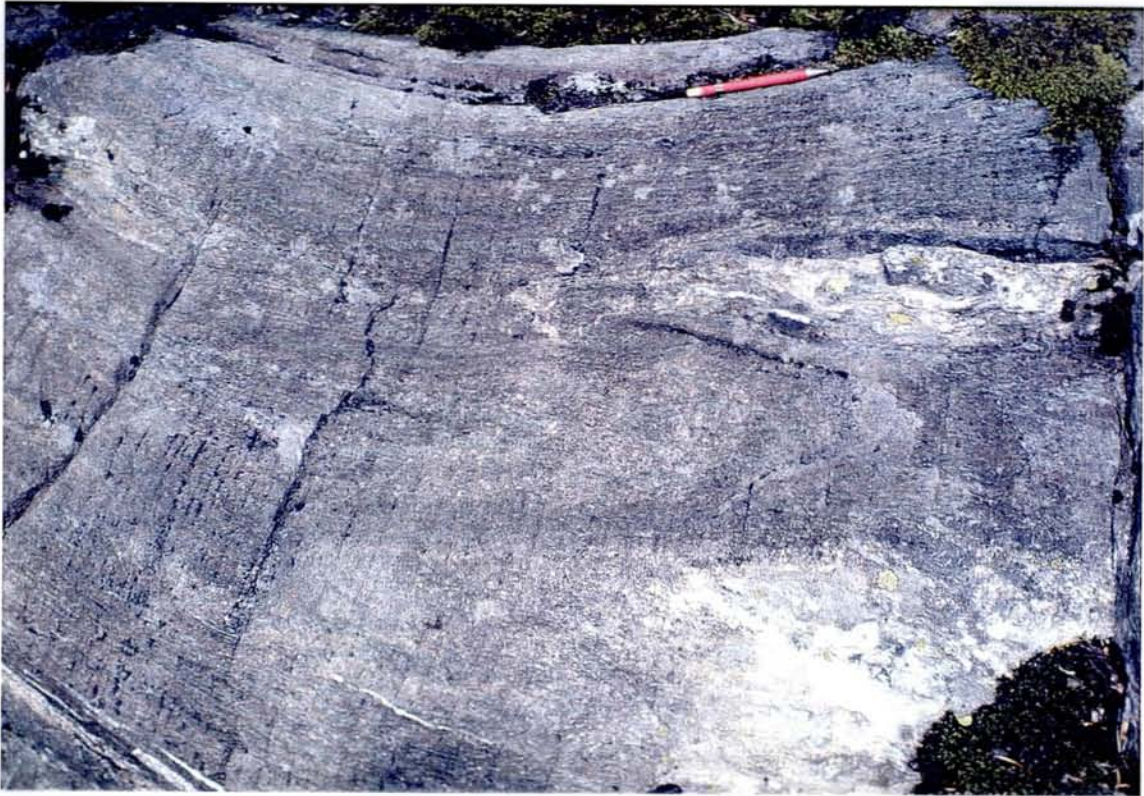


Fig.A4.5. Isoclinal F_2 -fold of the S_1 foliation in sheared ferro eclogite. The S_1 foliation is transposed into a S_2 foliation parallel to the fold-limbs. Note the fractures (S_5) that cross-cut both the fold and the foliations

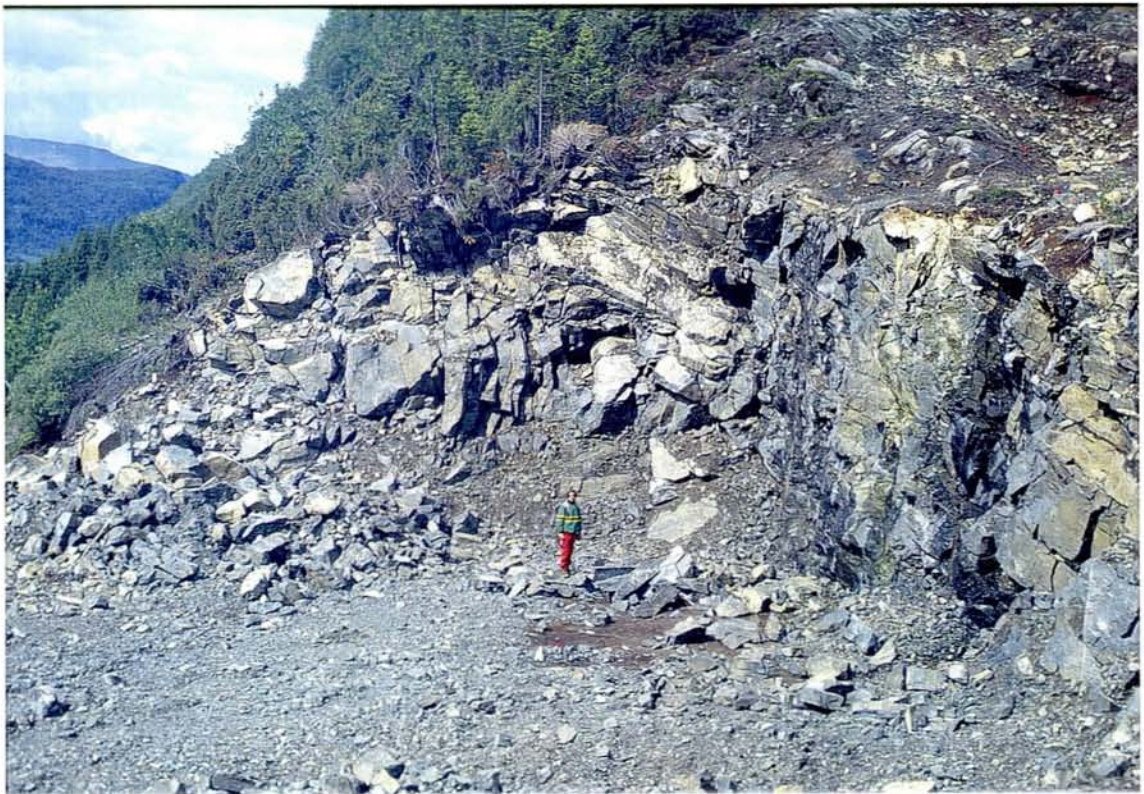


Fig.A4.6. Tight F_3 -antiform of S_2 foliation(?) in ferro eclogite. The fold-hing is located behind the person on the photograph. Both fold-limbs show retrograde, amphibolitic shear-zones where the S_2 (?) foliation is partly reactivated or truncated at a low angle. The photograph is oriented to the west in the quarry



Fig.A4.7. Strongly sheared, isoclinally folded lenses of partly retrograded eclogite in amphibole-gneiss (retrograded eclogite) with a dominant amphibolitic S_3 foliation. The photograph is from one exposure along the dirt road south of the quarry, i.e. outside the first order eclogite lens.

4.3. Orientation of mesoscale structures

Measurements of strike and dip of foliations and fractures (surfaces), and plunge and trend of folds and lineations (lines), were collected during fieldwork. This material is presented in equal area, lower hemisphere stereonet (Figs. 3.9 to 3.11). Most surfaces are plotted as poles to the plane, whereas lines are plotted in their true orientation. Fractures are also presented as a mirrored rose diagram, then with basis in the strike to the fractures.

Plot of F_1 -folds suggests that the primary layering/banding of the rocks were folded around a subhorizontal ENE-WSW axis (Fig.A4.9), corresponding to the long axis of the lens. The S_1 foliation, parallel to the limb and axial surface of these folds, is separated into three areas that differs in orientation (Fig.A4.9). Near the western end of the first order lens, the S_1 fabric and lithological contacts are folded into an anti-synform pair. This folding of the S_1 foliation is well displayed in the stereoplot, where poles to the foliation spreads along a great circle. This circle defines a fold axis ($p\beta$ -axis) that plunges moderately to the ENE, which is in accordance with orientations of parasitic folds. In the central part of the first order lens the S_1 fabric varies from one block to another. In the ferro-eclogite, the foliation strikes N-S and dips steeply west or east, when present. In the next block to the northeast, the S_1 foliation in the leucogabbroic eclogite strikes approximately E-W and dips moderately to the

south. Further ENE the entire block is folded and the strike varies from E-W to N-S, whereas the dip changes from steeply south to steeply west or east. In total, the S_1 fabric of the central area defines a rough fold-axis that plunges steeply north. In the third area, to the east, folding of the S_1 foliation results in steeply dipping S_1 orientations that varies from E-W to N-S strike. Again, a vaguely defined fold axis plunges steeply to the north.

The D_2 structural data reveal F_2 -folds that plunge steeply NW and SE (Fig.A4.10). These fold-axes plot along a vague great circle that strike ESE-WNW and dips steeply north. The same orientation is evident for the strike and dip of the S_2 foliation and the distribution of the stretching lineation. This S_2 fabric dips NNE and SSW in both the western and central part of the first order eclogite lens, whereas the L_2 stretching lineation has a dominant moderate to subhorizontal plunge to the WNW, subordinate ESE to SE.

D_3 structures show a consistent orientation throughout the area (Fig.A4.11). The S_3 foliation strikes E-W and dips steeply north, subordinate to the south. The L_3 stretching lineation plunges moderate to subhorizontal to the east and west, as is also the case for the F_3 -folds.

The D_4 shear zone of the eastern area strikes ESE-WNW and dips steeply north (Fig.A4.12). Oriented amphibole, biotite and quartz of the stretching lineation within the zone plunge subhorizontal to the ESE. This shear zone and all other foliations are cut by tensile fractures or joints. These fractures have a consistent N-S, subvertical orientation throughout the first order eclogite lens, however, similar fractures strike NW-SE in other eclogite lenses further south, outside the study area. Thus, these fractures may be folded on a regional scale (see discussion).



Fig.A4.8. Partly retrograded eclogite lenses in quartz-mica matrix. The S_3 foliation is revealed as distinct banding marginal to the dark lens. The significant mechanical contrast between the competent eclogite and the soft quartz-mica rock controls the formation of concentric and similar folds, respectively, and the generation of pinch-and-swell and boudinage structures. However, some of this deformation may relate to earlier eclogite facies episodes. The photograph is from the eastern opening of the road tunnel.

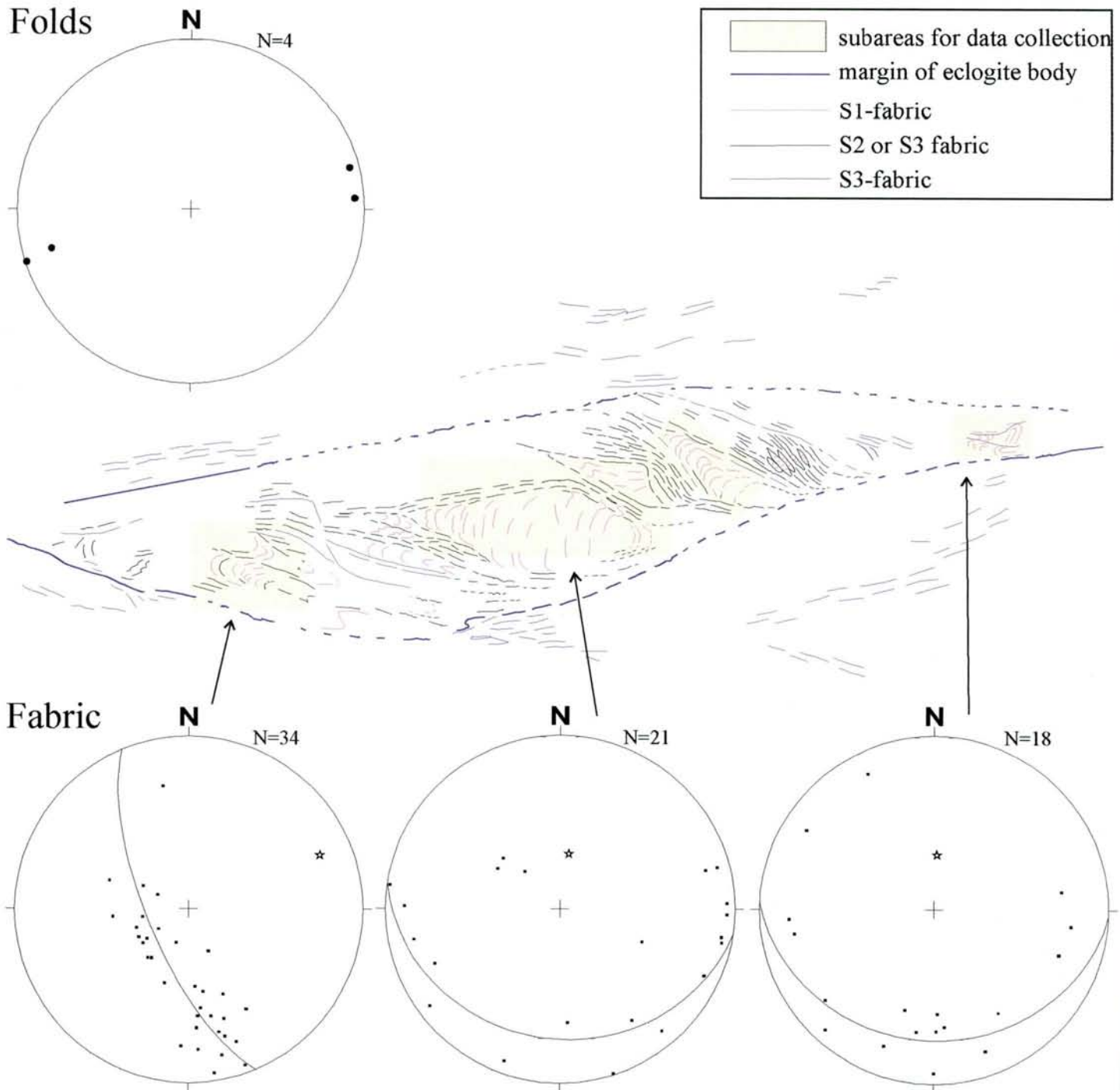


Fig.A4.9: D₁ structural data of the Engebøfjellet eclogite. Star indicates the best-fit fold-axis, based on poles to fabric, for each plot (equal area, lower hemisphere stereonets). The three lower plots present S₁-foliation/banding from three distinct subareas. The upper plot presents measured fold axes for the entire area.

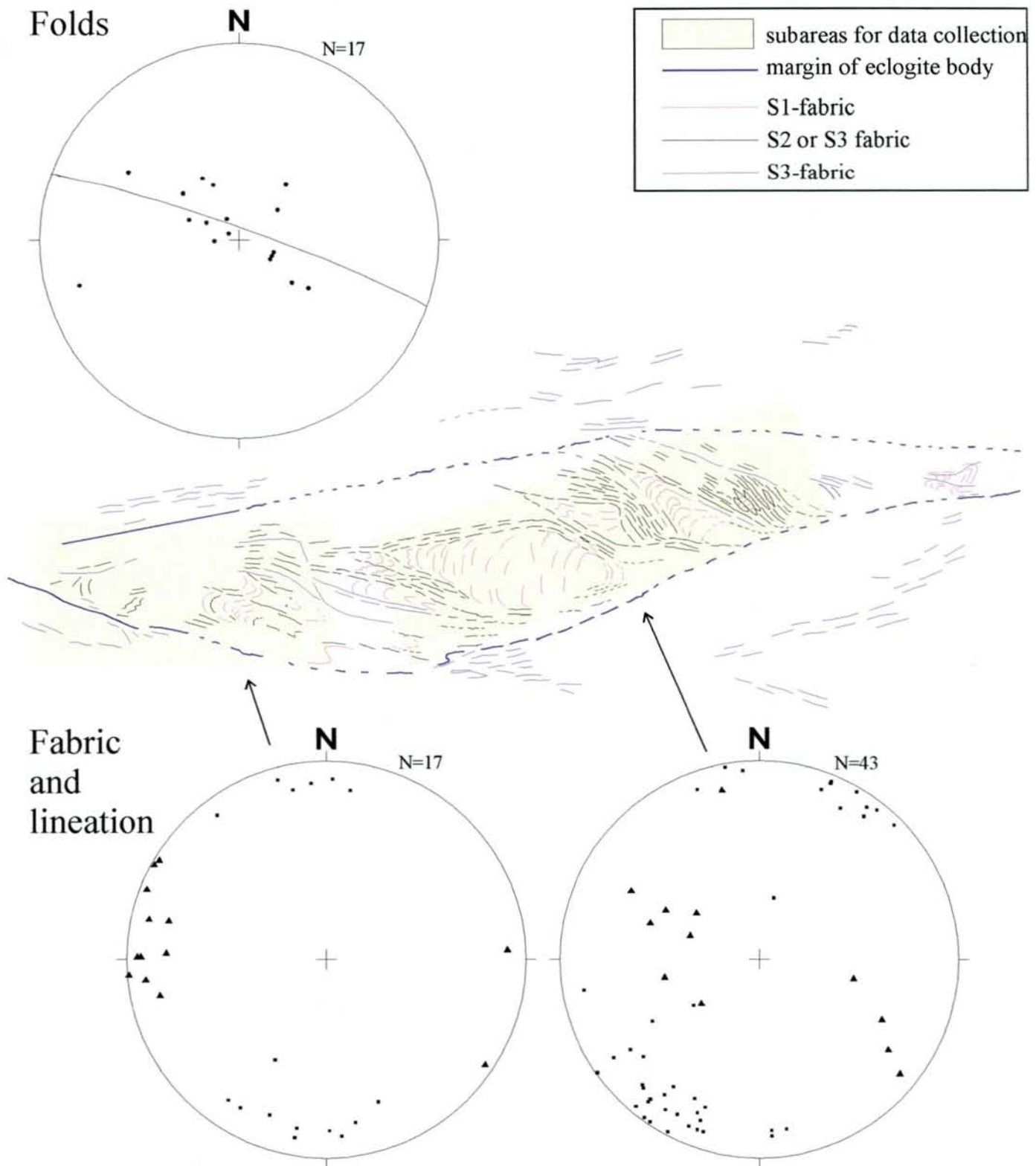


Fig.A4.10: D₂ structural data of the Engebøfjellet eclogite. Folds are presented for the whole area, whereas foliation (sq.) and lineation (tri.) data are separated into two subplots

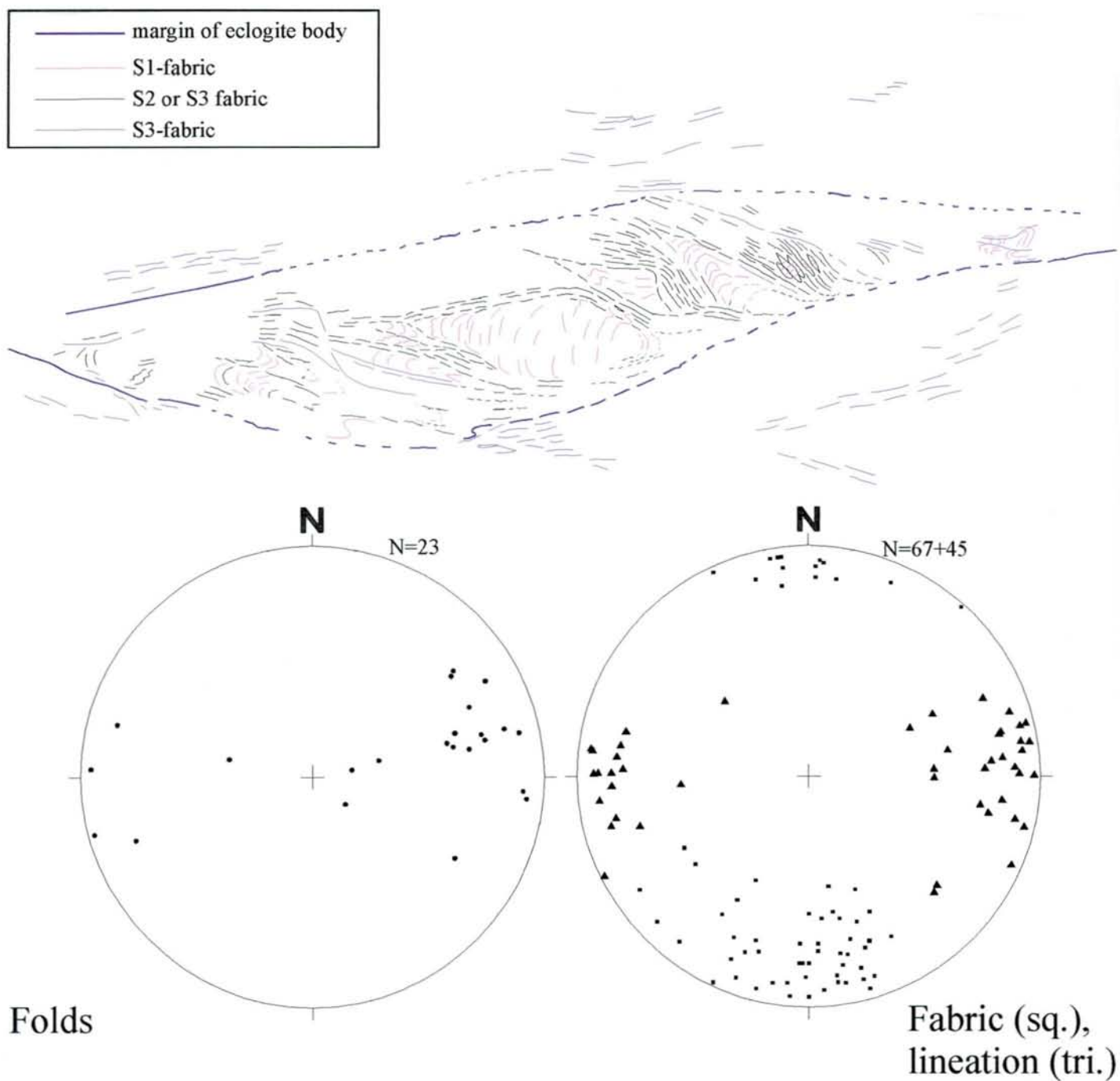


Fig.A4.11: D₃ structural data of the Engebøfjellet eclogite. Data presented in the stereoplots are collected from the entire area.

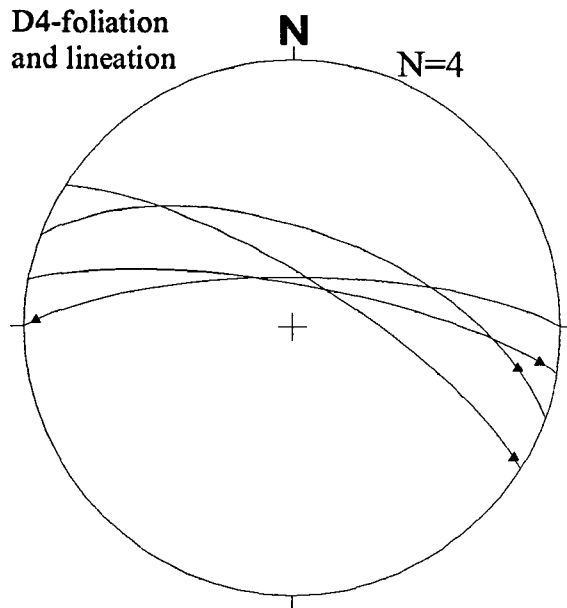
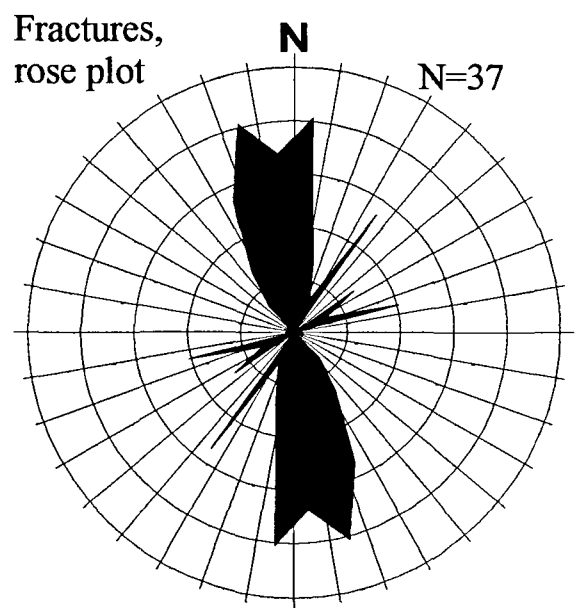
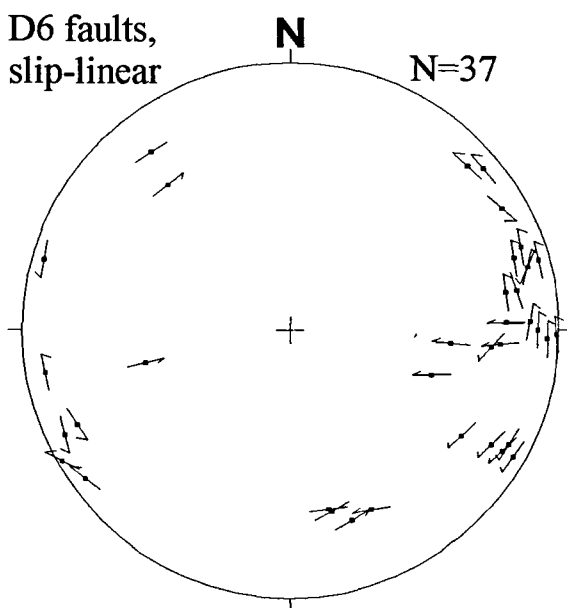
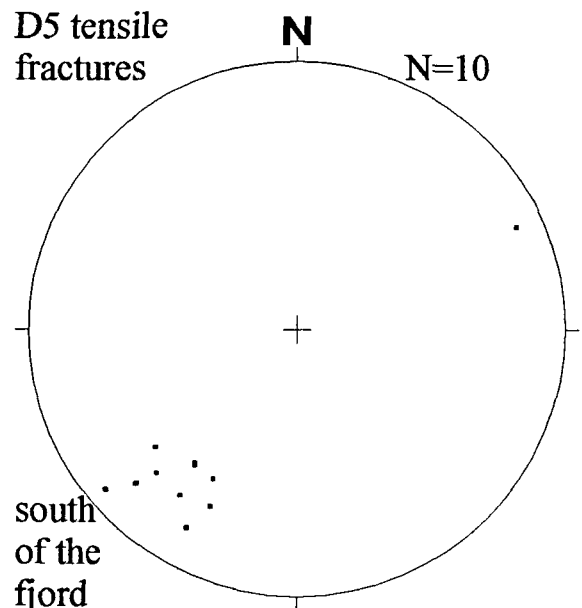
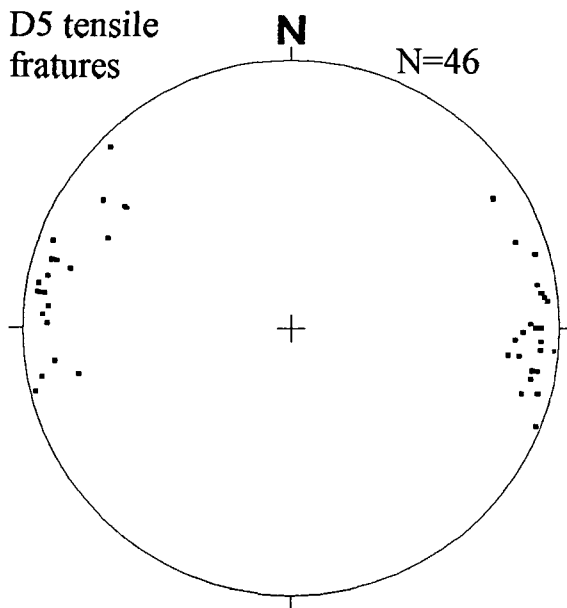


Fig.A4.12: Stereoplots of D₄, D₅ and D₆ structural data. Great circle with triangle, foliation with lineation; Square, pole to joint or fracture.



Mesoscopic faults (D_6) of the Engebøfjellet Eclogite may be separated into two populations; strike-slip faults and normal faults (Fig.A4.12). The first population of fractures, all with steep dips, strikes NE-SW or NNW-SSE. The other population strikes N-S and dips steeply east or west. Slip-lines on the faults, indicating the movement along the surface, suggest that the faults form a conjugate set of strike-slip faults (NE-SW and NNW-SSE strike), which are bisected by normal faults (N-S strike). In the rose diagram these orientations are well displayed. Here, the N-S and NNW-SSE strikes dominate whereas NE-SW and ENE-WSW fractures form a subordinate orientation.

4.4. Micro-structures and fabrics

Extensive descriptions of rocks of the Engebøfjellet eclogite, based on macroscopic and thin sections studies, are presented in chapter 3.3. This section focuses strictly on differences in mineral composition and crystal shape between the various foliations.

A primary layering, with potential primary textures of magmatic origin, is not reflected in the mineralogy. All rocks suffered eclogite facies metamorphism and recrystallization, although relict magmatic textures may be found (see chapter 3.3).

The S_1 foliation is defined by fine-grained, elongated and oriented minerals such as omphacite, blue-green amphibole, clinozoisite, white mica, oxides, quartz and apatite, which varies in concentration dependent on the rock type. Garnet forms euhedral crystals in many cases. This mineralogy and texture is present along the S_2 foliation and F_2 -related cleavage as well (Fig.A4.13). Along both foliations the grain size is very fine (< 0.5 mm). Elongated minerals are anhedral, in the form of wedge-shaped lenses, which are surrounded by even finer grained matrix - especially along the S_2 foliation. This suggests dynamic recrystallization during deformation/shearing of the rocks.

In places, late omphacite porphyroblasts overprint S_1 foliation. These crystals, which can be more than 1-2 cm long, have an apparent monoclinic shape. They are randomly oriented and seem to be found near F_1 fold-knees. The same overgrowth is not documented for the S_2 foliation, thus it appears that this late omphacite postdates the S_1 foliation and predates the S_2 foliation. Euhedral crystal shape also suggests growth under static conditions.

In the amphibolitic S_3 shear zones, common minerals are green amphibole, garnet, plagioclase and quartz, and subordinate zoisite, chlorite, epidote, white mica and brownish biotite. All minerals are fine to very fine grained, with an- to subhedral grain shapes. They have their long axis oriented parallel to the foliation (Fig.A4.14). Distinct planar banding, platy mosaics of euhedral quartz, wings around some garnets, and a well defined orientation of individual mineral grains, all suggest mineral growth under dynamic conditions, i.e. during shear deformation.

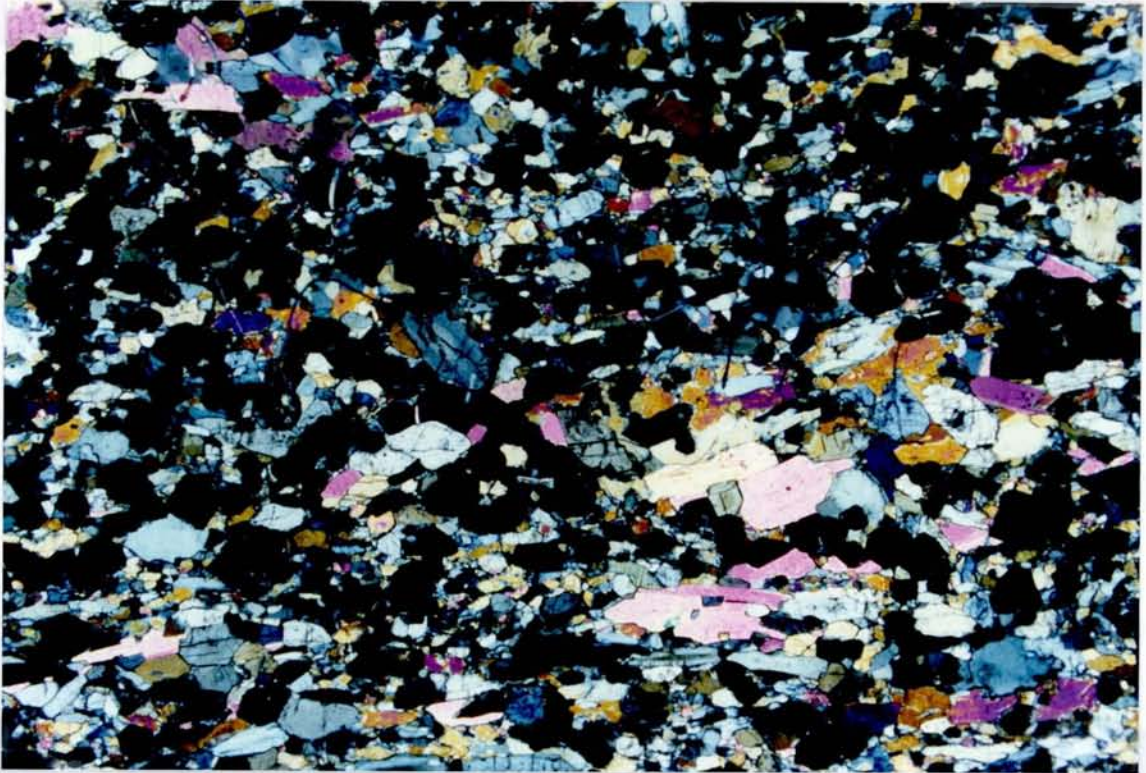


Fig.A4.13. Microphotograph of thin section (polarised transmitted light, 25x) showing garnet (black), pyroxene and amphibole (light colours) and quartz (white) in a well-defines S_2 foliation.

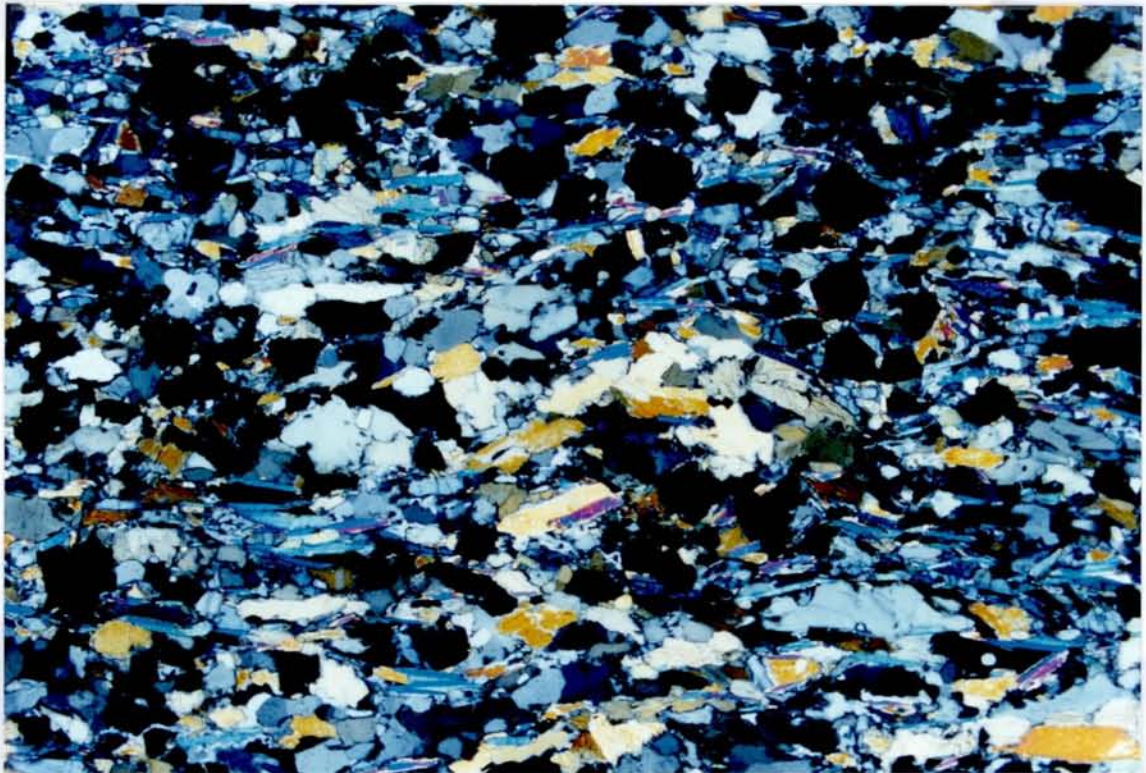


Fig.A4.14. Microphotograph of thin section showing a well developed S_3 foliation of amphibole, white mica and quartz. The relict eclogite facies mineralogy is present in sigmoidal-shaped lenses. Polarised transmitted light (25x).

Similar minerals, grain sizes, and textures occur along the S_4 foliation, however, garnet disappears and biotite constitutes a major part of the rock. Also in this case, there are indications for mineral growth during deformation.

The tensile fractures that cross-cut all foliations, i.e. the D_5 fractures, reveal green fibrose amphibole (actinolite), plagioclase, epidote, quartz and subordinate carbonate and chlorite (Fig.A4.15). Grain size varies from fine-grained to very fine-grained (< 0.1 mm). Wall-rock to the fractures show retrogression of omphacite, blue amphibole and garnet to green amphibole, as well as transformation of rutile to ilmenite (see chapter 3.3).

The final stage of deformation, present as brittle faults of the D_6 stage, did not result in any significant recrystallization. Mineral growth at this stage is limited to the fractures, which, in many cases, are linings coated with fibrose epidote or quartz. At a few locations, the fractures are filled with brown carbonate.

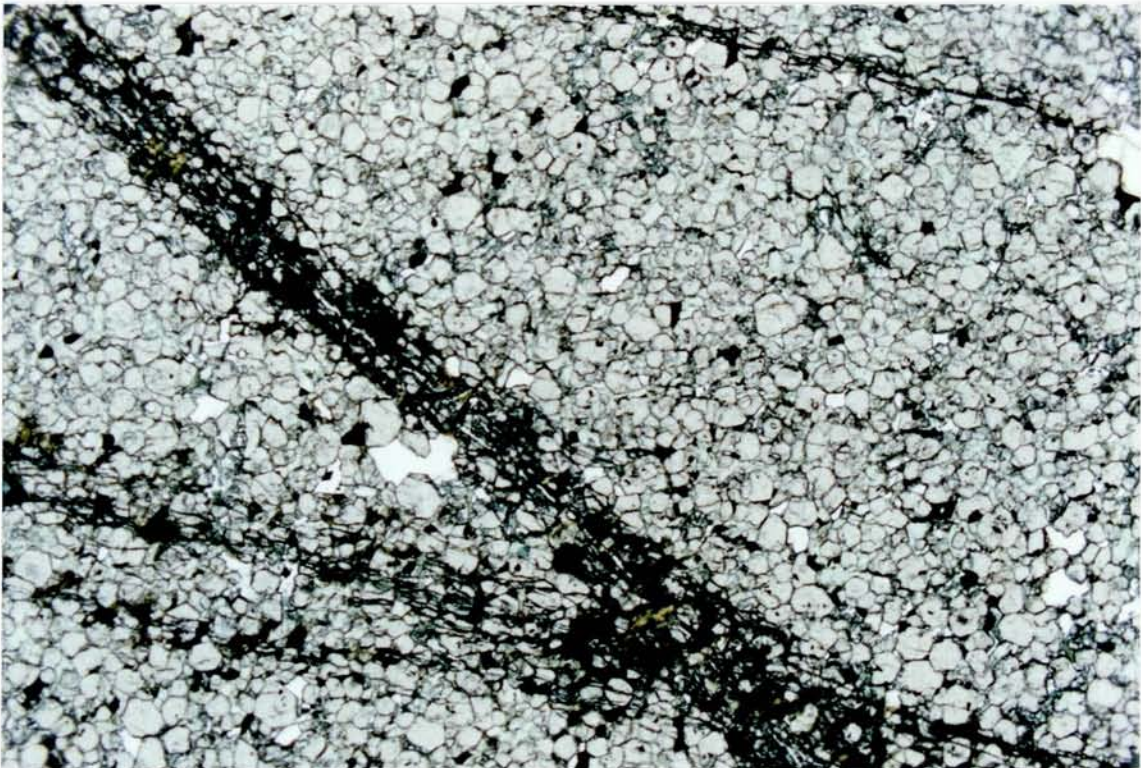


Fig.A4.15. Microphotograph of thin section showing a D_5 tensile fracture in the garnet-rich ferro eclogite. Greenish amphibole constitutes the main retrograde mineral along the fracture. Scale bar in the lower left corner.

Appendix 5

Mineralogy, Engebøfjellet

By Muriel Erambert

Contents

- 5.1 Eclogite texture**
- 5.2 Eclogite-facies minerals**
- 5.3 Pressure and temperature estimates for the eclogite-facies event**
- 5.4 Retrogressive reaction textures**
- 5.5 Secondary minerals**

Mineralogy, Engebøfjellet (by Muriel Erambert)

About 100 thin sections cut from drill core and surface samples have been studied, including fresh and retrograded "ferro-" and "leuco-" eclogites, and a few amphibolites and eclogite-facies "gneisses". In all studied eclogite samples, although pseudomorphic texture (= relict magmatic texture) is common, the first recorded mineral assemblage is eclogitic. No relics of magmatic minerals has been observed. Detailed textural, mineralogical and mineral chemistry study has been focused on the eclogitic assemblages from the main body.

5.1. Eclogitic texture

Textures observed in eclogites from Engebøfjellet are characteristic of those displayed during the transition from gabbro to coronite to eclogite (Gjelsvik, 1952; Godard, 1981; Pognante and Kienast, 1987; Mørk, 1985). This textural evolution reflects the extent to which the rocks have been subjected to deformation during eclogitisation and is well illustrated by the leuco-eclogites. The coronitic stage is preserved within the "massive leuco-eclogite". Coronas of garnet separate fine-grained mafic (amphibole, omphacite) and felsic (phengite + zoisite + albite + quartz) domains (Fig. A.5.1). Towards the deformed margins of this massive leucocratic body or along internal shear zones, progressive recrystallization gives rise to a range of textures. It evolves from deformed coronitic texture to an oriented texture of "coarse-grained" omphacite, amphibole, garnet, clinozoisite and quartz ribbons, and small granular felsic domains (phengite + paragonite + clinozoisite) (Fig. A.5.2). These fine-grained domains disappear in completely recrystallized leuco-eclogite (Fig. A.5.3).

Mafic eclogites are generally completely recrystallized. Tabular texture with oriented omphacite, amphibole and strings of small rutile grains parallel to the foliation results from strong deformation during the eclogite-facies D1 and D2 events (Fig. A.5.4). Garnets are generally small and euhedral. A few relicts of transitional stages (honeycomb texture, atoll garnets) are found.

On average, eclogites from Engebøfjellet are fine-grained rocks either as a result of strong deformation (ferro-eclogite) or lack of complete recrystallization (coronitic leuco-eclogite). Post-D1 growth of porphyroblasts (amphibole, omphacite) is however recorded in leuco- and "transitional" (i.e. intermediate in composition between ferro- and leuco-eclogites) eclogites (Fig. A.5.3). Further detail on the habitus of each eclogitic mineral is given below.

Fluid-rock interaction was frequent at all stages in the history of these rocks: abundant volatile-bearing phases characterize the eclogite parageneses (amphibole, phengite, clinozoisite, carbonate, apatite...) and retrogression is dominated by amphibole + plagioclase symplectites (the anhydrous counterpart, diopside + plagioclase, is rarely seen here). Numerous eclogite-facies veins (containing quartz, omphacite, garnet, carbonate, amphibole, sulfides...), particularly well represented in the E part of the body, indicate a high fluid pressure during peak metamorphism. The general availability of fluid may account for the complete "pseudomorphic" (static) eclogitisation of the massive leuco-eclogites, a feature unusual in coronitic gabbros and dolerites from the WGR that often preserve relict magmatic minerals when undeformed (e.g. Gjelsvik, 1952; Mørk, 1985; Cuthbert, 1985). Interplay of deformation and metamorphism (Rutter and Brodie, 1995) and reaction-enhanced ductility (Rubie, 1990) may explain that Fe-rich gabbros first to react (Green and Ringwood, 1967) are totally recrystallized and highly strained.

5.2. Eclogite-facies minerals

A few samples (4 ferro-, 2 ferro- /transitional, 1 layered and 1 leuco- eclogites) have been selected for microprobe analysis. In addition, compositions of minerals from felsic segregations in two leuco-coronites/eclogites have been analysed. Considering the limited number of samples, the mineral compositions presented below may not encompass the entire range in eclogites at Engebøfjellet, especially within the poorly represented but quite variable leuco- / layered eclogite group.

Mineral analyses were performed on a CAMECA Camebax Microbeam microprobe at the Mineralogical Museum, Oslo, operated in wavelength dispersive mode. Analytical conditions were: accelerating voltage 15 kV, counting time 10 s on peak and 5 s on background on both sides of peak. Sample current of 20 nA and focused beam were used to analyze garnet, pyroxene, amphibole, epidote and sphene; 10 nA and scan over an area of 5 by 5 (m on feldspar, micas, carbonate. Natural and synthetic silicates and oxides were used as standards (Si and Ca on wollastonite, Al₂O₃, Fe₂O₃, MgO, Cr₂O₃, NiO, Mn and Ti on pyrophanite, Na on omphacite or albite, K on orthoclase). Analyses were corrected according to the PAP procedure. Representative analyses are reported in Tables A5.1 to A5.4.

Garnet: In the mafic eclogites, modal abundance of garnet ranges from 25-30 % to 55%. In the leuco-eclogites, its abundance is usually less than 20%. Garnet distribution tends to be homogeneous in recrystallized granuloblastic eclogites, e.g. especially the mafic ones. Honeycomb texture is characteristic of many leuco-eclogites, resulting from coarsening of the garnet coronas without complete recrystallization. Garnet “coronas” or strings of small euhedral garnets separate fine-grained domains of clinozoisite + phengite, pseudomorphs after magmatic plagioclase, from mafic clinopyroxene- or amphibole-rich domains (Fig. A.5.1). In mafic eclogites, honeycomb texture and atoll garnets are occasionally seen. Partial garnet coronas, with euhedral faces towards the matrix, are commonly found around rutile.

In recrystallised mafic eclogites, garnet is generally small ((0.5 mm), euhedral to subhedral. In leuco- and layered eclogites, garnet size is variable and can reach 1 cm. In many garnets, inclusions are common (most common are carbonate, rutile, quartz, omphacite and amphibole) and range in size from a few (m (“dusty garnet”) to several 10 (m in the largest garnets; the poikilitic core is often surrounded by a inclusion-free rim.

Garnet is almandine-rich (see Table A5.1 and Fig. A.5.7). Core compositions range from Alm 56.3-64.7 Spe 1.0-5.5 Pyr 9.2-16.9 Gro 17.0-24.5 And 1.3-6.7 in mafic and transitional eclogites to Alm 51.6 Spe 1.8 Pyr 23.6 Gro 21.2 And 2.0 in the leucocratic one. Within a single sample, local variations in garnet composition depend on the adjacent mineral and reflect incomplete chemical homogenisation during eclogitisation. Rim compositions have higher Alm and lower Spe and And compared to the core; Pyr is generally higher. The zoning trend in Ca depends on the adjacent mineral. Compositional profiles in two euhedral garnets from a mafic eclogite show different trends (Fig. A.5.8). Notably, Ca increases from the poikilitic core to the inclusion-free rim, then decreases again towards the outer rim. This variation is balanced mainly by change in Fe in one garnet, in Mg + Fe in the other. Increase in

Table A5.1: Garnet compositions in eclogites from Engebøfjellet

	Mafic eclogites						Mafic to intermediate eclogites					Layered eclogite		Leucogabbroic eclogite			
Sample	E4/97.3	E4/97.3	E4/97.3	E4/130.3	E4/130.3	E3/159.8	E3/159.8	E1/101.9	E1/101.9	E1/101.9	E8/229.0	E8/229.0	E1/164.2	E1/164.2	E3/33.9	E3/33.9	E3/33.9
Analysis	2.1	1.2	2.2	1.4	1.2	2.1	2.3	3.1	1.2	3.7	1.2	1.3	2.2	2.3	2.1	2.4	2.9
Comment	core	core	rim	core	rim	core	rim	core	core	rim	"core"	rim	rim	rim	core	rim	rim
SiO ₂	38.14	38.33	38.38	37.57	38.10	38.46	38.75	38.34	38.55	37.80	37.54	37.79	37.89	38.18	38.97	38.87	38.78
TiO ₂	0.19	0.07	0.03	0.09	0.06	0.22	0.00	0.15	0.05	0.02	0.10	0.06	0.08	0.05	0.06	0.05	0.00
Al ₂ O ₃	20.62	20.94	21.27	20.66	20.63	20.92	21.34	20.76	21.01	20.60	20.36	20.57	20.45	21.28	21.46	21.58	21.46
Cr ₂ O ₃	0.01	0.00	0.03	0.00	0.00	0.00	0.01	0.00	0.00	0.00	0.03	0.03	0.00	0.00	0.05	0.08	0.09
FeO _t	26.88	27.29	28.84	30.35	31.27	26.92	27.80	28.43	28.15	29.41	30.44	30.82	30.59	29.15	24.54	25.13	25.07
MnO	0.53	0.79	0.52	1.84	0.91	0.69	0.51	0.55	0.95	0.53	1.02	0.47	1.02	0.28	0.80	0.54	0.57
MgO	3.78	3.50	4.08	2.32	3.36	3.91	4.99	3.09	2.97	3.24	2.39	2.19	2.94	4.34	6.13	6.17	5.72
CaO	9.73	9.49	8.00	7.68	6.43	9.64	7.66	10.01	10.04	8.16	8.51	8.74	7.67	7.55	8.37	7.89	8.31
Na ₂ O	0.05	0.02	0.00	0.04	0.02	0.06	0.00	0.06	0.03	0.04	0.07	0.01	0.04	0.04	0.04	0.02	0.02
K ₂ O	0.00	0.03	0.00	0.00	0.01	0.01	0.01	0.00	0.00	0.00	0.01	0.00	0.00	0.01	0.01	0.00	0.00
NiO	0.03	0.04	0.00	0.00	0.00	0.01	0.01	0.01	0.00	0.04	0.00	0.00	0.00	0.00	0.00	0.04	0.05
Sum	99.96	100.50	101.14	100.55	100.78	100.83	101.08	101.38	101.76	99.85	100.46	100.69	100.68	100.89	100.44	100.38	100.06
Structural formula (on 24 oxygens and 16 cations)																	
Si	6.00	6.01	5.98	5.97	6.02	5.99	6.00	5.98	5.99	6.00	5.96	5.99	5.99	5.96	6.01	6.00	6.02
Ti	0.02	0.01	0.00	0.01	0.01	0.03	0.00	0.02	0.01	0.00	0.01	0.01	0.01	0.01	0.01	0.01	0.00
Al	3.82	3.87	3.90	3.87	3.84	3.84	3.90	3.82	3.85	3.85	3.81	3.84	3.81	3.91	3.90	3.93	3.93
Cr	0.00	0.00	0.00	0.00	0.00	0.00	0.00	0.00	0.00	0.00	0.00	0.00	0.00	0.00	0.01	0.01	0.01
Fe ³⁺	0.15	0.09	0.13	0.18	0.12	0.14	0.10	0.21	0.17	0.16	0.26	0.16	0.20	0.18	0.08	0.04	0.02
Fe ²⁺	3.39	3.49	3.63	3.86	4.01	3.36	3.51	3.50	3.49	3.74	3.78	3.93	3.84	3.63	3.09	3.21	3.24
Mn	0.07	0.10	0.07	0.25	0.12	0.09	0.07	0.07	0.12	0.07	0.14	0.06	0.14	0.04	0.10	0.07	0.07
Mg	0.89	0.82	0.95	0.55	0.79	0.91	1.15	0.72	0.69	0.77	0.57	0.52	0.69	1.01	1.41	1.42	1.32
Ca	1.64	1.59	1.34	1.31	1.09	1.61	1.27	1.67	1.67	1.39	1.45	1.48	1.30	1.26	1.38	1.31	1.38
Na	0.02	0.00	0.00	0.01	0.00	0.02	0.00	0.02	0.01	0.01	0.02	0.00	0.01	0.01	0.01	0.00	0.00
K	0.00	0.00	0.00	0.00	0.00	0.00	0.00	0.00	0.00	0.00	0.00	0.00	0.00	0.00	0.00	0.00	0.00
Ni	0.00	0.00	0.00	0.00	0.00	0.00	0.00	0.00	0.00	0.01	0.00	0.00	0.00	0.00	0.00	0.00	0.01
Garnet end-members																	
Alm	56.58	58.10	60.70	64.68	66.66	56.33	58.46	58.67	58.43	62.72	63.73	65.54	64.34	61.12	51.59	53.40	53.80
Spe	1.18	1.74	1.14	4.14	2.04	1.52	1.12	1.22	2.08	1.19	2.30	1.06	2.30	0.62	1.75	1.18	1.23
Pyr	14.81	13.62	15.83	9.23	13.18	15.20	19.21	12.05	11.52	12.86	9.54	8.63	11.61	16.98	23.56	23.66	22.01
Gro	23.65	24.31	19.18	17.46	15.09	23.35	18.82	22.78	23.81	19.23	17.76	20.82	16.71	16.84	21.15	20.76	22.57
And	3.77	2.23	3.15	4.49	3.02	3.60	2.40	5.27	4.16	4.01	6.67	3.95	5.04	4.43	1.95	0.99	0.39

Table A5.2: Eclogitic pyroxenes from Engebøfjellet

	Mafic eclogites						Mafic to intermediate eclogites						Leucogabbroic eclogite	
Sample	E4/97.3	E4/97.3	E4/97.3	E3/159.8	E3/159.8	E7/074.0	E7/074.0	E1/101.9	E1/101.9	E8/229.0	E8/229.0	E3/33.9	E3/33.9	
Analysis	2.5	2.8	1.3	1.6	2.2	1.5d	4	3.4	1.6	1.1	1.5	2.3	2.8	
Comment	core	rim	incl.	core	rim	core	near vein	core	rim	core	core			
SiO ₂	54.99	54.82	54.73	55.04	55.00	55.13	55.05	55.73	55.62	54.73	55.13	56.68	56.95	
TiO ₂	0.09	0.09	0.06	0.10	0.11	0.10	0.25	0.09	0.09	0.10	0.08	0.11	0.03	
Al ₂ O ₃	7.33	6.82	7.04	7.66	7.70	7.70	7.32	8.11	8.33	6.80	7.58	10.88	11.14	
Cr ₂ O ₃	0.03	0.05	0.00	0.02	0.00	0.03	0.05	0.00	0.04	0.05	0.07	0.19	0.01	
FeO _t	8.66	8.99	9.22	9.20	8.55	8.58	8.38	9.54	10.18	12.33	11.96	4.19	4.05	
MnO	0.00	0.01	0.05	0.01	0.00	0.01	0.00	0.00	0.00	0.00	0.02	0.00	0.03	
MgO	8.11	7.84	8.48	7.55	8.41	7.66	8.27	7.13	6.49	6.27	5.76	8.15	8.16	
CaO	14.69	14.11	14.91	13.40	14.27	13.71	14.15	12.24	11.70	11.31	11.18	13.42	13.04	
Na ₂ O	6.10	6.56	5.75	6.92	6.34	6.79	6.47	8.04	7.88	8.22	8.42	7.40	7.39	
K ₂ O	0.00	0.00	0.04	0.04	0.00	0.00	0.00	0.00	0.00	0.01	0.01	0.00	0.00	
NiO	0.00	0.02	0.00	0.01	0.00	0.01	0.00	0.00	0.00	0.00	0.04	0.00	0.00	
Sum	100.00	99.30	100.29	99.94	100.38	99.73	99.93	100.90	100.34	99.81	100.25	101.01	100.80	
Structural formula (on 6 oxygens and 4 cations)														
Si	1.99	1.99	1.98	1.98	1.97	1.99	1.98	1.98	1.99	1.98	1.98	1.99	2.00	
Ti	0.00	0.00	0.00	0.00	0.00	0.00	0.01	0.00	0.00	0.00	0.00	0.00	0.00	
Al	0.31	0.29	0.30	0.33	0.33	0.33	0.31	0.34	0.35	0.29	0.32	0.45	0.46	
Cr	0.00	0.00	0.00	0.00	0.00	0.00	0.00	0.00	0.00	0.00	0.00	0.01	0.00	
Fe ³⁺	0.13	0.18	0.15	0.19	0.16	0.16	0.16	0.25	0.20	0.32	0.29	0.07	0.05	
Fe ²⁺	0.13	0.09	0.13	0.09	0.10	0.10	0.10	0.03	0.10	0.05	0.07	0.05	0.07	
Mn	0.00	0.00	0.00	0.00	0.00	0.00	0.00	0.00	0.00	0.00	0.00	0.00	0.00	
Mg	0.44	0.42	0.46	0.41	0.45	0.41	0.44	0.38	0.35	0.34	0.31	0.43	0.43	
Ni	0.00	0.00	0.00	0.00	0.00	0.00	0.00	0.00	0.00	0.00	0.00	0.00	0.00	
Ca	0.57	0.55	0.58	0.52	0.55	0.53	0.55	0.47	0.45	0.44	0.43	0.50	0.49	
Na	0.43	0.46	0.40	0.48	0.44	0.48	0.45	0.55	0.55	0.58	0.59	0.50	0.50	
K	0.00	0.00	0.00	0.00	0.00	0.00	0.00	0.00	0.00	0.00	0.00	0.00	0.00	
Pyroxene end-members														
Acmite	12.94	18.07	14.54	18.53	16.10	16.02	15.70	25.30	20.10	32.00	29.10	7.19	4.55	
Jadeite	29.70	28.08	25.93	29.99	28.06	31.44	29.38	30.10	34.60	25.50	29.50	42.58	45.67	
Ca-Ts	0.51	0.35	1.91	1.01	1.96	0.40	0.21	1.70	0.10	1.50	1.10	0.93	0.13	

Table A5.3: Eclogite-facies amphiboles from Engebøfjellet

	Mafic eclogites					Intermediate eclogites				Layered leucog. ecl.		Leucogabb. Ecl.	
Sample	E4/97.3	E4/97.3	E4/130.3	E4/130.3	E4/130.3	E8/229.0	E8/229.0	E101.9	E101.9	E1/164.2	E1/164.2	E3/33.3	E3/33.3
Analysis	1.4	2.10	1.6	1.5	1.9	1.6	1.14	1.5	1.4	1.1	1.2	2.6	2.5
Comment	core	rim w.Rut	core	rim w. Gt	rim w.Rut/Gt	core	rim w.Gt	core	rim w.Gt	core	rim	core	
SiO ₂	54.03	51.48	52.89	50.12	51.10	51.62	46.88	49.11	42.40	47.01	43.64	53.24	48.86
TiO ₂	0.11	0.31	0.12	0.24	0.47	0.13	0.32	0.29	0.25	0.42	0.46	0.11	0.17
Al ₂ O ₃	4.96	6.53	4.10	6.99	7.12	7.96	11.21	10.33	15.56	13.26	13.68	10.06	12.16
Cr ₂ O ₃	0.00	0.00	0.00	0.01	0.00	0.00	0.02	0.08	0.00	0.00	0.00	0.02	0.01
FeO _t	11.29	12.13	14.31	15.74	14.37	16.35	16.48	15.80	17.34	14.82	18.50	8.52	9.71
MnO	0.00	0.06	0.14	0.05	0.02	0.10	0.15	0.04	0.07	0.00	0.29	0.08	0.08
MgO	15.55	14.79	14.29	12.36	12.78	11.27	10.61	10.95	8.47	10.06	8.23	14.64	13.74
CaO	9.23	9.15	8.92	8.49	8.91	4.41	7.08	6.49	7.90	6.51	7.89	7.03	9.35
Na ₂ O	2.60	2.92	2.58	3.31	3.25	5.17	4.47	4.55	4.81	4.32	3.25	3.94	3.14
K ₂ O	0.18	0.20	0.12	0.26	0.18	0.07	0.13	0.41	0.96	0.37	0.55	0.16	0.26
NiO	0.02	0.05	0.04	0.00	0.00	0.00	0.05	0.03	0.00	0.00	0.00	0.05	0.06
Sum	97.96	97.62	97.50	97.56	98.20	97.06	97.40	98.07	97.76	96.77	96.49	97.86	97.52
Structural formula on "Sum cations - (Ca, Na, K) =13" *													
Si	7.59	7.30	7.54	7.23	7.31	7.32	6.77	7.01	6.26	6.77	6.44	7.35	6.90
Ti	0.01	0.03	0.01	0.03	0.05	0.01	0.04	0.03	0.03	0.05	0.05	0.01	0.02
Al IV	0.41	0.70	0.46	0.77	0.70	0.68	1.24	0.99	1.74	1.24	1.56	0.65	1.10
Al VI	0.41	0.40	0.23	0.41	0.51	0.65	0.67	0.74	0.96	1.01	0.82	0.98	0.93
Cr	0.00	0.00	0.00	0.00	0.00	0.00	0.00	0.01	0.00	0.00	0.00	0.00	0.00
Fe 3+	0.46	0.61	0.74	0.71	0.44	1.22	1.02	0.86	0.67	0.85	1.11	0.47	0.38
Fe 2+	0.87	0.83	0.96	1.19	1.28	0.72	0.97	1.03	1.47	0.94	1.17	0.51	0.77
Mn	0.00	0.01	0.02	0.01	0.00	0.01	0.02	0.00	0.01	0.00	0.04	0.01	0.01
Mg	3.25	3.13	3.04	2.66	2.72	2.38	2.28	2.33	1.86	2.16	1.81	3.01	2.90
Ni	0.00	0.01	0.00	0.00	0.00	0.00	0.01	0.00	0.00	0.00	0.00	0.01	0.01
Ca	1.39	1.39	1.36	1.31	1.37	0.67	1.09	0.99	1.25	1.00	1.25	1.04	1.42
Na	0.71	0.80	0.72	0.92	0.90	1.42	1.25	1.26	1.38	1.21	0.93	1.05	0.86
K	0.03	0.04	0.02	0.05	0.03	0.01	0.02	0.07	0.18	0.07	0.10	0.03	0.05
Sum	15.13	15.24	15.10	15.28	15.30	15.10	15.38	15.33	15.80	15.28	15.28	15.13	15.33
mg **	0.79	0.79	0.76	0.69	0.68	0.77	0.70	0.69	0.56	0.70	0.61	0.86	0.79
	subcalcic Actinolite	subcalcic actinolitic Hb	subcalcic Actinolite	subcalcic Edenite/ barroisite	subcalcic actinolitic Hb	barroisite	barroisite	barroisite	Mg-taramite/ Fe Parg.Hb	barroisite	barroisite	barroisite	subcalcic Mg-Hb

* To satisfy crystal-chemical criteria, structural formula for these amphiboles can only be recalculated on "Sum cations - (Ca, Na, K) =13" corresponding to the highest possible Fe³⁺ value and on "Sum oxygens =23" corresponding to Fe³⁺ = 0.

** mg = Mg / Mg + Fe²⁺

Table A5.4: Eclogitic minerals from Engebøfjellet

Phengite and Paragonite								Clinzoisites				Dolomite/Ankerite																																																																																								
Mafic eclogite		Layered eclogite		Leucogabbroic eclogites				Mafic eclogite		Leucogab. ecl.		Mafic eclogites																																																																																								
Sample	E3/159.8	E3/159.8	E1/164.2	E1/164.2	ME39/96	E3/101.9	E3/101.9	E3/159.8	E3/159.8	E3/33.9	E3/101.9	E4/97.3	E4/97.3	E4/97.3	E3/159.8	E3/159.8																																																																																				
Analysis	3	4	mc4	mc2	1.4	1.5	1.8	1.5	2.4	2.7	1.7	cc1	cc2	cc3	cc1	cc2																																																																																				
Comment	core	rim	core	rim	segreg.		segreg.	incl.	incl.	incl.	segreg.	core incl.	core	rim	core	core																																																																																				
SiO ₂	50.87	49.86	49.95	48.90	49.85	49.73	47.11	38.32	38.67	38.52	38.66	28.68	28.70	28.14	28.44	28.99																																																																																				
TiO ₂	0.39	0.45	0.43	0.50	0.33	0.28	0.13	0.11	0.14	0.08	0.04	8.75	7.19	8.88	6.01	5.98																																																																																				
Al ₂ O ₃	25.36	26.45	27.48	27.78	28.21	27.83	38.84	25.53	25.21	27.04	27.73	15.38	16.33	15.01	17.05	17.02																																																																																				
Cr ₂ O ₃								0.06	0.03	0.06		0.00	0.04	0.05	0.00	0.07																																																																																				
FeO _t	3.08	3.09	3.46	3.81	1.20	1.76	0.37	9.11	10.09	6.44	6.79																																																																																									
MnO	0.00	0.00	0.00	0.00	0.06	0.01	0.00	0.00	0.10	0.09	0.02																																																																																									
MgO	3.69	3.16	2.77	2.52	3.14	3.44	0.17	0.00	0.00	0.07	0.00																																																																																									
CaO	0.00	0.03	0.03	0.00	0.11	0.00	0.30	23.44	23.14	23.95	24.18																																																																																									
Na ₂ O	0.39	0.29	0.53	0.44	0.84	0.71	7.23	0.00	0.00	0.02	0.04																																																																																									
K ₂ O	10.85	11.08	10.16	10.42	9.83	9.90	0.67	0.01	0.00	0.00	0.01																																																																																									
NiO								0.00	0.03	0.03																																																																																										
Sum	94.63	94.40	94.79	94.37	93.57	93.66	94.82	96.57	97.42	96.32	97.47	52.81	52.26	52.08	51.50	52.06																																																																																				
Structural formula on 22 oxygens								Structural formula on 12.5 oxygens and 8 cations				Structural formula on 2 cations																																																																																								
Si	6.89	6.78	6.74	6.65	6.73	6.72	6.05	3.03	3.04	3.03	3.00																																																																																									
Ti	0.04	0.05	0.04	0.05	0.03	0.03	0.01	0.01	0.01	0.00	0.00																																																																																									
Al	4.05	4.24	4.37	4.46	4.49	4.44	5.88	2.38	2.33	2.51	2.54																																																																																									
Cr								0.00	0.00	0.00	0.00																																																																																									
Fe ³⁺								0.55	0.57	0.42	0.44																																																																																									
Fe ²⁺ = Fet	0.35	0.35	0.39	0.43	0.14	0.20	0.04	0.05	0.09	0.01	0.00																																																																																									
Mn	0.00	0.00	0.00	0.00	0.01	0.00	0.00	0.00	0.01	0.01	0.00																																																																																									
Mg	0.74	0.64	0.56	0.51	0.63	0.69	0.03	0.00	0.00	0.01	0.00																																																																																									
Ni								0.00	0.00	0.00	0.00																																																																																									
Ca	0.00	0.00	0.00	0.00	0.02	0.00	0.04	1.98	1.95	2.02	2.01																																																																																									
Na	0.10	0.08	0.14	0.12	0.22	0.19	1.80	0.00	0.00	0.00	0.01																																																																																									
K	1.87	1.92	1.75	1.81	1.69	1.71	0.11	0.00	0.00	0.00	0.00																																																																																									
Sum	14.04	14.06	13.98	14.03	13.95	13.98	13.96	8.00	8.00	8.00	8.00	52.24	53.02	52.30																																																																																						
mg*	0.68	0.65	0.59	0.54	0.82	0.78		Ps**	18.88	19.70	14.44	14.79																																																																																								
* mg = Mg/(Mg+ Mn+ Fet)								** Ps = 100 * Fe ³⁺ /(Fe ³⁺ + Al)				<table border="1"> <thead> <tr> <th></th> <th>E 4/130.3</th> <th>E 4/130.3</th> <th>E 4/130.3</th> <th></th> <th></th> </tr> <tr> <th></th> <th>cc1</th> <th>cc2</th> <th>cc3</th> <th></th> <th></th> </tr> <tr> <th></th> <th>core</th> <th>core</th> <th>core</th> <th></th> <th></th> </tr> </thead> <tbody> <tr> <td>CaO</td> <td>28.60</td> <td>28.78</td> <td>28.34</td> <td></td> <td></td> </tr> <tr> <td>FeO_t</td> <td>8.40</td> <td>9.17</td> <td>8.30</td> <td></td> <td></td> </tr> <tr> <td>MgO</td> <td>15.20</td> <td>14.92</td> <td>15.56</td> <td></td> <td></td> </tr> <tr> <td>MnO</td> <td>0.04</td> <td>0.15</td> <td>0.10</td> <td></td> <td></td> </tr> <tr> <td>Sum</td> <td>52.24</td> <td>53.02</td> <td>52.30</td> <td></td> <td></td> </tr> <tr> <td colspan="6">Structural formula on 2 cations</td> </tr> <tr> <td>Ca</td> <td>1.02</td> <td>1.01</td> <td>1.00</td> <td></td> <td></td> </tr> <tr> <td>Fet</td> <td>0.23</td> <td>0.25</td> <td>0.23</td> <td></td> <td></td> </tr> <tr> <td>Mg</td> <td>0.75</td> <td>0.73</td> <td>0.77</td> <td></td> <td></td> </tr> <tr> <td>Mn</td> <td>0.00</td> <td>0.00</td> <td>0.00</td> <td></td> <td></td> </tr> <tr> <td>mg*</td> <td>0.76</td> <td>0.74</td> <td>0.77</td> <td></td> <td></td> </tr> </tbody> </table>						E 4/130.3	E 4/130.3	E 4/130.3				cc1	cc2	cc3				core	core	core			CaO	28.60	28.78	28.34			FeO _t	8.40	9.17	8.30			MgO	15.20	14.92	15.56			MnO	0.04	0.15	0.10			Sum	52.24	53.02	52.30			Structural formula on 2 cations						Ca	1.02	1.01	1.00			Fet	0.23	0.25	0.23			Mg	0.75	0.73	0.77			Mn	0.00	0.00	0.00			mg*	0.76	0.74	0.77		
	E 4/130.3	E 4/130.3	E 4/130.3																																																																																																	
	cc1	cc2	cc3																																																																																																	
	core	core	core																																																																																																	
CaO	28.60	28.78	28.34																																																																																																	
FeO _t	8.40	9.17	8.30																																																																																																	
MgO	15.20	14.92	15.56																																																																																																	
MnO	0.04	0.15	0.10																																																																																																	
Sum	52.24	53.02	52.30																																																																																																	
Structural formula on 2 cations																																																																																																				
Ca	1.02	1.01	1.00																																																																																																	
Fet	0.23	0.25	0.23																																																																																																	
Mg	0.75	0.73	0.77																																																																																																	
Mn	0.00	0.00	0.00																																																																																																	
mg*	0.76	0.74	0.77																																																																																																	

Mg, decrease in Mn and “oscillatory “ behaviour of Ca and Fe has also been noted by Krogh (1980) in eclogite garnets from nearby Kvineset. In all these relatively low-temperature eclogites (ca. 550-600 oC, see below), the observed zoning is likely to be mainly growth-related. Diffusion in garnet at $T < 700$ oC is not effective enough to either completely erase any pre-existent zoning or to create any substantial one. It is tempting to use this growth zoning to deduce variations in P and T during eclogitisation. However, such interpretation is only possible if the growth direction is known. When eclogitization proceeds through a coronitic stage as it is the case here, growth patterns of garnet by coarsening of the coronas are complex, including growth from “rim” to poikilitic “core” (Godard, 1981). Contemporaneous garnets may have widely different growth patterns and zoning patterns, even within a single sample. The two composition profiles illustrated here cannot then be considered representative for the entire garnet population in these eclogites, and P-T interpretation of the zoning must await more detailed study.

Mg, decrease in Mn and “oscillatory “ behaviour of Ca and Fe has also been noted by Krogh (1980) in eclogite garnets from nearby Kvineset. In all these relatively low-temperature eclogites (ca. 550-600 oC, see below), the observed zoning is likely to be mainly growth-related. Diffusion in garnet at $T < 700$ oC is not effective enough to either completely erase any pre-existent zoning or to create any substantial one. It is tempting to use this growth zoning to deduce variations in P and T during eclogitisation. However, such interpretation is only possible if the growth direction is known. When eclogitization proceeds through a coronitic stage as it is the case here, growth patterns of garnet by coarsening of the coronas are complex, including growth from “rim” to poikilitic “core” (Godard, 1981). Contemporaneous garnets may have widely different growth patterns and zoning patterns, even within a single sample. The two composition profiles illustrated here cannot then be considered representative for the entire garnet population in these eclogites, and P-T interpretation of the zoning must await more detailed study.

Clinopyroxene: The clinopyroxene is pale to medium green. In all studied samples, pyroxenes are metamorphic; no relict of magmatic pyroxene was recorded. However, although chemical re-equilibration appears complete, some textures indicate pseudomorphic replacement of the magmatic pyroxene, e.g. large dusty clinopyroxenes with numerous oriented inclusions of tiny oxides found in leucocratic samples. In fine-grained and thoroughly recrystallized mafic eclogites, it is generally small ((0.5 mm) and its shape orientation is parallel to the eclogitic foliation. In leuco- and some transitional eclogites, the omphacite frequently forms elongate euhedral poikiloblasts (up to several cm in length), that include other eclogitic phases (garnet, rutile, quartz, clinozoisite...) (Fig. A.5.3). In coarser-grained mafic eclogites, large omphacite porphyroclasts are surrounded by small oriented omphacite, garnet, amphibole, carbonate and mica defining the foliation. These textural relationships indicate several recrystallization/ deformation stages under eclogite-facies conditions (see structural chapter).

In mafic and transitional eclogites, its composition lies at the limit between omphacite, sodian augite and chloromelanite (Jadeite 21.6-34.6 Acmite 14.4-32.3 Ca-Tschermak 0.0-2.3). In the leucogabbroic eclogite, it is omphacitic (Jd 42.6-45.7 Ac 4.0-7.2 Ca-Ts 0.1-0.9). No clear zoning from core to rim was recorded (Table A5.2).

Amphibole I: Amphibole is a major constituent of the eclogite-facies paragenesis in these rocks. It is present in most samples, its amount ranging from trace to major (up to 40%, visual estimate). In some samples, it may totally replace the clinopyroxene as main Na- and Ca-bearing eclogitic phase. This pleochroic amphibole is typically blue green to grey blue. It is

often zoned towards the rim to a green amphibole. When a minor phase, the amphibole is often seen to crystallize along grain boundaries between garnet and omphacite. This indicates that it is a late phase, although belonging to the eclogite paragenesis since it establishes textural equilibrium with other eclogitic phases. In fine-grained amphibole-rich eclogites, the amphibole is part of the granuloblastic texture. Porphyroblasts are common in leuco-/transitional eclogites and include garnet, omphacite, rutile, mica, clinozoisite and carbonate (Ex: Fig. A.5.2).

Composition ranges from subcalcic actinolitic hornblende to barroisite (Leake, 1978; Table A5.3; Fig. A.5.9). Core compositions are on average richer in Al in transitional and leuco- eclogites (amphibole is generally a barroisite) than in mafic eclogites (mostly actinolitic hornblende), reflecting the bulk Al content of the rock (Fig. A.5.10). However, in coronitic leuco-eclogite, the amphibole within mafic clusters is a magnesio-hornblende / tremolitic hornblende; this probably reflects the lack of large-scale chemical equilibrium in these rocks. Amphibole rim zoning corresponds generally to an increase in Al and $(\text{Na}+\text{K})\text{A}$, through increase in the substitutions Edenite - $(\text{Na})\text{A} + \text{Si} (\text{NaA} + \text{AlIV} - \text{and Tschermak} (+ \text{Ferri-Tschermak}) - \text{Si} + \text{Mg} (\text{AlIV} + (\text{AlVI}, \text{Fe}^{3+}))$. The increase in Ed reflects a relative increase in temperature (or a decrease in P at T constant). Increase in Ts (AlVI) may indicate that P also increased (Helz, 1973; Gilbert et al, 1982), although Cho and Ernst (1991) recorded increase in Ts with both T and P (at P= 8-12 kbar) but decrease with P at P= 12-21 kbar. Glaucofane substitution is strongly dependent on P, being present only at high P and increasing with P (Graham et al., 1989). A marked decrease in the substitution Glaucofane (+ Mg-Riebeckite) - $\text{Ca} + \text{Mg} (\text{NaM4} + (\text{AlVI}, \text{Fe}^{3+}))$ - is observed towards rim in amphiboles from transitional/ leuco- eclogites. This contrasts with a slight increase in this substitution in amphiboles from mafic eclogites. It is possible that this difference in zoning behaviour reflects a difference in timing, with eclogite-facies zoning preserved in "fresh" mafic eclogites (P and T increase during this event) and retrogressive zoning in transitional/ leuco- eclogites with incipient retrogression (drop in P).

Phengite: Phengite is characteristic of the leuco- and quartz-rich eclogites, but minor/trace amounts of it are also found in mafic eclogites. Depending on its abundance in the rock and its habitus (e.g. large parallel oriented laths), it gives a foliation to the rock. In leuco-eclogites, it often forms very fine-grained segregations, together with zoisite + albite + quartz, or is associated with paragonite and clinozoisite in coarser aggregates; both types are pseudomorphs after magmatic plagioclase (Figs. A.5.1 and A.5.2). Available data do not allow to decide whether finer-grained phengite + zoisite + albite + quartz segregations belong to an earlier stage of recrystallization than paragonite + phengite + clinozoisite assemblages, or represent local compositional variations in the rock. Only minor variation in composition is found (Table A5.4). Large phengites from the layered quartz-rich eclogite and the leuco-eclogites and small crystals in both types of segregations have all $\text{Si} = 6.62\text{-}6.88$ atoms per formula unit ("p.f.u", normalized to 22 oxygens) and minor Na substitution (0.07-0.23 p.f.u, higher in leuco-eclogites). $(\text{Mg} + \text{Fe}) = 0.67\text{-}1.09$ atoms p.f.u. always higher than the excess in Si (e.g. Si over 6) confirms that the involved substitution is celadonic (as expected in high-P micas). A slight decrease in Si and Mg + Fe is observed from core to rim. Traces of Ba were recorded in small phengites within pseudomorphs.

Paragonite: Paragonite is found associated with phengite and clinozoisite, forming fine-grained pseudomorphs after plagioclase in partly recrystallized leuco-eclogites (e.g. sample

3/101.9). A minor substitution of K for Na occurs, with K= 0.09-0.11 atoms (p.f.u. on 22 oxygens) (Table A5.4).

Epidote minerals: Clinozoisite/epidote is abundant in the matrix from leuco- eclogites, occasional and minor in the mafic eclogites. It may have been a transient phase in some eclogites where it is found only as minute inclusions within pyrite, garnet or other eclogitic silicates.

The pistacite content ($Ps = Fe^{3+} / (Fe^{3+} + Al)$) of the few analyzed clinozoisites ranges from Ps 14 in mafic eclogites to Ps 22 in leuco-eclogites (matrix crystals, inclusions and associated with paragonite, Table A5.4). In the fine-grained pseudomorphs with albite, quartz and phengite, it is zoisite/clinozoisite (Ps 04).

Clinozoisite remains stable during the first stages of retrogression but it is replaced by epidote (higher birefringence) during the late amphibolite- to greenschist-facies fracturing.

Carbonate: Carbonate is a common minor phase in most eclogites. It may be very abundant in some samples. The eclogite-facies carbonate is a dolomite/ankerite (Table A5.4). It may form segregations together with quartz and rutile (trace of former veins?) or be disseminated within the matrix. Its habitus varies from anhedral dusty inclusions within pyroxene (in some eclogites, its only occurrence) to anhedral matrix crystals, in textural equilibrium with eclogitic silicates (Fig. A.5.5). It often forms large poikilitic crystals. It may be fresh or exhibit a rusty colour; this alteration does not show any obvious correlation with the degree of retrogression of the rock. It is likely that in-situ replacement by secondary carbonate (calcite) occurs in some retrograded samples since carbonate is also common in amphibolites and greenschist-facies veins from this locality.

Quartz: Its abundance ranges from a few disseminated grains (mafic rocks) to deformed ribbons (layered and leucocratic rocks). It is often concentrated along quartz + mica \pm garnet \pm clinozoisite \pm carbonate schlieren. It is a major mineral in eclogitic “gneisses” (some of these “gneisses” are undoubtedly mobilisats or pressure shadows linked to the eclogite-facies shear deformation), where it is associated to clinozoisite, phengite, minor amphibole, carbonate and plagioclase.

Oxides: Eclogite-facies oxides are mainly rutile. Matrix rutile is found as disseminated discrete grains (anhedral, generally (0.5 mm, up to 1 mm in size), small clusters or strings of grains oriented parallel to the foliation (Fig. A.5.4). In fresh eclogites, grains consist generally of (nearly) pure rutile although minor ilmenite (volume ratio $Ilm / (Ilm + Rut) < 5$ to 10%) may be found. In such case, a frequent texture consists of broad lamellae of ilmenite within rutile. This ambiguous texture could be either a primary (eclogitic) or a replacement texture. Rutile also form abundant inclusions within silicate minerals, generally as small euhedral grains of pure rutile. In one mafic eclogite (4/120.9), the abundance of ilmenite compares to that of rutile, forming even single grains; it is probably primary (eclogitic) in this sample.

Secondary transformation of rutile to ilmenite during retrogression is seen as coronas or replacement along fractures (Fig. A.5.13 a and c). Secondary sphene is observed in only a few samples (Fig. A.5.13 b and d).

Sulphides: Pyrite is common in many eclogites, mafic or leucogabbroic, as disseminated subhedral crystals. Textural relationships show that it belongs to the eclogite facies

paragenesis. Some mixed grains of pyrite and minor rutile can also be seen. It often contains inclusions of clinozoisite.

Traces of chalcopyrite (few isolated minute grains) occur in some samples.

Other minerals: Apatite is a common accessory and may be very abundant in some samples, mafic or leucocratic ones.

Allanite is present in trace amounts in some samples, as minute brownish inclusions within eclogitic minerals, e.g. within amphibole where it is easily recognised by its pleochroic halo.

Zircon is a rare accessory mineral observed in some few samples (see chapter on trace element data)

Table A5.5: Temperature estimates on eclogites from Engebøfjellet

Partitioning of Fe ²⁺ and Mg between garnet and clinopyroxene			For P = 15 kbar												
Sample	Min.pair	Comment	Cations p.f.u in Cpx		Cations p.f.u in Gt							Ellis & Green	Krogh	Powell	
			Mg -cpx	Fet -cpx	Mg -gt	Fet -gt	Fe2+ -gt	Mn -gt	Ca -gt	XCaGT	Kd (Fet)	Kd (Fe2+)	T(Fe2+)	T(Fe2+)	T(Fe2+)
E 4/97.3	2.6,2.7	rim	0.47	0.25	0.90	3.74	3.64	0.06	1.42	0.23	7.88	19.84	606.00	554.00	583.00
	2.8,2.9	rim	0.43	0.27	0.89	3.51	3.44	0.07	1.60	0.26	6.11	17.70	680.00	640.00	660.00
	1.3,1.2	Grt core/Cpx incl	0.46	0.28	0.81	3.58	3.49	0.10	1.59	0.26	7.22	14.70	645.00	601.00	623.00
E 3/33.9	2.3,2.4	rim Gt incl/Omph	0.43	0.12	1.42	3.25	3.21	0.07	1.31	0.22	7.94	18.98	591.00	533.00	567.00
	2.8,2.10	rim Gt incl/Omph	0.43	0.12	1.37	3.23	3.19	0.07	1.36	0.23	8.44	13.52	586.00	531.00	563.00
E 3/159.8	2.2,2.3	rim	0.45	0.26	1.15	3.60	3.51	0.07	1.27	0.21	5.48	14.31	667.00	612.00	644.00
	2.8,2.10	rim	0.45	0.24	0.90	3.51	3.45	0.05	1.63	0.27	7.28	25.53	645.00	602.00	624.00
	1.3,1.4	rim	0.46	0.23	0.93	3.65	3.57	0.06	1.46	0.24	7.76	23.34	614.00	564.00	592.00
	1.7,1.8	rim	0.43	0.24	0.94	3.57	3.52	0.06	1.46	0.24	6.75	28.94	643.00	595.00	621.00
E 1/101.9	1.6,1.7	rim	0.35	0.31	0.73	3.80	3.66	0.09	1.49	0.24	5.93	16.71	677.00	633.00	656.00
E 8/229.0	1.4,1.3	rim Gt incl./Omph	0.32	0.36	0.52	4.09	3.93	0.06	1.48	0.24	6.96	40.41	641.00	593.00	619.00
	1.1,1.2	rim Gt incl./Omph	0.34	0.37	0.57	4.04	3.78	0.14	1.45	0.23	6.48	43.04	657.00	608.00	635.00

T estimated assuming Fe³⁺/Fet in Cpx = 0.40 (see text)

5.3. Pressure and temperature estimates for the eclogite-facies event

Although the microprobe study was not designed primarily for thermobarometric study, some inference on the eclogite-facies P and T conditions can be made.

P estimates: The highest jadeite content recorded here in clinopyroxene is found in omphacite from the leuco-eclogite (Jd= ca. 45%, see Table A5.2) where this mineral coexists with quartz. In the absence of coexisting plagioclase, this allows a minimal pressure estimate of ca. 15 kbar assuming $T = 600\text{ }^{\circ}\text{C}$ (Holland, 1980).

The persistence of albite (An 05) in fine-grained pseudomorphs may indicate that P never exceeded 16-17 kbar (for $T = 600\text{ }^{\circ}\text{C}$) although the possibility of disequilibrium breakdown of plagioclase cannot be ruled out.

T estimates: Partitioning of Fe^{2+} and Mg between garnet and clinopyroxene is dependent on temperature. Considering the complex growth zoning of garnet (and erratic zoning in the coexisting clinopyroxene), it is uncertain whether cores of matrix minerals are in equilibrium. Therefore, pairs of rim analyses at stable grain boundaries between garnet and clinopyroxene and one pair Gt “core” + Cpx inclusion have been used. A major problem is the accuracy of Fe^{3+} estimates calculated by charge balance assuming stoichiometry (normalized to 6 oxygens and 4 cations for Cpx, to 24 oxygens and 16 cations for garnet). This results in $\text{Fe}^{3+}/\text{Fe}^{2+}$ in Cpx ranging from 0.33 to 0.89; the higher values corresponding to chloromelanitic pyroxenes from ferro-eclogites are probably unrealistic (see Table A5.2). K_d values and resulting T are strongly dependent on this ratio: calculated T for calibrations used here (Ellis and Green, 1979; Powell, 1985; Krogh, 1988) were inversely correlated to the acmite content in Cpx. In order to estimate T, $\text{Fe}^{3+}/\text{Fe}^{2+} = 0.40$ was assumed for Cpx. For $P = 15$ kbar, T estimates range from 586 to 680 $^{\circ}\text{C}$ (Ellis and Green, 1979), from 563 to 660 $^{\circ}\text{C}$ (Powell, 1985) and from 531 to 640 $^{\circ}\text{C}$ (Krogh, 1988). The pair with garnet core + Cpx inclusion gives $T = 645\text{ }^{\circ}\text{C}$ (Ellis and Green, 1979), 623 $^{\circ}\text{C}$ (Powell, 1985) or 601 $^{\circ}\text{C}$ (Krogh, 1988) (Table A5.5). The spreading in calculated T and the uncertainties on the actual $\text{Fe}^{3+}/\text{Fe}^{2+}$ ratio do not allow a precise estimate, but T around or slightly above 600 $^{\circ}\text{C}$ seems likely during eclogitisation.

Krogh (1980) estimated P and T conditions of $540 \pm 35\text{ }^{\circ}\text{C}$ and 12.5 ± 2.5 kbar for the Kvineset eclogite, further east along Fordefjord, and of $630 \pm 35\text{ }^{\circ}\text{C}$ and 15 ± 2.5 kbar for the very similar Naustdal eclogite, located ca. 20 km to the east of Engebøfjellet.

5.4. Retrogressive reaction textures

Many of the studied eclogites are unaltered or show only trace of retrogression, limited to incipient symplectitic breakdown of omphacite rims. Minor to extensive retrogression corresponds to the progressive development of kelyphite around garnet and symplectitic breakdown of omphacite and phengite. Eclogite-facies amphibole generally remains stable but re-equilibrates at the rim to a green-blue amphibole. Frozen-in stages of reaction are observed in rocks where retrogression remained static (coronitic and symplectitic). Within a sample, the coronitic retrogression can be pervasive or limited to areas adjacent to late fractures. The degree of reaction depends on the amount of fluid present, either released by dehydration breakdown of eclogitic silicates or externally derived. The persistence of fresh amphibole- and mica- rich eclogites alongside their retrograded equivalents demonstrates that

at least some externally derived fluid is necessary to induce retrogression - even when dehydration reactions take place. The overall good preservation of these eclogites rich in eclogitic volatile-bearing minerals (amphibole, mica, clinozoisite/epidote) makes it likely that continued infiltration of fluid is required to drive further the process. The coronitic retrogression eventually reaches a stage where the mineral assemblages belong principally to amphibolite-facies (green hornblende + plagioclase + epidote \pm biotite \pm relict garnet \pm carbonate) although the eclogitic texture may still be seen ("ghost" texture preserved by in situ symplectitic replacement). Complete textural and mineralogical re-equilibration requires in addition deformation and leads here to amphibolites (D3 and D4 stages, see structural chapter). Re-equilibrated amphibolites within shear-zones have not been studied.

Fractures cutting the eclogites belong to the late D5 and D6 brittle deformation events. These fractures acted as channelways for fluid infiltration, promoting in different degrees the alteration of the wall-rock (Fig. A.5.6). Larger veins are filled by variable amounts of albitic plagioclase, quartz, actinolite, epidote, magnetite, ilmenite, chlorite, calcite and sphene (rare). These mineral assemblages indicate P-T conditions compatible with epidote-amphibolite or greenschist facies.

The extent of alteration along late fractures/veins correlates generally with the thickness of these fractures (Fig. A.5.6). Thin fractures lead most often to limited cryptocrystalline alteration of minerals in the wall-rock eclogite. Similarly, veins filled solely by carbonate do not generally induce significant retrogression of the wall-rock. Within a single sample, veins, parallel or not, can have different fillings. This could reflect different generations of fractures (see structural study) or alternatively the presence of several contemporaneous sets channelling fluids of different composition.

In the following, observed reaction textures are described. Our purpose was solely to complete the mineralogical description of Engebøfjellet by including the secondary minerals. Neither a discussion of reaction mechanisms and timing nor P-T estimates for the retrogression path will be presented.

Garnet breakdown: Garnet breakdown generally starts along rim and fractures with crystallization of a bluish green amphibole. At a more advanced reaction stage, the texture evolves inwards to a radiating intergrowth of amphibole + plagioclase \pm magnetite \pm epidote (kelyphite). Variations in texture, mode and mineralogy of the kelyphite are observed, depending on bulk and local composition (i.e. composition of garnet and adjacent minerals) and reaction site (corona around, or fractures within garnet). The presence of epidote seems to characterize transitional/ felsic rocks. Magnetite is often present, either disseminated in the kelyphite already at an early stage (and typically within garnet fractures) or appearing first at an advanced stage adjacent to garnet (earlier and more abundant where Alm component in garnet is higher?). Within fractures, zonation is also present: the central part consists of amphibole and frequently magnetite, as minute vermicular or euhedral crystals, bordered on both sides by symplectites of amphibole + plagioclase.

Some leuco- and layered eclogites contain kelyphites of biotite + epidote + plagioclase + magnetite (Fig. A.5.11). The biotite, pleochroic from green to brown, may also form the external corona. Local factors (local chemistry, diffusion) control this reaction: other garnets from the same sample form kelyphite with amphibole + epidote + plagioclase.

In totally amphibolitized eclogites, "round" pseudomorphs with amphibole, plagioclase, epidote and biotite may indicate the location of former garnets.

Garnet cut by late fractures (D5) is often replaced in-situ by epidote.

Omphacite breakdown: Incipient breakdown of the eclogitic pyroxene is marked by alteration along rim and fractures to cryptocrystalline greyish symplectites (Ex: Figs. A.5.3 and A.5.12). More advanced retrogression is marked by progressive replacement of omphacite and increase in grain size of the symplectite. Hydration is the rule; coarser symplectites are formed by amphibole + plagioclase \pm clinopyroxene (Figs. A.5.11 and A.5.13b). Complete amphibolitisation leads to a “coarse” symplectite matrix consisting mainly of green hornblende, plagioclase and epidote (Fig. A.5.13a).

Garnet and omphacite breakdown proceeds generally at the same rate, at least in mafic eclogites. Some leuco- /layered eclogites show a more or less complete replacement of omphacite (higher Jd) by microcrystalline symplectites of amphibole + plagioclase \pm diopside while other eclogitic minerals (including garnet) remain largely unaltered.

Phengite breakdown: Incipient breakdown is marked by a symplectitic rim of microcrystalline biotite and plagioclase (Fig. A.5.11). Advanced retrogression leads to a more or less complete replacement by coarse-grained symplectites of biotite + plagioclase \pm epidote (epidote present only at very advanced stages or only in some samples?). The crystal orientation of the biotite II often follows that of the parent phengite. An outer corona of plagioclase separates the symplectite from quartz.

In quartz-rich layers, phengite may be zoned to biotite (pleochroic rim from light brown to colourless) when adjacent to garnet.

Amphibole zoning and breakdown: Minor retrogression of the rock corresponds to a rim zoning of the amphibole. Its colour changes from blue-grey to blue green or green (Fig. A.5.12). With increasing retrogression, zoning gradually extends to the whole amphibole and rim breakdown to symplectites of green amphibole + plagioclase may be seen.

Clinozoisite zoning: Breakdown of clinozoisite was not observed during coronitic retrogression, but zoning to epidote occurs along fractures and rim.

Carbonate alteration: Alteration of dolomite does not strictly correlate with the degree of retrogression of the rock. The carbonate may remain apparently unaltered in eclogites with minor retrogression. Conversely, in fresh eclogites, dolomite may be cloudy or display rim alteration to a brownish micaceous assemblage. Intergrowths of calcite + minor talc associated to clusters and coronas of green biotite may be found as replacement of dolomite in extensively retrograded quartz- and carbonate-rich layered eclogites. In late veins, carbonate is calcite.

5.5. Secondary minerals

Amphibole II: The kelyphitic and symplectitic amphiboles are green magnesio-hornblendes. In the late veins, the pale green and fibrose amphibole is an actinolite.

Plagioclase: It is found within symplectites after omphacite and phengite and in kelyphite around garnet. Microprobe EDS spectra indicate that it is a Na-Ca plagioclase. It differs in composition from a reaction site to another. Within a reaction site, zoning of plagioclase in response to the diffusion gradient is also observed. Only few analyses are available, unlikely to encompass all possible compositions. In one symplectite after phengite, plagioclase is an

oligoclase An 22 to 28; in the same sample, plagioclase in a garnet kelyphite ranges in composition from An 03 to An 34.

The plagioclase in the late greenschist-facies veins is an albite An 04.

Epidote II: In eclogites showing minor to extensive retrogression, small anhedral grains are found within symplectites after phengite or, in some few samples, in kelyphite around garnet. In strongly amphibolitized rocks, it is common within pseudomorphs after garnet and phengite or as disseminated anhedral grains in the symplectitic matrix. It also crystallizes within late fractures, as new subhedral to anhedral crystals or as in-situ replacement of clinozoisite and garnet cut by these fractures. The few available analyses show that the composition of kelyphitic epidote II lies around Ps 26. The yellow epidote from the late veins is Ps 31-38.

Transformation of rutile to ilmenite II and sphene:

The abundance of ilmenite relative to rutile remains (10% (volume ratio Ilm/Ilm + Rut, visual estimate) in eclogites showing only minor retrogression. In extensively retrograded eclogites, it ranges from ca. 20% to more than 95% (totally amphibolitised samples, Ex: Fig. A.5.13a). Replacement occurs along fractures or as coronas. Rutile cut by late fractures (D5) is systematically replaced, albeit often only partially, by ilmenite (Fig. A.5.13c). A few exceptions involve direct replacement by sphene.

Sphene is a rare secondary mineral in these eclogites. It is found either as coronas around rutile/ ilmenite grains (most often within symplectites of amphibole and plagioclase) or as subhedral crystals within a few late veins (Figs. A.5.13b and d).

Magnetite II: It forms minute crystals within kelyphites and symplectites. Its abundance seems largely determined by the Fe/Fe+Mg ratio of the reactant mineral. For example, it is particularly abundant in the mafic/transitional eclogite E8/229.0 (Fig. A.5.12) and the layered eclogite E1/164.2 (Fig. A.5.11) containing some of the most Fe-rich garnets recorded (Alm 63.7-65.5 and Alm 61.1-64.5 respectively, Table A5.1).

Biotite II: It is mainly a breakdown product after phengite. Small crystals, pleochroic from green to beige, are also present within kelyphite around garnet, associated to epidote, plagioclase and magnetite in some samples. Biotite is found as small crystals in symplectitic matrix and within garnet pseudomorphs in strongly amphibolitized rocks.

Chlorite: Within late veins in a few samples, green chlorite with anomalous birefringence forms spherulitic clusters. It is also found as in-situ replacement of garnet in the adjacent wall-rock. Chlorite clusters present in some few amphibolites may represent garnet pseudomorphs (rare in the studied samples).

Green chlorite is also present in variable amounts in eclogitic “gneisses” (as late alteration?).

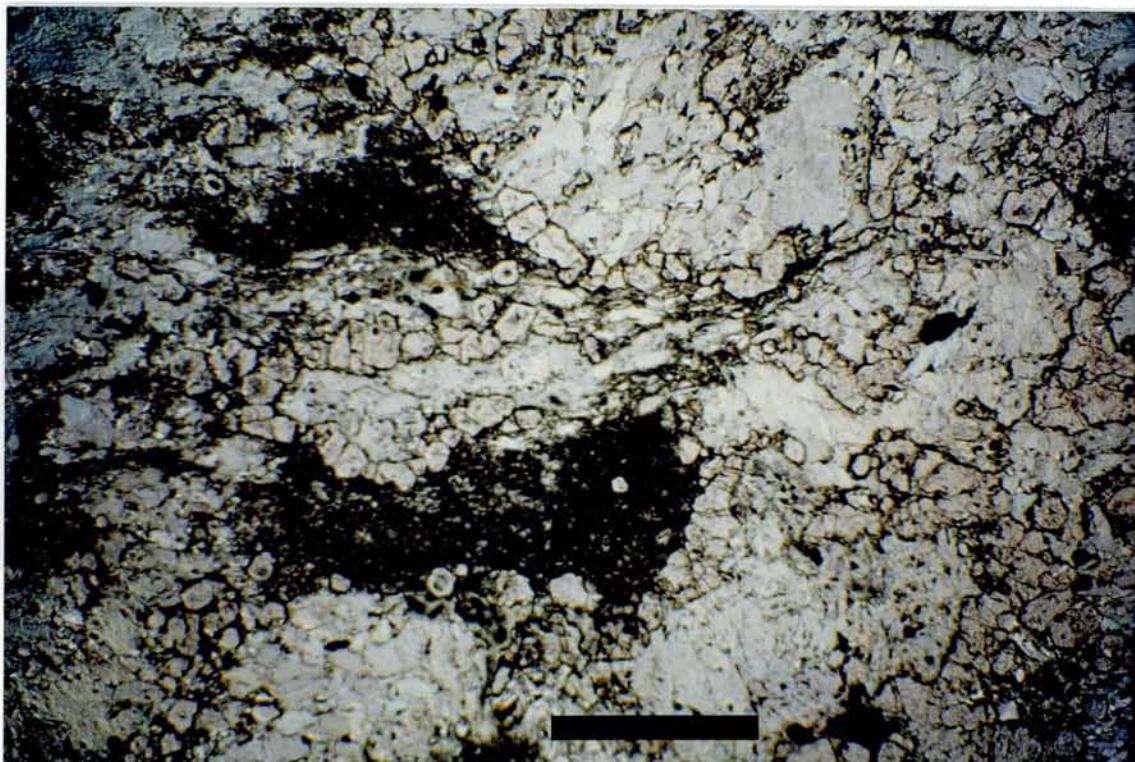


Fig. A.5.1 : Coronitic texture in massive leuco- eclogite (= pseudomorphosis of the gabbroic texture). Mineralogy is eclogitic. Coronas of garnet divide mafic domains with granuloblastic clinopyroxene and amphibole (light grey-green) from extremely fine-grained felsic domains (dark grey) composed of clinozoisite + phengite + quartz + albite (former plagioclase). Microphotograph (polarized transmitted light). Scale bar = 1 mm. Sample ME 39/96.

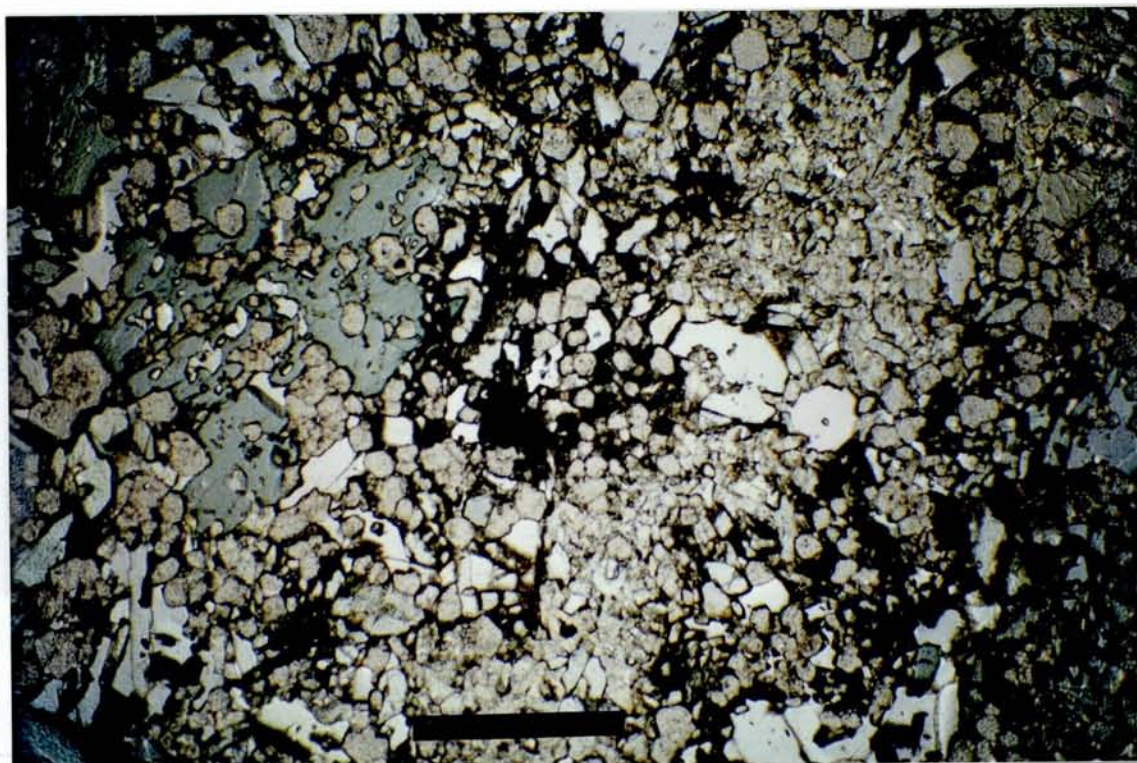


Fig. A.5.2 : Partly recrystallized leuco- eclogite showing persistence of granular domains of small clinozoisite + phengite \pm paragonite. Intermediate stage between coronitic eclogite (Fig. A.5.1) and texturally equilibrated eclogite. Other minerals are small euhedral garnet, matrix phengite, quartz and amphibole (blue porphyroblast). Sample: E 4/35.9. Microphotograph (polarized transmitted light). Scale as on Fig A.5.1



Fig. A.5.3 : Recrystallized leuco-eclogite. "Late" omphacite (Jd 45) porphyroblasts with no preferred orientation postdate the D1 eclogitic texture, with phengite (F1 foliation), small euhedral garnet, amphibole (grey-green), clinozoisite, quartz, rutile \pm ilmenite II, pyrite and traces of dolomite. Incipient retrogression marked by cryptocrystalline symplectites (dark grey) around omphacite. Sample E3/33.9. Microphotograph (polarized transmitted light). Scale bar = 1 mm.

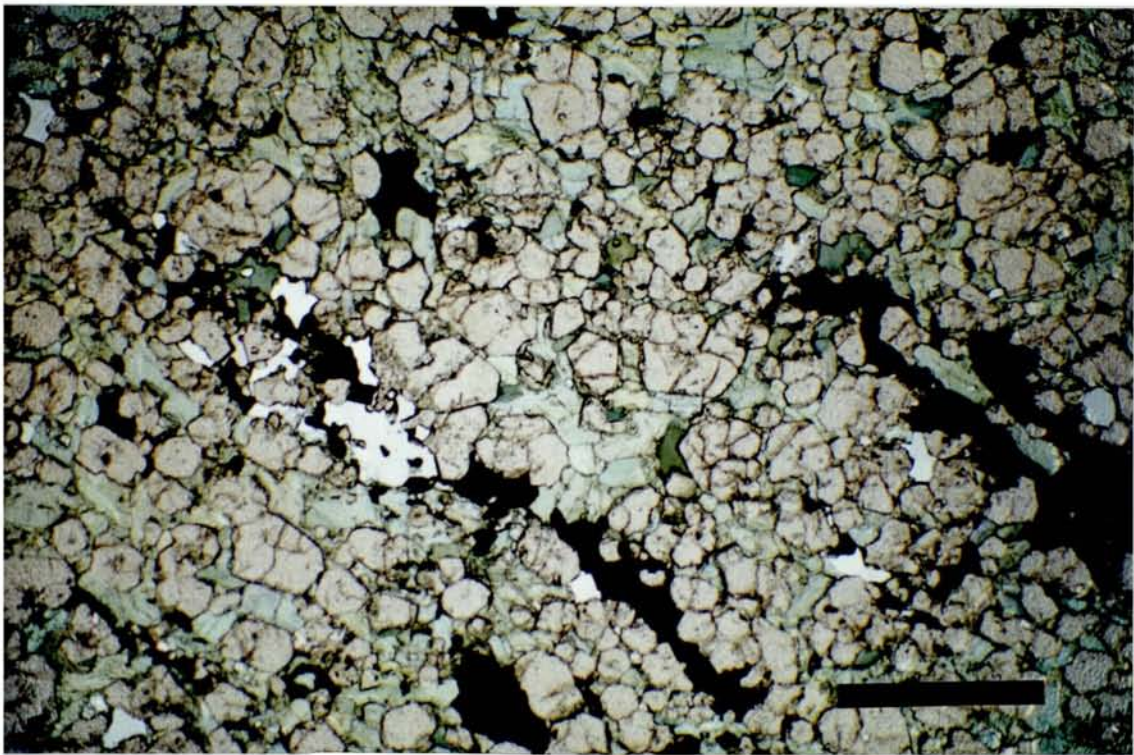


Fig. A.5.4 : Recrystallized mafic eclogite (eclogite mylonite). Granuloblastic texture with omphacite (medium green), minor amphibole (darker green) and quartz (white). Grain size ((0.5 mm) representative for mafic eclogites from Engebøfjellet. Strings of oxides (rutile, minor ilmenite; dark) indicate strong deformation (of a former magmatic ilmenite?) prior to recrystallization. Sample E4/79.9. Microphotograph (polarized transmitted light). Scale as on Fig A.5.3.

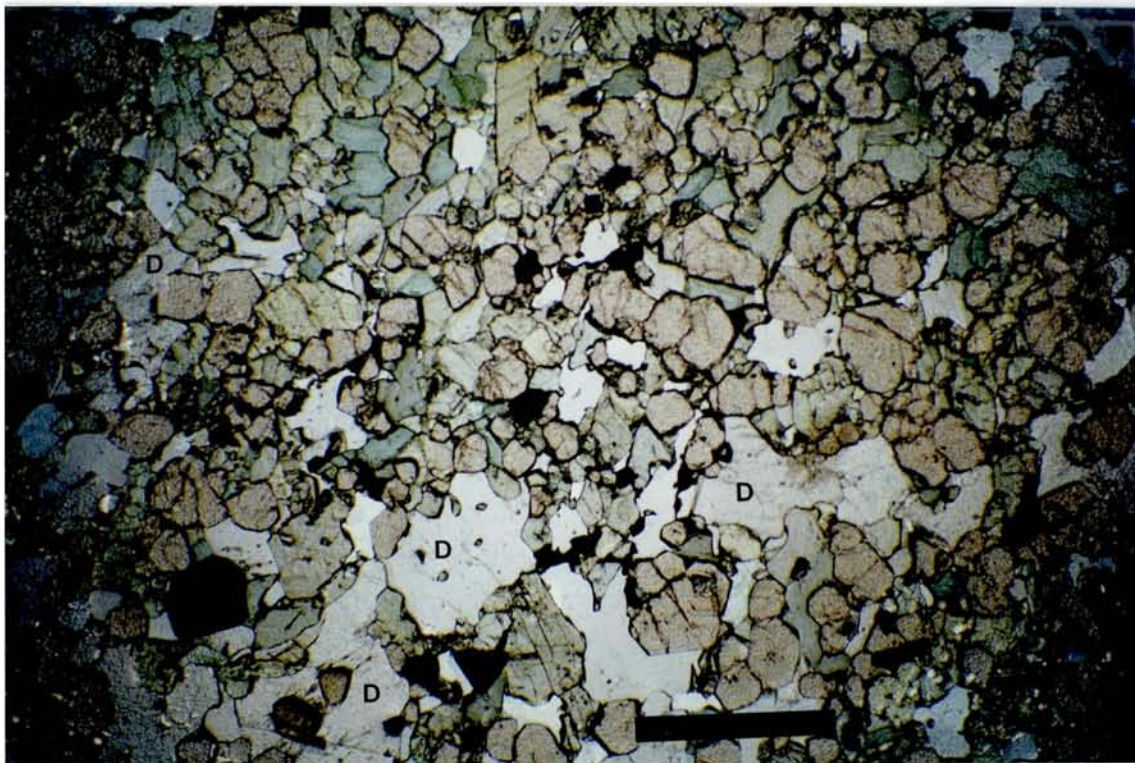


Fig. A.5.5 : Carbonate-rich eclogite showing textural equilibrium between garnet, omphacite, amphibole, dolomite (D), polycrystalline quartz areas, rutile and pyrite (black). Sample E3/146.9. Microphotograph (polarized transmitted light). Scale bar = 1 mm.

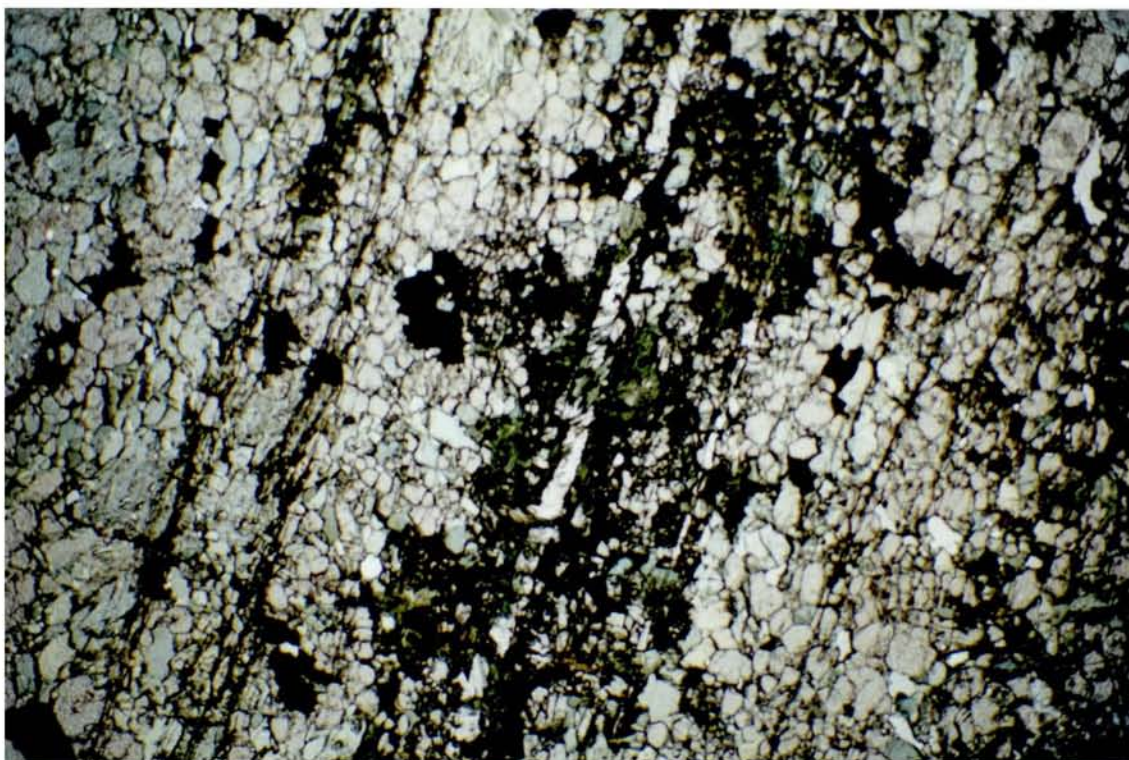


Fig. A.5.6 : Microphotograph showing retrograde alteration of the wall-rock (replacement by dark green actinolite/hornblende) adjacent to late fractures. Away from the fractures, the eclogite remains unaltered. Vein filling consists of epidote, actinolite, albite, quartz, chlorite, calcite, ilmenite \pm sphene (see Fig. A.5.13 c and d) indicating Ep-amphibolite- to greenschist facies conditions. Ferro- eclogite E7/074.0. Scale as on Fig A.5.5.

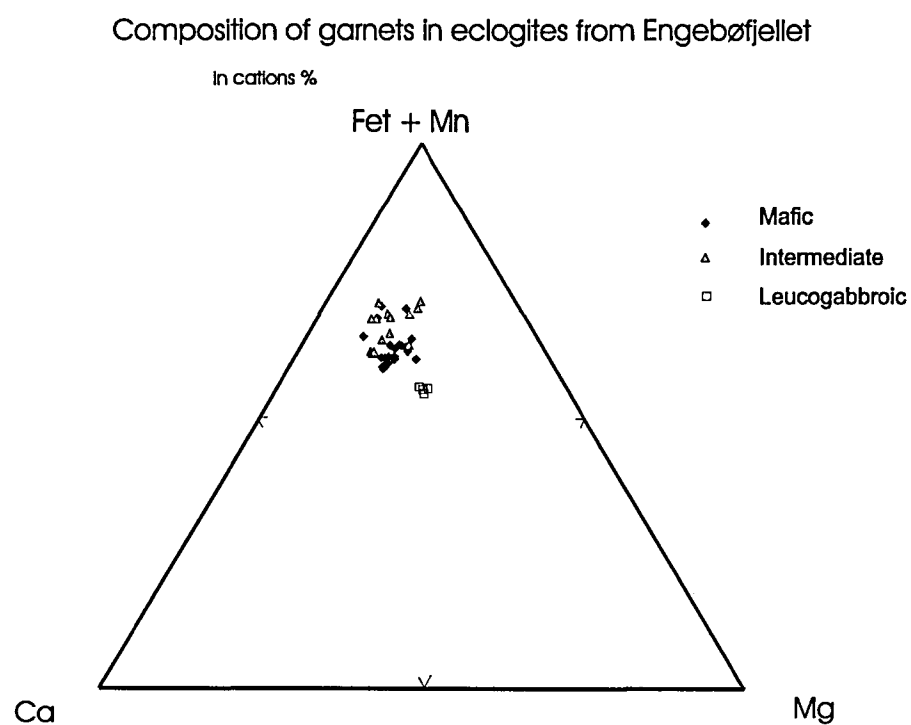


Fig. A.5.7 : Compositions of garnets in eclogites from Engebøfjellet, in atomic proportions of Fet+Mn, Mg and Ca. See table A5.1 for calculation of end-members Alm, Pyr, Spe, Gro and And. Symbols: ferro- (black diamonds), transitional (open triangles), leuco- (open squares) and light layered eclogites (open circles).

Ferrogabbroic eclogite E4/130.3

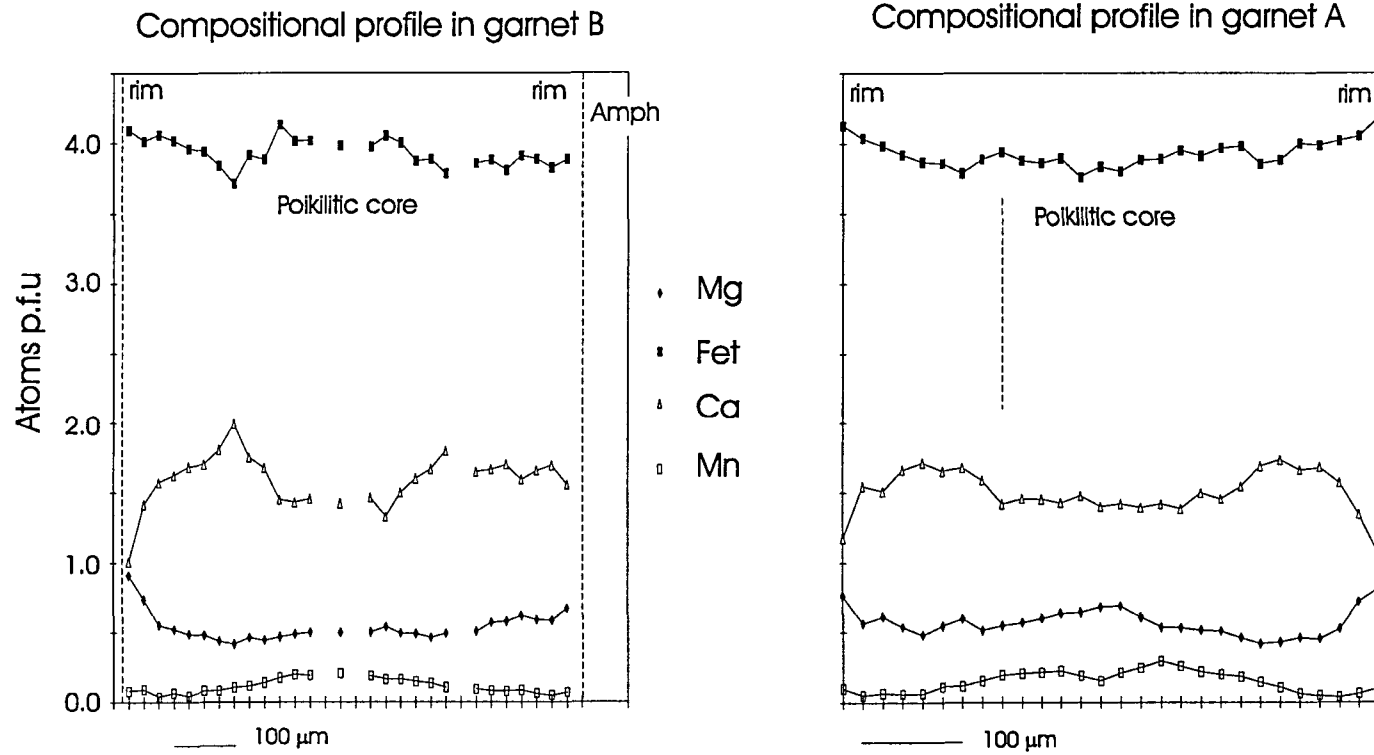


Fig. A.5.8 : Compositional profiles in two garnets with poikilitic cores from the ferro-eclogite E 4/130.3. Variations in Fet, Mg, Mn and Ca atoms p.f.u normalized to 24 oxygens.

Classification of amphiboles from Engebøfjellet

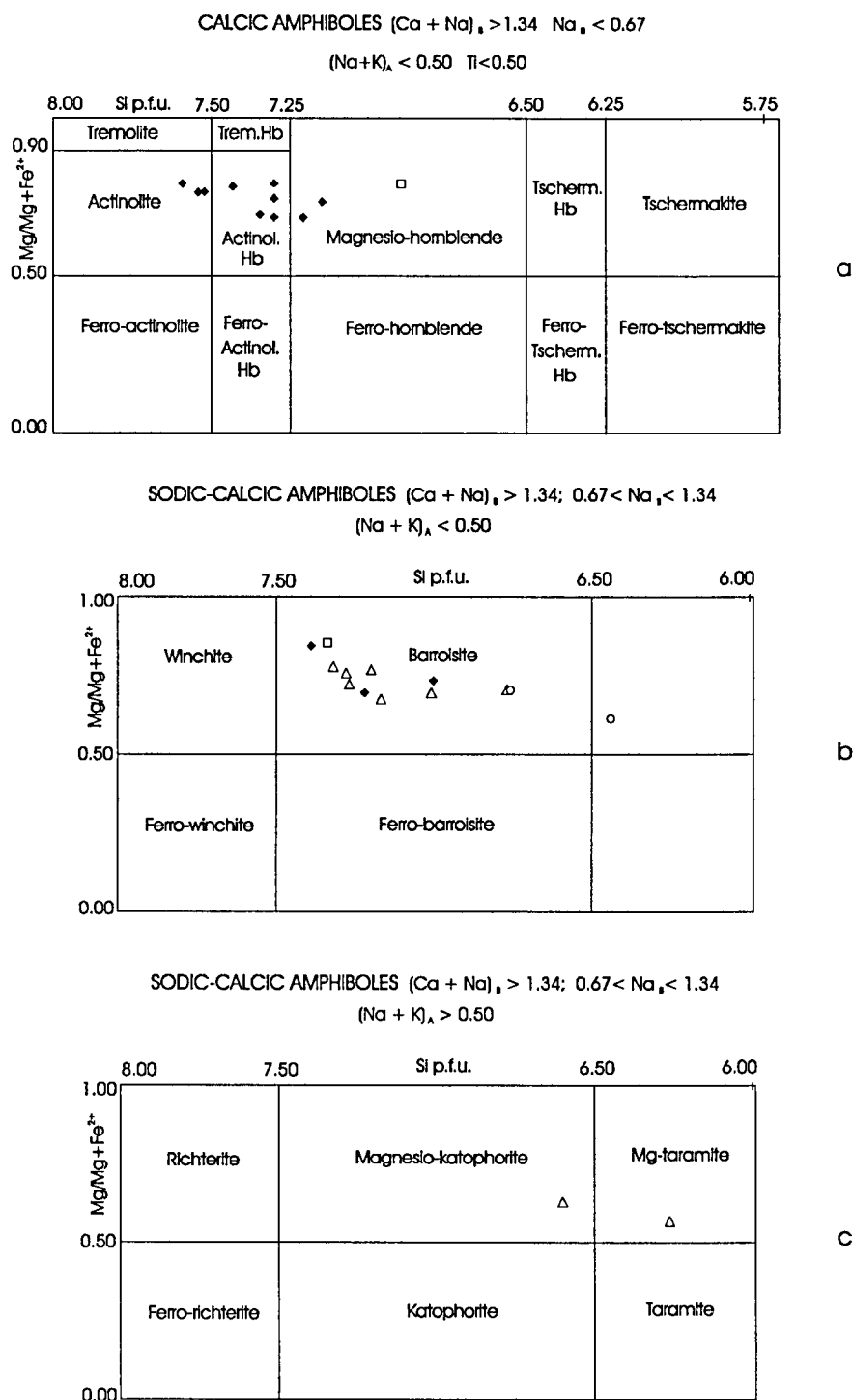


Fig. A.5.9 : Compositions of eclogite-facies amphiboles from Engebøfjellet (nomenclature: Leake, 1978). Structural formula of amphiboles normalized to sum cations exclusive of $Ca + Na + K = 13$ (leading to maximal Fe^{3+} , Al^{IV} and Na_{MA} estimates). Symbols: ferro- (black diamonds), intermediate (open triangles), leuco- (open squares) and light layered eclogites (open circles). Amphiboles in ferro-eclogites are mainly subcalcic actinolitic hornblendes (a), zoned towards rim to barroisite (b); in intermediate, layered and leuco- eclogites, amphiboles are sodic-calcic, mainly barroisitic (b and c), with rim zoning to magnesio-hornblende

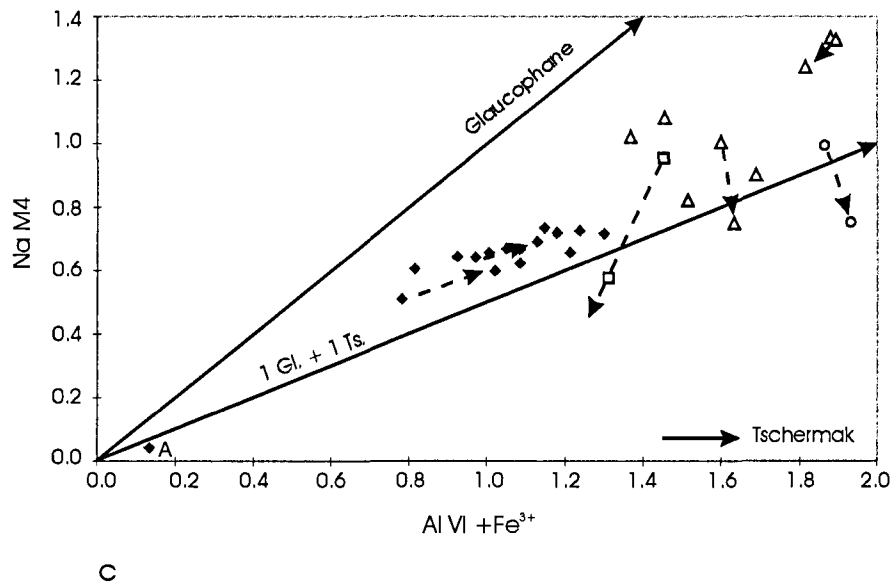
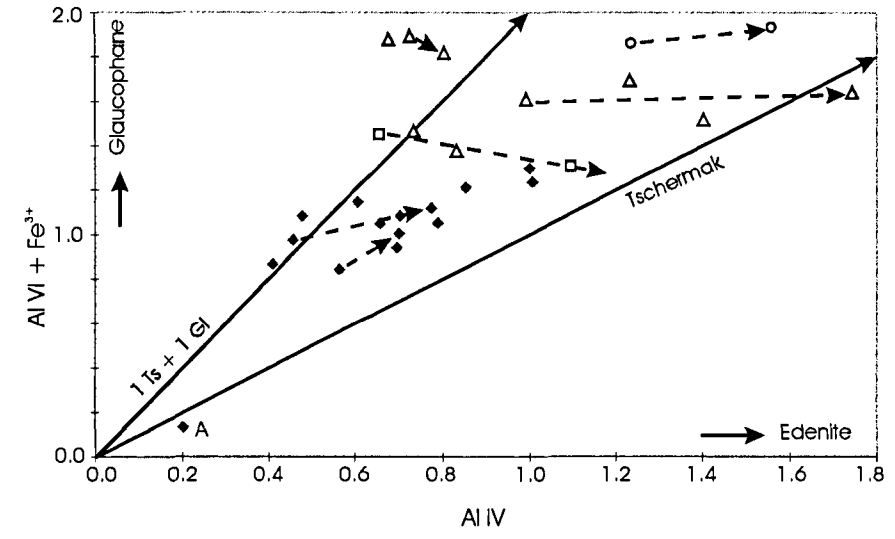
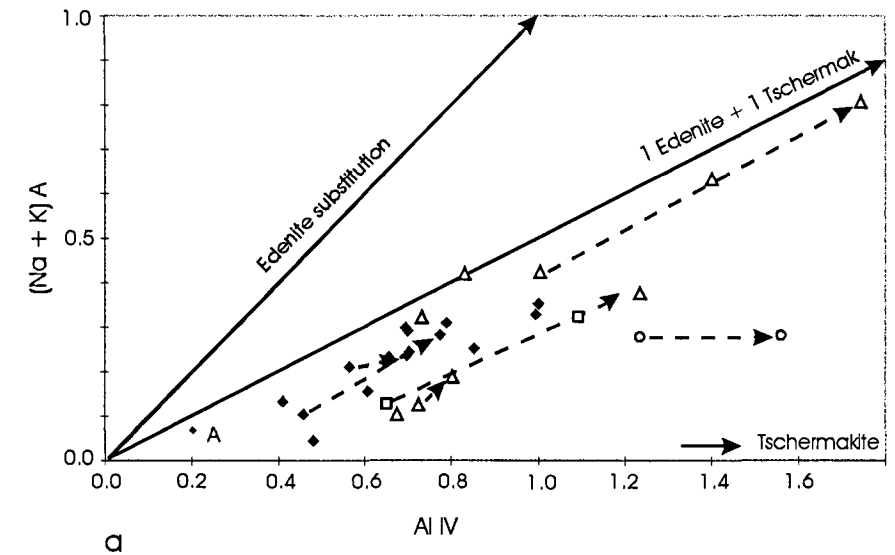


Fig. A5.10: Substitutions in eclogitic amphiboles. Same symbols as in Fig. A5.9; A= actinolite in late fractures; stippled arrows from core to rim analyses within a single crystal; plain arrows indicate variation trend for each of the 3 substitutions: Edenite (Ed), Tschermak (Ts; + ferri-tschermak) and Glaucofane (Gl; + Mg-riebeckite), see text. (a) (Na,K) in site A vs Al IV: most amphiboles show higher substitutions in Ts than in Ed. Variations from core to rim correspond to increase in substitutions Ed and Ts in amphiboles from all groups except layered eclogite (retrograde zoning? see text) - (b) Al VI + Fe³⁺ vs Al IV - (c) Na M4 vs Al VI + Fe³⁺ shows a notable Gl (+ Mg-riebeckite) component in these high-pressure amphiboles (filling of site M4 by Na ranges from ca. 25 to 70%). Mafic eclogites show an increase in Gl substitution from core to rim (P increase during eclogite-facies? see text) while the other eclogite types show a marked decrease in Gl (retrograde zoning?).



Fig. A.5.11 : Extensive symplectitic breakdown in layered eclogite E1/164.2. Microphotograph (polarized transmitted light). Matrix omphacite is replaced by microcrystalline amphibole + plagioclase symplectites (dark green). Kelyphite around garnet consists of biotite, epidote, plagioclase and magnetite. Phengite is rimmed by symplectites of biotite + plagioclase (within quartz area, middle of picture). Scale bar = 1 mm.

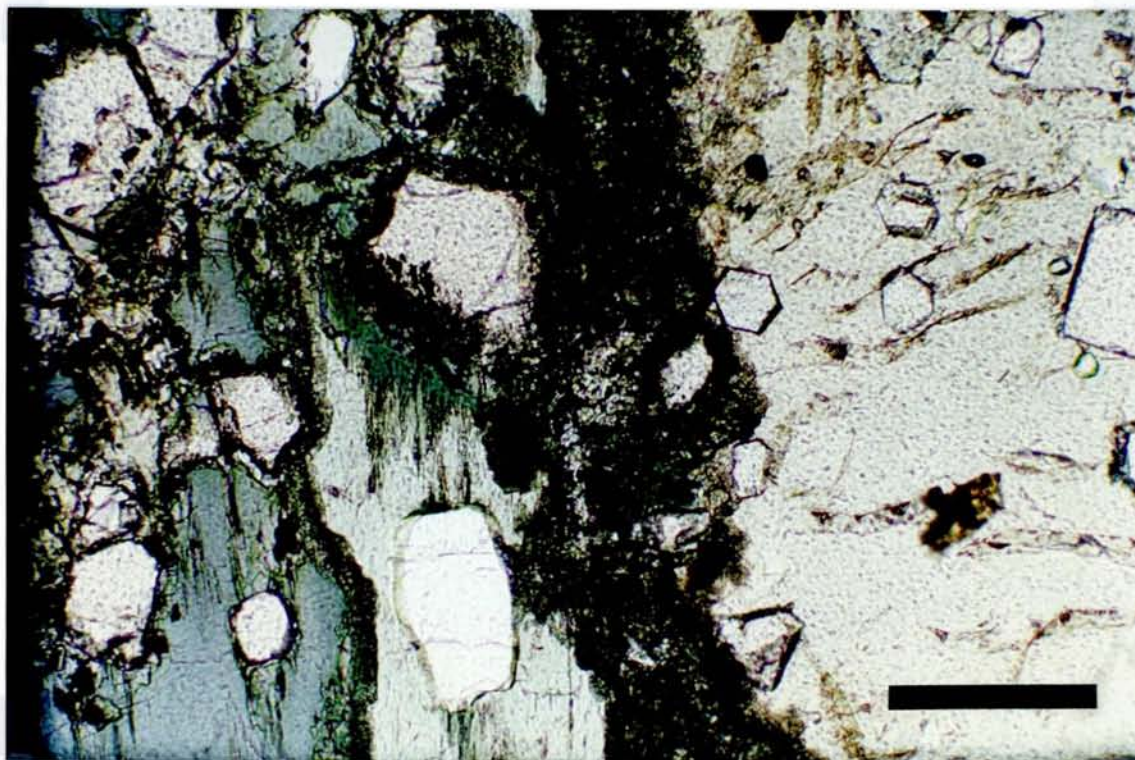


Fig. A.5.12 : Microphotograph of transitional eclogite E8/229.0 showing incipient retrogression along grain boundaries. Secondary magnetite (vermicular to small subhedral grains, black) within symplectites around omphacite (light green, with euhedral garnet inclusions) and amphibole (blue) porphyroblasts, and within kelyphite, adjacent to garnet. Magnetite II is particularly abundant in this sample with high Fe/Mg ratio in garnet. Scale bar = 0.25 mm.

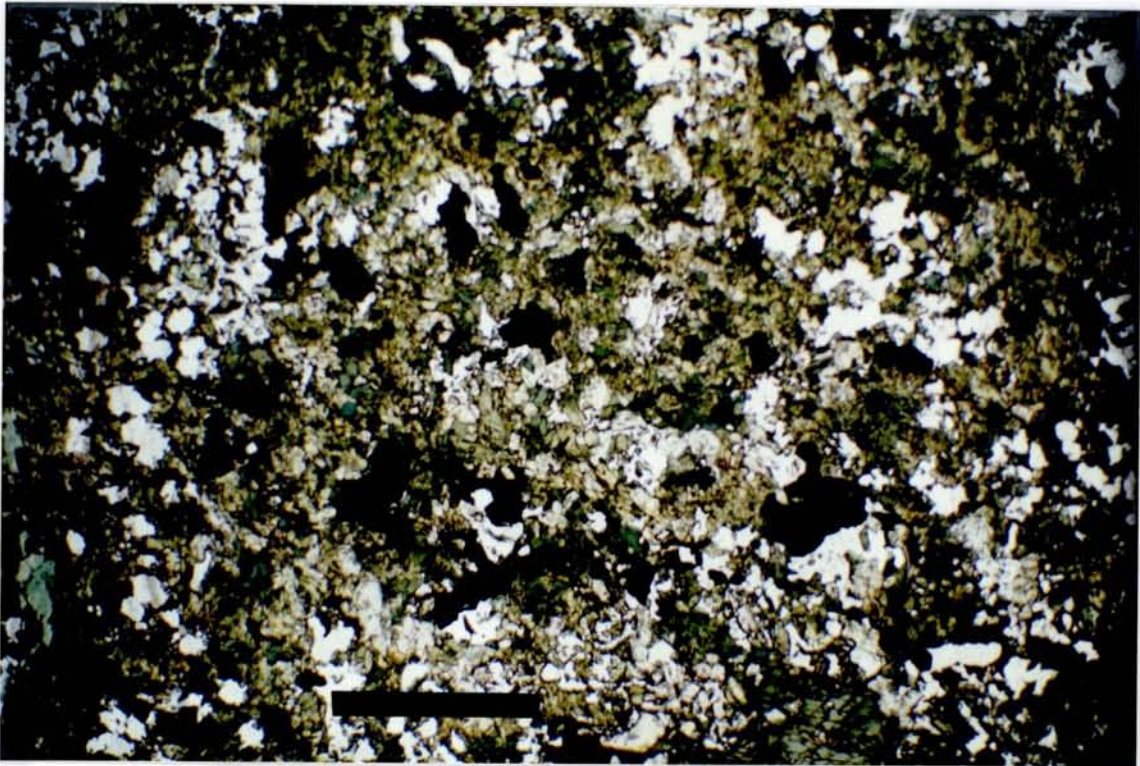


Fig. A.5.13a : See text below

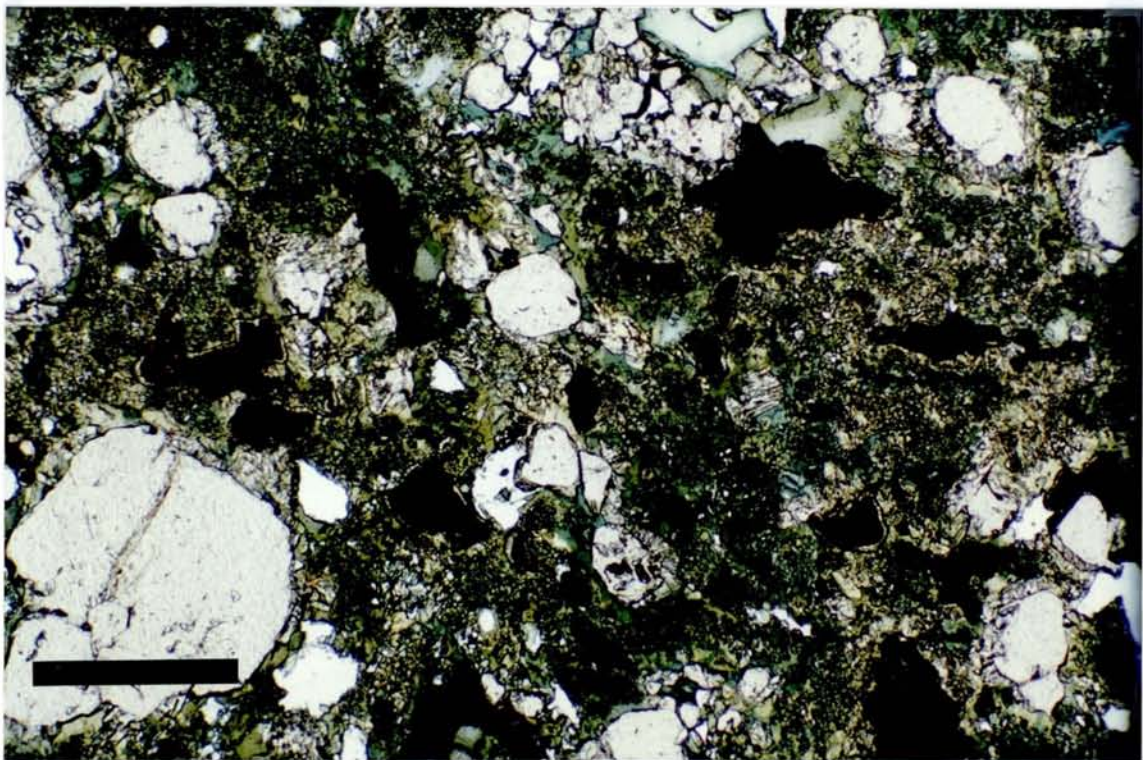


Fig. A.5.13b : See text below

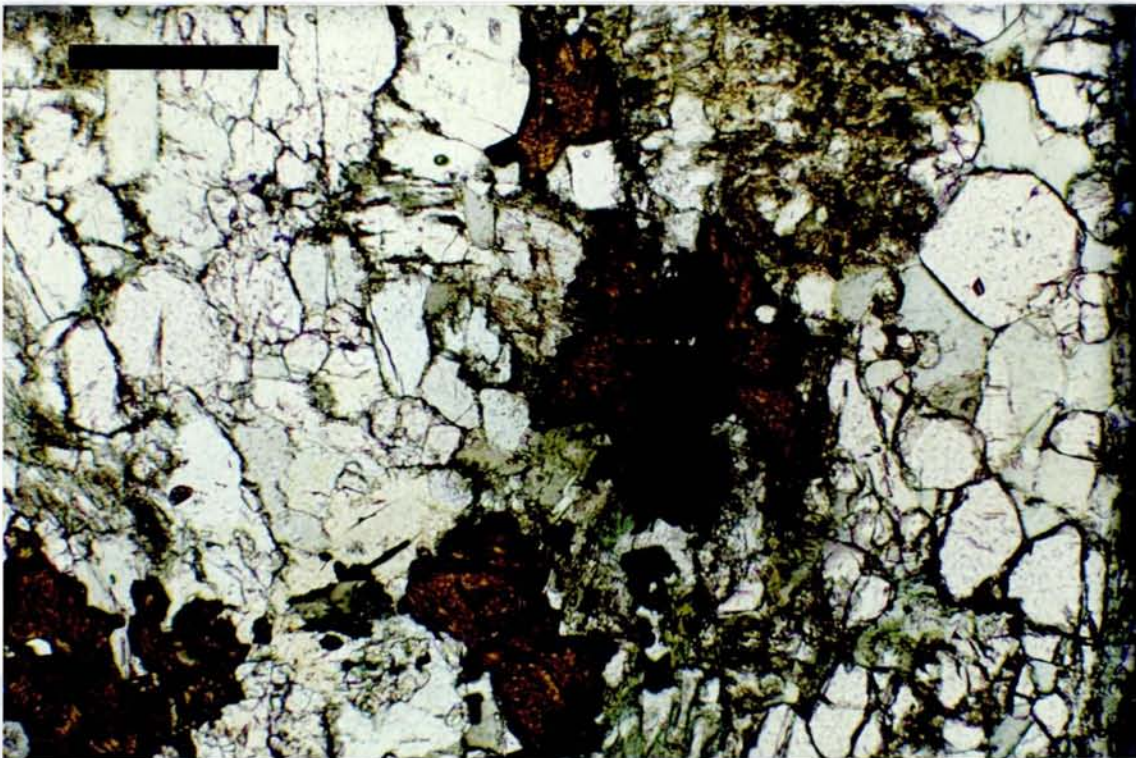


Fig. A.5.13c : See text below



Fig. A.5.13 : Retrogressive textures of Ti-oxides. (a) Ilmenite corona around rutile in amphibolitised eclogite; replacement of rutile is partial to complete in this sample. Static retrogression: eclogitic minerals have been replaced by a fine-grained matrix of amphibole + plagioclase + epidote. Sample E4/81.9. Scale bar = 1 mm - (b) Sphene corona (thin beige rim) around rutile/ilmenite grains embedded within a symplectitic matrix of amphibole + plagioclase. Towards garnet, sphene corona is less developed or missing. Sphene is a rare mineral in Engebøfjellet eclogites. Extensively retrograded sample E4/72.9. Scale bar = 0.5 mm - (c) Partial replacement of rutile by ilmenite II along late fractures. Sample E7/074.0. Scale bar = 0.25 mm - (d) Sphene crystallization (beige with euhedral crystal faces) upon wall-rock rutile cut by a late vein. In the adjacent wall-rock, rutile is rimmed by ilmenite II. Sample E7/074.0. Scale bar = 0.25 mm.

Appendix 6

Miscellaneous plots of analytical data

By Are Korneliussen

CONTENTS

	page
Fig.A6.1: Fe ₂ O ₃ -TiO ₂ plot of X-Met core analyses of leuco-, transitional- and ferro eclogites	2
Fig.A6.2: Fe ₂ O ₃ -TiO ₂ plot of X-Met core analyses of leuco eclogites	3
Fig.A6.3: Fe ₂ O ₃ -TiO ₂ plot of X-Met core analyses of transitional eclogites	4
Fig.A6.4: Fe ₂ O ₃ -TiO ₂ plot of X-Met core analyses of ferro eclogites	5
Fig.A6.5: Fe ₂ O ₃ -TiO ₂ plot of X-Met core analyses of amphibolite unit rocks	6
Fig.A6.6: Fe ₂ O ₃ -TiO ₂ plot of X-Met core analyses of amphibolites	7
Fig.A6.7: Fe ₂ O ₃ -TiO ₂ plot of X-Met core analyses of garnet amphibolites	8
Fig.A6.8: Fe ₂ O ₃ vs. TiO ₂ , P ₂ O ₅ , La and Zr for core samples analysed by XRF	9
Fig.A6.9: Fe/Mg vs. TiO ₂ , P ₂ O ₅ , La and Zr for core samples analysed by XRF ...	10
Fig.A6.10: Zr - Y*3 - Ti/100 triangular diagram, Engebøfjell core samples	11
Fig.A6.11: Chondrite normalised REE-patterns for Engebøfjell core samples	12

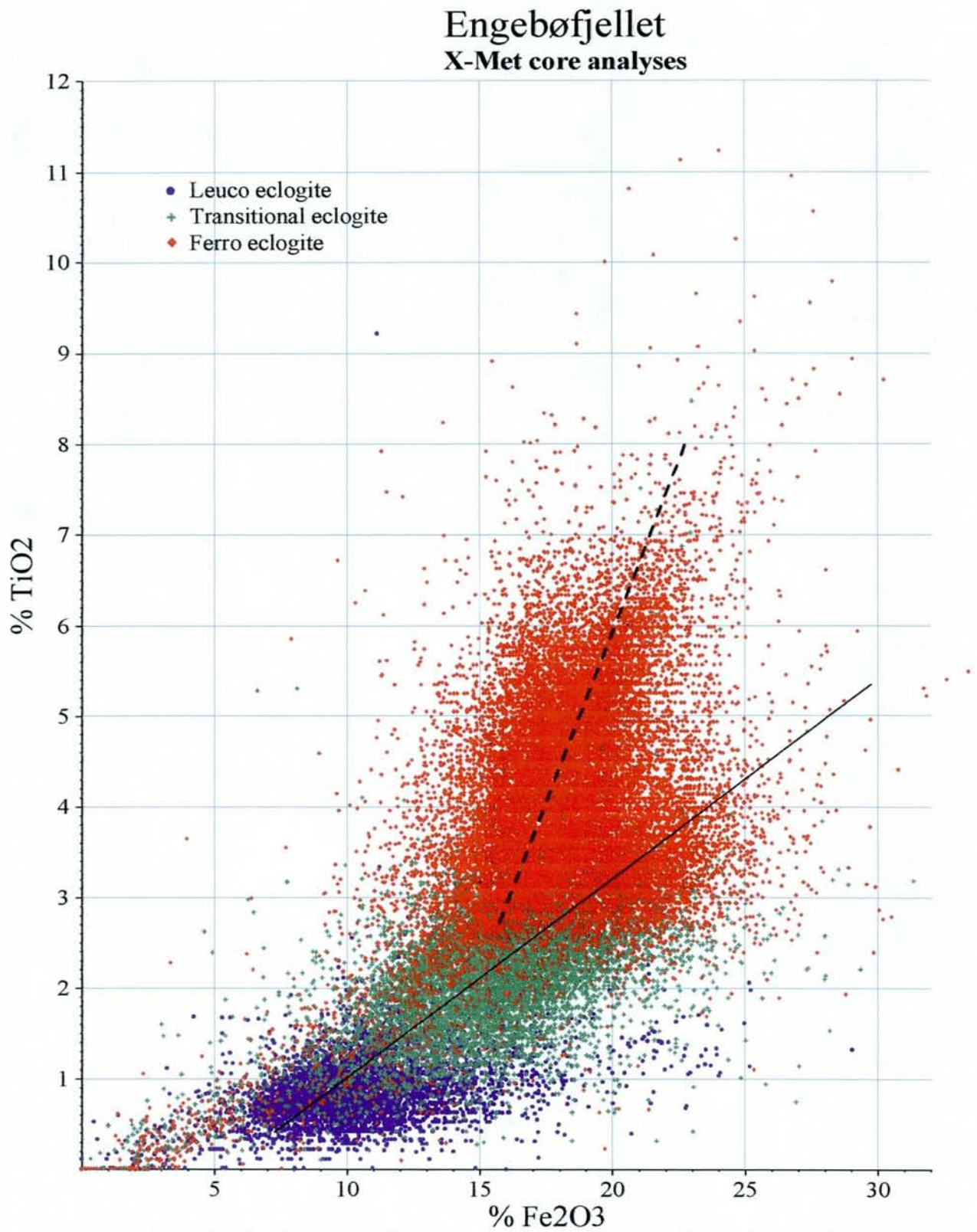


Fig. A6.1: Fe₂O₃ -TiO₂ plot of X-Met core analyses of core sections defined as leuco eclogite, transitional eclogite and ferro eclogite, based on data from the corelog database (Englog.mdb). The plot contains approx. 40.000 points. The solid line indicates the «normal» Fe₂O₃ -TiO₂ enrichment trend; the dashed line indicates the TiO₂-rich trend for the ferro eclogite.

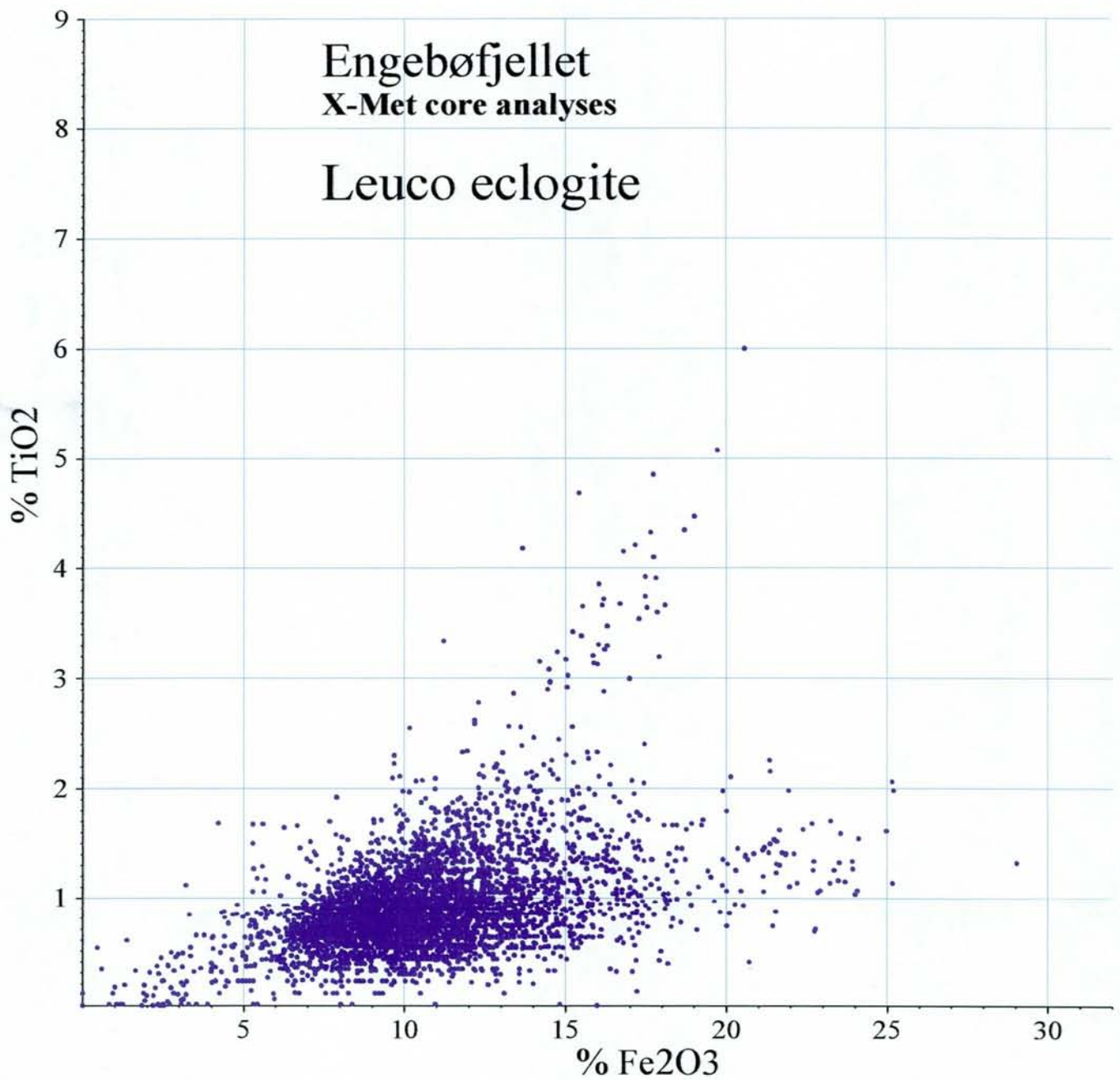


Fig. A6.2: Fe_2O_3 - TiO_2 plot of core analyses done by the X-Met portable XRF instrument directly on cores defined as leuco eclogite. The plot is based on data from the corelog database (Englog.mdb). Samples with relatively high Fe_2O_3 or TiO_2 values are caused by small-scale inhomogeneities in Fe_2O_3 - TiO_2 contents in the leuco eclogite.

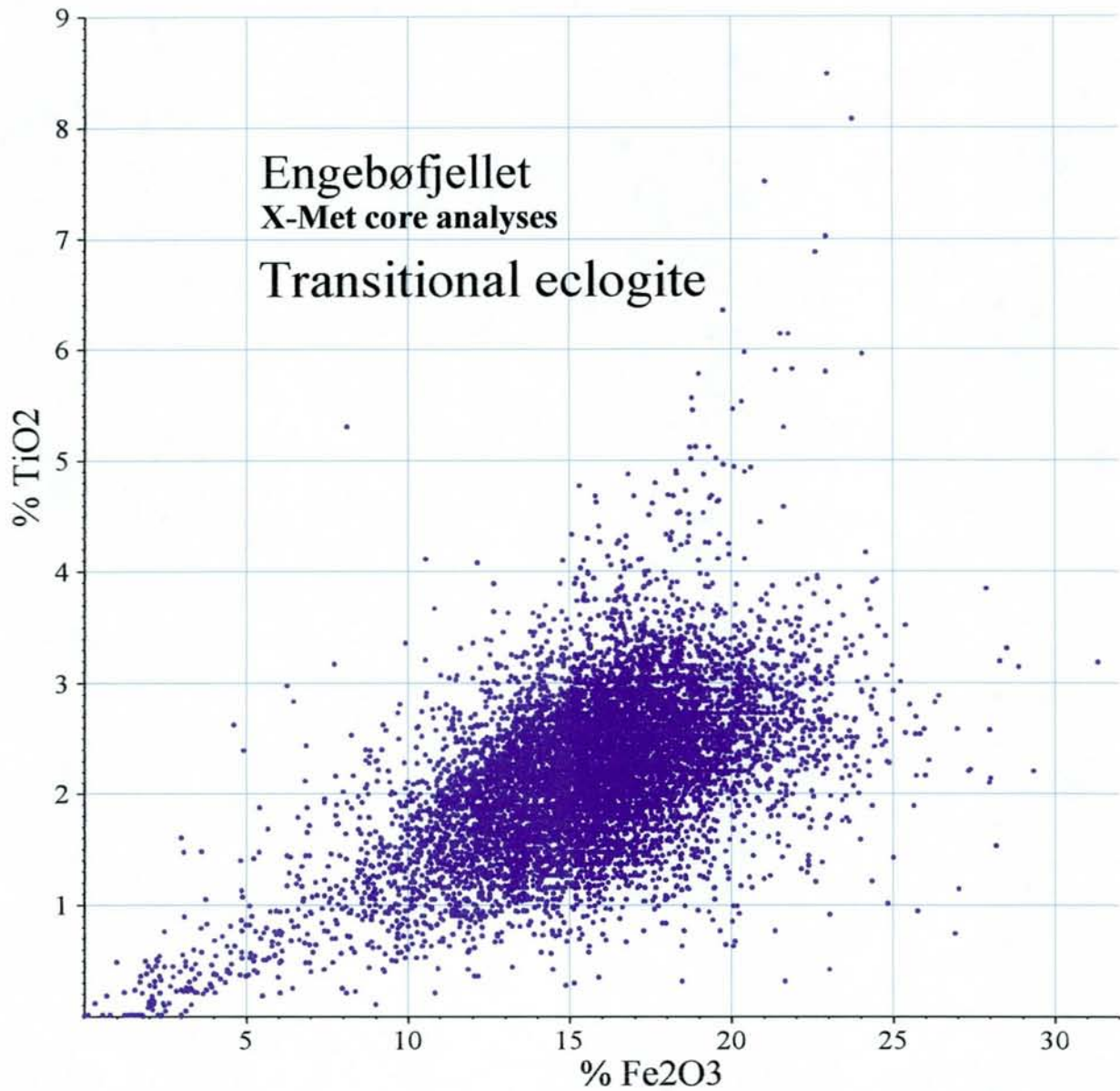


Fig. A6.3: Fe_2O_3 - TiO_2 plot of core analyses done by the X-Met portable XRF instrument directly on cores defined as transitional eclogite. The plot is based on data from the corelog database (Englog.mdb). Samples with anomalously high or low Fe_2O_3 or TiO_2 values are caused by small-scale inhomogeneities in the contents of these elements within the rocktype.

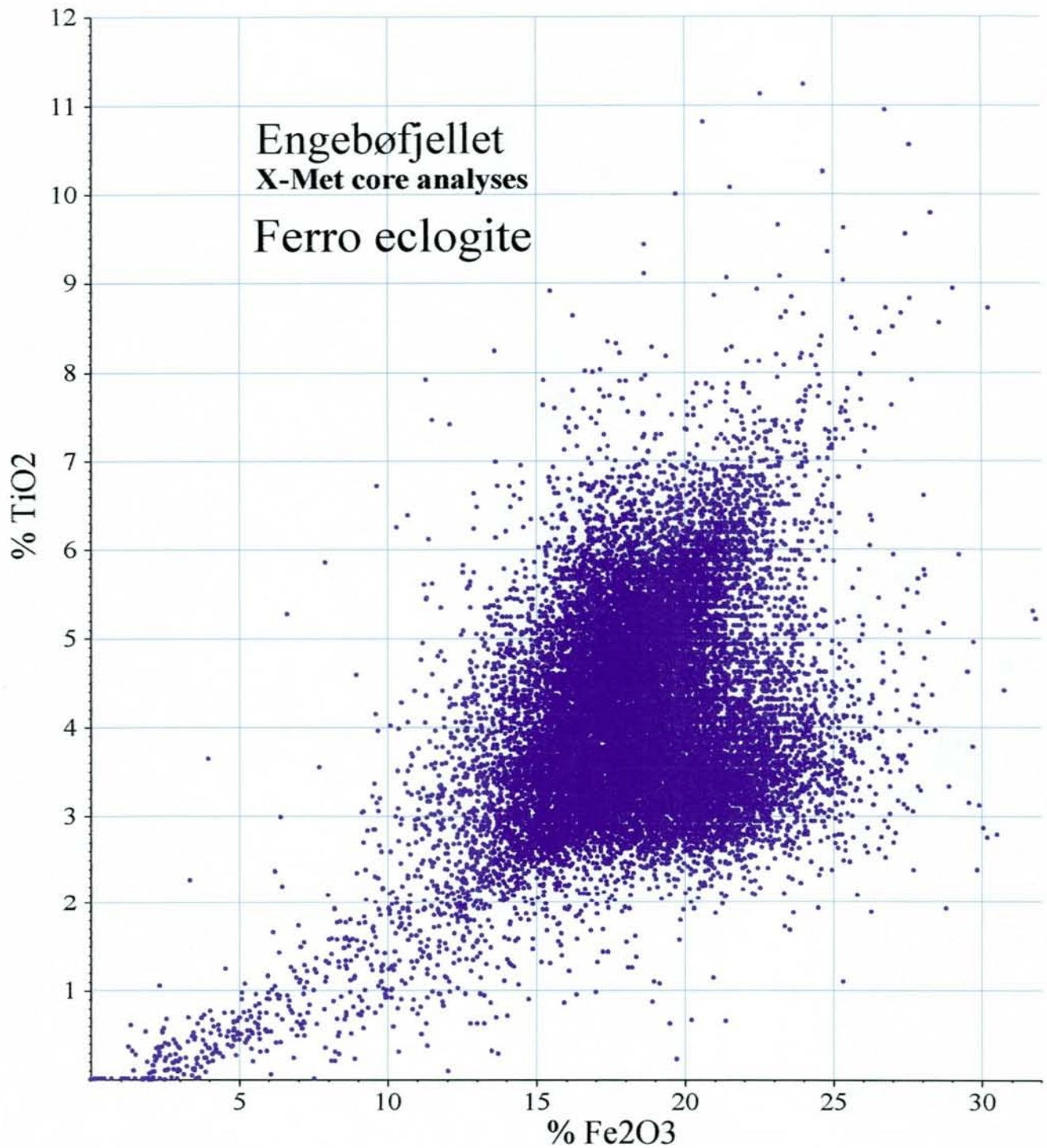


Fig. A6.4: Fe_2O_3 - TiO_2 plot of core analyses done by the X-Met portable XRF instrument directly on cores defined as ferro eclogite. The plot is based on data from the corelog database (Englog.mdb). Samples with anomalously high or low Fe_2O_3 or TiO_2 values are caused by small-scale inhomogeneities in the contents of these elements within the rocktype.

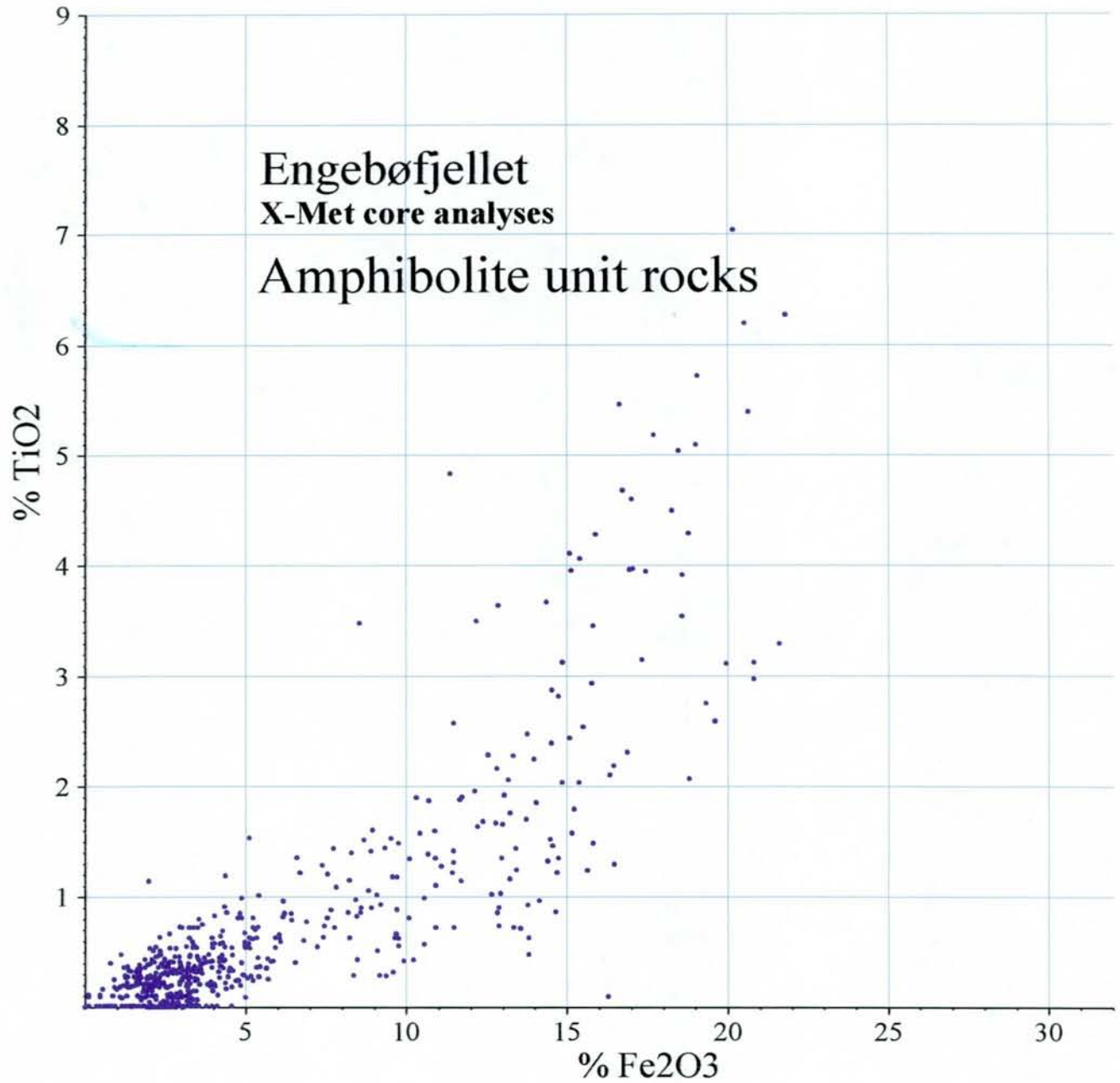


Fig. A6.5: Fe_2O_3 - TiO_2 plot of core analyses done by the X-Met portable XRF instrument directly on cores defined to belong to the amphibolite unit, i.e. country-rocks to the Engebøfjell eclogite body. The plot is based on data from the corelog database (Englog.mdb).

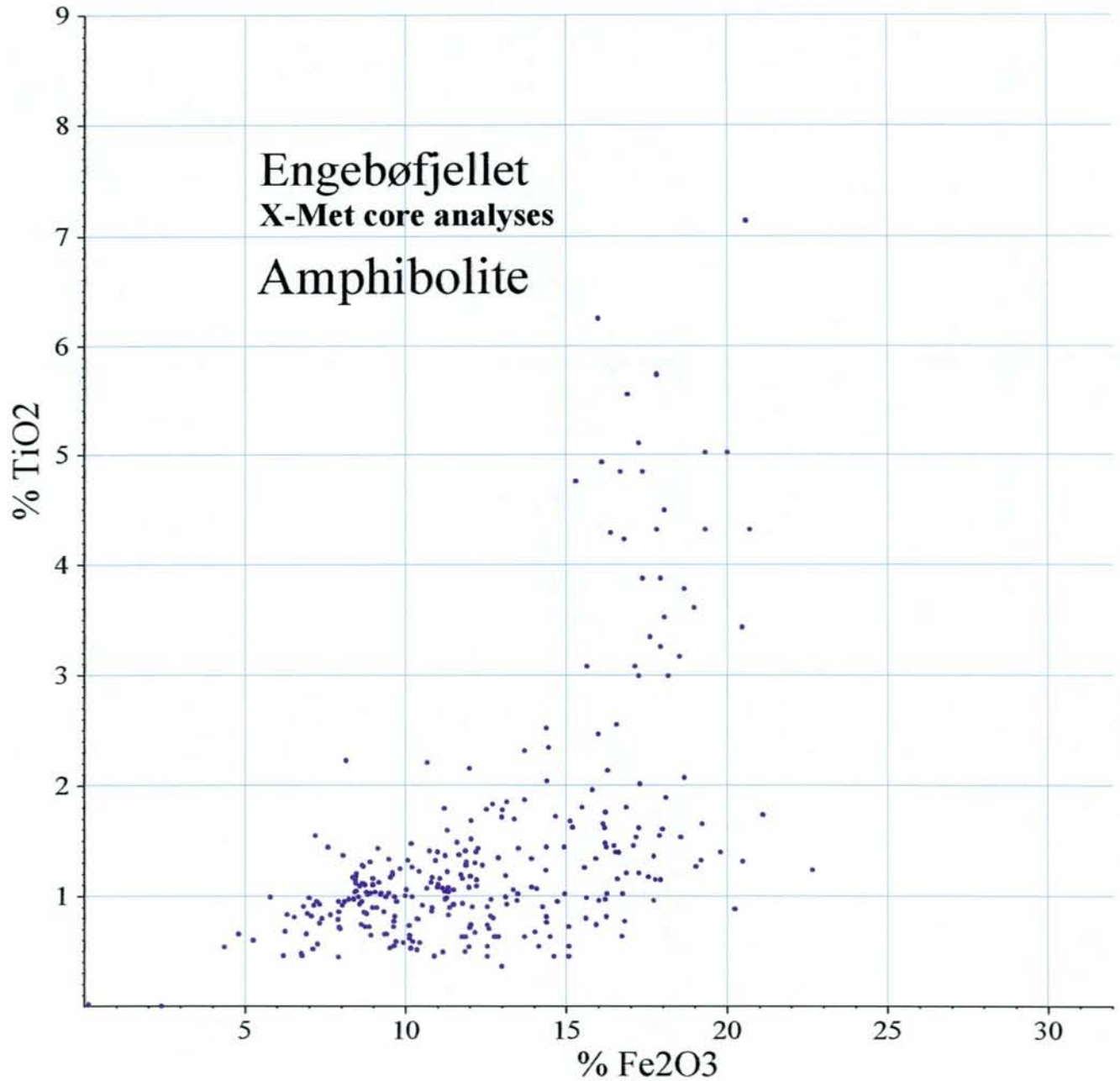


Fig. A6.6: Fe_2O_3 - TiO_2 plot of core analyses done by the X-Met portable XRF instrument directly on cores defined as amphibolite. These amphibolites occur within the Engebøfjell eclogite body. Most of these samples probably represent retrograded leuco-, transitional- or ferro eclogites. The plot is based on data from the corelog database (Englog.mdb).

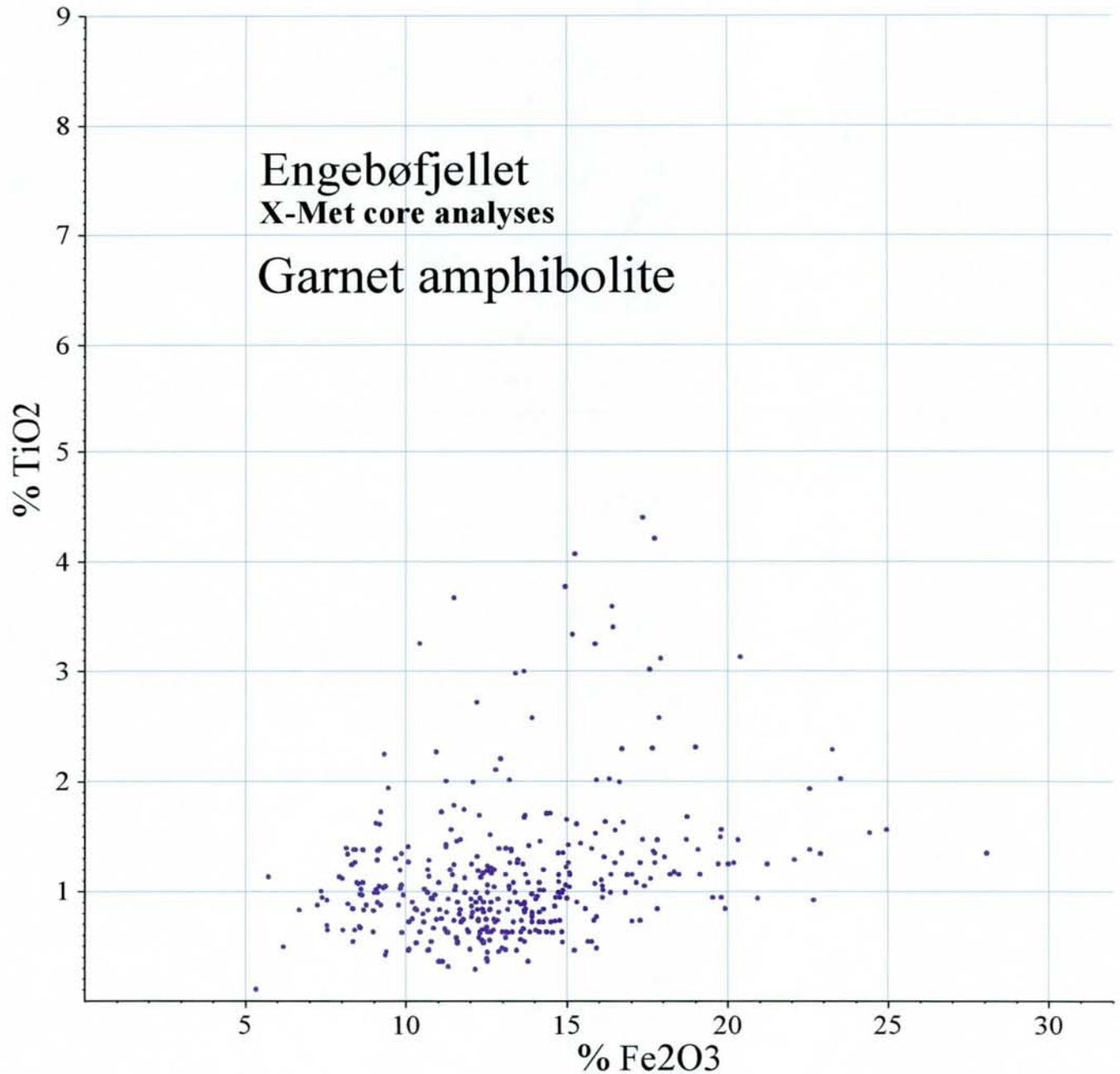


Fig. A6.7: Fe_2O_3 - TiO_2 plot of core analyses done by the X-Met portable XRF instrument directly on cores defined as garnet amphibolite. These garnet amphibolites occur within the Enggebøfjell eclogite body. Most of these samples probably represent retrograded leuco-, transitional- or ferro eclogites, others might be infolded amphibolite unit rocks. The plot is based on data from the corelog database (Englog.mdb).

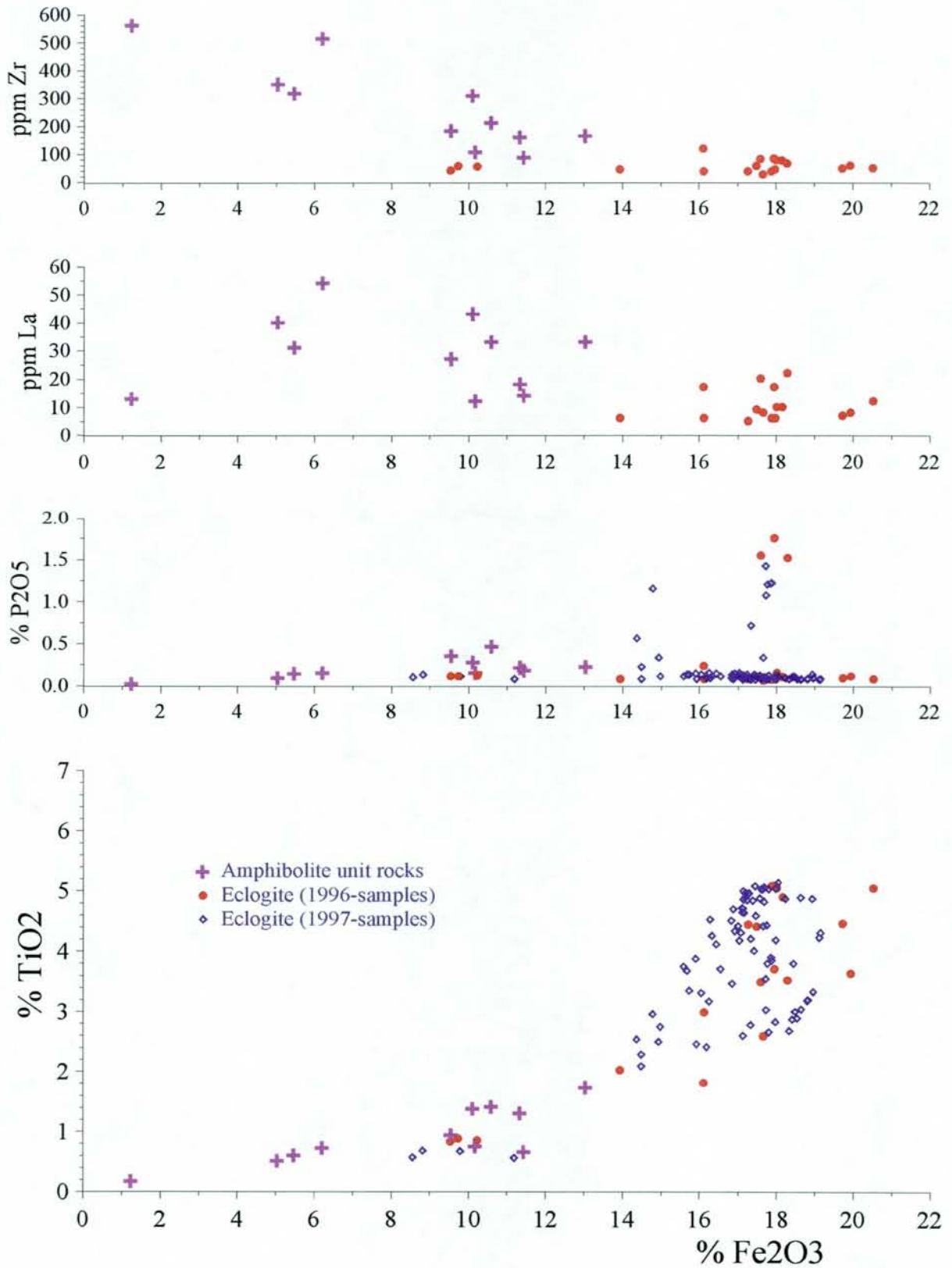


Fig. A6.8: Scattergram plots showing Fe_2O_3 vs. TiO_2 , P_2O_5 , La and Zr for core samples analysed by XRF. The analytical data are given in Appendix 8.

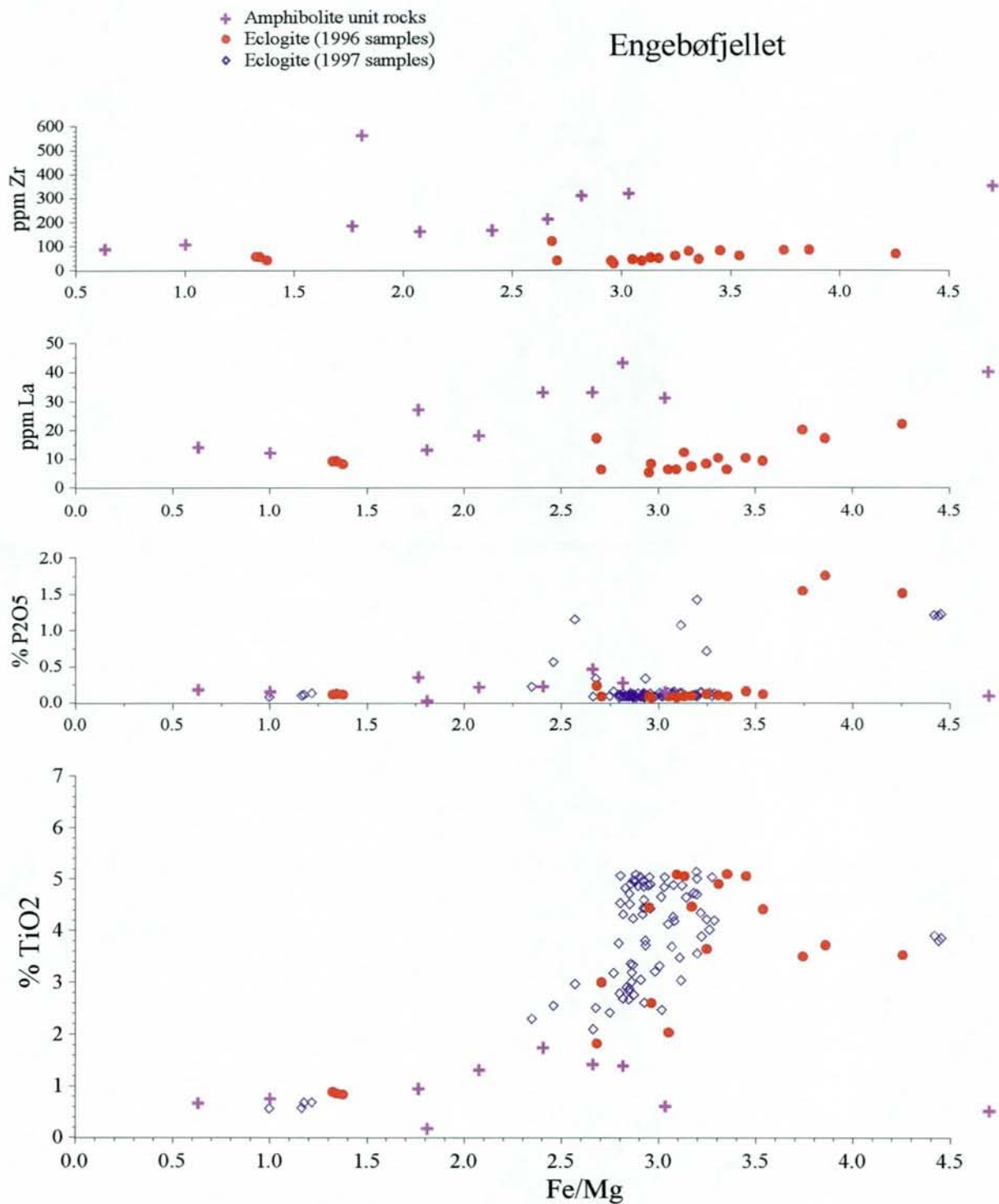


Fig. A6.9: Scattergram plots showing Fe/Mg vs. TiO₂, P₂O₅, La and Zr for core samples analyses by XRF. The analytical data are given in Appendix 8.

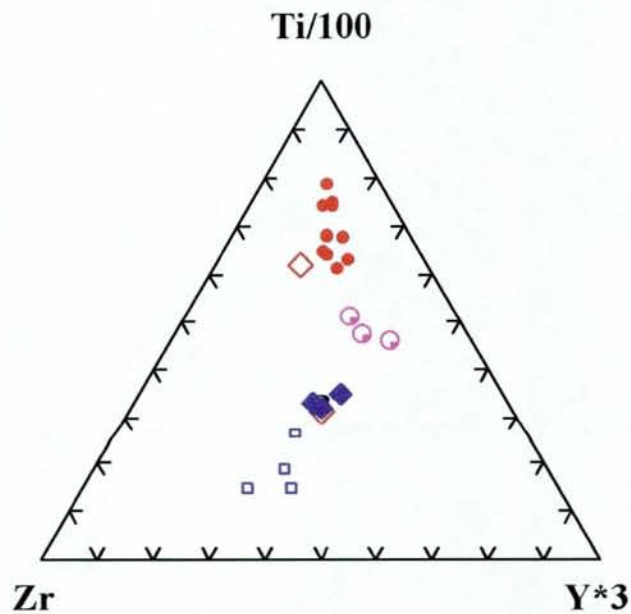


Fig. A6.10: Zr - Y*3 - Ti/100 triangular diagram. Symbols: Filled red circles (ferro eclogite, normal type), Tilted open squares (low-Ti ferrogabbroic eclogites), Circles with quarter-filled purple (P-rich ferrogabbroic eclogite), Tilted dark-blue squares (leucogabbroic eclogite), Open squares (composite samples of amphibolite unit rocks with cm-dm scale alternating mafic/felsic bands). The complete analytical data are given in Appendix 8.

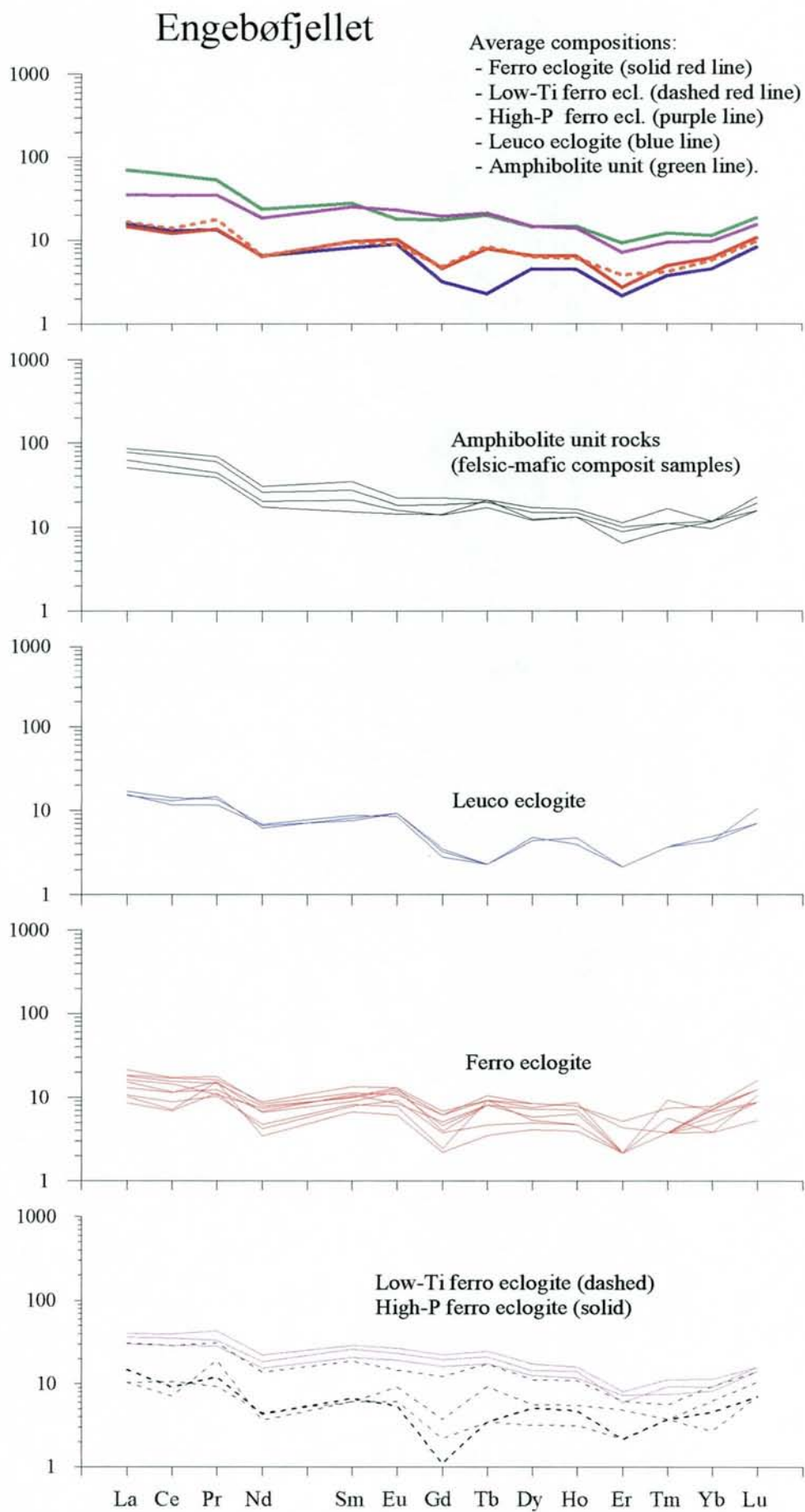


Fig. A6.11: REE-patterns for Engebøfjell core samples analysed by ICP.

Appendix 7: Surface samples, Engebøfjellet.
Sample list, UTM coordinates and TiO₂- and Fe₂O₃ data,

SampleType	SampleNo1	East (wgs84)	North (wgs84)	dasl	TiO2	Fe2O3	Ti/Fe	Comments
chip96-NGU	K471A.96	309935	6822676	210	3.27	16.54	0.20	Chip-sampl. 1996 by NGU
chip96-NGU	K471B.96	309995	6822671	210	2.98	15.28	0.20	(XMET analyses)
chip96-NGU	K471C.96	310035	6822664	210	3.47	16.24	0.21	Chip-sampl. 1996 by NGU
chip96-NGU	K472A.96	309760	6822719	220	1.13	12.86	0.09	(XMET analyses)
chip96-NGU	K473A.96	309780	6822761	130	3.46	13.96	0.25	Chip-sampl. 1996 by NGU
chip96-NGU	K473B.96	309780	6822586	130	3.91	14.96	0.26	(XMET analyses)
chip96-NGU	K474.96	309560	6822696	90	3.21	14.39	0.22	Chip-sampl. 1996 by NGU
chip96-NGU	K475.96	309520	6822921	70	1.09	12.13	0.09	(XMET analyses)
chip96-NGU	K476A.96	310145	6822677	245	4.40	15.95	0.28	Chip-sampl. 1996 by NGU
chip96-NGU	K476B.96	310145	6822647	222	4.46	18.28	0.24	(XMET analyses)
chip96-NGU	K476C.96	310145	6822626	202	4.06	16.87	0.24	Chip-sampl. 1996 by NGU
chip96-NGU	K476D.96	310145	6822606	165	5.35	18.05	0.30	(XMET analyses)
chip96-NGU	K476E.96	310145	6822596	150	8.60	14.67	0.59	Chip-sampl. 1996 by NGU
chip96-NGU	K477A.96	310907	6822942	250	3.55	14.70	0.24	(XMET analyses)
chip96-NGU	K477B.96	310910	6822931	228	3.34	13.03	0.26	Chip-sampl. 1996 by NGU
chip96-NGU	K477C.96	310914	6822925	225	3.10	15.62	0.20	(XMET analyses)
chip96-NGU	K477D.96K480	310918	6822911	190	2.35	15.71	0.15	Chip-sampl. 1996 by NGU
chip96-NGU	K480A.96	312250	6823356	390	2.29	13.27	0.17	(XMET analyses)
chip96-NGU	K480B.96	312465	6823376	444	2.81	14.33	0.20	Chip-sampl. 1996 by NGU
chip96-NGU	K480C.96	312323	6823306	375	2.19	13.24	0.17	(XMET analyses)
chip96-NGU	K480D.96	312115	6823103	280	1.99	13.55	0.15	Chip-sampl. 1996 by NGU
chip96-NGU	K480E.96	311880	6823196	200	2.43	15.00	0.16	(XMET analyses)
chip96-NGU	K481A.96	310064	6822669	238	2.67	13.26	0.20	Chip-sampl. 1996 by NGU
chip96-NGU	K481B.96	310064	6822656	225	2.90	15.50	0.19	(XMET analyses)
chip96-NGU	K481C.96	310064	6822642	210	2.65	14.30	0.19	Chip-sampl. 1996 by NGU
chip96-NGU	K481D.96	310064	6822626	200	3.26	17.66	0.18	(XMET analyses)
chip96-NGU	K481E.96	310060	6822611	170	4.61	17.83	0.26	Chip-sampl. 1996 by NGU
chip96-NGU	K482A.96	310058	6822601	130	3.51	15.85	0.22	(XMET analyses)
chip96-NGU	K483A.96	310710	6822906	275	2.56	13.07	0.20	Chip-sampl. 1996 by NGU
chip96-NGU	K483B.96	310810	6822881	245	3.99	13.21	0.30	(XMET analyses)
chip96-NGU	K483C.96	310745	6822849	212	4.21	13.28	0.32	Chip-sampl. 1996 by NGU
chip96-NGU	K483D.96	310745	6822828	200	2.44	12.42	0.20	(XMET analyses)
chip96-NGU	K483E.96	310734	6822794	155	3.79	13.74	0.28	Chip-sampl. 1996 by NGU
chip96-NGU	XK482.01	310006	6822671	215	2.18	12.18	0.18	(XMET analyses)
chip96-NGU	XK482.02	310006	6822656	202	2.67	13.01	0.21	Chip-sampl. 1996 by NGU
chip96-NGU	XK482.03	310006	6822666	190	2.27	11.58	0.20	(XMET analyses)
chip96-NGU	XK482.04	310006	6822631	170	2.74	12.64	0.22	Chip-sampl. 1996 by NGU
chip96-NGU	XK482.05	310006	6822619	140	2.68	14.20	0.19	(XMET analyses)
chip96-NGU	XK482.06	310004	6822611	130	2.96	14.83	0.20	Chip-sampl. 1996 by NGU
chip96-NGU	XK482.07	310000	6822598	220	3.00	15.95	0.19	(XMET analyses)
chip96-NGU	XK482.08	309995	6822595	100	3.53	17.91	0.20	Chip-sampl. 1996 by NGU
chip96-NGU	XK482.09	309990	6822588	90	3.46	15.49	0.22	(XMET analyses)
chip96-NGU	XK482.10	309985	6822586	70	3.42	15.42	0.22	Chip-sampl. 1996 by NGU
chip96-NGU	XK482.11	309980	6822581	60	4.23	16.62	0.25	(XMET analyses)
Chip97-NGU	1	309720	6822701		0.94	10.23	0.09	Chip-samples 1997 (see ENV 27)
Chip97-NGU	2	309718	6822699		0.96	11.24	0.09	(these analyses are by XMET
Chip97-NGU	3	309716	6822697		0.63	11.47	0.05	on pulverised samples)
Chip97-NGU	4	309715	6822696		0.75	9.27	0.08	Chip-samples 1997 (see ENV 27)
Chip97-NGU	5	309713	6822694		0.64	10.80	0.06	(these analyses are by XMET
Chip97-NGU	6	309712	6822693		3.96	17.53	0.23	on pulverised samples)
Chip97-NGU	7	309710	6822691		5.08	19.25	0.26	Chip-samples 1997 (see ENV 27)
Chip97-NGU	8	309740	6822691		1.32	11.39	0.12	(these analyses are by XMET
Chip97-NGU	9	309740	6822687		0.96	10.36	0.09	on pulverised samples)
Chip97-NGU	10	309740	6822683		2.32	17.61	0.13	Chip-samples 1997 (see ENV 27)
Chip97-NGU	11	309740	6822679		4.10	19.57	0.21	(these analyses are by XMET
Chip97-NGU	12	309740	6822675		5.07	19.63	0.26	on pulverised samples)
Chip97-NGU	13	309740	6822671		3.35	15.33	0.22	Chip-samples 1997 (see ENV 27)
Chip97-NGU	14	309770	6822686		3.04	15.15	0.20	(these analyses are by XMET
Chip97-NGU	15	309770	6822683		3.93	18.55	0.21	on pulverised samples)

SampleType	SampleNo1	East (wgs84)	North (wgs84)	dasl	TiO2	Fe2O3	Ti/Fe	Comments
Chip97-NGU	16	309770	6822680		3.82	16.77	0.23	Chip-samples 1997 (see ENV 27)
Chip97-NGU	17	309770	6822676		3.93	17.08	0.23	(these analyses are by XMET
Chip97-NGU	18	309770	6822673		1.39	9.05	0.15	on pulverised samples)
Chip97-NGU	19	309770	6822670		3.66	16.85	0.22	Chip-samples 1997 (see ENV 27)
Chip97-NGU	20	309770	6822666		3.02	15.83	0.19	(these analyses are by XMET
Chip97-NGU	21	309810	6822686	205	2.81	16.93	0.17	on pulverised samples)
Chip97-NGU	22	309810	6822683		2.05	13.52	0.15	Chip-samples 1997 (see ENV 27)
Chip97-NGU	23	309810	6822680		2.53	15.12	0.17	(these analyses are by XMET
Chip97-NGU	24	309810	6822677		3.04	18.53	0.16	on pulverised samples)
Chip97-NGU	25	309810	6822675		3.02	17.73	0.17	Chip-samples 1997 (see ENV 27)
Chip97-NGU	26	309810	6822672		3.24	16.40	0.20	(these analyses are by XMET
Chip97-NGU	27	309810	6822670		3.03	18.48	0.16	on pulverised samples)
Chip97-NGU	28	309810	6822668		2.57	15.86	0.16	Chip-samples 1997 (see ENV 27)
Chip97-NGU	29	309810	6822666		2.88	15.78	0.18	(these analyses are by XMET
Chip97-NGU	30	309780	6822661	2	2.51	15.28	0.16	on pulverised samples)
Chip97-NGU	31	309780	6822659		3.05	17.24	0.18	Chip-samples 1997 (see ENV 27)
Chip97-NGU	32	309780	6822658		2.01	13.53	0.15	(these analyses are by XMET
Chip97-NGU	33	309780	6822657		3.02	17.66	0.17	on pulverised samples)
Chip97-NGU	34	309780	6822656		3.09	17.01	0.18	Chip-samples 1997 (see ENV 27)
Chip97-NGU	35	309765	6822661		3.13	17.75	0.18	(these analyses are by XMET
Chip97-NGU	36	309765	6822659		2.43	13.74	0.18	on pulverised samples)
Chip97-NGU	37	309765	6822658		2.67	16.54	0.16	Chip-samples 1997 (see ENV 27)
Chip97-NGU	38	309765	6822657		2.78	17.34	0.16	(these analyses are by XMET
Chip97-NGU	39	309765	6822656		2.87	15.50	0.18	on pulverised samples)
Chip97-NGU	40	309750	6822661		2.55	16.21	0.16	Chip-samples 1997 (see ENV 27)
Chip97-NGU	41	309750	6822659		3.17	17.84	0.18	(these analyses are by XMET
Chip97-NGU	42	309750	6822658		3.41	18.92	0.18	on pulverised samples)
Chip97-NGU	43	309750	6822656		3.20	17.58	0.18	Chip-samples 1997 (see ENV 27)
Chip97-NGU	44	309730	6822661		3.65	17.28	0.21	(these analyses are by XMET
Chip97-NGU	45	309730	6822659		3.78	17.21	0.22	on pulverised samples)
Chip97-NGU	46	309730	6822657		2.86	16.21	0.18	Chip-samples 1997 (see ENV 27)
Chip97-NGU	47	309555	6822711		3.75	19.00	0.20	(these analyses are by XMET
Chip97-NGU	48	309552	6822706		4.33	19.34	0.22	on pulverised samples)
Chip97-NGU	49	309549	6822701		5.09	19.79	0.26	Chip-samples 1997 (see ENV 27)
Chip97-NGU	50	309546	6822696		4.67	18.87	0.25	(these analyses are by XMET
Chip97-NGU	51	309543	6822691		3.98	13.92	0.29	on pulverised samples)
Chip97-NGU	52	309539	6822686		3.77	18.17	0.21	Chip-samples 1997 (see ENV 27)
Chip97-NGU	53	309535	6822681		1.21	11.61	0.10	(these analyses are by XMET
Chip97-NGU	54	309580	6822706		4.69	18.60	0.25	on pulverised samples)
Chip97-NGU	55	309578	6822700		3.24	15.78	0.21	Chip-samples 1997 (see ENV 27)
Chip97-NGU	56	309576	6822695		5.38	20.21	0.27	(these analyses are by XMET
Chip97-NGU	57	309573	6822689		4.99	20.18	0.25	on pulverised samples)
Chip97-NGU	58	309571	6822683		2.90	14.82	0.20	Chip-samples 1997 (see ENV 27)
Chip97-NGU	59	309568	6822678		2.02	13.69	0.15	(these analyses are by XMET
Chip97-NGU	60	309565	6822674		4.77	20.59	0.23	on pulverised samples)
Chip97-NGU	61	309563	6822670		1.30	12.90	0.10	Chip-samples 1997 (see ENV 27)
Chip97-NGU	62	309560	6822666		1.21	9.81	0.12	(these analyses are by XMET
Chip97-NGU	63	309685	6822646		2.46	14.64	0.17	on pulverised samples)
Chip97-NGU	64	309685	6822641		3.06	16.48	0.19	Chip-samples 1997 (see ENV 27)
Chip97-NGU	65	309685	6822636		3.40	17.37	0.20	(these analyses are by XMET
Chip97-NGU	66	309685	6822631		4.84	20.13	0.24	on pulverised samples)
Chip97-NGU	67	309685	6822626		3.97	19.18	0.21	Chip-samples 1997 (see ENV 27)
Chip97-NGU	68	309685	6822621		3.47	18.81	0.18	(these analyses are by XMET
Chip97-NGU	69	309685	6822616		3.73	19.92	0.19	on pulverised samples)
Chip97-NGU	70	309715	6822636		2.79	16.87	0.17	Chip-samples 1997 (see ENV 27)
Chip97-NGU	71	309715	6822631		2.84	17.38	0.16	(these analyses are by XMET
Chip97-NGU	72	309715	6822626		3.31	18.85	0.18	on pulverised samples)
Chip97-NGU	73	309715	6822622		2.82	16.27	0.17	Chip-samples 1997 (see ENV 27)
Chip97-NGU	74	309715	6822618		3.17	17.57	0.18	(these analyses are by XMET
Chip97-NGU	75	309715	6822614		2.80	17.07	0.16	on pulverised samples)
Chip97-NGU	76	309715	6822610		2.95	16.45	0.18	Chip-samples 1997 (see ENV 27)
Chip97-NGU	77	309715	6822606		3.12	17.28	0.18	(these analyses are by XMET
Chip97-NGU	78	309760	6822626		3.05	15.05	0.20	on pulverised samples)
Chip97-NGU	79	309760	6822620		3.13	18.68	0.17	Chip-samples 1997 (see ENV 27)
Chip97-NGU	80	309760	6822614		3.39	18.82	0.18	(these analyses are by XMET

SampleType	SampleNo1	East (wgs84)	North (wgs84)	dasl	TiO2	Fe2O3	Ti/Fe	Comments
Chip97-NGU	81	309760	6822608		1.91	14.58	0.13	on pulverised samples)
Chip97-NGU	82	309760	6822602		1.81	12.85	0.14	Chip-samples 1997 (see ENV 27)
Chip97-NGU	83	309760	6822596		3.06	17.69	0.17	(these analyses are by XMET
Chip97-NGU	84	309600	6822696		4.85	20.37	0.24	on pulverised samples)
Chip97-NGU	85	309595	6822690		3.92	16.75	0.23	Chip-samples 1997 (see ENV 27)
Chip97-NGU	86	309590	6822684		4.85	19.32	0.25	(these analyses are by XMET
Chip97-NGU	87	309585	6822678		4.75	19.48	0.24	on pulverised samples)
Chip97-NGU	88	309580	6822672		2.79	15.30	0.18	Chip-samples 1997 (see ENV 27)
Chip97-NGU	89	309575	6822666		2.48	12.44	0.20	(these analyses are by XMET
Chip97-NGU	90	309610	6822686		5.55	20.61	0.27	on pulverised samples)
Chip97-NGU	91	309606	6822680		5.08	19.78	0.26	Chip-samples 1997 (see ENV 27)
Chip97-NGU	92	309602	6822674		5.11	19.70	0.26	(these analyses are by XMET
Chip97-NGU	93	309598	6822668		2.90	15.53	0.19	on pulverised samples)
Chip97-NGU	94	309594	6822662		2.95	14.62	0.20	Chip-samples 1997 (see ENV 27)
Chip97-NGU	95	309590	6822656		3.35	16.35	0.20	(these analyses are by XMET
Chip97-NGU	96	309625	6822676		2.78	15.24	0.18	on pulverised samples)
Chip97-NGU	97	309623	6822671		3.82	15.01	0.25	Chip-samples 1997 (see ENV 27)
Chip97-NGU	98	309621	6822667		2.48	12.21	0.20	(these analyses are by XMET
Chip97-NGU	99	309619	6822663		3.31	15.99	0.21	on pulverised samples)
Chip97-NGU	100	309616	6822659		4.54	18.97	0.24	Chip-samples 1997 (see ENV 27)
Chip97-NGU	101	309613	6822655		2.06	13.53	0.15	(these analyses are by XMET
Chip97-NGU	102	309610	6822651		2.84	17.00	0.17	on pulverised samples)
Chip97-NGU	103	309640	6822666		4.42	19.80	0.22	Chip-samples 1997 (see ENV 27)
Chip97-NGU	104	309639	6822661		3.41	17.14	0.20	(these analyses are by XMET
Chip97-NGU	105	309637	6822656		4.90	18.84	0.26	on pulverised samples)
Chip97-NGU	106	309636	6822652		4.91	19.21	0.26	Chip-samples 1997 (see ENV 27)
Chip97-NGU	107	309635	6822648		5.10	19.42	0.26	(these analyses are by XMET
Chip97-NGU	108	309633	6822644		4.67	17.89	0.26	on pulverised samples)
Chip97-NGU	109	309631	6822640		4.64	18.90	0.25	Chip-samples 1997 (see ENV 27)
Chip97-NGU	110	309630	6822636		3.86	17.79	0.22	(these analyses are by XMET
Chip97-NGU	111	309660	6822666		1.91	13.16	0.15	on pulverised samples)
Chip97-NGU	112	309660	6822661		3.14	17.59	0.18	Chip-samples 1997 (see ENV 27)
Chip97-NGU	113	309660	6822656		3.43	18.56	0.19	(these analyses are by XMET
Chip97-NGU	114	309660	6822651		4.07	19.12	0.21	on pulverised samples)
Chip97-NGU	115	309660	6822646		5.13	20.83	0.25	Chip-samples 1997 (see ENV 27)
Chip97-NGU	116	309660	6822641		4.50	18.31	0.25	(these analyses are by XMET
Chip97-NGU	117	309660	6822636		2.50	14.50	0.17	on pulverised samples)
Chip97-NGU	118	309660	6822631		4.93	20.96	0.24	Chip-samples 1997 (see ENV 27)
Chip97-NGU	119	309660	6822626		2.24	14.02	0.16	(these analyses are by XMET
Chip97-NGU	120	309485	6822716		0.94	6.58	0.14	on pulverised samples)
Chip97-NGU	121	309480	6822713		5.14	19.46	0.26	Chip-samples 1997 (see ENV 27)
Chip97-NGU	122	309475	6822709		4.78	18.45	0.26	(these analyses are by XMET
Chip97-NGU	123	309470	6822705		2.87	15.06	0.19	on pulverised samples)
Chip97-NGU	124	309465	6822701		3.09	15.83	0.20	Chip-samples 1997 (see ENV 27)
Chip97-NGU	125	309510	6822731		4.56	18.28	0.25	(these analyses are by XMET
Chip97-NGU	126	309508	6822727		3.57	15.81	0.23	on pulverised samples)
Chip97-NGU	127	309506	6822723		5.05	18.93	0.27	Chip-samples 1997 (see ENV 27)
Chip97-NGU	128	309504	6822719		4.31	17.99	0.24	(these analyses are by XMET
Chip97-NGU	129	309502	6822715		2.51	14.88	0.17	on pulverised samples)
Chip97-NGU	130	309500	6822711		2.67	15.29	0.17	Chip-samples 1997 (see ENV 27)
Chip97-NGU	131	309498	6822708		3.22	16.58	0.19	(these analyses are by XMET
Chip97-NGU	132	309496	6822705		1.71	12.72	0.13	on pulverised samples)
Chip97-NGU	133	309494	6822702		1.13	12.96	0.09	Chip-samples 1997 (see ENV 27)
Chip97-NGU	134	309492	6822699		1.23	9.34	0.13	(these analyses are by XMET
Chip97-NGU	135	309490	6822696		0.76	8.51	0.09	on pulverised samples)
Chip97-NGU	136	309535	6822716		4.45	18.76	0.24	Chip-samples 1997 (see ENV 27)
Chip97-NGU	137	309530	6822711		5.59	20.20	0.28	(these analyses are by XMET
Chip97-NGU	138	309525	6822706		5.42	20.96	0.26	on pulverised samples)
Chip97-NGU	139	309520	6822701		4.24	17.40	0.24	Chip-samples 1997 (see ENV 27)
Chip97-NGU	140	309515	6822696		3.60	18.27	0.20	(these analyses are by XMET
Chip97-NGU	141	309660	6822611	25	4.04	17.24	0.23	on pulverised samples)
Chip97-NGU	142	309660	6822609		4.75	18.77	0.25	Chip-samples 1997 (see ENV 27)
Chip97-NGU	143	309660	6822607		4.55	18.68	0.24	(these analyses are by XMET
Chip97-NGU	144	309660	6822604		3.87	17.20	0.22	on pulverised samples)
Chip97-NGU	145	309660	6822601		0.83	8.75	0.09	Chip-samples 1997 (see ENV 27)

SampleType	SampleNo1	East (wgs84)	North (wgs84)	dasl	TiO2	Fe2O3	Ti/Fe	Comments
Chip97-NGU	146	309640	6822626	25	3.56	17.25	0.21	(these analyses are by XMET
Chip97-NGU	147	309639	6822622		2.39	12.86	0.19	on pulverised samples)
Chip97-NGU	148	309638	6822618		2.23	14.31	0.16	Chip-samples 1997 (see ENV 27)
Chip97-NGU	149	309637	6822614		3.49	17.13	0.20	(these analyses are by XMET
Chip97-NGU	150	309636	6822610		2.22	14.56	0.15	on pulverised samples)
Chip97-NGU	151	309635	6822606		0.87	9.30	0.09	Chip-samples 1997 (see ENV 27)
Chip97-NGU	152	309621	6822626	25	4.60	19.14	0.24	(these analyses are by XMET
Chip97-NGU	153	309620	6822624		0.96	10.19	0.09	on pulverised samples)
Chip97-NGU	154	309619	6822622		1.01	9.67	0.10	Chip-samples 1997 (see ENV 27)
Chip97-NGU	155	309618	6822620		1.95	14.06	0.14	(these analyses are by XMET
Chip97-NGU	156	309617	6822617		1.63	13.20	0.12	on pulverised samples)
Chip97-NGU	157	309616	6822614		3.97	15.79	0.25	Chip-samples 1997 (see ENV 27)
Chip97-NGU	158	309615	6822611		1.19	8.23	0.14	(these analyses are by XMET
Chip97-NGU	159	309585	6822641	25	0.90	9.57	0.09	on pulverised samples)
Chip97-NGU	160	309585	6822638		1.06	9.13	0.12	Chip-samples 1997 (see ENV 27)
Chip97-NGU	161	309585	6822636		0.87	8.14	0.11	(these analyses are by XMET
Chip97-NGU	162	309585	6822634		1.63	13.10	0.12	on pulverised samples)
Chip97-NGU	163	309585	6822632		3.03	15.58	0.19	Chip-samples 1997 (see ENV 27)
Chip97-NGU	164	309585	6822630		1.33	10.62	0.13	(these analyses are by XMET
Chip97-NGU	165	309585	6822628		2.78	13.64	0.20	on pulverised samples)
Chip97-NGU	166	309585	6822626		4.30	17.75	0.24	Chip-samples 1997 (see ENV 27)
Chip97-NGU	167	309550	6822666	30	3.25	16.02	0.20	(these analyses are by XMET
Chip97-NGU	168	309546	6822660		0.99	10.11	0.10	on pulverised samples)
Chip97-NGU	169	309543	6822653		1.02	9.28	0.11	Chip-samples 1997 (see ENV 27)
Chip97-NGU	170	309540	6822646		1.88	11.91	0.16	(these analyses are by XMET
Chip97-NGU	171	309510	6822681	30	3.58	16.42	0.22	on pulverised samples)
Chip97-NGU	172	309508	6822676		4.51	19.81	0.23	Chip-samples 1997 (see ENV 27)
Chip97-NGU	173	309506	6822671		2.76	14.94	0.18	(these analyses are by XMET
Chip97-NGU	174	309503	6822656		3.58	16.66	0.22	on pulverised samples)
Chip97-NGU	175	309500	6822661		1.10	10.83	0.10	Chip-samples 1997 (see ENV 27)
Chip97-NGU	176	309785	6822631		2.72	16.13	0.17	(these analyses are by XMET
Chip97-NGU	177	309785	6822626		2.90	15.78	0.18	on pulverised samples)
Chip97-NGU	178	309785	6822621		2.48	14.41	0.17	Chip-samples 1997 (see ENV 27)
Chip97-NGU	179	309785	6822616		3.22	19.38	0.17	(these analyses are by XMET
Chip97-NGU	180	309785	6822611		2.80	15.95	0.18	on pulverised samples)
Chip97-NGU	181	309785	6822606		2.49	15.87	0.16	Chip-samples 1997 (see ENV 27)
Chip97-NGU	182	309785	6822601		2.38	16.31	0.15	(these analyses are by XMET
Chip97-NGU	183	309785	6822596		2.40	15.78	0.15	on pulverised samples)
Chip97-NGU	184	309845	6822716	227	2.04	13.00	0.16	Chip-samples 1997 (see ENV 27)
Chip97-NGU	185	309845	6822706	224	2.81	17.61	0.16	(these analyses are by XMET
Chip97-NGU	186	309845	6822696	219	2.47	14.92	0.17	on pulverised samples)
Chip97-NGU	187	309845	6822686	213	2.30	14.05	0.16	Chip-samples 1997 (see ENV 27)
Chip97-NGU	188	309845	6822681	207	2.02	13.13	0.15	(these analyses are by XMET
Chip97-NGU	189	309845	6822676	203	2.39	15.35	0.16	on pulverised samples)
Chip97-NGU	190	309845	6822671	198	2.51	15.10	0.17	Chip-samples 1997 (see ENV 27)
Chip97-NGU	191	309845	6822666	192	2.44	15.05	0.16	(these analyses are by XMET
Chip97-NGU	192	309845	6822661	183	1.92	12.94	0.15	on pulverised samples)
Chip97-NGU	193	309845	6822656	176	2.24	14.31	0.16	Chip-samples 1997 (see ENV 27)
Chip97-NGU	194	309846	6822652	170	1.93	12.65	0.15	(these analyses are by XMET
Chip97-NGU	195	309848	6822648	165	2.41	13.52	0.18	on pulverised samples)
Chip97-NGU	196	309849	6822644	159	2.51	14.55	0.17	Chip-samples 1997 (see ENV 27)
Chip97-NGU	197	309851	6822640	155	2.22	13.89	0.16	(these analyses are by XMET
Chip97-NGU	198	309852	6822636	145	2.66	16.70	0.16	on pulverised samples)
Chip97-NGU	199	309854	6822631	136	3.82	18.94	0.20	Chip-samples 1997 (see ENV 27)
Chip97-NGU	200	309855	6822626	130	2.85	16.42	0.17	(these analyses are by XMET
Chip97-NGU	201	309857	6822621	121	2.38	15.55	0.15	on pulverised samples)
Chip97-NGU	202	309858	6822616	117	2.39	15.35	0.16	Chip-samples 1997 (see ENV 27)
Chip97-NGU	203	309860	6822611	106	2.09	14.39	0.15	(these analyses are by XMET
Chip97-NGU	204	309885	6822601	45	4.81	20.07	0.24	on pulverised samples)
Chip97-NGU	205	309885	6822594	41	2.76	15.74	0.18	Chip-samples 1997 (see ENV 27)
Chip97-NGU	206	309885	6822586	30	3.67	19.29	0.19	(these analyses are by XMET
Chip97-NGU	207	309885	6823576	10	3.67	18.80	0.20	on pulverised samples)
Chip97-NGU	208	309880	6822691	227	0.85	7.92	0.11	Chip-samples 1997 (see ENV 27)
Chip97-NGU	209	309881	6822687		2.29	15.51	0.15	(these analyses are by XMET
Chip97-NGU	210	309882	6822683		2.75	16.81	0.16	on pulverised samples)

SampleType	SampleNo1	East (wgs84)	North (wgs84)	dasl	TiO2	Fe2O3	Ti/Fe	Comments
Chip97-NGU	211	309883	6822679		2.21	13.57	0.16	Chip-samples 1997 (see ENV 27)
Chip97-NGU	212	309884	6822675		1.77	12.19	0.15	(these analyses are by XMET
Chip97-NGU	213	309885	6822671		1.70	11.28	0.15	on pulverised samples)
Chip97-NGU	214	309885	6822667		1.55	11.12	0.14	Chip-samples 1997 (see ENV 27)
Chip97-NGU	215	309885	6822663		2.53	15.82	0.16	(these analyses are by XMET
Chip97-NGU	216	309885	6822659		1.74	11.16	0.16	on pulverised samples)
Chip97-NGU	217	309885	6822655		2.77	16.69	0.17	Chip-samples 1997 (see ENV 27)
Chip97-NGU	218	309885	6822651		3.37	18.28	0.18	(these analyses are by XMET
Chip97-NGU	219	309885	6822647		2.64	15.96	0.17	on pulverised samples)
Chip97-NGU	220	309885	6822643		2.65	13.78	0.19	Chip-samples 1997 (see ENV 27)
Chip97-NGU	221	309885	6822639		2.31	14.83	0.16	(these analyses are by XMET
Chip97-NGU	222	309885	6822635		0.96	9.13	0.11	on pulverised samples)
Chip97-NGU	223	309885	6822631		2.13	14.95	0.14	Chip-samples 1997 (see ENV 27)
Chip97-NGU	224	309885	6822627		2.11	15.26	0.14	(these analyses are by XMET
Chip97-NGU	225	309885	6822623		2.48	15.67	0.16	on pulverised samples)
Chip97-NGU	226	309885	6822619		2.57	15.77	0.16	Chip-samples 1997 (see ENV 27)
Chip97-NGU	227	309885	6822615		2.57	15.95	0.16	(these analyses are by XMET
Chip97-NGU	228	309885	6822611		2.84	17.17	0.17	on pulverised samples)
Chip97-NGU	229	309885	6822606		2.19	13.75	0.16	Chip-samples 1997 (see ENV 27)
dd95-NGU	1046,01	311600	6823111	90	2.61	16.81	0.16	Drill-dust 1996 by NGU
dd95-NGU	1046,02	311575	6823108	105	1.94	14.51	0.13	(XMET analyses)
dd95-NGU	1046,03	311555	6823096	115	0.39	1.42	0.27	Drill-dust 1996 by NGU
dd95-NGU	1046,04	311520	6823096	130	1.60	14.68	0.11	(XMET analyses)
dd95-NGU	1046,05	311485	6823096	145	2.34	16.98	0.14	Drill-dust 1996 by NGU
dd95-NGU	1046,06	311460	6823101	155	3.51	18.51	0.19	(XMET analyses)
dd95-NGU	1046,07	311430	6823104	160	3.75	18.44	0.20	Drill-dust 1996 by NGU
dd95-NGU	1046,08	311400	6823094	155	2.59	16.08	0.16	(XMET analyses)
dd95-NGU	1046,09	311375	6823086	155	3.41	17.46	0.20	Drill-dust 1996 by NGU
dd95-NGU	1046,1	311350	6823084	160	4.24	18.22	0.23	(XMET analyses)
dd95-NGU	1046,11	311328	6823079	160	1.39	14.22	0.10	Drill-dust 1996 by NGU
dd95-NGU	1046,12	311306	6823071	165	3.84	18.22	0.21	(XMET analyses)
dd95-NGU	1046,13	311284	6823071	170	5.50	19.32	0.28	Drill-dust 1996 by NGU
dd95-NGU	1046,14	311262	6823071	175	2.68	16.17	0.17	(XMET analyses)
dd95-NGU	1046,15	311240	6823069	175	0.70	10.73	0.07	Drill-dust 1996 by NGU
dd95-NGU	1046,16	311218	6823066	175	0.48	10.49	0.05	(XMET analyses)
dd95-NGU	1046,17	311199	6823056	180	1.67	15.66	0.11	Drill-dust 1996 by NGU
dd95-NGU	1046,18	311180	6823049	185	2.10	14.52	0.14	(XMET analyses)
dd95-NGU	1046,19	311140	6823026	190	5.39	19.77	0.27	Drill-dust 1996 by NGU
dd95-NGU	1046,21	311070	6822976	205	5.44	19.83	0.27	(XMET analyses)
dd95-NGU	1046,22	311060	6822986	210	3.16	20.25	0.16	Drill-dust 1996 by NGU
dd95-NGU	1046,23	311050	6822986	215	3.54	19.29	0.18	(XMET analyses)
dd95-NGU	1046,24	311035	6822986	225	5.47	19.45	0.28	Drill-dust 1996 by NGU
dd95-NGU	1046,25	311005	6823001	240	3.55	18.94	0.19	(XMET analyses)
dd95-NGU	1046,26	310975	6823006	250	0.81	7.65	0.11	Drill-dust 1996 by NGU
dd95-NGU	1046,27	310953	6823006	260	1.12	10.91	0.10	(XMET analyses)
dd95-NGU	1046,28	310945	6823001	265	2.69	15.86	0.17	Drill-dust 1996 by NGU
dd95-NGU	1046,29	310938	6822986	270	3.01	18.73	0.16	(XMET analyses)
dd95-NGU	1046,3	310930	6822983	275	2.72	16.16	0.17	Drill-dust 1996 by NGU
dd95-NGU	1046,31	310920	6822981	285	3.11	17.17	0.18	(XMET analyses)
dd95-NGU	1046,32	310903	6822979	295	3.30	18.34	0.18	Drill-dust 1996 by NGU
dd95-NGU	1046,33	310883	6822979	305	1.56	14.55	0.11	(XMET analyses)
dd95-NGU	1046,34	310848	6822991	310	1.99	13.65	0.15	Drill-dust 1996 by NGU
dd95-NGU	1046,35	310840	6822994	315	3.14	19.45	0.16	(XMET analyses)
dd95-NGU	1046,36	310833	6822991	320	1.61	6.85	0.24	Drill-dust 1996 by NGU
dd95-NGU	1046,37	310818	6822989	325	3.84	21.82	0.18	(XMET analyses)
dd95-NGU	1046,38	310800	6822984	325	2.64	17.31	0.15	Drill-dust 1996 by NGU
dd95-NGU	1046,39	310785	6822984	330	1.21	11.27	0.11	(XMET analyses)
dd95-NGU	1046,4	310765	6822979	330	1.07	8.81	0.12	Drill-dust 1996 by NGU
dd95-NGU	1046,41	310745	6822974	330	1.22	10.72	0.11	(XMET analyses)
dd95-NGU	1046,42	310715	6822986	325	1.54	12.54	0.12	Drill-dust 1996 by NGU
dd95-NGU	1046,43	310685	6823006	325	2.06	14.97	0.14	(XMET analyses)
dd95-NGU	1046,44	310655	6823026	330	2.20	14.81	0.15	Drill-dust 1996 by NGU
dd95-NGU	1046,45	310625	6823016	330	2.06	13.61	0.15	(XMET analyses)
dd95-NGU	1046,46	310595	6823006	325	3.40	19.59	0.17	Drill-dust 1996 by NGU
dd95-NGU	1046,47	310565	6823001	325	1.93	13.85	0.14	(XMET analyses)

SampleType	SampleNo1	East (wgs84)	North (wgs84)	dasl	TiO2	Fe2O3	Ti/Fe	Comments
dd95-NGU	1046,48	310635	6822991	330	1.08	10.21	0.11	Drill-dust 1996 by NGU
dd95-NGU	1046,49	310500	6822979	330	0.00	0.00		(XMET analyses)
dd95-NGU	1046,5	310480	6822979	330	0.50	8.31	0.06	Drill-dust 1996 by NGU
dd95-NGU	1046,51	310445	6822979	335	0.39	7.74	0.05	(XMET analyses)
dd95-NGU	1046,52	310420	6822981	335	0.46	7.02	0.07	Drill-dust 1996 by NGU
dd95-NGU	1046,53	310390	6822996	335	2.71	16.23	0.17	(XMET analyses)
dd95-NGU	1046,54	310370	6823006	335	0.54	9.65	0.06	Drill-dust 1996 by NGU
dd95-NGU	1046,55	310350	6823009	330	0.62	8.18	0.08	(XMET analyses)
dd95-NGU	1046,56	310320	6823011	325	0.59	8.12	0.07	Drill-dust 1996 by NGU
dd95-NGU	1046,57	310295	6823006	320	1.07	10.66	0.10	(XMET analyses)
dd95-NGU	1046,58	310270	6823004	315	0.36	3.83	0.09	Drill-dust 1996 by NGU
dd95-NGU	1046,59	310250	6823003	310	0.73	7.92	0.09	(XMET analyses)
dd95-NGU	1046,6	310225	6823001	300	3.77	18.06	0.21	Drill-dust 1996 by NGU
dd95-NGU	1046.2	311105	6823011	200	5.85	19.91	0.29	(XMET analyses)
dd95-NGU	1047,01	310200	6823071	300	0.61	8.88	0.07	Drill-dust 1996 by NGU
dd95-NGU	1047,02	310220	6823066	310	0.45	5.78	0.08	(XMET analyses)
dd95-NGU	1047,03	310250	6823061	315	0.00	0.00		Drill-dust 1996 by NGU
dd95-NGU	1047,04	310280	6823056	325	1.24	11.76	0.11	(XMET analyses)
dd95-NGU	1047,05	310310	6823051	330	0.99	10.82	0.09	Drill-dust 1996 by NGU
dd95-NGU	1047,06	310340	6823046	330	0.74	9.05	0.08	(XMET analyses)
dd95-NGU	1047,07	310370	6823041	335	0.84	11.55	0.07	Drill-dust 1996 by NGU
dd95-NGU	1047,08	310400	6823061	335	0.49	8.00	0.06	(XMET analyses)
dd95-NGU	1047,09	310430	6823056	330	2.46	14.98	0.16	Drill-dust 1996 by NGU
dd95-NGU	1047,1	310460	6823046	330	1.26	5.71	0.22	(XMET analyses)
dd95-NGU	1047,11	310460	6823071	325	0.65	9.72	0.07	Drill-dust 1996 by NGU
dd95-NGU	1047,12	310490	6823071	325	0.64	8.66	0.07	(XMET analyses)
dd95-NGU	1047,13	310510	6823086	320	1.92	13.70	0.14	Drill-dust 1996 by NGU
dd95-NGU	1047,14	310560	6823086	320	2.19	15.65	0.14	(XMET analyses)
dd95-NGU	1047,15	310610	6823086	320	2.68	16.33	0.16	Drill-dust 1996 by NGU
dd95-NGU	1047,16	310650	6823086	320	2.84	17.96	0.16	(XMET analyses)
dd95-NGU	1047,17	310700	6823066	315	1.41	11.94	0.12	Drill-dust 1996 by NGU
dd95-NGU	1047,18	310743	6823048	310	0.99	8.25	0.12	(XMET analyses)
dd95-NGU	1047,19	310760	6823051	305	3.58	20.35	0.18	Drill-dust 1996 by NGU
dd95-NGU	1047,2	310776	6823056	300	1.31	9.35	0.14	(XMET analyses)
dd95-NGU	1047,21	310792	6823058	290	2.14	14.52	0.15	Drill-dust 1996 by NGU
dd95-NGU	1047,22	310808	6823060	285	1.05	8.83	0.12	(XMET analyses)
dd95-NGU	1047,23	310823	6823062	280	2.41	15.46	0.16	Drill-dust 1996 by NGU
dd95-NGU	1047,24	310838	6823064	275	3.34	18.94	0.18	(XMET analyses)
dd95-NGU	1047,25	310860	6823111	265	1.73	14.82	0.12	Drill-dust 1996 by NGU
dd95-NGU	1047,26	310880	6823101	260	2.91	16.59	0.18	(XMET analyses)
dd95-NGU	1047,27	310900	6823096	250	2.89	16.23	0.18	Drill-dust 1996 by NGU
dd95-NGU	1047,28	310920	6823106	235	0.82	12.65	0.06	(XMET analyses)
dd95-NGU	1047,29	310940	6823106	225	0.66	8.61	0.08	Drill-dust 1996 by NGU
dd95-NGU	1047,3	310960	6823111	220	1.63	12.07	0.14	(XMET analyses)
dd95-NGU	1047,31	310980	6823096	215	1.73	12.20	0.14	Drill-dust 1996 by NGU
dd95-NGU	1047,32	311000	6823076	210	0.89	8.12	0.11	(XMET analyses)
dd95-NGU	1047,33	311025	6823076	200	3.02	17.67	0.17	Drill-dust 1996 by NGU
dd95-NGU	1047,34	311045	6823096	195	1.27	11.52	0.11	(XMET analyses)
dd95-NGU	1047,35	311070	6823096	185	1.30	11.75	0.11	Drill-dust 1996 by NGU
dd95-NGU	1047,36	311078	6823071	185	0.65	9.56	0.07	(XMET analyses)
dd95-NGU	1047,37	311170	6823086	175	3.91	17.41	0.22	Drill-dust 1996 by NGU
dd95-NGU	1047,38	311195	6823101	170	1.12	10.07	0.11	(XMET analyses)
dd95-NGU	1047,39	311230	6823111	165	1.65	11.61	0.14	Drill-dust 1996 by NGU
dd95-NGU	1047,4	311183	6823026	180	5.32	19.15	0.28	(XMET analyses)
dd95-NGU	1047,41	311223	6823030	180	0.61	8.53	0.07	Drill-dust 1996 by NGU
dd95-NGU	1047,42	311248	6823024	170	5.48	19.96	0.27	(XMET analyses)
dd95-NGU	1047,43	311255	6823022	170	1.67	16.22	0.10	Drill-dust 1996 by NGU
dd95-NGU	1047,44	311273	6823021	165	0.55	9.27	0.06	(XMET analyses)
dd95-NGU	1047,45	311285	6823026	160	4.51	18.62	0.24	Drill-dust 1996 by NGU
dd95-NGU	1047,46	311305	6823026	155	4.06	18.58	0.22	(XMET analyses)
dd95-NGU	1047,47	311330	6823036	150	4.28	18.20	0.24	Drill-dust 1996 by NGU
dd95-NGU	1047,48	311400	6823026	145	2.18	14.99	0.15	(XMET analyses)
dd95-NGU	1047,49	311427	6823016	145	1.16	11.20	0.10	Drill-dust 1996 by NGU
dd95-NGU	1047,5	311458	6823009	145	1.89	14.75	0.13	(XMET analyses)
dd96-DuPont	1000	310077	6822760	284	5.60	15.43	0.36	Drill-dust 1996 by DuPont

SampleType	SampleNo1	East (wgs84)	North (wgs84)	dasl	TiO2	Fe2O3	Ti/Fe	Comments
dd96-DuPont	1000	310077	6822785	284	3.59	15.21	0.24	(ASOMA analyses)
dd96-DuPont	1000	310080	6822781	281	4.75	16.21	0.29	Drill-dust 1996 by DuPont
dd96-DuPont	1000	310080	6822754	281	5.15	15.33	0.34	(ASOMA analyses)
dd96-DuPont	1000	310080	6822806	281	2.86	16.86	0.17	Drill-dust 1996 by DuPont
dd96-DuPont	1000	310076	6822820	0	3.01	17.19	0.18	(ASOMA analyses)
dd96-DuPont	1000	310074	6822831	277	2.17	13.55	0.16	Drill-dust 1996 by DuPont
dd96-DuPont	1000	310075	6822770	277	4.84	14.79	0.33	(ASOMA analyses)
dd96-DuPont	1000	310078	6822798	284	2.79	17.36	0.16	Drill-dust 1996 by DuPont
dd96-DuPont	1000	310073	6822749	272	5.00	14.84	0.34	(ASOMA analyses)
dd96-DuPont	1050	310127	6822768	284	5.31	15.68	0.34	Drill-dust 1996 by DuPont
dd96-DuPont	1050	310128	6822740	289	4.81	16.22	0.30	(ASOMA analyses)
dd96-DuPont	1050	310129	6822810	298	4.91	15.52	0.32	Drill-dust 1996 by DuPont
dd96-DuPont	1050	310129	6822759	288	5.78	16.82	0.34	(ASOMA analyses)
dd96-DuPont	1050	310129	6822729	283	3.82	15.01	0.25	Drill-dust 1996 by DuPont
dd96-DuPont	1050	310129	6822829	292	3.30	9.08	0.36	(ASOMA analyses)
dd96-DuPont	1050	310129	6822879	281	1.08	2.15	0.50	Drill-dust 1996 by DuPont
dd96-DuPont	1050	310130	6822858	288	2.10	12.77	0.16	(ASOMA analyses)
dd96-DuPont	1050	310128	6822780	291	5.22	15.72	0.33	Drill-dust 1996 by DuPont
dd96-DuPont	1050	310130	6822886	275	2.33	12.97	0.18	(ASOMA analyses)
dd96-DuPont	1050	310129	6822850	287	2.49	13.05	0.19	Drill-dust 1996 by DuPont
dd96-DuPont	1050	310130	6822821	299	4.92	14.74	0.33	(ASOMA analyses)
dd96-DuPont	1050	310131	6822748	281	5.11	15.90	0.32	Drill-dust 1996 by DuPont
dd96-DuPont	1050	310132	6822867	281	2.64	15.78	0.17	(ASOMA analyses)
dd96-DuPont	1050	310133	6822724	274	3.82	14.90	0.26	Drill-dust 1996 by DuPont
dd96-DuPont	1050	310139	6822710	275	3.20	14.48	0.22	(ASOMA analyses)
dd96-DuPont	1050	310129	6822849	290	4.27	18.09	0.24	Drill-dust 1996 by DuPont
dd96-DuPont	1050	310131	6822792	294	5.17	14.91	0.35	(ASOMA analyses)
dd96-DuPont	1050	310128	6822805	293	5.15	15.05	0.34	Drill-dust 1996 by DuPont
dd96-DuPont	1100	310176	6822769	291	2.73	14.65	0.19	(ASOMA analyses)
dd96-DuPont	1100	310179	6822759	289	2.61	12.82	0.20	Drill-dust 1996 by DuPont
dd96-DuPont	1100	310179	6822789	301	2.79	13.06	0.21	(ASOMA analyses)
dd96-DuPont	1100	310179	6822812	294	3.54	13.87	0.26	Drill-dust 1996 by DuPont
dd96-DuPont	1100	310179	6822802	305	3.70	14.00	0.26	(ASOMA analyses)
dd96-DuPont	1100	310180	6822866	299	2.81	16.76	0.17	Drill-dust 1996 by DuPont
dd96-DuPont	1100	310177	6822746	288	2.87	14.07	0.20	(ASOMA analyses)
dd96-DuPont	1100	310180	6822737	289	2.04	12.46	0.16	Drill-dust 1996 by DuPont
dd96-DuPont	1100	310178	6822828	298	3.73	15.59	0.24	(ASOMA analyses)
dd96-DuPont	1100	310180	6822862	300	4.76	15.33	0.31	Drill-dust 1996 by DuPont
dd96-DuPont	1100	310178	6822819	295	5.11	15.15	0.34	(ASOMA analyses)
dd96-DuPont	1100	310183	6822847	301	5.14	15.34	0.34	Drill-dust 1996 by DuPont
dd96-DuPont	1100	310180	6822841	296	5.16	15.91	0.32	(ASOMA analyses)
dd96-DuPont	1150	310226	6822789	300	2.44	12.98	0.19	Drill-dust 1996 by DuPont
dd96-DuPont	1150	310229	6822766	288	1.66	12.17	0.14	(ASOMA analyses)
dd96-DuPont	1150	310231	6822863	309	2.18	15.62	0.14	Drill-dust 1996 by DuPont
dd96-DuPont	1150	310232	6822814	302	2.52	14.69	0.17	(ASOMA analyses)
dd96-DuPont	1150	310246	6822767	293	3.55	14.62	0.24	Drill-dust 1996 by DuPont
dd96-DuPont	1150	310236	6822837	306	2.94	18.67	0.16	(ASOMA analyses)
dd96-DuPont	1150	310228	6822870	304	2.30	12.72	0.18	Drill-dust 1996 by DuPont
dd96-DuPont	1150	310226	6822799	297	3.10	16.97	0.18	(ASOMA analyses)
dd96-DuPont	1150	310228	6822849	307	2.73	16.93	0.16	Drill-dust 1996 by DuPont
dd96-DuPont	1150	310230	6822807	301	3.32	13.88	0.24	(ASOMA analyses)
dd96-DuPont	1150	310226	6822830	303	4.84	17.08	0.28	Drill-dust 1996 by DuPont
dd96-DuPont	1150	310228	6822780	295	3.33	14.24	0.23	(ASOMA analyses)
dd96-DuPont	1150	310226	6822739	293	3.19	15.18	0.21	Drill-dust 1996 by DuPont
dd96-DuPont	1200	310281	6822787	297	4.12	15.98	0.26	(ASOMA analyses)
dd96-DuPont	1200	310280	6822798	298	5.22	16.09	0.32	Drill-dust 1996 by DuPont
dd96-DuPont	1200	310282	6822810	303	4.31	15.38	0.28	(ASOMA analyses)
dd96-DuPont	1200	310281	6822819	308	2.93	17.53	0.17	Drill-dust 1996 by DuPont
dd96-DuPont	1200	310283	6822828	304	2.64	16.70	0.16	(ASOMA analyses)
dd96-DuPont	1200	310280	6822838	307	2.32	15.49	0.15	Drill-dust 1996 by DuPont
dd96-DuPont	1200	310284	6822758	291	4.24	15.13	0.28	(ASOMA analyses)
dd96-DuPont	1200	310276	6822767	303	4.27	14.50	0.29	Drill-dust 1996 by DuPont
dd96-DuPont	1200	310279	6822768	296	4.23	16.51	0.26	(ASOMA analyses)
dd96-DuPont	1200	310281	6822786	300	3.80	16.51	0.23	Drill-dust 1996 by DuPont
dd96-DuPont	1250	310337	6822788	303	4.43	17.88	0.25	(ASOMA analyses)

SampleType	SampleNo1	East (wgs84)	North (wgs84)	dasl	TiO2	Fe2O3	Ti/Fe	Comments
dd96-DuPont	1250	310328	6822797	300	5.14	17.13	0.30	Drill-dust 1996 by DuPont
dd96-DuPont	1250	310329	6822803	303	3.00	16.45	0.18	(ASOMA analyses)
dd96-DuPont	1250	310331	6822815	306	2.49	13.60	0.18	Drill-dust 1996 by DuPont
dd96-DuPont	1250	310334	6822824	307	2.58	15.86	0.16	(ASOMA analyses)
dd96-DuPont	1250	310332	6822830	312	2.04	13.48	0.15	Drill-dust 1996 by DuPont
dd96-DuPont	1250	310327	6822783	310	5.24	15.60	0.34	(ASOMA analyses)
dd96-DuPont	1350	310427	6822825	299	5.34	15.93	0.34	Drill-dust 1996 by DuPont
dd96-DuPont	1350	310429	6822834	311	3.62	14.24	0.25	(ASOMA analyses)
dd96-DuPont	1350	310424	6822845	312	2.52	15.26	0.17	Drill-dust 1996 by DuPont
dd96-DuPont	1350	310430	6822854	312	2.65	16.62	0.16	(ASOMA analyses)
dd96-DuPont	1350	310433	6822871	316	0.51	13.64	0.04	Drill-dust 1996 by DuPont
dd96-DuPont	1400	310486	6822857	303	2.04	14.62	0.14	(ASOMA analyses)
dd96-DuPont	1400	310482	6822860	306	1.96	10.72	0.18	Drill-dust 1996 by DuPont
dd96-DuPont	1400	310484	6822875	316	2.21	13.65	0.16	(ASOMA analyses)
dd96-DuPont	1400	310489	6822886	314	2.12	12.26	0.17	Drill-dust 1996 by DuPont
dd96-DuPont	1400	310481	6822898	317	1.08	9.00	0.12	(ASOMA analyses)
dd96-DuPont	1500	310607	6822923	313	1.70	12.45	0.14	Drill-dust 1996 by DuPont
dd96-DuPont	1500	310603	6822942	311	3.97	15.96	0.25	(ASOMA analyses)
dd96-DuPont	1500	310595	6822849	322	3.29	13.63	0.24	Drill-dust 1996 by DuPont
dd96-DuPont	1600	310689	6822952	307	2.99	13.39	0.22	(ASOMA analyses)
dd96-DuPont	850	309935	6822689	229	1.68	11.09	0.15	Drill-dust 1996 by DuPont
dd96-DuPont	850	309937	6822696	233	1.95	15.97	0.12	(ASOMA analyses)
dd96-DuPont	850	309931	6822707	233	1.97	15.00	0.13	Drill-dust 1996 by DuPont
dd96-DuPont	850	309953	6822711	236	1.70	13.66	0.12	(ASOMA analyses)
dd96-DuPont	850	309942	6822718	244	1.08	11.11	0.10	Drill-dust 1996 by DuPont
dd96-DuPont	850	309932	6822730	250	0.56	7.26	0.08	(ASOMA analyses)
dd96-DuPont	850	309929	6822743	250	0.42	2.05	0.20	Drill-dust 1996 by DuPont
dd96-DuPont	850	309935	6822754	253	0.55	5.44	0.10	(ASOMA analyses)
dd96-DuPont	850	309932	6822761	252	0.53	4.77	0.11	Drill-dust 1996 by DuPont
dd96-DuPont	900	309976	6822780	256	2.34	12.09	0.19	(ASOMA analyses)
dd96-DuPont	900	309978	6822728	245	0.60	6.10	0.10	Drill-dust 1996 by DuPont
dd96-DuPont	900	309979	6822716	243	1.47	6.31	0.23	(ASOMA analyses)
dd96-DuPont	900	309983	6822803	259	2.47	16.16	0.15	Drill-dust 1996 by DuPont
dd96-DuPont	900	309984	6822769	258	0.80	11.67	0.07	(ASOMA analyses)
dd96-DuPont	900	309987	6822739	254	3.88	17.04	0.23	Drill-dust 1996 by DuPont
dd96-DuPont	900	309989	6822746	250	3.49	16.55	0.21	(ASOMA analyses)
dd96-DuPont	900	310003	6822689	236	2.30	13.58	0.17	Drill-dust 1996 by DuPont
dd96-DuPont	900	309982	6822811	243	2.41	12.30	0.20	(ASOMA analyses)
dd96-DuPont	900	309981	6822790	254	2.53	14.71	0.17	Drill-dust 1996 by DuPont
dd96-DuPont	900	310003	6822697	225	2.25	13.23	0.17	(ASOMA analyses)
dd96-DuPont	900	310003	6822763	264	3.20	16.99	0.19	Drill-dust 1996 by DuPont
dd96-DuPont	950	310025	6822719	249	1.27	13.52	0.09	(ASOMA analyses)
dd96-DuPont	950	310031	6822802	266	3.05	17.55	0.17	Drill-dust 1996 by DuPont
dd96-DuPont	950	310032	6822789	272	2.64	15.65	0.17	(ASOMA analyses)
dd96-DuPont	950	310033	6822770	267	3.25	17.16	0.19	Drill-dust 1996 by DuPont
dd96-DuPont	950	310034	6822783	268	2.96	17.14	0.17	(ASOMA analyses)
dd96-DuPont	950	310035	6822735	253	5.11	15.84	0.32	Drill-dust 1996 by DuPont
dd96-DuPont	950	310037	6822741	264	4.62	14.71	0.31	(ASOMA analyses)
dd96-DuPont	950	310038	6822810	269	2.29	13.87	0.17	Drill-dust 1996 by DuPont
dd96-DuPont	950	310038	6822745	265	4.60	15.22	0.30	(ASOMA analyses)
dd96-DuPont	950	310033	6822758	264	4.38	15.72	0.28	Drill-dust 1996 by DuPont
dd96-DuPont	950	310032	6822848	282	2.56	15.84	0.16	(ASOMA analyses)
dd96-NGU	DD10-96	310379	6822868	319	0.90	16.70	0.05	Drill-dust 1996 by NGU
dd96-NGU	DD11-96	310374	6822858	316	0.90	10.00	0.09	(XMET analyses)
dd96-NGU	DD12-96	310373	6822843	306	1.90	13.70	0.14	Drill-dust 1996 by NGU
dd96-NGU	DD13-96	310380	6822834	308	3.40	20.50	0.17	(XMET analyses)
dd96-NGU	DD14-96	310380	6822817	304	3.30	21.20	0.16	Drill-dust 1996 by NGU
dd96-NGU	DD15-96	310374	6822807	302	5.40	19.60	0.28	(XMET analyses)
dd96-NGU	DD16-96	310375	6822794	289	5.50	18.00	0.31	Drill-dust 1996 by NGU
dd96-NGU	DD18-96	310244	6822941	296	1.00	10.70	0.09	(XMET analyses)
dd96-NGU	DD1-96	310381	6822967	315	4.10	19.70	0.21	Drill-dust 1996 by NGU
dd96-NGU	DD19-96	310240	6822932	301	1.00	10.60	0.09	(XMET analyses)
dd96-NGU	DD20-96	310232	6822925	304	2.10	20.20	0.10	Drill-dust 1996 by NGU
dd96-NGU	DD21-96	310225	6822916	300	1.00	11.70	0.09	(XMET analyses)
dd96-NGU	DD22-96*	310219	6822906	305	0.90	10.20	0.09	Drill-dust 1996 by NGU

Appendix 8: Major and trace element analyses, Engebøfjellet core samples

XrfSampleNo	Rock	Anal. file	Anal number	Rutil	Rutile vs. TiO2	%	%	%	%	%	%	%	%	%	%	%	%	%	TiO2	S
						SiO2	Al2O3	Fe2O3	TiO2	MgO	CaO	Na2O	K2O	MnO	P2O5	LOI	Sum	icp	leco	
						xrf	xrf	xrf	xrf	xrf	xrf	xrf	xrf	xrf	xrf	xrf	xrf	xrf	icp	leco
1/20-30	amph. unit	1996.0046	1	0.32	34 %	56.41	13.74	9.54	0.94	5.41	6.38	3.41	1.56	0.14	0.35	1.30	99.17	0.37		
1/65-66	leucogab. ecl.	1996.0046	2	1.71	94 %	46.24	15.04	16.12	1.81	6.01	9.57	2.77	0.91	0.18	0.23	0.96	99.83	0.06	0.14	
1/101-103	ferrog. ecl.	1996.0046	3	3.22	92 %	45.65	13.47	17.60	3.49	4.70	9.40	2.57	0.52	0.23	1.54	0.12	99.29	0.16	0.13	
1/126-127	ferrog. ecl.	1996.0046	4	3.29	89 %	45.26	13.00	17.95	3.71	4.65	9.55	2.37	0.56	0.23	1.75	0.38	99.42	0.25	0.14	
1/160-170	amph. unit	1996.0046	5	0.76	54 %	57.45	13.12	10.59	1.41	3.98	6.43	3.05	1.52	0.16	0.46	1.38	99.54	0.39		
2/95-105	amph. unit	1996.0046	6	1.36	79 %	52.12	14.09	13.04	1.73	5.42	6.77	3.54	1.24	0.17	0.22	0.78	99.12	0.22		
2/115-116	ferrog. ecl.	1996.0046	7	4.65	95 %	44.59	13.67	18.17	4.90	5.49	9.94	2.54	0.27	0.21	0.10	-0.01	99.89	0.15	0.15	
2/150-155	ferrog. ecl.	1996.0046	8	3.36	93 %	44.64	12.85	19.94	3.63	6.14	10.01	2.26	0.25	0.21	0.11	0.01	100.06	0.16	0.24	
2/165-170	ferrog. ecl.	1996.0046	9	4.90	97 %	44.56	13.15	18.02	5.05	5.22	9.76	2.30	0.40	0.21	0.15	0.01	98.83	0.09	0.18	
2/200-205	ferrog. ecl.	1996.0046	10	3.14	89 %	42.59	13.38	18.31	3.52	4.30	9.50	2.23	0.52	0.25	1.51	0.10	96.22	0.23	0.12	
2/260-270	amph. unit	1996.0046	11	0.88	64 %	56.69	15.27	10.11	1.38	3.59	5.67	3.17	1.91	0.16	0.27	0.85	99.05	0.30		
3/15-20	leucogab. ecl.	1996.0046	12	0.84	95 %	51.10	17.60	9.74	0.88	7.35	8.22	2.47	0.42	0.14	0.11	1.70	99.75	0.03	0.05	
3/60-65	leucogab. ecl.	1996.0046	13	0.78	94 %	51.03	18.42	9.54	0.83	6.93	8.48	2.79	0.56	0.14	0.11	1.69	100.51	0.03	0.35	
3/80-85	gneiss	1996.0046	14	0.15	88 %	82.77	8.77	1.23	0.17	0.68	1.47	1.28	1.35	0.01	0.02	0.98	98.75	0.01		
3/110-111	leucogab. ecl.	1996.0046	15	0.78	92 %	50.10	17.40	10.23	0.85	7.61	8.07	2.96	0.70	0.15	0.12	1.85	100.03	0.04	0.12	
3/135-136	leucogab. ecl.	1996.0046	16	1.97	98 %	47.77	16.93	13.95	2.02	4.57	10.19	2.64	0.31	0.13	0.08	0.52	99.10	0.03	0.15	
3/159-160	ferrog. ecl.	1996.0046	17	4.97	98 %	43.76	13.53	17.89	5.08	5.78	10.23	2.25	0.21	0.20	0.07	0.21	99.22	0.06	0.17	
4/36-40	leucogab. ecl.	1996.0046	18	2.36	91 %	45.05	15.22	17.67	2.59	5.96	9.88	2.72	0.27	0.18	0.06	0.17	99.77	0.14	0.20	
4/75-77	ferrog. ecl.	1996.0046	19	4.91	96 %	43.12	13.99	17.98	5.09	5.36	9.81	2.11	0.43	0.21	0.08	0.95	99.13	0.11	0.13	
4/97-98	ferrog. ecl.	1996.0046	20	4.34	98 %	44.68	13.37	17.28	4.44	5.85	10.35	2.26	0.13	0.21	0.08	0.18	98.82	0.06	0.19	
4/120-121	ferrog. ecl.	1996.0046	21	3.85	76 %	43.09	11.29	20.53	5.05	6.55	10.10	1.82	0.08	0.26	0.08	0.26	99.11	0.72	0.20	
4/130-131	ferrog. ecl.	1996.0046	22	4.19	94 %	44.01	11.78	19.73	4.46	6.22	9.87	2.13	0.18	0.25	0.09	0.22	98.95	0.16	0.31	
4/106-108	ferrog. ecl.	1996.0046	23	2.88	96 %	46.37	13.49	16.13	2.99	5.96	10.27	2.25	0.22	0.22	0.08	0.84	98.83	0.07	0.18	
4/151-152	ferrog. ecl.	1996.0046	24	4.14	94 %	45.51	14.15	17.49	4.41	4.94	9.47	2.51	0.33	0.21	0.11	0.44	99.57	0.16	0.07	
10/120-125	ferrog. ecl.	1996.0285	1	2.56	98 %	45.90	15.39	17.13	2.60	5.85	10.54	2.57	0.22	0.15	0.07	0.22	100.65	0.04		
10/145-150	ferrog. ecl.	1996.0285	2	4.77	98 %	45.88	13.32	18.64	4.89	6.30	10.22	2.07	0.18	0.21	0.07	-0.07	99.70	0.12		
10/290-295	ferrog. ecl.	1996.0285	3	4.52	96 %	45.53	13.51	16.88	4.70	5.28	9.32	2.05	0.59	0.19	0.08	1.11	99.24	0.18		
10/240-245	ferrog. ecl.	1996.0285	4	4.71	97 %	45.16	13.69	17.39	4.84	5.74	9.86	2.25	0.28	0.20	0.10	0.05	99.57	0.13		
13/100-105	eclogite	1997.0086	1	4.66	96 %	43.18	12.57	18.43	4.85	5.89	10.12	2.03	0.19	0.20	0.07	-	98.31	0.19		
13/130-140	eclogite	1997.0086	2	4.99	99 %	44.01	13.71	18.02	5.06	5.16	9.73	2.02	0.31	0.20	0.07	-	98.97	0.07		
13/180-181	eclogite, retr.	1997.0086	3	4.46	94 %	44.17	13.93	16.62	4.73	4.95	9.50	2.09	0.66	0.18	0.07	-	98.37	0.27		
13/182-183	eclogite	1997.0086	4	4.95	97 %	43.40	13.72	17.44	5.10	5.26	9.85	2.05	0.45	0.20	0.07	-	98.26	0.15		
13/190-200	eclogite, retr.	1997.0086	5	4.67	96 %	44.38	13.01	17.30	4.88	5.75	9.85	1.95	0.43	0.21	0.08	-	98.23	0.21		
13/230-240	eclogite	1997.0086	6	2.90	94 %	45.30	13.07	18.42	3.07	5.91	10.12	1.78	0.29	0.19	0.05	-	98.85	0.17		
13/259.1-260	eclogite, mica-rich	1997.0086	7	2.24	91 %	40.71	13.71	12.18	2.47	5.39	10.22	0.17	2.78	0.15	0.61	-	98.17	0.23		
13/257-258	eclogite	1997.0086	8	3.08	97 %	43.80	13.39	18.68	3.16	5.87	9.91	1.87	0.38	0.19	0.07	-	98.79	0.09		
13/150-160	eclogite	1997.0086	9	4.81	98 %	43.88	13.40	17.87	4.90	5.49	10.16	2.01	0.23	0.20	0.08	-	98.33	0.09		
11/140-150	eclogite	1997.0086	10	2.80	97 %	44.65	14.07	18.70	2.90	6.06	10.14	1.85	0.29	0.19	0.06	-	98.96	0.10		

XrfSampleNo	Rock	Anal. file	Anal number	Rutil	Rutile vs. TiO2	SiO2	Al2O3	Fe2O3	TiO2	MgO	CaO	Na2O	K2O	MnO	P2O5	LOI	Sum	TiO2 icp	S leco
I1/200-210	eclogite	1997.0086	11	4.76	99 %	44.97	13.38	17.16	4.83	5.48	9.81	1.98	0.36	0.19	0.06	-	98.17	0.07	
I2/270-280	eclogite	1997.0086	12	4.91	98 %	44.71	13.54	17.26	4.98	5.51	10.19	2.07	0.28	0.20	0.08	-	98.63	0.08	
I2/370-380	eclogite	1997.0086	13	4.62	98 %	45.13	13.59	17.22	4.73	5.18	9.87	1.97	0.39	0.20	0.08	-	98.49	0.11	
I(20-60)A	leucocratic layers	1997.0086	14	-	-	71.16	13.22	5.03	0.51	1.07	2.47	1.76	2.28	0.08	0.09	-	98.53	-	
I(20-60)B	mafic layers	1997.0086	15	-	-	50.66	15.02	11.33	1.30	5.46	8.13	3.74	1.38	0.16	0.21	-	98.39	-	
I(176-179)	doneioritic gneiss	1997.0086	16	-	-	67.44	14.60	6.20	0.72	0.68	3.05	3.35	1.75	0.10	0.15	-	98.68	-	
I(160-196)A	leucocratic layers	1997.0086	17	-	-	70.21	13.23	5.46	0.60	1.80	2.42	2.39	2.42	0.09	0.14	-	99.49	-	
I(160-196)B	mafic layers	1997.0086	18	-	-	51.34	11.98	10.17	0.75	10.16	8.49	3.38	0.60	0.14	0.15	-	98.79	-	
9/(350-355)	hornblende	1997.0086	19	-	-	47.76	5.45	11.43	0.66	18.11	11.51	0.26	0.33	0.15	0.18	-	98.37	-	
102/10-20	ferrog. ecl.	1997.0220	1	3.16	91 %	46.91	13.86	16.85	3.47	5.42	9.61	2.62	0.43	0.21	0.13	0.68	100.18	0.31	
102/120-130	ferrog. ecl.	1997.0220	2	2.68	95 %	47.06	12.98	17.97	2.83	6.31	9.74	2.05	0.38	0.19	0.08	0.62	100.21	0.15	
102/180-190	ferrog. ecl.	1997.0220	3	4.47	95 %	44.42	12.50	17.13	4.71	6.01	9.70	2.31	0.38	0.20	0.08	0.98	98.41	0.24	
102/250-260	ferrog. ecl.	1997.0220	4	4.08	88 %	45.00	13.70	17.16	4.64	5.46	9.37	2.63	0.36	0.20	0.09	1.00	99.62	0.56	
103/50-60	leucog. ecl.	1997.0220	5	0.63	94 %	50.49	16.78	9.79	0.67	8.32	7.84	2.63	0.48	0.15	0.11	2.36	99.62	0.04	
103/110-120	ferrog. ecl.	1997.0220	6	3.14	94 %	43.70	12.87	18.96	3.33	6.61	10.48	2.14	0.30	0.20	0.09	0.77	99.44	0.19	
103/220-230	ferrog. ecl.	1997.0220	7	2.71	97 %	46.05	13.88	17.33	2.78	6.19	9.94	2.50	0.34	0.18	0.07	1.08	100.34	0.07	
103/360-370	ferrog. ecl.	1997.0220	8	3.88	83 %	44.73	13.47	17.12	4.65	5.68	9.54	2.45	0.38	0.20	0.10	0.72	99.06	0.77	
202/20-30	ferrog. ecl.	1997.0220	9	3.60	97 %	47.13	13.42	16.55	3.71	5.64	9.78	2.50	0.41	0.21	0.11	0.44	99.90	0.11	
202/70-80	ferrog. ecl.	1997.0220	10	3.90	97 %	46.31	14.27	17.42	4.01	5.34	9.58	2.59	0.38	0.22	0.13	0.14	100.39	0.11	
202/180-190	ferrog. ecl.	1997.0220	11	2.69	91 %	48.36	13.19	14.78	2.96	5.75	9.36	2.61	0.37	0.19	1.15	1.03	99.75	0.27	
203/20-30	ferrog. ecl.	1997.0220	12	3.99	96 %	45.71	14.11	17.04	4.18	5.53	9.24	2.92	0.39	0.21	0.15	1.22	100.70	0.19	
104/90-100	ferrog. ecl.	1997.0220	13	4.33	98 %	43.61	13.56	17.75	4.43	6.07	10.09	2.50	0.41	0.21	0.08	0.51	99.21	0.10	
104/200-210	ferrog. ecl.	1997.0220	14	2.55	96 %	45.03	14.03	17.80	2.66	6.25	10.12	2.48	0.27	0.18	0.08	0.30	99.19	0.11	
104/330-340	ferrog. ecl.	1997.0220	15	4.03	93 %	44.28	13.38	19.15	4.31	6.56	10.42	2.31	0.26	0.21	0.08	0.18	101.14	0.28	
204/10-20	ferrog. ecl.	1997.0220	16	4.03	96 %	45.47	13.97	17.98	4.19	5.47	9.67	2.58	0.22	0.22	0.12	0.06	99.94	0.16	
204/130-140	ferrog. ecl.	1997.0220	17	3.52	94 %	47.08	13.05	15.59	3.75	5.58	9.78	2.62	0.40	0.20	0.11	1.35	99.52	0.23	
203/170-180	ferrog. ecl.	1997.0220	18	2.45	89 %	49.09	14.21	14.98	2.75	5.21	9.02	2.74	0.66	0.20	0.11	0.58	99.55	0.30	
107/50-60	ecl	1997.0298	1	0.54	96 %	49.94	14.71	11.19	0.56	11.21	7.36	2.01	0.29	0.18	0.08	1.64	99.16	0.02	
107/190-200	ecl	1997.0298	2	2.93	97 %	45.24	13.79	18.65	3.04	6.41	10.06	2.33	0.29	0.20	0.08	-0.20	99.90	0.11	
108/50-60	ecl	1997.0298	3	0.55	97 %	51.05	19.62	8.55	0.57	7.35	9.09	2.74	0.30	0.13	0.10	1.28	100.78	0.02	
108/130-140	ecl	1997.0298	4	4.04	96 %	43.81	12.75	19.12	4.23	6.66	10.40	2.24	0.26	0.20	0.07	-0.01	99.74	0.19	
108/200-210	ecl	1997.0298	5	2.68	89 %	46.29	13.93	17.73	3.03	5.69	9.25	2.59	0.47	0.22	1.07	0.11	100.38	0.35	
108/340-350	ecl	1997.0298	6	4.30	85 %	44.61	13.14	17.45	5.08	6.05	9.70	2.44	0.42	0.20	0.07	0.01	99.17	0.78	
109/140-150	ecl	1997.0298	7	3.73	96 %	47.96	13.54	15.91	3.88	4.94	8.89	2.74	0.70	0.20	0.14	0.54	99.44	0.15	
109/200-210	ecl	1997.0298	8	4.87	97 %	44.92	13.42	17.65	5.03	5.39	9.52	2.45	0.41	0.20	0.09	0.45	99.53	0.16	
110/110-120	ecl	1997.0298	9	1.73	83 %	49.75	14.79	14.49	2.09	5.44	8.89	3.13	0.83	0.15	0.08	0.89	100.52	0.36	
110/170-180	ecl	1997.0298	10	4.77	96 %	43.95	12.66	17.26	4.95	5.99	10.12	2.46	0.33	0.20	0.09	0.07	98.07	0.18	
110/290-300	ecl	1997.0298	11	4.52	90 %	44.56	13.26	17.14	5.00	5.36	9.39	2.44	0.50	0.19	0.09	0.66	98.59	0.48	
207/60-70	ecl	1997.0298	12	3.14	98 %	44.48	13.74	18.82	3.20	6.31	10.20	2.28	0.33	0.20	0.08	0.10	99.74	0.06	
207/110-120	ecl	1997.0298	13	4.77	95 %	43.69	12.57	17.99	5.04	6.19	10.21	2.46	0.24	0.21	0.08	0.09	98.76	0.27	
207/130-140	ecl	1997.0298	14	4.71	95 %	44.21	13.65	17.29	4.96	5.92	9.88	2.36	0.35	0.19	0.09	0.01	98.90	0.25	
208/50-60	ecl	1997.0298	15	2.35	94 %	46.66	15.41	14.94	2.50	5.58	9.12	2.44	1.10	0.16	0.33	1.30	99.55	0.15	
208/130-140	ecl	1997.0298	16	4.42	98 %	47.34	13.40	16.28	4.53	5.81	9.35	2.32	0.71	0.19	0.09	0.34	100.35	0.11	
208/270-280	ecl	1997.0298	17	4.44	94 %	46.78	12.64	17.11	4.72	5.38	9.14	2.32	0.38	0.19	0.10	0.67	99.43	0.28	
209/90-100	ecl	1997.0298	18	3.13	98 %	44.61	13.64	18.81	3.18	6.57	10.52	2.27	0.19	0.19	0.08	-0.02	100.02	0.05	

XrfSampleNo	Rock	Anal. file	Anal number	Rutil vs. TiO2	SiO2	Al2O3	Fe2O3	TiO2	MgO	CaO	Na2O	K2O	MnO	P2O5	LOI	Sum	TiO2 iep	S leco	
209/150-160	ecl	1997.0298	19	4.94	98 %	44.58	13.44	17.61	5.03	5.96	10.17	2.74	0.30	0.19	0.08	0.01	100.13	0.09	
210/100-110	ecl	1997.0298	20	2.40	97 %	45.92	16.63	15.93	2.46	5.28	10.73	2.63	0.27	0.15	0.08	0.47	100.55	0.06	
210/240-250	ecl	1997.0298	21	4.48	93 %	44.51	13.58	17.68	4.82	6.25	10.36	2.53	0.25	0.20	0.09	0.27	100.52	0.34	
210/340-350	ecl	1997.0298	22	2.96	93 %	46.37	14.01	16.25	3.17	5.87	9.37	2.64	0.54	0.21	0.15	0.90	99.47	0.21	
111/60-70	ecl	1997.0342	1	0.66	97 %	50.60	18.48	8.81	0.68	7.25	8.80	2.81	0.35	0.13	0.13	1.27	99.30	0.02	
111/200-210	ecl	1997.0342	2	4.19	91 %	44.22	13.38	17.47	4.59	5.97	9.87	2.30	0.40	0.20	0.11	0.18	98.69	0.40	
111/330-340	ecl	1997.0342	3	4.09	96 %	46.07	13.78	16.33	4.26	5.31	9.19	2.74	0.47	0.19	0.11	0.54	99.00	0.17	
112/180-190	ecl	1997.0342	4	4.81	97 %	44.11	13.22	17.20	4.97	5.99	9.87	2.38	0.38	0.20	0.09	0.46	98.87	0.16	
112/260-270	ecl	1997.0342	5	1.83	76 %	46.78	14.09	16.19	2.41	5.89	9.60	2.55	0.40	0.16	0.09	0.60	98.78	0.58	
112/360-370	ecl	1997.0342	6	4.15	94 %	45.48	13.48	17.01	4.42	5.75	9.30	2.17	0.74	0.19	0.12	0.26	98.94	0.27	
113/170-180	ecl	1997.0342	7	2.92	75 %	47.44	11.66	17.86	3.90	4.04	8.32	2.70	0.88	0.24	1.21	0.22	98.48	0.98	
113/240-250	ecl	1997.0342	8	2.81	94 %	43.99	13.51	18.49	3.00	6.46	9.99	2.50	0.26	0.19	0.10	-0.03	98.45	0.19	
211/130-140	ecl	1997.0342	9	2.02	53 %	47.56	11.49	17.77	3.80	4.00	7.89	2.44	1.05	0.25	1.20	0.73	98.19	1.78	
211/210-220	ecl	1997.0342	10	3.90	90 %	44.84	13.64	16.92	4.34	5.26	9.63	2.64	0.38	0.21	0.14	0.30	98.30	0.44	
211/310-320	ecl	1997.0342	11	4.85	96 %	43.06	12.96	17.80	5.03	5.87	9.82	2.37	0.31	0.20	0.12	0.48	98.03	0.18	
211/410-420	ecl	1997.0342	12	3.40	79 %	44.34	13.29	17.08	4.31	6.06	9.88	2.35	0.43	0.21	0.12	0.65	98.71	0.91	
212/70-80	ecl	1997.0342	13	4.81	98 %	44.15	13.46	17.20	4.90	6.02	10.10	2.42	0.25	0.19	0.10	-0.13	98.67	0.09	
212/170-180	ecl	1997.0342	14	3.91	95 %	45.76	14.13	16.44	4.12	5.39	9.61	2.72	0.39	0.21	0.14	0.11	99.03	0.21	
212/270-280	ecl	1997.0342	15	3.40	92 %	46.90	13.82	15.68	3.68	5.11	8.45	2.53	0.72	0.19	0.13	1.07	98.27	0.28	
213/40-50	ecl	1997.0342	16	4.67	96 %	43.86	13.13	17.57	4.88	5.71	9.93	2.42	0.37	0.21	0.12	0.17	98.37	0.21	
213/130-140	ecl	1997.0342	17	2.16	94 %	46.01	14.49	14.49	2.29	6.17	9.43	2.79	0.59	0.20	0.22	2.58	99.26	0.13	
213/210-220	ecl	1997.0342	18	3.01	91 %	46.74	13.48	16.05	3.31	5.34	9.48	2.55	0.52	0.21	0.13	1.33	99.13	0.30	
301/40-50	ecl	1997.0342	19	4.76	98 %	43.94	12.91	18.24	4.87	6.19	9.75	2.27	0.28	0.20	0.09	0.21	98.95	0.11	
301/100-110	ecl	1997.0342	20	2.60	97 %	44.38	14.25	18.34	2.68	6.51	10.42	2.36	0.20	0.18	0.08	0.33	99.73	0.08	
301/190-200	ecl	1997.0342	21	4.10	97 %	44.70	13.79	17.34	4.21	5.34	9.73	2.56	0.28	0.22	0.71	0.41	99.30	0.11	
302/30-40	ecl	1997.0342	22	4.43	98 %	44.74	13.58	16.83	4.51	5.90	9.79	2.50	0.43	0.19	0.09	0.47	99.02	0.08	
302/190-200	ecl	1997.0342	23	4.84	96 %	43.53	12.96	17.69	5.06	6.31	10.19	2.29	0.21	0.21	0.10	0.22	98.76	0.22	
302/330-340	ecl	1997.0342	24	4.98	97 %	43.82	13.52	18.05	5.14	5.65	9.88	2.33	0.32	0.21	0.11	-0.15	98.88	0.16	
303/40-50	ecl	1997.0342	25	3.71	98 %	44.55	13.16	18.45	3.80	6.29	10.06	2.29	0.30	0.21	0.11	0.11	99.34	0.09	
303/90-100	ecl	1997.0342	26	2.74	95 %	44.23	13.70	18.54	2.89	6.54	10.31	2.35	0.26	0.18	0.08	0.28	99.36	0.15	
303/140-150	ecl	1997.0342	27	4.30	97 %	44.75	13.30	17.66	4.42	6.02	9.62	2.28	0.31	0.21	0.33	0.12	99.01	0.12	
303/230-240	ecl	1997.0342	28	3.22	96 %	47.56	13.81	15.74	3.35	5.51	9.10	2.69	0.52	0.19	0.13	0.67	99.28	0.13	
214/200-210	ecl	1997.0342	29	4.59	94 %	43.74	12.35	18.94	4.87	6.07	9.94	2.26	0.15	0.24	0.13	-0.03	98.65	0.28	
214/310-320	ecl	1997.0342	30	2.33	92 %	45.73	14.22	14.37	2.54	5.84	9.29	2.80	0.87	0.19	0.56	2.37	98.78	0.21	
114/100-110	ecl	1997.0342	31	2.13	55 %	47.27	11.68	17.87	3.85	4.01	8.19	2.88	0.51	0.21	1.22	0.74	98.42	1.72	
214/40-50	ecl	1997.0342	32	4.78	98 %	44.46	13.60	17.15	4.86	5.92	10.28	2.47	0.27	0.20	0.12	0.03	99.36	0.08	
304/80-90	ecl	1997.0342	33	2.81	98 %	44.49	14.00	18.42	2.87	6.46	10.28	2.42	0.25	0.19	0.10	-0.02	99.46	0.06	
304/200-210	ecl	1997.0342	34	4.65	96 %	44.31	13.55	17.24	4.85	5.89	9.97	2.50	0.34	0.20	0.13	-0.11	98.86	0.20	
304/330-340	ecl	1997.0342	35	3.33	94 %	44.39	13.34	17.72	3.55	5.54	9.65	2.58	0.33	0.23	1.42	0.13	98.87	0.22	
				3.42	92 %	46.82	13.69	16.10	3.52	5.78	9.31	2.42	0.52	0.19	0.22	0.56	99.21	0.23	

Appendix 8:

XrfSampleNo	ppm		ppm																																		
	Y	Y icp	Zr	Nb	Sr	Rb	Ba	Cu	Zn	Pb	Se	V	Ni	Cr	Ga	Yb	Co	Ce	La	Nd	La icp	Ce icp	Pr icp	ne icp	Sm icp	Eu icp	Gd icp	Tb icp	dy icp	Ho icp	Er icp	Tm icp	Yb icp	Lu icp			
1/20-30	45	47.6	183	10	202	43	388	62	143	33	20	120	102	217	21	-10	31	55	27	14	28.1	63.5	7.9	28.2	7.5	1.9	6.5	1.8	7.2	1.7	2.4	0.5	4.3	1.1			
1/65-66	39	39.6	119	-5	256	24	401	83	136	12	42	379	72	51	26	-10	51	51	15	-10	16.9	41.1	6.4	22.1	6.5	1.9	5.6	1.5	6.4	1.4	2.3	0.3	3.5	0.8			
1/101-103	48	49.0	82	8	294	17	170	26	166	11	38	206	15	44	25	-10	43	75	20	34	19.7	49.9	6.8	29.1	8.9	3.0	8.9	1.8	8.1	1.8	2.2	0.5	3.4	0.9			
1/126-127	49	43.3	83	-5	288	16	174	27	165	17	30	207	11	9	26	-10	51	82	31	38	16.5	40.9	5.8	24.6	7.1	2.5	7.3	1.5	7.1	1.5	2.7	0.4	3.0	0.8			
1/160-170	54	51.2	210	9	181	36	502	25	114	-10	22	144	59	125	21	-10	26	86	33	23	42.7	99.1	12.3	41.7	9.5	2.4	8.5	1.7	8.7	1.9	3.8	0.6	4.4	1.3			
2/95-105	40	42.8	164	6	128	29	414	48	137	-10	27	221	77	106	25	-10	42	79	33	14	34.2	75.4	9.1	32.3	7.2	2.1	6.4	1.5	7.0	1.7	3.3	0.6	3.6	0.9			
2/115-116	23	28.6	77	-5	119	-5	94	29	143	-10	48	404	15	69	27	-10	58	46	10	20	9.8	21.9	3.0	12.5	3.4	1.6	2.8	0.9	4.8	1.0	1.9	0.4	2.9	0.9			
2/150-155	22	25.8	58	-5	135	-5	96	42	158	-10	50	597	17	48	30	-10	68	40	15	-10	8.3	16.5	2.5	10.9	3.7	1.1	2.3	0.7	4.1	0.9	0.8	0.2	2.6	0.7			
2/165-170	26	27.8	79	-5	139	11	123	26	135	-10	47	406	12	36	27	-10	60	44	11	24	10.1	24.0	3.3	14.0	4.6	1.7	3.1	0.8	4.3	1.1	0.8	0.5	2.5	0.5			
2/200-205	48	59.9	66	6	250	14	158	28	163	-10	36	178	10	23	27	-10	48	88	16	34	22.0	56.2	8.8	35.2	9.8	3.5	10.1	2.1	9.8	2.0	3.0	0.6	4.2	0.9			
2/260-270	62	54.7	308	11	216	40	752	22	103	16	22	133	53	84	24	-10	24	79	43	28	47.1	111.4	14.3	48.7	12.0	2.9	10.1	1.8	9.9	2.1	4.2	0.9	4.4	0.9			
3/15-20	17	17.1	56	-5	369	7	134	24	83	-10	19	130	84	261	19	-10	39	-10	-10	-10	9.3	20.5	2.8	10.9	3.0	1.1	1.3	0.2	2.5	0.6	0.8	0.2	1.6	0.6			
3/60-65	15	17.0	41	-5	327	14	186	37	76	12	17	128	76	280	22	-10	40	-10	-10	-10	8.3	18.7	3.0	9.9	2.8	1.2	1.5	0.2	2.7	0.5	0.8	0.2	1.6	0.4			
3/80-85	18	15.4	56	-5	169	40	1093	6	25	-10	-10	15	-5	24	-10	-10	-10	-10	-10	-10	21.8	39.0	5.7	12.4	2.7	0.7	1.1	0.5	1.3	0.4	1.4	0.2	2.4	0.7			
3/110-111	16	18.2	54	-5	307	26	256	40	92	-10	25	129	87	287	17	-10	45	13	-10	-10	8.6	16.6	2.4	10.6	2.6	1.2	1.6	0.2	2.5	0.6	0.8	0.2	1.8	0.4			
3/135-136	11	10.0	44	-5	285	8	115	68	87	-10	34	554	56	56	25	-10	54	22	-10	-10	5.7	10.2	3.9	5.8	2.1	0.8	1.0	0.3	1.8	0.4	0.8	0.2	1.0	0.4			
3/159-160	11	14.5	37	-5	70	-5	84	29	128	-10	51	474	15	108	24	-10	64	38	-10	15	5.6	10.1	3.1	5.5	2.3	0.8	1.0	0.3	2.3	0.5	0.8	0.2	1.4	0.6			
4/36-40	17	18.3	26	-5	144	7	84	42	130	-10	44	572	28	103	25	-10	75	24	-10	-10	8.1	13.1	2.5	6.9	2.3	0.7	0.5	0.3	2.9	0.6	0.8	0.2	1.7	0.4			
4/75-77	16	19.6	44	-5	163	12	115	38	127	-10	49	433	19	19	25	-10	66	35	-10	-10	5.8	12.5	2.1	7.6	2.8	1.0	1.1	0.8	3.0	0.6	0.8	0.2	1.8	0.5			
4/97-98	19	16.5	37	-5	194	-5	53	30	125	-10	50	355	14	74	24	-10	63	25	-10	13	4.7	9.8	2.3	6.7	2.7	1.2	1.7	0.4	2.8	0.6	0.8	0.3	1.4	0.3			
4/120-121	20	18.2	50	-5	81	-5	37	36	149	-10	56	399	26	29	24	-10	68	49	13	16	11.6	24.4	3.6	13.3	3.9	1.4	2.8	0.8	4.8	1.0	1.6	0.2	2.9	0.7			
4/130-131	20	26.4	48	6	319	-5	60	46	159	-10	52	341	24	45	25	-10	64	24	-10	-10	7.1	16.2	3.1	10.5	3.1	1.5	2.1	0.7	4.1	0.9	0.8	0.2	2.7	0.7			
4/106-108	18	22.2	38	-5	237	-5	77	21	122	-10	47	338	18	68	25	-10	54	16	-10	-10	5.7	15.2	1.9	7.2	2.1	1.2	1.7	0.8	3.2	0.7	1.8	0.2	2.3	0.6			
4/151-152	17	21.8	57	7	117	6	110	45	131	-10	46	266	15	16	29	-10	55	42	24	17	8.9	20.6	2.2	11.9	3.5	1.7	1.8	0.7	3.3	0.8	0.8	0.2	2.2	0.5			
10/120-125																																					
10/145-150																																					
10/290-295																																					
10/240-245																																					
13/100-105	15	16.8	40	2.5	152	2.5	60	34	140	5	60	510	17	115	26	5	65	35	5	12	4.7	5.3	4.1	3.7	0.3	0.9	2.2	0.9	1.6	1.1	0.4	0.1	1.6	0.2			
13/130-140	14	18.2	50	7	170	9	90	27	126	22	60	435	16	22	25	5	57	35	18	15	5.6	11.1	4.5	6.6	0.6	1.4	2.6	0.7	1.8	1.1	0.4	0.1	1.8	0.3			
13/180-181	15	18.7	46	6	268	21	167	29	116	5	52	430	16	26	28	5	52	29	5	5	5.5	10.4	5.0	8.1	0.9	1.4	3.5	0.7	1.6	1.1	1.4	0.2	1.8	0.3			
13/182-183	17	18.9	45	2.5	194	13	122	21	126	5	59	434	16	42	22	5	57	21	5	5	5.3	8.6	4.4	6.5	0.3	1.2	3.0	0.9	1.8	1.1	2.0	0.2	1.9	0.4			
13/190-200	16	21.1	48	2.5	222	12	114	30	125	5	60	429	14	18	27	5	57	27	5	5	5.4	9.9	5.2	6.2	1.0	1.3	3.3	0.5	1.2	1.2	1.7	0.1	2.1	0.3			
13/230-240	15	16.2	26	2.5	207	6	87	33	128	5	55	599	18	59	25	5	67	28	5	5	6.4	8.9	5.1	5.2	0.3	0.9	2.3	0.6	0.8	1.0	0.4	0.3	1.5	0.3			
13/259.1-260	25	23.2	190	6	688	89	1113	12	71	54	33	547	53	96	28	5	28	206	111	84	112.4	213.9	25.9	82.2	11.4	4.2	8.4	0.8	2.3	1.1	0.4	0.1	1.7	0.2			
13/257-258	13	13.6	32	2.5	192	10	152	36	137	5	51	618	26	29	22	5	71	37	5	5	7.6	13.7	5.3	7.1	0.3	1.0	2.3	0.6	1.0	0.8	1.1	0.3	1.3	0.2			
13/150-160	18	18.6	44	5	168	2.5	73	21	130	22	57	442	18	28	25	5	58	28	5	12	4.4	9.2	6.7	3.6	0.3	1.1	2.6	0.8	1.2	1.2	0.9	0.2	1.8	0.2			
11/140-150	17	14.6	29	2.5	168	5	83	33	132	5	49	612	24	109	26	5	67	24	5	5	2.6	5.3	6.2	3.5	0.3	0.9	2.2	0.4	1.0	1.0	0.4	0.5	1.4	0.2			

Appendix 9

Miscellaneous photographs

Engebøfjellet



Fig. A9.1: Photographs of representative ferro eclogite. The upper photo is a core sample from Dh10 (sample 10/97.1) of a garnet-rich, massive ferro eclogite. Retrogression is minimal; omphacite (light green) is unaltered. The brown dots are small cavities after a leached mineral. Elsewhere in the Engebøfjell cores a white, tabular mineral identified by XRD to be celestite (SrSO_4), has been found in patches resembling these cavities. The central photo is a microphotograph (transmitted light) of a similar rutile- (black) and garnet-rich fresh eclogite from Dh10 at 292.9 m (thin-section 10/292.9). Other minerals are omphacite (light green), minor amphibole (blue-green) and colorless minerals (phengite, quartz, carbonate). The lower photo shows the same thin-section seen in reflected light, with rutile (gray) and pyrite (white).



Fig. A9.2: Representative, massive ferro eclogite from Dh9 at 87.7 m (upper photo) and Dh10 at 282.5 m (lower photo). For the darker part of sample 9/87.7 there are two possible explanations that both are fairly common: (a) during retrogression (amphibolitization) the primary amphibole * and the omphacitic clinopyroxene are replaced by a secondary amphibole (hornblende). Such retrogression occurs in gradual variations from hardly noticeable to very extensive. In the very extensive retrogression, rutile is often altered to ilmenite or even to titanite. (b) Alternatively, the darker area in the eclogite corresponds to an infiltration of fluid during eclogite facies metamorphism; in such cases the darker rock is due to the abundance of blue-green eclogite facies amphibole. Another common retrogression occurs along thin veins in the eclogite, as most clearly seen in the lower photo. In such retrograde veins, rutile is often partly retrograded to ilmenite and occasionally also to titanite (see Fig. 16).

* New electron microprobe analyses indicate that the primary amphibole in the fresh ferro eclogite is an actinolitic hornblende, not barroisite as previously regarded. A possibility is that the composition of the primary eclogite-facies amphibole varies.

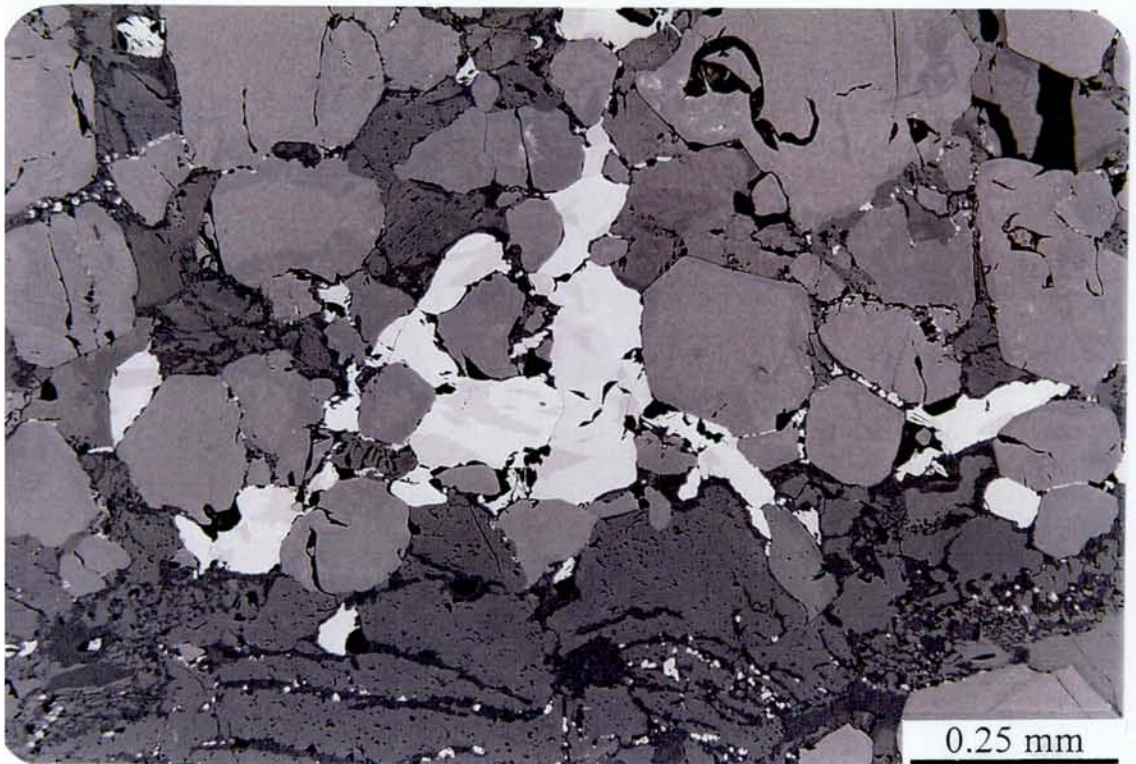
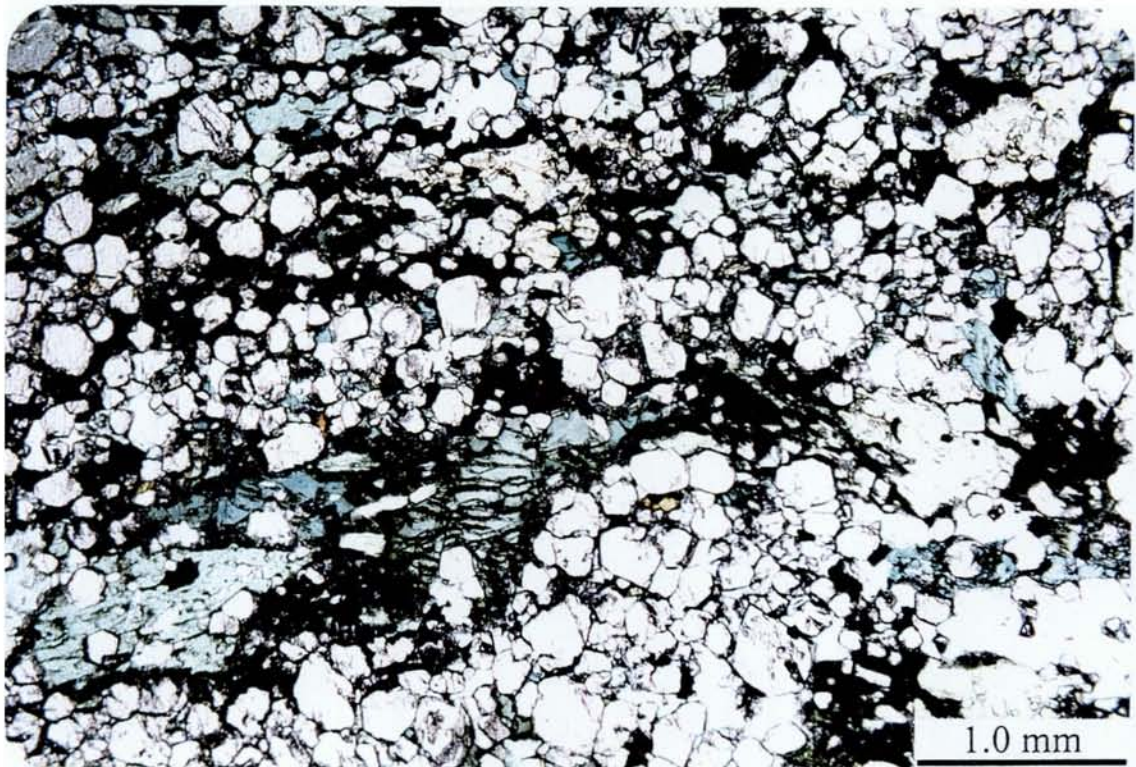


Fig. A9.3: Microphotographs of retrograded eclogite from Dh8 (thin section 8/229.0). In the upper photo (transmitted light), the barroisitic (or actinolitic) amphibole is altered to hornblende (green) and the omphacite to very fine-grained symplectitic aggregates of hornblende-plagioclase-diopside-magnetite (dark green to black). Alteration happens along lines and fractures within minerals. The lower photo (reflected light) shows rutile (gray) with ilmenite exsolutions (brownish) and fine-grained secondary magnetite (white patches mainly within symplectites after omphacite).

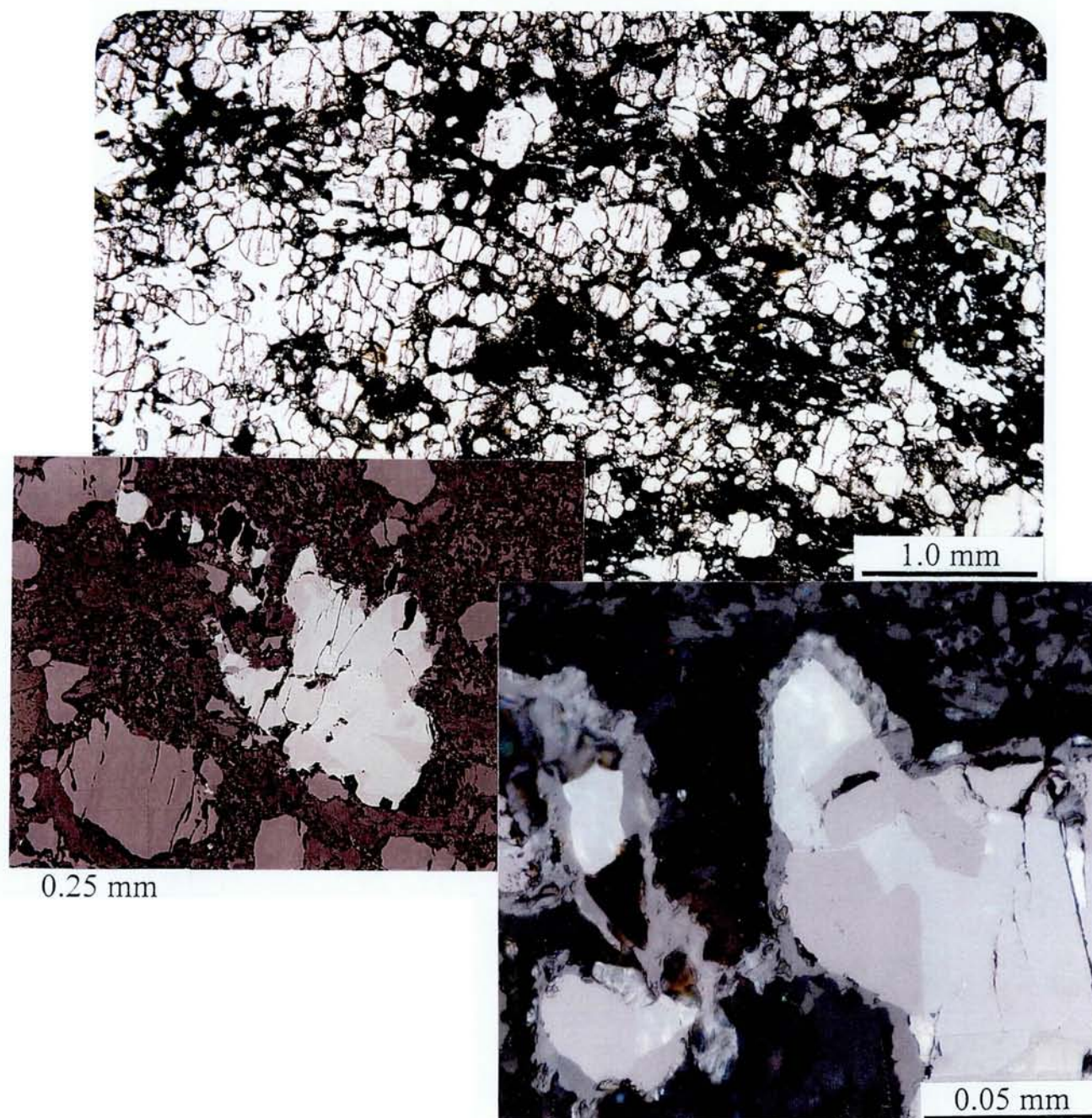


Fig. A9.4: Microphotographs of strongly retrograded, garnet- and rutile-rich ferro eclogite from Dh8 (thin-section 8/170.0). The dark green to black fine-grained matrix in the upper photo (transmitted light) is an alteration product after barroisite and omphacite. Rutile (gray) - ilmenite (brownish) intergrowths (reflected light) are shown in the central photo. The lower photo is an enlargement of the previous image showing titanite corona at the rim of the rutile/ilmenite grain.

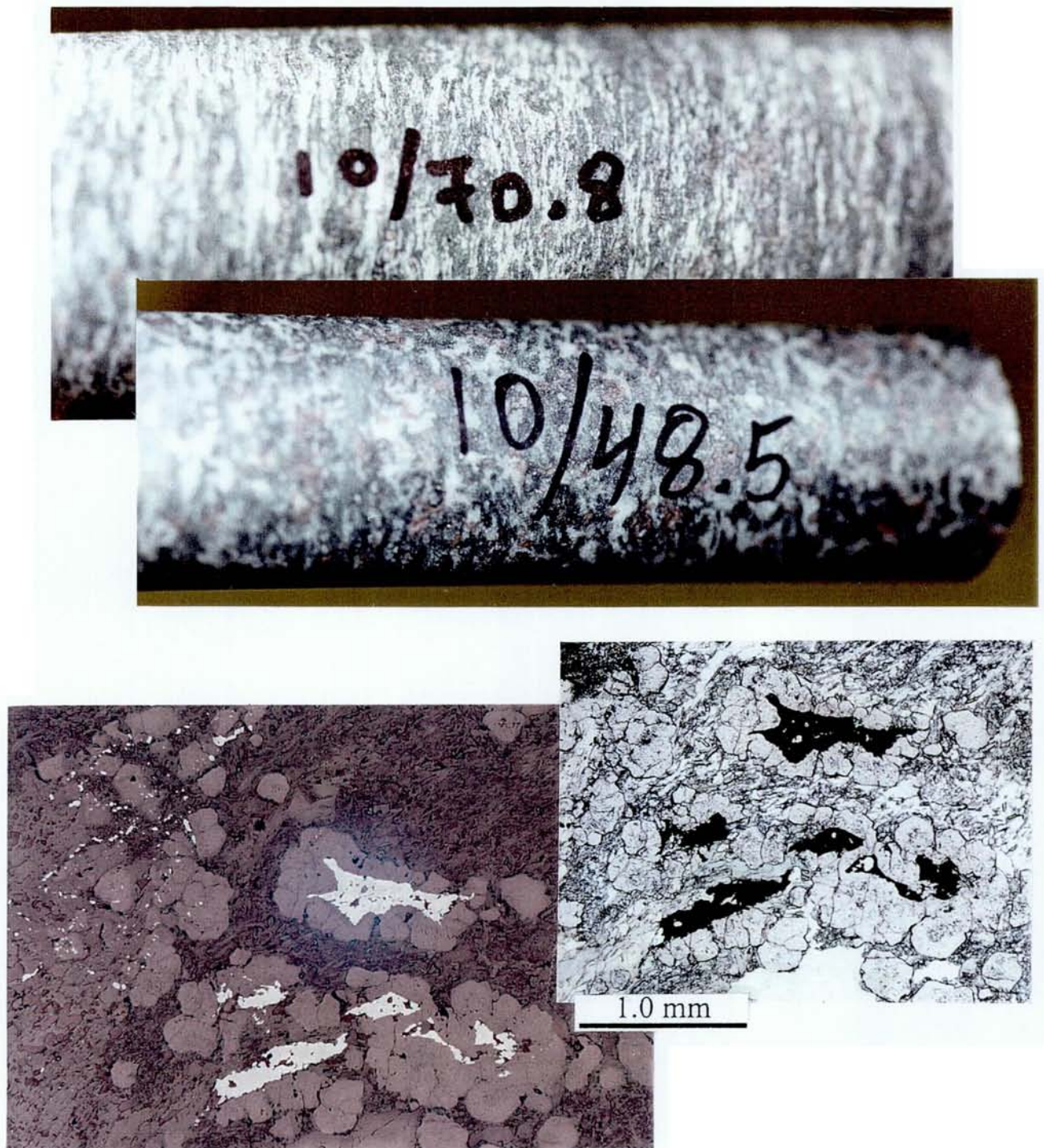


Fig. A9.5: Photographs of core and thin-section of leuco eclogite. Upper photo: representative, slightly sheared leuco eclogite from Dh10 at 70.8 m. Upper central photo: Massive leuco eclogite with preserved gabbroic texture from Dh10 at 48.5 m. Photo at lower right: microphotograph (thin section 10/46.9; reflected light) of rutile (black) in leuco eclogite. Garnet corona (around rutile) and fine-grained areas of clinzoisite + phengite + quartz + amphibole + omphacite after magmatic plagioclase are typical of partly recrystallized gabbroic textures. Photograph at lower left: same rutile grains (light gray; reflected light) as in the previous photo. The light gray patches in the left part of the photo are fine-grained rutile. Rutile in leuco eclogite normally occurs as fairly large grains or aggregates of grains and as scattered (dusty) grains as shown on this photograph. In retrograded leuco eclogites the fine-grained oxide dust is usually magnetite.



Fig. A9.6: Some retrograded eclogite varieties. Upper photo: core-sample of amphibolite/hornblendite with quartz vein from Dh10 at 255.7 m. Central photo: core-sample of slightly retrograded eclogite with coarse-grained garnets from Dh10 at 173.8 m. The light green areas consist mainly of diopside + plagioclase symplectites after omphacite and minor amphibole. In this kind of rock, the rutile is often partly altered to ilmenite and occurs as rutile/ilmenite exsolutions. Lower photo: core-sample of a strongly retrograded rock with retrograde coronas of amphibole + plagioclase (\pm epidote?) around the garnet crystals and amphibolitized matrix. At this stage of retrogression, rutile is more or less totally altered to ilmenite and occasionally also to titanite.

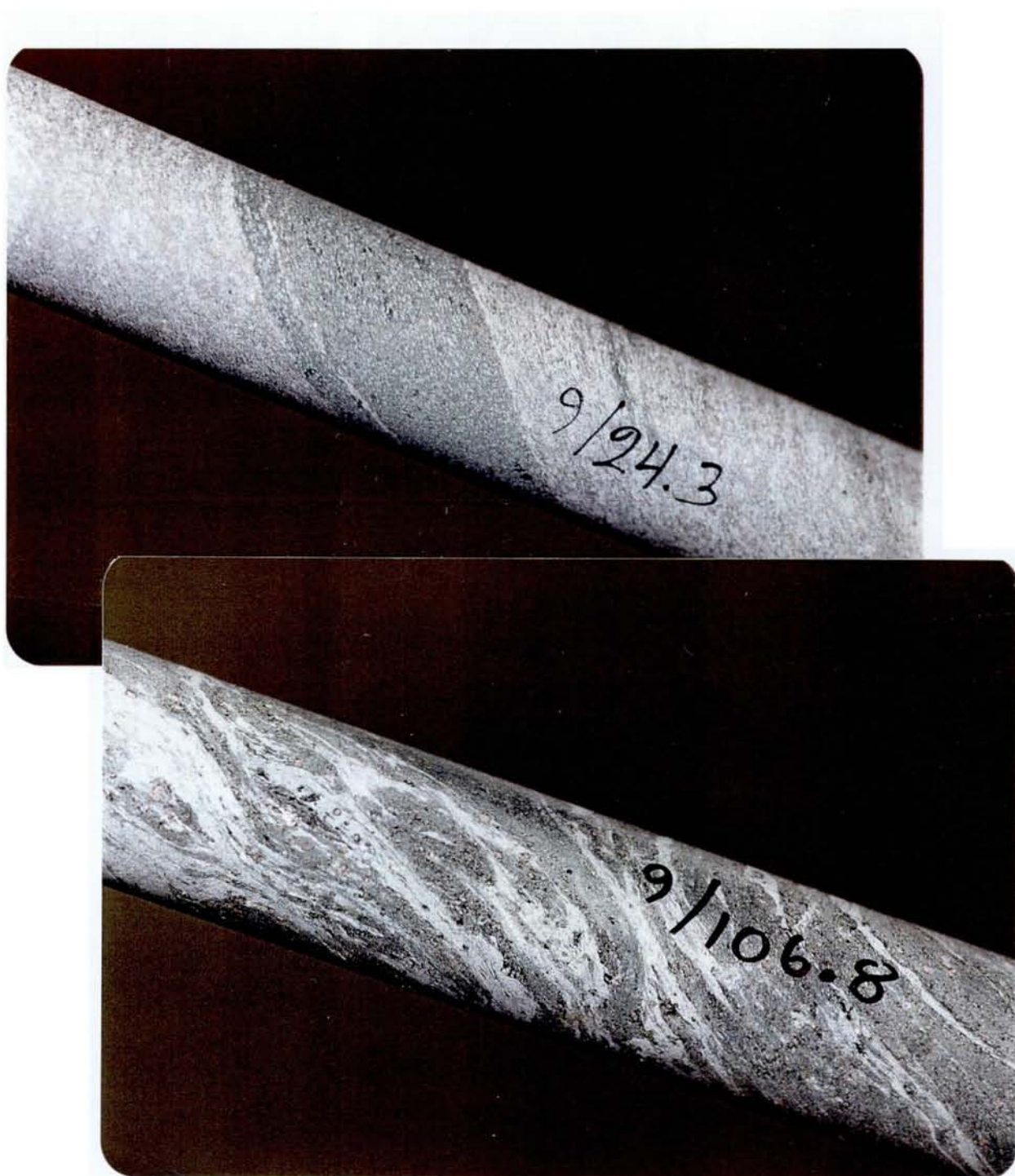


Fig. A9.7: Typical amphibolite unit rocks; upper photo: gray gneiss (dioritic) with amphibolite bands from Dh9 at 24.3 m. Lower photo: strongly amphibolitized eclogite with numerous mm- to cm-thick bands, often intensely folded, of a leucocratic gneiss.



Fig. A9.8: Sharp contact between a patchy amphibolite (left part of the core-sample) and massive ferrogabbroic eclogite (right). The eclogite is fresh and foliated with the foliation more or less parallel to the amphibolite contact.